INTERFACIAL PHENOMENA AND RATE PROCESSES IN THE EXTRACTION OF NICKEL BY MIXED REAGENTS

By

Cesar Alberto SAVASTANO

Ingeniero Químico (San Juan, Argentina, 1978)
M.Sc., Nuclear Fuels Technology (London University, 1981)
Diploma of Imperial College (DIC, 1981)
M.S., Chem. Eng. (Syracuse University, USA, 1984)

A thesis submitted for the degree of Doctor of Philosophy of the University of London

Department of Chemical Engineering and Chemical Technology,
Imperial College of Science and Technology,
London SW7 England

1988

ABSTRACT

The liquid-liquid extraction of nickel ions from nitrate media by di-nonylnaphthalenesulphonic acid (DNNSA), the commercial hydroxyoxime LIX63 and their mixtures in hexane has been studied. Equilibrium distributions were determined. Extraction rates were measured in a non-dispersive contactor under controlled hydrodynamic conditions. The effect of concentrations, turbulence, temperature and interfacial area on fluxes was investigated. The partition and dynamic solubilization of DNNSA was investigated, as well as the solubilization of water by reversed DNNSA micelles.

Novel criteria based on extractant aqueous solubility and dissolution kinetics were implemented to identify the interface as the locale of the rate controlling step in nickel extraction.

Rate models were derived to simulate the initial extraction fluxes by single and mixed reagents under conditions free from controlling mass transfer resistances. In addition to concentrations, the models incorporate interfacial parameters and transfer coefficients estimated from physical transfer experiments.

The problem of interfacial reaction with convective-diffusion was modelled following the two-film and the penetration-surface renewal theories of mass transfer. The analyses successfully predict the plateaux reached by the fluxes as stirring speeds were increased.

Synergic and rate-enhanced extraction by the mixtures was observed. Organic bulk and interfacial speciation of single reagents and mixtures were modelled. Based on thermodynamic consideration of changes in aggregation and micellar solubilization, the synergism shown by mixtures was justified. Concurrent changes in bulk and interfacial speciation were found responsible for the rate enhancements by mixtures.

The explaination proposed for the rôle of catalytic extractants differs from existing models in two respects:
i) it integrates the analysis of bulk and interfacial speciation,
ii) it does not assume formation of metal complexes with mixed reagents.

To Gladys, Gemi and Luis,
for coping
with a student husband and dad.

ACKNOWLEDGEMENTS

My supervisors, Susana Ortiz and the late Henry Sawistowski, organized this project thus making possible my work at Imperial College. For this reason I am much obliged to them. Talking to Dr. Ortiz has always been cheering, and her advice useful.

During this work, I have been very fortunate in counting with the help of top class professionals and individuals. Advice and encouragement from Ian Drummond, Dick Wood and Malcom Dix were always forthcoming. The Glassblowers, and the PG Services and mechanical workshop Technicians did a great job of each piece of work I took to them. Their high standard of workmanship did much for the success of this project.

My colleages Filomena Pinto, Philippe Alinat and Christophe Haunold spent some time working in my laboratory. Zaki El-Hassan and Ini Urua showed me how to stop being 'computer-unfriendly'. I much appreciate their help and the privilege of their friendship.

Dr. Peter Clay helped with organization, advice and facilities in the work with radioactive tracers.

During the last three years I have benefitted from discussions with Dr. K. Osseo-Asare from Pennsylvania State University.

Elios Jorisi, Mark Sadler, and Peter Poggioli worked hard to analize my samples and to help me in all respects.

Financial support from the Science and Engineering Research Council of the U.K. is gratefully acknowledged.

TABLE OF CONTENTS

	Page
Abstract	2
Acknowledgements	4
Table of contents	5
List of Tables	8
List of Figures	10
Notation	12
I. INTRODUCTION	16
II. LITERATURE REVIEW	20
II.1. Amphipathy and other extractant properties.	21
II.1.1. Adsorption and aggregation.	22
II.1.2. Aqueous solubility of extractants.	29
II.1.3. Interfacial pressure and excess.	31
II.1.4. Interfacial potentials.	36
II.2. Surfactants and mass transfer.	40
II.2.1. Micellar solubilization.	40
II.2.2. Dynamic phase transfer.	44
II.3. Equilibria and rates of metal extraction.	52
II.3.1. Equilibria of extraction by single reagents	52
II.3.2. Rates of extraction by single reagents.	56
II.3.3. Synergism in metal extraction by mixtures.	60
II.3.4. Rate enhancements by extractant mixtures.	64
II.3.5. Microemulsions as metal extractants.	69
III. EXPERIMENTAL	71
III.1. Reagents	71
III.1.1. DNNSA.	71
III.1.2. LIX63.	73
III.1.3. Other reagents and chemicals.	73
III.2. Interfacial tension measurements.	74
III.3. Water analysis in micellar solutions.	74
III.4. Water solubilization experiments.	77

Page

III.5. DNNSA solubilization experiments. 82

III.6. Nickel extraction equilibrium experiments. 84

III.7. (K-H)DNNS exchange equilibrium experiments. 85

III.8. Nickel extraction rate experiments. 86

III.9. Miscellaneous measurements. 88

IV. RESULTS AND DISCUSSION OF RESULTS 89

IV.1. Characterization of DNNSA solutions and DNNSA-LIX63 mixtures. 89

IV.1.1. Physical properties of solutions. 90

IV.1.2. Interfacial tensions and π-A isotherms. 91

IV.1.3. Correction of interfacial potentials. 103

IV.1.4. Direct measurement of reversed micelles. 104

IV.2. Aqueous solubility of DNNSA. 106

IV.2.1. Partition equilibrium results. 106

IV.2.2. Dynamic solubilization. 108

IV.3. Electrolyte solubilization by DNNSA micelles. 121

IV.3.1. Solubilization capacity. 121

IV.3.2. Transfer across hydrophilic membranes. 124

IV.3.3. Transfer in the NDSC. 130

IV.3.4. Initial solubilization and core exchange 136

IV.4. Ni(II)-K(I)-H(I)-DNNS exchange equilibria. 137

IV.4.1. (K-H)DNNS exchange equilibrium. 137

IV.4.2. (Ni-K-H)DNNS exchange equilibrium. 150

IV.5. Equilibrium of Ni(II) extraction by LIX63. 155

IV.6. Equilibrium of Ni(II) extraction by DNNSA-LIX63 mixtures. 165

IV.7. Kinetics of Ni(II) extraction by DNNSA. 174

IV.8. Kinetics of Ni(II) extraction by LIX63. 190

IV.9. Kinetics of Ni(II) extraction by DNNSA-LIX63 mixtures. 191

V. MODELLING 197

V.1. Physical mass transfer. 197

V.1.1. DNNSA aqueous solubilization dynamics. 197

V.1.2. Solubilization by reversed micelles. 199

Page

V.2. Solubilization contribution to initial extraction fluxes. 207

V.3. Kinetic modelling of nickel extraction by DNNSA. 211

V.4. Interfacial kinetics and the two-film theory. 227

V.5. Interfacial kinetics and the penetration-surface renewal theory. 232

V.6. Kinetic modelling of nickel extraction by LIX63. 236

V.7. Speciation in DNNSA-LIX63 mixtures. 242

V.8. Kinetic modelling of extraction by mixtures. 247

VI. CONCLUSIONS AND SUGGESTIONS FOR FURTHER WORK 258

VI.1. Conclusions. 258

VI.2. Suggestions for further work. 260

Bibliography 262

Appendices

A. Purification of DNNSA. 274

B. Purification of LIX63. 275

C. Operation of the NDSC. 276

D. Austin's solution to the problem of unsteady mass transfer in a diffusion layer. 278

E. Solution to the problem of diffusion and simultaneous interfacial reaction with the "radiation" BC. 280

F. Experimental data. 284

G. Estimation of diffusion coefficients. 323

H. Computer codes. 325

ERRATA

Page Numbering: Number 131 was given to no page, and
Number 203 was given to two pages.

LIST OF TABLES

Full captions are included in the heading of each table.

Name	Description	Page
III.1	Ultimate loading of DNNSA.	76
III.2	Gas phase chromatography of DNNSA solutions.	76
IV.1	CACs and CMCs of organic feeds.	100
V.2	Fractional interfacial coverages.	100
IV.3	Rates and fluxes in ^{32}P solubilization.	139
IV.4	Equilibrium of nickel extraction by mixtures.	167
IV.5	Equilibrium of nickel extraction by mixtures.	167
IV.6	Activation energy from nickel fluxes by DNNSA.	189
V.1	Estimation of δ and $\mathfrak{D}$ in the NDSC.	206
V.2	MTCs in initial solubilization and core exchange.	206
F.1	Ternary water-hexane-ethanol standards.	284
F.2	^{32}P tracer specifications.	285
F.3	Density of organic feeds.	286
F.4	Viscosity of organic feeds.	286
F.5	σ and adsorption isotherm of DNNSA.	287
F.6	σ and adsorption isotherms of DNNSA-LIX63.	288
F.7	σ and adsorption isotherms of LIX63.	290
F.8	σ and adsorption isotherms of LIX63 (from literature values).	290
F.9	Interfacial potentials for DNNSA.	291
F.10	Interfacial potentials for mixtures.	292
F.11	PCS measurements of reversed micelles.	293
F.12	Partition of DNNSA.	299
F.13	Effect of ionic strength on DNNSA solubility.	300
F.14	Rates and fluxes in DNNSA transfer.	301
F.15	Moisture content of purified DNNSA.	302
F.16	Calibration of solubilized ^{32}P.	302
F.17	Water solubilization across membranes.	303
F.18	Rates of water transfer across membranes.	303

		Page
F.19	Electrolyte solubilization in the NDSC.	304
F.20	^{32}P solubilization by DNNSA micelles	305
F.21	(K-H)DNNS equilibrium.	309
F.22	(Ni-K-H)DNNS equilibrium.	310
F.23	Aggregation number of DNNSA.	312
F.24	Nickel-LIX63 extraction equilibrium.	313
F.25	Effect of pH on nickel extraction by LIX63.	314
F.26	Equilibrium of nickel extraction by mixtures.	315
F.27	Equilibrium constants in extraction by mixtures.	316
F.28	Effect of stirring on nickel fluxes by DNNSA.	316
F.29	Effect of concentrations on nickel fluxes by DNNSA	317
F.30	Effect of concentrations on nickel fluxes by LIX63	318
F.31	Effect of pH on nickel fluxes by LIX63.	318
F.32	Effect of concentrations on fluxes by mixtures.	319
F.33	Effect of pH on nickel fluxes by mixtures.	320
F.34	Effect of nickel concn. on fluxes by mixtures.	320
F.35	Aqueous phase MTCs in the NDSC.	321
F.36	Organic phase MTCs in the NDSC.	321
F.37	Solubilization and nickel fluxes.	322

LIST OF FIGURES

Name	Description	Page
II.1	Formula of DNNSA.	21
III.1a	Non-dispersive, stirred contactor.	79
III.1b	Membrane contactor.	81
III.2	UV absorbance of DNNSA solutions.	83
III.3	UV absorbance of DNNSA; calibration.	83
IV.1	Viscosity of feeds.	94
IV.2	Interfacial tension of extractants and mixtures.	95
IV.3	Interf. tensions and UV-VIS absorbance of DNNSA.	96
IV.4	Interfacial excesses.	101
IV.5	Adsorption ('π-A') isotherms.	102
IV.6	Interfacial potentials.	105
IV.7	Aqueous solubility of DNNSA.	109
IV.8	Partition coefficients of DNNSA.	110
IV.9	Effect of concns. on DNNSA solubilization rate.	115
IV.10	Effect of I on DNNSA solubilization rate.	116
IV.11	Effect of nickel on DNNSA solubilization rate.	117
IV.12	Presaturation and DNNSA solubilization rate.	118
IV.13	DNNSA fluxes and ionic strength.	119
IV.14	DNNSA fluxes and stirring speeds.	120
IV.15	Drying of purified DNNSA.	125
IV.16	Effect of I on water loading capacity of DNNSA.	126
IV.17	Effect of concentration on capacity of water loading and rate of transfer across membranes.	127
IV.18	^{32}P solubilization. Calibration.	128
IV.19	Dynamic water solubilization across membranes.	129
IV.20	Effect of stirring on water solubilization across membranes.	133
IV.21	Dynamic water solubilization in the NDSC.	134
IV.22	Effect of stirring on water fluxes.	135
IV.23	Initial solubilization of ^{32}P tracer.	138
IV.24	Exchange of ^{32}P tracer.	139
IV.25	Effect of pH on DNNSA exchange equilibria.	149

		Page
IV.26	Effect of concentrations on the equilibrium of nickel extraction by DNNSA.	154
IV.27	Equilibrium of nickel extraction by LIX63.	162
IV.28	Effect of pH on nickel extraction by LIX63.	163
IV.29	Estimation of LIX63 dimerization constants.	164
IV.30	Equilibrium of nickel extraction by mixtures.	168
IV.31	Data from nickel extraction in the NDSC.	183
IV.32	Effect of stirring and DNNSA concn. on nickel fluxes.	184
IV.33	Nickel fluxes and interfacial area.	185
IV.34	Effect of nickel concentrations on fluxes by DNNSA.	186
IV.35	Effect of pH on nickel fluxes.	187
IV.36	Effect of stirring and concentrations on DNNSA and nickel fluxes in the NDSC.	188
IV.37	Effect of extractant concns. on nickel fluxes.	195
IV.38	Effect of nickel concentration on fluxes by mixtures.	196
V.1	MTCs in the NDSC.	203
V.2	Predictions of dynamic water solubilization in the NDSC.	204
V.3	Mechanism of micelles-interface interaction.	205
V.4	Effect of presaturation on nickel fluxes.	209
V.5	Nickel fluxes in NDSC and in RD experiments.	210
V.6	Reaction mechanism for nickel-DNNSA.	214
V.7	Concentration profiles as in the film theory.	228
V.8	Effect of stirring on physical transfer in the NDSC.	234
V.9	Nickel flux by LIX63.	241
V.10	Speciation of mixtures, [LIX63]=5.10^{-3}M.	245
V.11	Speciation of mixtures, [LIX63]=1.10^{-3}M.	246
V.12	Rate enhancements with mixed extractants.	255
V.13	Predicted nickel fluxes by mixtures.	256
V.14	Fit of experimental mixed fluxes, regions I,II.	257

NOTATION

A : interfacial area in the NDSC, m^2.

A : area of interfacially adsorbed molecule, $nm^2 molecule^{-1}$ or $m^2 kmol^{-1}$.

A_o : limiting area of interfacially adsorbed molecule.

a : interfacial area per unit volume, m^{-1}.

C : concentration, kmol m^{-3}.

D : metal distribution coefficient.

D : DNNSA monomer, in speciation analysis.

$\mathfrak{D}$: diffusion coefficient, $m^2 s^{-1}$.

E : rate enhancement factor in extraction by mixtures.

F : Faraday electrochemical constant.

F : ratio of film renewal rates.

I : ionic strength, $kmol m^{-3}$.

J : interfacial flux, kmol $m^{-2} s^{-1}$.

k' : kinetic rate constant.

k : apparent kinetic rate constant.

K_a : DNNSA ionization constant.

K_{aq} : aqueous phase MTC, ms^{-1}.

K_e : equilibrium constant for nickel exchange.

K_s : equilibrium constant for metal solvation.

K_s : KDNNS ionization constant.

K_h : hydrolysis constant.

L : LIX63 monomer, in speciation analysis.

L : equilibrium nickel loading capacity in section V.5.

m : aggregation number of DNNSA in organic phase.

n : aggregation number of DNNSA in aqueous phase.

p : partition coefficient.

R : correlation coefficient of regressions.

r : rate of transfer per unit volume, $kmol m^{-3} s^{-1}$.

S : aqueous solubility of surfactants, $kmol m^{-3}$.

s : subphase renewal frequency, s^{-1}.

s : Laplace domain variable (in appendix E).

t : time, s.

T : temperature, ^{o}C or K.

V : volume, m^3.

v : molecular volume (m^3/molec), and volume per unit area in the NDSC (m).

W : water molecules solubilized per surfactant molecules.

z : electrical charge or ionic valency.

ACRONYMS and ABBREVIATIONS

BC : boundary condition.

CAC : critical adsorption concentration, $kmolm^{-3}$.

CMC : critical micellar concentration, $kmolm^{-3}$.

Concn. : concentration.

D2EHPA : di-2-ethylhexylphosphoric acid.

DNNSA : di-nonyl naphthalenesulphonic acid.

DP : discrete particle.

EM : electrophoretic mobility.

FE : fluid element of organic phase.

HD : monomer of DNNSA.

H_2L : monomer of LIX63.

KD : monomer of K-soap of DNNSA.

LMA : law of mass action.

MIC : concentration of micellar species, $kmolm^{-3}$.

MT : mass transfer.

MTC : mass transfer coefficient, ms^{-1}.

NDSC : non-dispersive, stirred contactor.

PCS : photon-correlation spectroscopy.

RD : rising drop.

RDS : rate-determining step.

Re : Reynolds number.

RM : reversed micelle.

sd : standard deviation of a set of values.

SMA : sub-micellar aggregate, or concn. of SMAs ($kmolm^{-3}$).

TBP : tri-n-butylphosphate.

Bq : Becquerel

SUPERSCRIPTS

ad : adsorbed at the o/w interface.

h : in hexane (e.g. moisture).

i : interfacial.

s : at saturation.

I,II,III: regions in figure V.12.

SUBSCRIPTS

a : anion.

aq : aqueous phase.

D : refers to DNNSA, and to ionized sulphonate.

e : exchange.

eq : equilibrium.

f : feed.

i : ith species in rate modelling.

p : DNNSA micelle.

T : formal (total) concentration.

H : hydrogen ion.

K : potassium ion.

L : refers to LIX63.

M : mixed system, also refers to Metal (i.e. nickel).

Ni : nickel.

o : organic phase.

s : refers to KD soap, or ionized naphthalene sulphonate.

so : solvation.

w : water, in micellar solubilization work.

1 : monomer, also refers to MD^+, and to pre-synergic equilibrium (in section IV.6).

2 : dimer, also refers to MD_2, and to synergic equilibrium (in section IV.6).

GREEK SYMBOLS

δ : thickness of diffusion film (in section V.4), m.

δ : thickness of reaction film (in section V.5), m.

ε : time required for chemical conversion of a FE.

ϕ : surface renewal frequency distribution.

Γ : interfacial adsorption density, $kmolm^{-2}$ and molec nm^{-2}.

η : refractive index.

ψ : interfacial potential, mV.

λ : adsorbed film thickness, nm.

μ : viscosity, mPas.

ν : kinematic viscosity, cS.

π : interfacial pressure, mNm^{-1}.

θ_j : fractional interfacial coverage by species j.

ρ : density, $kgdm^{-3}$.

σ : interfacial tension, mNm^{-1}.

τ : time required for full water loading of a FE.

ζ : zeta potential, mV.

[ ] : concentration, $kmol\ m^{-3}$.

CHAPTER I. INTRODUCTION

The research and development efforts invested over the last three decades or so in the optimisation of hydrometallurgical liquid-liquid extraction processes can be classified into two areas of arguably similar importance: equipment engineering and process fundamentals. In respect of the former, although conventional mixer-settlers are still in use in most mills, a number of technical innovations are gradually being introduced. Contactors such as combined mixer-settlers and columns of various designs tend to show a better performance than conventional plant.

The fundamentals of metal extraction processes have lately received much attention. Research on the process chemistry has lead to the development of later-generation reagents that are more selective, have higher loading capacity, or are more stable than earlier extractants. Modifiers have also been developed that facilitate the stripping and phase disengagement and reduce crud formation.

As processes become well established, there appears the understandable reticence of speciality chemicals manufacturers to invest funds in the development of new reagents or processes (Price, 1987). Instead, considerable effort is currently being devoted to discovering and exploiting the advantages resulting from mixing available well known extractants. The desirable effects usually sought are increases in selectivity or in loading capacity (synergism), enhancements in the extraction or stripping rates, or a combination of these effects.

The hydroxyoximes developed as the LIX series by General Mills (now Henkel Corp.) in the late 1960s are the best known example of synergic/rate-enhancing effects in one proprietory reagent mixture. Aimed at the large tonnage copper industry, LIX64N is a mixture of mostly 2-hydroxy-5-nonyl benzophenone oxime (LIX

65N) with small amounts of 5,8-diethyl 7-hydroxy 6 dodecanone oxime (LIX63). The molecules of these acidic extractants can exchange protons by copper cations, and also chelate the metal ion. The small additions of LIX63 to the highly copper-selective LIX65N increase the rate of extraction.

Reports of synergic and rate enhancing effects observed with mixtures of LIX reagents and other acidic extractants of the sulphonate, carboxylate, and phosphate families abound in the literature, yet there appears to be little understanding of the physico-chemical and transport phenomena underlying such observations. Further, because of the modelling difficulties posed by the heterogeneous nature and the chemistry of the reactions involved and the amphipathic character of the extractants, conflictive conclusions are sometimes reached.

Satisfactory models of extraction rates by extractant mixtures or the conclusive identification of the locus of rate determining steps in the mechanisms involved cannot be readily substantiated without a comprehensive research approach. Such a study must encompass the bulk phases as well as the interfacial region. Information about all species present in the organic and in the aqueous phase, and on interfacial parameters such as pressure, electrostatic potential and adsorption density should be combined with the study of the effect of chemical and hydrodynamic parameters in the interpretation of kinetic data. Perusal of the literature reveals that this is not the approach usually followed. Instead, models are derived from partial analyses of extraction systems.

As a consequence, disparate opinions are found in the literature on aspects such as reaction orders and the locale of the rate determining step (RDS). There is, for example, an ongoing argument about the site of RDSs. A correlation between aqueous solubility of the extractant dithizone and extraction rates suggested to

Akiba and Freiser (1982) that reactions in the bulk aqueous phase controlled the rate of extraction of Cu(II), whereas a similar dependence of the rate on the interfacial adsorption density of LIX65N le d Flett (1977) to propose an interfacial control.

The interfacial physical chemistry and bulk speciation of extraction systems with dinonylnaphthalene sulphonic acid (DNNSA or HD, Kings Industries, Conn., USA) and the hydroxyoxime LIX63 (Henkel Corp., previously General Mills) have been extensively studied by the research group lead by Dr. K. Osseo-Asare at Pennsylvania State University. The availability of information generated by that work makes this extractant mixture a good model system for an integrated approach to kinetic extraction modelling.

Although these mixtures may have little commercial relevance at present, understanding the complicated phenomena underlying the catalytic and synergic interactions in them is expected to contribute to the understanding of the behaviour of other extractant mixtures.

In addition, because of its intense surface activity, DNNSA has potential applications not limited to metal extraction. Its ability to form aggregates in organic diluents may be exploited to solubilize hydrophiles that are virtually insoluble in the absence of surfactant. Potential uses are in medicine, biotechnological separations, and catalytic processes in heterogeneous systems. Double tailed molecules such as that of DNNSA favour the attainment of very low interfacial tensions. This property may be used to benefit in enhanced oil recovery (Aveyard, 1987). Thus furthering our understanding of the surface chemistry and colloidal properties of DNNSA has a significant niche in the research and development effort which may eventually translate into novel separation techniques.

The aim of this work was to obtain mechanistic models that adequately describe the kinetics of nickel extraction by LIX63 -DNNSA mixtures. To this effect, experimental work was performed covering the following areas:

-aqueous solubility and dynamic phase-transfer of DNNSA,

-interfacial tensions,

-equilibrium and dynamic loading of water by solutions of reversed micelles,

-metal extraction equilibria, and

-metal extraction kinetics.

Experiments are described in chapter III, and results are presented and discussed in chapter IV. Chapter V deals with the modelling of metal extraction kinetics by single and mixed extractants and of physical mass transfer. The literature relevant to all areas of this work is reviewed in chapter II.

CHAPTER II. LITERATURE REVIEW

The major subject of this thesis belongs in the field of hydrometallurgical liquid-liquid extraction using reagents mixtures. The relevant bibliography is covered in section II.3.

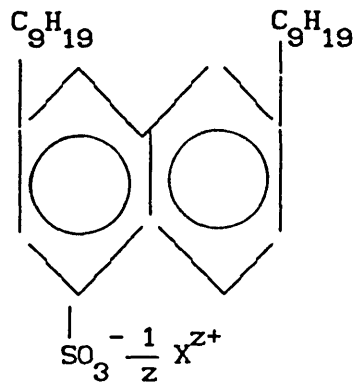
The secondary thrust of this work was to investigate the ability of DNNSA to form micelles that can physically solubilize otherwise sparingly soluble substrata. Work on the solubilization of hydrophobic substances by surfactants and the symmetric phenomenon of hydrophiles solubilization is reviewed in section II.2. From the large body of literature focusing on these areas the most directly relevant work has been culled. Some reviews are included among the references.

It is believed that a satisfactory characterization of the bulk phases and the interface is needed to model extractive separations, whether with or without chemical reactions, in biphasic liquid systems. Thus the literature reports referred to in section II.1 concerning the interfacial activity of surfactants are of similar importance to all mechanisms here investigated.

II.1. AMPHIPATHY AND OTHER PROPERTIES OF EXTRACTANTS

The molecule of the DNNSA isomer shown in figure II.1 is composed of a non-polar part (two hydrocarbon tails and a naphthalene group), and a polar head, the sulphonate group (Högfeldt et al., 1981). The polar head is attracted toward polar diluents, whereas the tails are hydrophobic. Hartley (1936) coined the word "amphipathy" for such dual properties in one molecule.

Figure II.1



Hydrogen bonding causes liquid water to be strongly structured, and to show similar short-range ordering as that in ice (Tanford, 1973). Non-polar solutes such as the hydrocarbon tails of DNNSA increase that structuring, as evidenced by negative entropy changes on dissolution. Thus as the concentration of a surfactant in water (C_{DT}, for DNNSA) is increased, the Gibbs free energy of the system also increases and it is mostly localized at the interface between water and hydrocarbon tails (Elworthy et al., 1968). The system reacts to increases in C_{DT} according to Le Chatelier principle: the interfacial area shrinks.

Three mechanisms contribute to such reduction in interfacial area. The amphipathic molecules **adsorb** at the air-water interface, with the tails sticking out of the water. The molecules also **contract** down to about 70% of their length in hydrocarbon diluents

(Elworthy et al., 1968). As C_{DT} is increased even further, the interfacial population of adsorbed monomers eventually reaches saturation. Further surfactant additions result in aggregation. Micelles are formed in the bulk phase with the hydrocarbon tails in the centres, isolated from the aqueous environment by a shell of polar heads. Significant micellisation starts at the critical micellar concentration (CMC).

II.1.1. ADSORPTION AND AGGREGATION

The CMC of a surfactant or a mixture of surfactants is not a unique composition, instead it is a narrow concentration band. CMC values are experimentally found by locating the usually sharp break in the curve of concentration versus various physical properties, such as interfacial or surface tension, solubility of immiscible substrata, electrical conductivity, osmotic pressure, electrophoretic mobility, or turbidity (Elworthy et al.; 1968, Hall and Tiddy, 1981; Eicke, 1980).

Nagarajan and Ruckenstein (1979) have analized the molecular interactions resulting in aggregation of amphipathic agents in aqueous media. Electrostatic repulsions cause ionic surfactants to form larger micelles than similar, non-ionic surfactants. The thickness of the diffuse electrical layer is reduced by increasing the ionic strength (I), thus the repulsions also decrease and larger micelles can be stabilized at higher values of I. It has been reported that increasing values of I enhanced the solubilization of hydrophobes by aqueous micelles, consistent with a larger micellar size (Carroll, 1981; Lianos et al., 1984; Huang et al., 1981).

Fendler and Fendler (1975) collected micellar parameters of sulphonate-based and other types of surfactants in aqueous and non

-polar media. Temperature, chain length, ionic strength, the presence of additives, and the type of counterion are variables which affect the micellar size and the CMC.

There is also adsorption at interfaces and micellisation when surfactants are dissolved in organic diluents. Reversed micelles are formed in that case, with the polar heads in the centre, shielded from the non-polar environment by the hydrocarbon tails (Eicke and Christen, 1974a). The pairs of tails in DNNSA molecules form a hydrophobic shell that very efficiently screens the polar heads, resulting in values of the CMC as low as 5.10^{-6}kmolm^{-3} (Osseo-Asare and Keeney, 1980a). Reversed micelles are considerably smaller (aggregation numbers (m) $\cong$ 5 to 20) than aqueous micelles (m $\cong$ 50 and larger) (Fendler and Fendler, 1975).

In reversed micelles the polar heads are closer together, and are subjected to the aqueous environment of the core. Thus electrostatic repulsions may be even more important than in aqueous micelles. As I is increased, the repulsions among heads will decrease and more compact micelles would be expected. Reductions in the solubilizing ability of those micelles as I was increased (Goklen and Hatton, 1985; 1986) suggest that electrostatic interactions play a major role in stabilizing the micellar size.

It has not been conclusively demonstrated whether micellar sizes are affected by moisture. Kaufman and Singleterry (1955) reported that the sizes of NaDNNS and $Ba(DNNS)_2$ micelles were not sensitive to changing water concentrations. But the same authors later reported (1957) marked increases in $Zn(DNNS)_2$ micelles size as their water content increased.

Some of the work reviewed by Nagy (1982) has shown marked effects of the water content on micellar sizes. Much earlier, Markus and Kertes (1969) stated that, although DNNSA is dimeric in dry benzene, there were "some larger aggregates" in the presence of

water. Water, therefore, seems relevant to the formation of reversed micelles. Eicke and Christen (1978) suggested that it is indeed indispensable.

The micellar size depends on counterion type (Markovitz and Choppin, 1973; Eicke, 1980), although Markus and Kertes (1969) did not observe a large effect of this factor. The weight of a NaDNNS micelle in dry heptane was found to be around 2400, thus $m \cong 5.5$ (Wang and Li, 1965). The hydrophobic moiety of the molecule affects the micellar size more than the polar head. $Ba(DNNS)_2$ reversed micelles of 7 to 8 monomers were identified in wet benzene, whereas Ba-petroleum sulphonate was found to aggregate in micelles of 34 to 35 monomers (Kaufman and Singleterry, 1955).

The early literature data on DNNSA aggregation in organic diluents can be roughly arranged into two groups according to the dependence of the values of m on the polarity of the diluent (Markovitz and Choppin, 1973). In aromatic solvents m ranges from 5 to 10, whereas m increases to the range 15 to 20 in aliphatic diluents. NaDNNS and $Ba(DNNS)_2$ micelles in n-decane were roughly twice as large as those in benzene (Markovitz and Choppin, 1973).

The experimental difficulties involved in the determination of micellar sizes are evidenced in the disparity of the results available in the literature about aggregation numbers of DNNSA. Morris and Jones (1969) reported aggregation numbers around 20 in heptane, whereas Markovitz and Choppin (1973) estimated a value of 10, closer to the finding of van Dalen et al (1974a), 7, and the value $m = 7$ virtually constant in the range $1.10^{-3} \leq [DNNSA] \leq 0.15$ estimated recently by Zheng and Osseo-Asare (1987). From data on equilibrium transfer of aqueous halides into DNNSA and LiDNNS micellar solutions in heptane, m values around 17 were estimated (Högfeldt et al., 1981). Later revisions reported in the same paper corrected the estimate to around 9.

Kertes and Gutmann (1976) and Mukerjee (1974) have described the main approaches to the modelling of micellisation, namely:

1) the pseudo-phase model, and

2) the Law of Mass Action (LMA) model, which in turn has two different versions, as follows

2a) stepwise aggregation, and

2b) monomer-micelle equilibrium.

1) The pseudo-phase theory considers the micelles as a separate but discrete, non-coalescing phase which abruptly appears as the bulk surfactant concentration is increased beyond the CMC. All surfactant further added to the system is used in forming micelles, i.e. the monomer activity remains constant at about the CMC value. This picture of the aggregation phenomena is the simplest and it is based on the observation that micellisation shows several properties characteristic of phase separation (Berezin et al., 1973). The pseudo-phase theory represents well the physical situation only for large aggregation numbers (Elworthy et al., 1968) thus it is most suitable for aqueous phase micelles.

2a) According to the stepwise aggregation model monomers self-associate into dimers, and sequentially trimers and higher oligomers are formed. The activity of the i-th oligomer (i.e. of the aggregate of i monomers) a_i is related to a_{i+1} and to a_{i-1} by the LMA (Kertes and Gutmann, 1976). Aggregation proceeds stepwise. Polydispersity of aggregates and no abrupt discontinuity in the concentration versus physical property curves are expected from this approach. Thus the concept of CMC is no longer valid (Kertes, 1977). Some surfactant solutions in non-polar diluents do not show a sharp CMC, in contrast with most aqueous micellar systems.

2b) When the micellisation phenomenon is modelled as a one-step aggregation, the monomer activity (a_i) increases little beyond

that at the CMC. The LMA relates activities of monomer and micelle. The one-step aggregation approach is usually preferred to model the speciation in reversed micellar systems.

DNNSA adsorbs strongly at the hexane-water interface and reduces the interfacial tension (σ) from 50 mNm^{-1} to about 8 mNm^{-1} at [DNNSA]=5.10^{-6}(Osseo-Asare and Keeney,1980a;b).There is a sharp break in the σ versus log [DNNSA] curve near the latter value, indicating the CMC. The CMC in toluene was reported at around 2.10^{-5} $kmolm^{-3}$ by Chiarizia et al. (1976). This sharp break and the constant mean aggregation number found from VPO studies (Osseo-Asare and Zheng, 1987, Zheng and Osseo-Asare, 1987) suggest that DNNSA aggregates following the monomer-micelle equilibrium model 2b, used by Chiarizia et al.(1976), and Lin (1984).

The features of DNNSA reversed micelles most relevant to this work are summarized as follows (Gallacher, 1982):

1) DNNSA and its salts form micelles in non-polar diluents, with aggregation numbers around 10. Micellar sizes depend on the diluent dielectric constant, and to a lesser degree on the cation type, moisture quality and concentration, and DNNSA concentration.

2) The CMC in hydrocarbon diluents is around $10^{-6}kmolm^{-3}$.

Most hydrometallurgical extractants are less surface active than DNNSA, as indicated by the higher values of their critical adsorption concentration (CAC). They are thus expected to aggregate less than DNNSA. Carboxylic acids dimerize in organic diluents, and monomer-dimer binaries in aqueous media have been reported (Flett and Jaycock, 1973).

Hummelstedt (1977) presented data which showed that LIX63 and LIX65N aggregate more in i-octane than in aromatic hydrocarbons, in agreement with the difference in interfacial activity in those diluents.

Organophosphorous extractants dimerize in organic diluents. Cox et al. (1983) reported that di-2-ethyl hexyl phosphoric acid (D2EHPA), phosphonic, and phosphinic acid from commercial samples in toluene were dimers. Reversed micelles of D2EHPA (pCAC=3.6 in n-dodecane; Osseo-Asare, 1984) have been reported by Eicke and Christen (1974a), and by Gaonkar and Neuman (1986).

The dimerization of hydroxyoximes in anhydrous diluents was confirmed in the mid 1970's, but no work had been reported until 1977 on dimerization in wet organic phases (Cox and Flett, 1977).

The aggregation of the anti-isomer of 5,8-diethyl-7-hydroxy dodecanone oxime (the active extractant in LIX63, pCAC=3.7 in hexane, 2. in toluene) has been studied by Aguilar et al. (1983) using vapor pressure osmometry (VPO). Trimers and dimers were found. Zheng and Osseo-Asare (1987) used the same technique and estimated aggregation numbers higher than 2, and increasing as the concentration was increased beyond the CMC.

Atwood et al.(1975) found no evidence of LIX64N dimerizing from their IR and extraction equilibrium results.

Akiba and Freiser (1982) evaluated the dimerization constant of LIX65N in hexane and heptane. Inoue and Tsunomachi (1984) did the same for the active extractant in Shell's SME529, and Zheng and Osseo-Asare (1987) for LIX63.

The aggregation of extractant mixtures is less well known than that of single reagents. Their VPO work suggested van Dalen et al. (1974b) that one D2EHPA molecule was associated to 7 DNNSA molecules in a reversed micelle.

When LIX63 was added in varying proportions to hexane solutions of DNNSA, σ increased above that value for DNNSA alone

(Keeney and Osseo-Asare, 1982). The σ vs log[DNNSA] isotherms showed breaks almost as sharp as in the case of DNNSA alone, and values of CAC and the critical micellar concentration (CMC) could be estimated for the mixtures at each level of [LIX63].

Lin (1984) adopted the monomer-micelle one-stage equilibrium approach to model the aggregation of DNNSA and of DNNSA-LIX63 mixtures. Lin assumed that the formation of mixed binaries proposed by Keeney and Osseo-Asare (1982) destabilized LIX63 dimers and trimers (Aguilar et al., 1983, Zheng and Osseo-Asare, 1987), which were thus not included in Lin's analysis.

In their VPO work with LIX63-DNNSA mixtures in hexane, Osseo -Asare and Zheng (1987) and Zheng and Osseo-Asare (1987) found that the vapor pressure vs log[DNNSA] curves with [LIX63] as the parameter had minima at [DNNSA]/[LIX63] ratios of around 2/3. That finding agreed with the stoichiometry of metal complexes extracted by these mixtures (Osseo-Asare and Renninger, 1984), and lead the authors to propose the speciation analysis used in section V.7 of this work.

A molecular thermodynamic theory for mixed surfactant micelles has been presented by Nagarajan (1985).

When tri-n-butyl phosphate (TBP) was added to D2EHPA solutions in hexane, σ was found to increase, the rate of uranyl ion extraction to decrease, and the interfacial electrostatic potential took on less negative values. These observations indicated a decrease in adsorption, probably due to aggregation of both reagents in the bulk (Cox and Flett, 1977).

II.1.2. AQUEOUS SOLUBILITY OF EXTRACTANTS

One of the requirements of hydrometallurgical extractants and diluents is a low solubility in aqueous media. Otherwise losses in the raffinate would pose economic penalties in the form of inventories replenishment and pollution abatement. Besides this technological importance, the aqueous solubility concerns the modelling of metal extraction fundamentals.

There is a conspicuous discussion in the literature about the locale of the rate-controlling reaction step. In some systems, controlling reactions have been reported as taking place in the aqueous bulk, while in others the organic or the aqueous diffusion films have been proposed as the site to those reactions, and the interface is the choice of most researchers. If the reactions take place in aqueous media, then the aqueous solubility of the extractants is obviously important. It is also so when rate-limiting reactions between interfacially adsorbed complexes and extractants in the aqueous phase are proposed.

Coleman and Roddy (1971) warned that the solubility issue can be an important consideration in kinetic modelling. They reviewed data on alkyl phosphoric acids partition. The partition coefficient (P) of D2EHPA in n-octane was shown to depend on pH and [D2EHPA]. It may be estimated from the data shown that P doubled as the reagent concentration was increased one hundred -fold. The experimental difficulties involved in measuring the partition of surfactants were highlighted.

Akiba and Freiser (1982) have shown that extraction rates of Ni(II) by LIX65N increased in line with the aqueous solubility of the reagent. The authors found a correlation between reagent aggregation in the organic bulk and whether P was constant or varied as [LIX65N] was changed. Constant values of P were reported for LIX65N partitioning between a buffer and solvating, relatively

more polar (than hydrocarbons, for example) diluents. The oxime does not aggregate significantly in those diluents but it dimerizes in hexane and heptane (Akiba and Freiser, 1982), for which P was found to increase as [LIX65N] was increased. For all diluents a unique value of pK_a (8.7) was determined. Paatero and Golding (1983) reported $pK_a>10$ for most hydroxyoximes, and Flett et al. (1973) used in their calculations $pK_a=10$ for alkyl hydroxyoximes.

Whewell et al. (1977) included aqueous solubilities in rate models that assumed controlling reactions in the aqueous diffusion film. Those researchers presented data which show that aggregation and partition of hydroyoximes are related. The solubility vs [LIX63] line was curved, whereas solubility vs [monomer] was a straight line. It follows that partition coefficients of increasing value are to be expected at higher formal concentrations.

The non-linearity between organic and aqueous extractant solubilities due to the concentration dependency of P has not been considered by authors who proposed aqueous diffusion films as the locus of rate-controlling reactions (Hughes and Rod, 1983, 1984a, b).

The partition of SME529 (Shell Chemicals) was investigated by Inoue and Tsunomachi (1984). The aqueous solubility of the oxime was shown to be independent of pH up to pH 7, and to rise sharply at pH>7 as the reagent ionized more significantly. From the data plotted by those authors it may be estimated that a 30-fold increase in [oxime] resulted in a value of P around 3 times larger, and that P depended on $[\text{oxime}]^{\cong 0.35}$. In view of the relatively very large values of P (6000 to 20000) it is somewhat surprising that a rate controlling reaction involving the aqueous oxime be invoked for that chemical system (Inoue et al., 1985; Miyake et al., 1986).

Aqueous hydroxyoxime concentrations are usually measured following the spectrographic method developed by Ashbrook (1972).

Chaiko and Osseo-Asare (1987b) have estimated the aqueous solubilities of DNNSA and of LIX65N from monolayer dissolution rate experiments. No previous report concerning aqueous solubility of DNNSA or its salts was found by those authors in the literature. The solubility of the oxime may be compared to the value found by Komasawa et al. (1980b).

II.1.3. INTERFACIAL PRESSURE AND EXCESS

The potential contributions of interfacial properties measurements to the understanding of the physical-chemical mechanisms involved in metal ion liquid-liquid extraction were highlighted by Cox and Flett last decade (1977). However, few researchers undertake such work as an integral part of their investigations. The interfacial activity is also closely related to the aggregation and the resulting speciation of the extractants, as will be emphasized throughout this work.

The amphipathy of reagent molecules is responsible for both adsorption and aggregation. The extractant shows affinity for both media, thus it adsorbs at the o/w interface where its concentration becomes higher than in the bulk phases causing σ to fall below that value when surfactants are not present. The CAC is the lowest bulk concentration which can produce a saturated interface (Rosen, 1978), thus CAC values give an indication of the interfacial activity of surfactants: the lower the CAC value, the higher the activity. Osseo-Asare has tabulated CACs and CMCs of the more common acidic, basic, and amphoteric extractants in several diluents (1984).

DNNSA adsorbs very strongly, as indicated by its pCAC= 6.5 (Osseo-Asare and Keeney, 1980a). Its interfacial concentration is therefore approximately constant in the range of bulk concentrations of interest, an important consideration in the modelling of extraction kinetics (Danesi and Chiarizia, 1980).

The interfacial concentration thus is clearly different from that concentration in the bulk. The Gibbs equation of state relates the adsorption density (or "interfacial excess", Γ) to the reagent activity in the subphase. When electrolytes are added to the aqueous phase with the aim, for example, of regulating pH or ionic strength, the Gibbs equation may still be used, modified as proposed by Matijevic and Pethica (1958).

The adsorbed film has a finite volume, because its thickness is similar to the length of the adsorbed molecule. The length of a DNNSA molecule in the monolayer was estimated as 1.8nm by Chiarizia et al. (1976), on the basis of the molar volume (Kaufman and Singleterry, 1957) and assuming cylindrical shape. The length of the free monomer had previously been estimated as 0.8nm by van Dalen et al. (1974a). Thus Chiarizia et al. (1976) concluded that the adsorbed molecule was stretched, with the head opposite to the tails. The assumption of cylindrical geometry for the DNNSA molecule seems reasonable in view of the two tails (Aveyard, 1987).

Several factors affect σ and Γ of a surfactant at the organic /water (o/w) interface. Osseo-Asare (1984) has discussed such effects in the context of hydrometallurgical extraction reagents, while Lucassen-Reynders (1981) reviewed anionic tensoids.

Miyake et al. (1986) investigated the effect of alkyl chain length on σ, metal distribution at equilibrium, and rates of copper extraction by a series of homologue o-hydroxyacetophenone oximes in benzene.

DNNSA and LIX63 adsorb more strongly when dissolved in aliphatic hydrocarbons than when in aromatic hydrocarbons (Osseo-Asare, 1984). The latter are more polar than the paraffinic diluents, thus they repel less the polar heads. Similar diluent effect was observed for di-n-octyl phosphinic acid by Cox et al. (1983), who reported a $\Delta pCAC \cong 2$ from heptane to toluene. The monolayer was more packed in the former than in the latter (Γ=0.71 and 0.44 molecules nm^{-2}, respectively).

The effect of changing pH on σ for a variety of extraction systems suggests that as ionization of the extractant is favoured, adsorption becomes stronger. This effect is probably due to the increasing repulsion between organic diluent and extractant as the latter becomes more polar on ionization (Osseo-Asare, 1984).

As pH was reduced, the β alkenyl-8-hydroxy quinoline KELEX 100 (Sherex Chemicals Co.) protonated, and σ again decreased (Lee and Tavlarides, 1986).

Adsorbed LIX63 is largely deprotonated at pH≅10 (Al-Diwan et al., 1977). The value of σ increased as pH was reduced to about 4, probably due to lesser ionization, and σ decreased again when pH was reduced to around 1. Those authors attributed the decrease in σ as pH fell from 4 to 1 to the protonation of the oxime. Such protonation, however, would impart a positive charge to the interfaces at which LIX63 adsorb, in contradiction with the nil electrophoretic mobility (EM) of droplets observed in that pH range by Osseo-Asare et al(1983b). No effect of changing pH up to pH=9 on the adsorption of LIX63 had previously been reported (Cox and Flett, 1977).

Because DNNSA is a strong acid (pK_a=0.57; CRC, 1983-84), it is not expected that pH changes affect σ. However, the work of Flett et al. (1974; 1975a; b) concerning the variation of σ with pH in several acidic extractant systems showed that σ for DNNSA in hexane fell from about 20 mNm^{-1} at pH=2 to about 9 mNm^{-1} at pH=8.

Those values of σ seem surprisingly high considering that [DNNSA] was 2.10^{-3}.

Depending on the selectivity of an acidic extractant, the adsorbed film may resemble a mosaic composed of anions, acid, and various salts (Fyles, 1985; 1986). It is not expected that all counterions affect σ equally. For example, copper hydroxyoximates were less surface active than the hydroxyoximes (Cox and Flett, 1977). When nickel was present σ of LIX63 increased, again indicating that the complex was less active than the extractant (Flett et al., 1974).

Adsorption density data are usually presented as 'π-A' isotherms. The interfacial pressure π is defined as the drop in σ due to the adsorbed surfactant from the value of σ^{o} at the water/ hydrocarbon interface (around 50 mNm^{-1}). The area covered by each adsorbed molecule (A) is the reciprocal of Γ, thus it may be found by application of the Gibbs isotherm.

Lucassen-Reynders (1981) has reviewed the recent work on monolayer thermodynamics, such as the 2-d-gas and 2-d-solution approaches to the equation of adsorbed state.

The reagent *effectiveness of adsorption*, $\Gamma_o = A_o^{-1}$, can be found from the limiting value of A at high pressures by extrapolating the straight section of the π-A curve to π=0. Osseo-Asare (1984) listed values of A_o for a variety of extractants.

Some disparity is found in the literature concerning values of A_o for DNNSA. Osseo-Asare and Keeney (1980a) estimated $A_o = 0.38$ $nm^2 molecule^{-1}$, whereas Chaiko and Osseo-Asare (1983) reported $A_o = 1.21 nm^2 molecule^{-1}$. The variation was attributed to differences in the purity of the reagent. The lower value seems more probable, as other authors reported similar results. Chiarizia et al. (1976) estimated $A_o = 0.40$ $nm^2 molecule^{-1}$.

Results for LIX63 are more self-consistent in this respect. Al-Diwan et al. (1977) reported A_o=1.01 $nm^2 molecule^{-1}$, whereas Chaiko and Osseo-Asare (1983) estimated A_o=0.99 $nm^2 molecule^{-1}$ with the same diluent. Osseo-Asare and Keeney (1980a) found A_o= 1.08nm^2 $molecule^{-1}$.

The smaller the value of A_o a reagent has, the higher the interfacial concentration it reaches. A correlation would therefore be expected between Γ_o and the observed rate of heterogeneous reactions if the rate depended on interfacial density. Such a correlation was found by Flett (1977) for the extraction of copper by LIX65N. A_o was modified by using various diluents. Dalton et al. (1978) reported that σ increased and the extraction of copper by o-hydroxyaryl oximes slowed down as the percentage of aromatic component in the diluent increased from 0 to 100.

Additions of a second reagent may alter the bulk speciation of an extractant and its interfacial activity. [LIX63]=0.1 increases the CMC of DNNSA from 5.10^{-6}M to 2.10^{-2}M (Keeney and Osseo-Asare, 1982; Osseo-Asare and Keeney, 1980b). In other words, the mixture DNNSA-LIX63 is less surface active than DNNSA alone. DNNSA (pCAC=6.5) is more surface active than LIX63 (pCAC≅3), thus it populates the interface preferentially. Whether the adsorbed monolayer is a mosaic of mostly sulphonates and a few oximates, or it is composed of only sulphonates at a lower π, when LIX63 is present Γ_o is smaller than Γ_o with DNNSA alone.

DNNSA-LIX63 mixtures however extracted more nickel, and extracted it faster, than DNNSA alone (Osseo-Asare and Keeney, 1980b; Osseo-Asare et al., 1983a; Lin, 1984). The rate of tervalent cation extraction by DNNSA alone was found to be interfacially limited (Danesi et al., 1976). Postulating similar rate-limiting reactions for mixtures would apparently contradict Flett's correlation between Γ_o and rates (1977). A facile conclusion would

thus be that the extraction rate in this mixed system is not controlled by interfacial mechanisms. But Flett's correlation applies only when reactions between either cations or charged complexes and adsorbed extractant control the overall rate. The rate increases observed as Γ_o decreased in the nickel-DNNSA-LIX63 system thus suggest that reactions other than those limit the rate of extraction by DNNSA alone.

Dobson and van der Zeeuw (1976) showed that values of Γ of hydroxyoximes in n-heptane were higher than in toluene. Hummelstedt (1977) suggested that observation as the reason for the higher fluxes observed with aliphatic diluents. In other words, the author backed Flett's A_o-J correlation.

The classical methods to measure σ involve either the balance of forces between the weight of a pending drop and the tension over the perimeter at the suspension point, or the force required by a ring or plate to cross the interface (Adamson, 1967).

Measurements of dynamic interfacial tensions allow the estimation of extractant diffusion coefficients (Rodríguez de Carvalho and Slater, 1983).

II.1.4. INTERFACIAL POTENTIALS

Adsorption of ions at liquid-liquid interfaces gives rise to a concentration of charges at the plane of those functional groups (McRitchie, 1977). This interfacial charge leads to an interfacial potential (ψ). The electrostatic field generated by ψ between interface and bulk attracts ions of opposite and repels ions of equal charge sign. Attracted counterions therefore concentrate as a diffuse layer facing the adsorbed monolayer. The value of ψ depends on Γ and on the ionic strength of the aqueous phase (I)

according to the Gouy equation. For a univalent electrolyte at 20°C this relationship is (Ortiz, 1978):

$$\psi = 50.4 \sinh^{-1} \frac{134\ \Gamma}{I^{0.5}} \qquad (II.1)$$

DNNSA is a strong acid that upon adsorption at an o/w interface ionizes and confers negative charge to the interface. Because DNNSA is also a strong surfactant, Γ is relatively large in aliphatic diluents, and significant values of ψ are observed at moderate electrolyte concentrations (Lin, 1984; Lin and Osseo-Asare, 1983). Cations will thus be strongly attracted toward the interface.

Increasing ionization of adsorbed extractant molecules and decreasing polarity of the organic diluent turn the extractant more hydrophilic, thus σ and ψ are affected in the same way by both factors. Cante et al. (1975) measured σ and the electrophoretic mobility (EM) of lauric acid and four of its salts in six organic diluents. The σ measurements indicated that the adsorbed monolayers were of mixed acid-laurate salts, except when chloroform was the diluent, when only slight adsorption was observed. Low adsorption and low interfacial charge were consistent with the fact that chloroform was the most polar diluent used by those authors.

The distribution of ions between interface and bulk, across a diffuse double electrochemical layer, was originally modelled by Hartley and Roe (1940) assuming a Boltzman exponential variation as follows

$$C_j^i = C_j \exp(-z\psi F/RT) \qquad (II.2)$$

where C_j^i and C_j are the interfacial and bulk concentrations of the jth ion, respectively, and z is its charge. F is the Faraday electrochemical constant. The interfacial pH (pH^i) is thus given by:

$$pH^i = pH + \frac{z\,F\,\psi}{2.3\,RT} \qquad \text{(II.3)}$$

where pH is the bulk value. The "zeta potential" ζ rather than ψ is calculated from EM measurements, but Hartley and Roe (1940) found that ζ could be substituted for ψ in eqn. II.3. In that way, Cante et al. (1975) arrived at eqn II.4 for the interfacial pH:

$$pH^i = pH + \frac{\zeta(mV)}{59} \qquad \text{(II.4)}$$

Eqn. II.3 is equivalent to the relationship derived by Hartley and Roe (1940) to relate the ionization constant in the bulk (K_a) to that at the interface (K_a^i), eqn. II.5

$$pK_a^i = pK_a + \frac{\zeta}{60} \qquad \text{(II.5)}$$

In their review, Cox and Flett (1977) replaced the sign of the term $\zeta/59$ in eqn. II.4, which must be a plus. The values of pH^i are therefore lower than pH because ζ is negative when anionic surfactants are adsorbed. The values of ζ calculated by Cante et al. (1975) ranged from -50 to -100 mV, thus pH^i was about one to two units smaller than pH.

Variations of pH between bulk and interface have been investigated by means of fluorescent dyes which change colour upon protonating (Fromherz and Masters, 1974).

Al-Diwan et al. (1977) estimated three distinct values for deprotonation constants in biphasic systems of hydroxyoximes: in the organic bulk, in the aqueous bulk, and at the interface. The values were similar for most of the hydroxyoximes investigated. The ΔpK_a=1.50 between aqueous bulk and interface estimated by the authors corresponds to a value of ζ of around -90 mV.

From rates of dissolution of LIX65N monolayers, Chaiko and Osseo-Asare (1986b) estimated a value of pK_a^i around 3 units lower than the bulk value.

The EM of droplets of DNNSA, LIX63, D2EHPA, and ALIQUAT 336 (tri-caprylmethyl ammonium chloride) solutions in toluene and hexane were measured by Lin and Osseo-Asare (1983). Changes in pH only slightly affected the ionization of DNNSA. The oxime is a weak acid and required raising the pH above 4 to deprotonize significantly. D2EHPA showed an intermediate behaviour. ALIQUAT 336 protonized readily at pH below 9, thus assigning a positive charge to the surface of the droplets.

The concentrative effect of ψ explicit in eqn. II.2 means that the concentrations of reagents partaking in interfacial reactions are not the same as their concentrations in the aqueous bulk. Further, C_j^i depends on I via eqn. II.1. This dependence of C_j^i on I was suggested as the reason for the rate of Fe(III) extraction by D2EHPA slowing down as I was increased (Ortiz, 1978). Harada and Miyake (1986) and Fyles (1985; 1986) included interfacial potentials in their modelling of metal transfer rates. However, none of those authors reported attempts to measure ψ.

II.2. SURFACTANTS AND MASS TRANSFER

The literature reviewed in this section is concerned with solubilization mediated by aqueous and reversed micelles. Because the solubilization of water by reversed DNNSA micelles was one of the areas studied in this work, the investigations included in this section are directly relevant. The dynamic transfer of DNNSA to the aqueous phase was also studied. Because DNNSA aggregates in the aqueous as well as in the organic phase, the work here reviewed is related to the results reported in section IV.2. Mass transfer mechanisms from interface to bulk phases must incorporate adsorption/desorption steps, thus selected previous studies of those phenomena are also included.

II.2.1. MICELLAR SOLUBILIZATION

Surfactants in solution can increase the concentration of otherwise immiscible or sparingly soluble substances. This phenomenon is called *solubilization*, and it is a consequence of micellisation (Elworthy et al., 1968; Fendler and Fendler, 1975).

The early work on solubilization by reversed micelles was oriented toward assessing the water loading capacity and the related changes in micellar parameters. Fendler and Fendler (1975) tabulated the solubilization capacity of reversed micelles in a variety of diluent-surfactant systems. The capacity is affected by the same factors that change the micellar size, such as diluent type, hydrocarbon chain length, ionic strength of the solubilizate (I), and, to a lesser degree, the counterion. Temperature increases usually reduce the loading, suggesting hydrogen bonding between solubilizate and polar heads (Fendler and Fendler, 1975).

The work on solubilization by reversed DNNSA micelles only will be reviewed in detail in the following paragraphs. It must be

stated however that the application of solubilization by reversed micelles of other surfactants to the field of biotechnological separations has shown great potential. Enzymes in reversed micelles can catalyze the conversion of hydrophobes such as cholesterol and triglycerides (Luisi and Wolf, 1982; Luisi and Laane, 1986). Proteins and other biopolymers may be extracted and separated by reversed micelles and water in oil (w/o) micro-emulsions (Goklen and Hatton, 1985; Grandi at al., 1981).

Reversed micelles and microemulsions are two names sometimes interchanged in the literature because there is no formal difference between the two. Schulman and co-workers coined the word "microemulsions" (Bowcott and Schulman, 1955), which were also called "swollen micelles" by Adamson (1967) and Friberg (1977).

Högfeldt (1966) measured concentrations of water and mineral acids loaded at equilibrium by DNNSA in heptane, using a modified Karl Fischer method for water analysis and acid-base titration for acids. The ratio of water molecules solubilized at saturation per DNNSA molecule in the micelle (W^S) decreased to about 1 from around 9 as I was increased. Van Dalen et al. (1974a) found a value W^S=8 for DNNSA micelles saturated with 1N $HClO_4$ in aliphatic diluents.

Low angle X-ray scattering indicated that wet KDNNS micelles in heptane were about twice as large as the dry micelles (Högfeldt et al., 1981). This finding contradicted the previously reported insensitivity of micellar sizes to moisture content (Kaufman and Singleterry, 1955). This contradiction may be explained by a phenomenon similar to the formation of a relatively coarse microemulsion as water is solubilized by AOT in toluene, followed by the microemulsion collapse into a finer colloidal suspension as the system ages (Corkill et al., 1964).

Högfeldt et al. (1981) also showed that the value of W^S depends on the cation as well as on I. At unitary water activity, $W^S \cong$ 10 was estimated for DNNSA, whereas it was only around 2, unexpectedly low, for AgDNNS.

Water is desolubilized when LIX63 is mixed with water-saturated DNNSA solutions. Gallacher (1982) found 1.26% water (i.e. $W^S =$ 5.6) at I=4N H_2SO_4 in 0.1M DNNSA micelles in kerosene. Only 0.13% water at similar I was found in 0.1M DNNSA + 0.2M LIX63. Probable reason for this effects is the demicellisation resulting from the formation of mixed binaries (Keeney and Osseo-Asare, 1982), and submicellar aggregates (Zheng and Osseo-Asare, 1987).

Besides the amount of water solubilized by reversed micelles, the quality of the solubilizate may be a significant consideration in the understanding of micellar mediated mechanisms. Two aspects of the solubilization phenomenon are relevant, First, not all the water associated with a micelle is similarly bound, and second, there appear to be differences between bulk and solubilized water (Smith and Luisi, 1980). The status of the solubilizate, therefore, requires characterization. The work of El-Seoud et al. (1982a; b; 1983) with a variety of reversed micellar systems and dyes indicates variations in pH between the water pool and the bulk aqueous phase.

Balasubramanian (1981) used proton NMR to study reversed micelles of the non-ionic surfactant Triton X-100 in cyclohexane. The author concluded that around 33% of the solubilized water (5 to 5.5 in 14 molecules) was strongly bound to the surfactant, probably as water of hydration. The balance was less strongly bound, probably forming a "water pool" in the micellar core.

Some of the conclusions in Nagy's paper (1982) summarize the review done here. They are:

1) Reversed micelles in non-polar diluents always contain water, at least as water of hydration.

2) There are two types of water in loaded micelles, a shell strongly bound to the surfactant heads, and a "water pool" in the micellar core.

3) The stepwise association model describes most of these systems best.

Surfactant micelles in aqueous media can solubilize hydrophobic substrata in their hydrocarbon core. This phenomenon has been extensively studied because of its wide practical and biological importance. In detergency, the surfactant plays the two rôles of wetting agent and soil solubilizing agent (Cussler, 1986). The aqueous concentration of sparingly soluble drugs can be increased by solubilization (Carroll et al., 1981). The digestion of fatty acids in the human intestine is believed to be promoted by their solubilization by micelles of biliar acid and salts, the body's natural surfactants (Cussler, 1986). Cresols and other pollutants may be separated from streams by micellar solubilization (Bhat et al., 1987). Aqueous solutions of anionic surfactants are able to extract phenols from carbolic acids (Plucinski, 1985).

Inoue et al. (1983b) used IR spectra to show that acetic and oleic acids are solubilized by $Mg(DNNS)_2$, $Ca(DNNS)_2$, and $Ba(DNNS)_2$ micelles in hexane. The aggregation of LIX63 with reversed DNNSA micelles was interpreted as micellar solubilization of the oxime by Osseo-Asare and Zheng (1987). The interaction between DNNSA and D2EHPA reported by van Dalen et al. (1974b) can be similarly viewed.

Nagarajan et al. (1984) studied theoretically and experimentally the solubilization of hexane plus benzene by aqueous micelles of three surfactants.

II.2.2. DYNAMIC PHASE TRANSFER

Chan et al. (1976) studied the solubilization of long chain fatty acids by sodium dodecyl sulphate (SDS) solutions. Disks of mixed tagged (with ^{14}C) and untagged solid acids were spinned in the receiving media. The mass transfer characteristics of such a system are known (Levich, 1962). The tagged solute allowed measurements of rates of load exchange by presaturated micelles as well as initial loading rates by fresh micelles. The authors proposed mechanisms and derived rate models for both phenomena. Desorption of loaded micelles was treated as a reaction. Although full understanding of the mechanism of interaction between micelles and the macroscopic interface is still lacking, it is now believed that micelles are not interfacially active, thus they do not adsorb as aggregates. Applying theories of ternary diffusion coefficients (Cussler, 1976) to the system tagged acid/untagged acid/ mixed diluent (water plus detergent), apparent concentration dependent mass transfer coefficients were predicted.

When Chan et al. (1976) plotted their results as reciprocal flux versus reciprocal solubility (proportional to surfactant concentration) with Re as the parameter, they found a single positive y-intercept. Because it suggested a RDS which depended on interfacial rather than on bulk composition, that observation lent support to the **desorption**-controlled interfacial mechanism proposed. The overall rate was however mass transfer-limited as evidenced by the effect of changing hydrodynamic conditions.

When Carroll (1981) similarly plotted the reciprocal fluxes of oils solubilized by non-ionic surfactants, the plot intercepted the origin. Carroll therefore concluded that a bulk concentration-driven mechanism (i.e. **adsorption** at instead of desorption from the interface) was the slowest interfacial step in his experiments. Plots of rates vs detergent concentrations again passed through zero when Carroll et al. (1982) studied a similar system

under initial solubilization (<<1% saturation) conditions. The fluxes of two solubilized oils were not in the same ratio as their respective solubilities. Changes in aggregation number and shape as micelles age were suggested as the reason for such difference.

Disagreement between dynamic transfer and solubility was also observed by Lianos et al. (1984), who used fluorescence measurements to study the rates of pyrene solubilization by several surfactants of varying chain length. No attempt was done by those authors to characterize hydrodynamic conditions in their experiments.

The studies of solubilization of fatty acids by Chan et al. (1976) were continued by E. L. Cussler's research team. Later work focused on liquid substrata, and bile-related acids and salts as the surfactants. Huang et al. (1981) used a shallow rotating cylinder with a porous horizontal membrane separating solubilizate from receiving phase. The authors concluded that mass transfer controlled the rate at low Re, and a *surface reaction* at higher Re. The classical approach to heterogeneous reactions was followed, considering adsorption on vacant surface sites and a "reaction" between adsorbed surfactant and substrate at the interface.

Unlike Chan et al. (1976), Huang et al. (1981) envisaged some type of surfactant-solubilizate "complex" desorbing prior to aggregation "at the surface", presumably in the sublayer *adjacent* to the interface. Rates in 1M NaCl were more than three times higher than in water. Favoured adsorption due to the shielding of electrostatic charges and a salting-out effect as I was increased were tentatively suggested as the reasons for the observed rate enhancements. The same effect of NaCl on rates was observed by Lianos et al.(1984), who instead attributed the cause to increases in micellar size brought about by additions of the electrolyte. We note here that increases in I have in general opposite effects on the

size of aqueous and reversed micelles: they usually reduce the size of reversed micelles, and increase the size of aqueous micelles.

Stowe and Shaiewitz (1982) studied the rate of oleic acid solubilization by micelles of the bile salt Na-taurodeoxicholate in a diffusion cell fitted with two flat disks impellers. The fluxes depended on hydrodynamic conditions and surfactant concentration as in former work (Huang et al., 1981). The flux enhancements observed as I was increased corresponded to unrealistically high mass transfer coefficients and could not be explained solely on the basis of the increased substrate solubility. Transfer of solubilizate by inter-micellar communications were suggested as a possible explanation for the enhanced flux. It is not clear, however, why a second transfer mechanism may be in effect at high but not at low values of I.

The high rates observed by Stowe and Shaiewitz (1982) were reinterpreted by Raterman and Shaiewitz (1984). The latter authors proposed the formation of an oil/aqueous surfactant liquid crystal adjacent to the interface, with macroemulsions characteristics. The emulsion layer would shear off the interface under hydrodynamic stress and disperse as a microemulsion.

Concentration-dependent apparent diffusion coefficients ($\mathfrak{D}$) are a feature of surfactant systems under dynamic conditions, wherein tensoids aggregate and diffuse simultaneously (Cussler, 1986). Due to a higher extent of aggregation, the values of $\mathfrak{D}$ may decrease as the surfactant concentration is increased. Apparent values of $\mathfrak{D}$ in the range $\mathfrak{D}_{micelle} \leq \mathfrak{D} \leq \mathfrak{D}_{monomer}$ are to be expected in that case.

A relationship between $\mathfrak{D}_{monomer}$ and $\mathfrak{D}_{micelle}$ was found by McQueen and Hermans (1972), and Irandoust and Andersson (1986) reported a concentration dependent diffusion coefficient for benzoic acid in water.

The theory of simultaneous aggregation and diffusion of surfactants (Cussler, 1986) was partially contradicted by the work of Evans et al. (1983), who concluded that their results could only be explained by assuming that aqueous micelles dissociate, diffuse as monomers, and reaggregate in the bulk phase.

Shaiewitz et al. (1981) studied the solubilization rate of four fatty acids by aqueous solutions of ionic and non ionic detergents. They agreed with the mechanism proposed by Chan et al. (1976) at low temperature. The fluxes increased dramatically as the temperature was raised in the interval 30 to 50 ^{o}C, depending on the type of fatty acid. Those flux enhancements were explained as due to the formation of a liquid crystalline phase on the aqueous side of the interface.

Neogi et al. (1985) modelled the kinetics of oil solubilization by aqueous micelles of a non-ionic surfactant. Their model was based on the phase diagram previously reported by Friberg et al. (1985) for the ternary oil-water-surfactant system, and aimed at predicting the time required for the stabilization of the four distinct phases that appeared at equilibrium. The former authors concluded that adsorption/desorption at the o/w interface controlled the rate of solubilization, consistent with the formation of an interfacial liquid crystal.

The differences between interfacial transfer of adsorbing and non-adsorbing solutes were underlined by England and Berg (1971). The two main reasons for the different behaviours are that in the dynamic transfer of a surface-active substance:

1) the transient interfacial flux that starts across a freshly formed interface may be of different value than the steady flux observed once the adsorbed surfactant film has stabilized. Such

difference would be due to the finite rate of adsorptive accumulation taking place prior to the stabilization of a packed interfacial film, and,

2) a strong affinity of the solute for the interface may lead to adsorptive/desorptive resistance to mass transfer.

Those authors predicted and experimentally verified desorption barriers with effects lasting minutes. Their work, therefore, may have implications reaching far into the modelling of hydrometallurgical liquid-liquid extraction rates. When the control is assumed in an aqueous reaction film overlapping but not necessarily identical (Sherwood et al, 1975) to the aqueous diffusion film, the aqueous extractant concentration appears in the rate equations (Hughes and Rod, 1984a; b). When a desorption barrier controls the extractant dissolution rate, it follows that conditions in the aqueous film may be far removed from partition equilibrium. Thus estimating aqueous concentrations from bulk organic concentrations and partition coefficients may not be a good approximation in those cases.

Sawistowski (1982) reviewed work showing that interfacial resistances due to surfactants affect mass transfer coefficients (MTCs) in ternary systems. Surfactant concentrations increasing to the CMC reduce the MTC from that corresponding to the "clean" system. Further additions of surfactant to concentrations above the CMC resulted in increasing MTCs, apparently due to micellar solubilization (Nitsch and Hofman, 1981).

Ter Minassian-Saraga (1955) presented a model for the dynamic dissolution of a monolayer spread at the oil/water interface. Diffusion of desorbed surfactant through a saturated, stagnant sublayer was assumed to be rate-controlling, i.e. desorption was envisaged as a step in equilibrium, and the concentration in the sublayer as that given by the π-Γ relationship (i.e. the Gibbs ad-

sorption isotherm). The rate of film dissolution (R) was calculated by observing its contraction at constant π in a Langmuir trough.

Patlak and Gershfeld (1967) presented a theoretical analysis of the kinetics of adsorbed monolayer dissolution at constant π. Their analysis is more general than that by Ter Minassian-Saraga (1955) in that considers three possible rate controlling steps. The model that resulted from assuming full diffusive control fitted best the data from dynamic dissolution of monolayers at the air/water interface.

Chaiko and Osseo-Asare(1986a;1987a;b) have applied monolayer dissolution techniques to the study of hydrometallurgical extractants. From the comparison of film dissolution rates and of copper extraction fluxes, those authors derived a criterion to locate the RDS in metal extraction reactions. They calculated that initial fluxes of extractant due to monolayer dissolution at constant π (thus at constant Γ) were around 3 orders of magnitude lower than metal transfer fluxes. The authors considered that difference as an indication of an interfacial rate-control. The experiments they compared, however, were done under widely different hydrodynamic conditions. Metal extraction rate experiments done in a non-dispersive, stirred contactor (NDSC) under relatively high turbulence in the bulk phases yield transfer fluxes consistent with a value of δ as small as 10^{-5}m (Danesi et al., 1977a; b). In a Langmuir trough, on the other hand, values of $\delta \cong 0.1$ to 0.15 cm were estimated (Patlak and Gershfeld, 1967; Ter Minassian-Saraga, 1955). The difference in values of δ is thus similar to the difference in value of the fluxes, and comparison of both types of experiments does not help to identify the RDS.

The kinetic analysis of Ter Minassian-Saraga allows the estimation of surfactant solubility (S) and δ from dynamic monolayer dissolution experiments, if an estimate of $\mathcal{D}$ is available (Chaiko

and Osseo-Asare, 1987b). The method seems attractive because it minimizes the errors due to adsorption of reagents at the liquid -solid interfaces. The disadvantage with respect to direct measurements of concentrations, however, is that it depends on an estimated value of $\mathfrak{D}$ which may itself be in error. It is said above that because of aggregation, apparent $\mathfrak{D}$ values depend on surfactant concentration (Cussler, 1986; Irandoust and Andersson, 1986). It is not known however whether varying values of π (or Γ) affect the value of $\mathfrak{D}$, but that is probable as changes in S found when π was changed would affect $\mathfrak{D}$. The value of $\mathfrak{D}$ estimated by Chaiko and Osseo-Asare (1987b) presumably corresponds to the DNNSA monomer.

The dynamics of solubilization by *(swollen)* reversed micelles is related to the rate of communication of micelles among themselves and with the o/w interface (Luisi and Wolf, 1982). The exchange of material among reversed micelles is relatively very fast, thus it is assumed at equilibrium in most models.

The kinetics of micellar communications and the ensuing phenomenon of core exchange have been extensively studied by the group lead by Prof. B. Robinson at the University of Kent at Canterbury. Using three different reactions in the aqueous micellar cores as probes, Fletcher et al. (1987) investigated the rate of core exchange by AOT reversed micelles in n-heptane. Lean microemulsions and fast reactions were required to grant inter-micellar communications a rate-controlling rôle. The time-scale of core exchange was in the order of milliseconds, and depended on the micellar concentration. Eicke et al. (1976) observed exchanges of hydrophilic cores in time-scales shorter than one second.

Fletcher and Robinson (1981) proposed models to describe the dynamics of micellar communications. They envisaged a mechanism as follows:

1) two reversed micelles ("*droplets*") collide,

2) a (small) fraction of the resulting pairs fuse, exchanging cores.

3) the aggregate breaks ("*decoalesces*").

Microemulsions therefore undergo similar mechanisms of coalescence-breakage as droplets in macroscopic two-liquid dispersions. The size dispersity in both systems results from such dynamic equilibria. The main difference however is that particle dynamics is spontaneous in microemulsions whereas energy must be provided as turbulence to keep a dispersion as such. The spontaneity of interactions in microemulsions means that communications and core-exchange must always be present (Fletcher et al., 1987).

The catalytic effects of reversed micelles on the rate of a number of reactions of interest to organic chemists were compiled by Fendler and Fendler (1975). Berezin et al. (1973) did some pioneering work on the understanding of the physical-chemical fundamentals of micellar catalysis in aqueous media. Several authors have studied the reaction between Ni(II) and pyridine2-azo-p-dimethylaniline (PADA) as a model for aqueous micellar catalysis (James and Robinson, 1978; Hicks and Reinsborough, 1982; 1984).

Albery et al. (1987) measured rates of proton release by microemulsions at an o/w interface supported by a spinning membrane. They estimated rates of micelles-interface interaction which became constant at high surfactant concentration.

Tondre and Xenakis (1982) reported the transport of pyrene solubilized by o/w microemulsions of SDS from a source organic solution to another through water.

II.3. EQUILIBRIA AND RATES OF METAL EXTRACTION.

II.3.1. EQUILIBRIA OF EXTRACTION BY SINGLE REAGENTS

Most of the investigations concerning the extraction of metals by DNNSA and its salts reported before 1973 focused on the equilibria of extraction. Those early studies were reviewed by Markovitz and Choppin (1973).

Högfeldt et al. (1978) found that most sulphonate was as the K-salt rather than in the acidic form at I=0.1 (HCl + KCl) and pH ≥ 2.5. The investigations they conducted on the thermodynamics of cation exchange by DNNSA are relevant to this work because they supply an explanation to the observed pH effect on the nickel exchange equilibrium and rate.

Being a strong acid (pK_a=0.57, CRC, 1983-84), DNNSA is able to extract cations at pH<1, unlike carboxylic acids (Marcus and Kertes, 1969).

Van Dalen et al (1974a) applied to metal extraction a method previously used by Morris and Jones (1969) to estimate mean aggregation numbers from data on the equilibrium invasion by electrolytes of DNNSA solutions. Details of the method are given in section IV.4. Those authors estimated m=7 from the extraction equilibrium of Ce(III) by DNNSA in hexane and dodecane. Using the same procedure, Chiarizia et al. (1976) evaluated m=8 in their work on Eu(III) extraction from $HClO_4$ by DNNSA in toluene. Gallacher (1982) found m=9.5 treating in the same way data from the equilibrium of Cu(II) extraction by 0.1M DNNSA plus 0.2M LIX63 in kerosene.

Högfeldt et al. (1981) presented an extensive review of their work on the characterization of and extraction behaviour by DNNSA

and its salts. Their analysis started from the following general reaction:

$$M^{z+} + p\ \overline{(HD)}_m \Leftrightarrow \overline{MH_{(mp-z)}D_{mp}} + z\ H^+$$

(where superscripted bars assign the species to the organic phase), and it was aimed at confirming the micelle/metal ion=1/1 stoichiometry of the complex (i.e. p=1) and that equivalent number of charges are exchanged (i.e. z=constant on both sides of the reaction).

Preston (1975) investigated the equilibrium loading and extraction stoichiometry of several base metals by synthetic aliphatic α-hydroxy oximes in toluene. He found that the loading capacities decreased in the order Fe>Cu>Co≅Ni. Those findings mean that LIX63 could not separate nickel from iron in a leach liquor. Such a separation is possible when DNNSA is mixed with LIX63 (Zheng and Osseo-Asare, 1985). Preston (1975) found a 1:2 stoichiometry for the Ni-oximate complex in the pH range 6.5 to 8.5, and that Ni(II) was exchanged by two H^+.

Hummelstedt (1977) reviewed work showing that LIX63 reacted with copper in three different ways, depending on pH:
1) at high pH, the polymeric $\overline{(CuL)}_n$ formed;
2) at intermediate pH, the oxime exchanged one proton only to form $\overline{CuL_2}$;
3) at low pH, LIX63 did not deprotonate, thus there was no ion exchange, but copper was extracted by chelation. SO_4^{2-} and HSO_4^{2-} were transferred into the organic phase.

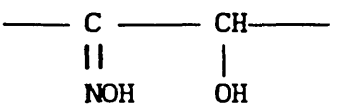
The equilibrium of nickel extraction from NH_4NO_3 by SME 529 was studied by Inoue et al. (1984). The formal oxime concentration was determined from the metal distribution under "ultimate loading" at high pH. The dimerization constant was evaluated. The proposed extraction by monomers instead of by dimers cannot be substantiated from the data presented by the authors.

The chemistry of nickel and cobalt extraction by LIX63 is complicated by the several complexes that appear to coexist in the extract. The concentration balance of those different complexes is dictated by the pH of the raffinate and the ratio of metal ion to extractant concentrations. Renninger and Osseo-Asare (1983) reviewed the work done on the extraction equilibria by this reagent and listed reported pH dependences of the distribution coefficient (D_L). For nickel, D_L has been found to vary as 1.3 pH to 2.0 pH at constant [LIX63] and relatively low acidity ($pH_{0.5} \cong 4.4$ to 7.2). Using spectrophotometric techniques, the authors found that the balance among the concentrations of the various complexes shifted with contact time. Co(II) probably oxidized to Co(III) after extraction, as was also concluded by Preston (1975). As pH decreases, the relative importance of the metal complexes would increase as follows:

$$[\overline{Ni(HL)_2}] < [\overline{Ni(HL)_2.H_2L}] < [\overline{Ni.HL(H_2L)_2}^{+}] < [\overline{Ni(H_2L)_3}^{++}]$$

$$pH(a) > pH(b) > pH(c) > pH(d)$$

LIX63 is symbolized as H_2L because it has two labile groups in its functional group that in principle can be exchanged (Preston, 1975), as shown below



The doubled charged complex (d) would predominate at pH below 4, where the log D_L vs pH curve flattened (Renninger and Osseo-Asare, 1983). LIX63 is a weak acid which does not ionize appreciably in that pH region, as suggested by EM measurements (Lin and Osseo-Asare, 1984). No cation exchange is involved in the formation of chelate (d).

The equilibrium distribution of copper between LIX63 in toluene and 1M KNO_3 has recently been investigated by Zapatero et al. (1986). Log D_L varied as 1.·pH at high acidity and as 2.*pH in the range 2.5≤pH≤3.0. The speciation assumed is listed next (Zapatero et al., 1986)

1) $Cu(NO_3)(HL)(H_2L)_2$: this solvated complex was the main species at higher [LIX63] and pH around 3. It was not significant at low [LIX63]. It is not common that a complex incorporating an inorganic anion be proposed.

2) $Cu(HL)_2$: this species was important at all levels of [LIX63] and at pH ≥ 3.5. The unsolvated 1:2 complex is the species accepted by most authors (Preston, 1975).

3) $Cu(HL)_2(H_2L)$: its concentration increased as 2) with increasing pH. Because of the increasing solvation effect, it was more important than 2) at higher [LIX63], and less important than 2) at lower [LIX63]. The main species at pH>4.

4) $(CuL)_{11}$: a polymeric species, the most important at the lowest [LIX63]/pH ratios. Negligible at [LIX63]=0.2 over the entire pH range.

5) $(Cu(NO_3)_2(H_2L))_{4,aq}$: these aqueous polynuclear complexes were the main species proposed at pH ≤ 3.5, when the organic phase loading was low. The tetramer was an average that explained the decrease in the values of D_L observed when C_M was increased at constant pH in that pH range.

The approach of Zapatero et al. (1986) to the speciation of LIX63/Cu(II) extracts seems more realistic than the analysis of Renninger and Osseo-Asare (1983). The charged complexes suggested

by the latter authors are not expected to readily dissolve in non-polar diluents. Zapatero et al., instead, used the partial neutralization of the cation charges by NO_3^- to explain the low pH dependence of D_L at lower pH. It also seems appropiate that those authors considered $Cu(NO_3)^+$ as the extractable species not $Cu(HO)^+$, because they worked at 1M KNO_3 under acidic conditions where hydrolysis of Cu^{++} would not be appreciable.

II.3.2. RATES OF EXTRACTION BY SINGLE REAGENTS

Komasawa et al. (1980a) used the rising drop technique to study the rate of copper extraction from sulphate media into n-heptane and toluene solutions of commercial LIX65N and the purified hydroxyoxime. Using previously measured MTCs, the authors estimated physical transfer fluxes 10 to 100 times higher than the metal transfer fluxes. They concluded on that criterion that their extraction experiments were fully controlled by chemistry when J was below around 5.10^{-8} $kmolm^{-2}s^{-1}$. Transfer experiments of non surface active solutes (iodine and acetic acid) were used to estimate the MTCs and correlate the transfer characteristics of the contactors, which may thus not be applicable to surface-active extractants.

Inoue et al. (1983a) followed a comprehensive research program to investigate the mechanism and kinetics of Ni(II) extraction from 1M NO_3NH_4 by the hydroxyoxime SME 529 in a proprietory diluent. Information concerning the extractant aqueous solubility, interfacial pressure, metal distribution and rate was obtained and applied to the formulation of a mechanistic model. Stirring speeds were varied by Inoue et al. in a latter work (1985) with the same chemical system and as the fluxes did not change the chemical regime was confirmed.

Miyake et al. (1986) presented an interesting work which showed how the relative values of the extractant aqueous solubility and interfacial activity may determine the locus of the rate controlling reaction. In a later paper, Harada and Miyake (1986) rederived the models of Miyake et al. (1986) and incorporated into that model based on interfacial reaction the concentrative effect of interfacial electrostatic potentials and the concept of fractional interfacial coverage (Fyles, 1985; Cohen and Cohen, 1981).

One of the first kinetic studies of DNNSA as metal extractant was reported by Kandil and Choppin (1975). In that work Tm(III) was extracted from 0.1M $NaClO_4$ by toluene solutions of either DNNSA or D2EHPA. The contacting phases were stagnant as no stirring was provided. The authors used least squares minimization to evaluate constants in a three-term rate model. Extraction rates (R) were linearly dependent on C_M and varied with [DNNSA] and C_H with fractional exponents.

Danesi et al. (1976) studied the kinetics of Fe(III) extraction from $HClO_4$ by DNNSA in toluene in a nondispersive reactor under conditions such that mass transfer resistances were negligible with respect to the interfacial resistence (i.e. under *chemical regime*). From the variation of extraction rates with the interfacial area and the phase volume, the authors concluded that "processes in proximity of the interface" controlled the rate. Both plots are indeed proof of rate control in the interfacial *region*. The "A/V-criterion" and the concentration dependences are not enough tools to identify the controlling reaction locale, however, because diffusion-controlled mechanisms mimic partial first order reactions (Danesi, 1983; 1984). Other criteria are thus needed. The slow reaction between interfacially adsorbed charged complexes and reversed HD micelles was proposed as the rate determining step (RDS). Such reaction is formally equivalent to a micellar-assisted desorption of metal complexes. Freed monomers are in principle able to adsorb, deprotonate, and continue the extraction cycle.

Probably the key contribution in the work of Danesi et al. (1976) was to envisage the RDS as the desorption of complexes. That idea is central to the modelling of metal extraction rates done in this work. The assumption that micelles be involved in such interaction was necessary to explain the stoichiometry and the rate dependence on formal DNNSA concentration. No hypothesis however was made about the possible rôle of micelles in the desorption mechanism. The aggregation number m=7 was chosen, the average from the work by Chiarizia et al. (1976), who evaluated m=6 from measurements of σ, and m=8 from metal distribution data. Non-ionized HD^{ad} was assumed to react with metal ions. The strong acidic character of HD translates in rather high negative values of ψ (Lin and Osseo-Asare, 1983) and suggests intense deprotonation of the adsorbed sulphonate at the hexane-aqueous interface. It may be somewhat less ionized at the toluene-aqueous interface.

Danesi et al. (1977) and Danesi and Chiarizia (1977) extended the kinetic model derived earlier (1976) to include mass transfer resistances into rate models for Eu(III) extraction from $HClO_4$ by DNNSA in toluene. Numerical simulations with the model reproduced the experiments for a diffusion film thickness $\delta \cong 10^{-5}$m.

Lin (1984) studied the rate of Ni(II) extraction from KNO_3 by DNNSA in hexane using the single rising drop technique. Lin's approach differed from the modelling of Danesi et al. (1976; 1977) in the following respects

(1) Lin considered the deprotonation of HD^{ad}.

(2) He also considered the K^+-H^+ exchange due to the low selectivity of DNNSA (Högfeldt et al., 1978).

Points (1) and (2) gave rise to a speciation analysis of the interface that included adsorbed ionized sulphonate, acid, K-, and Ni- salts.

(3) Based on the *interfacial inactivity* of reversed micelles, Lin proposed that **neutral** Ni-complexes first desorbed, then associated with micelles as both species diffused in opposite directions through the organic diffusion (thus also *reaction*) film. A system of two simultaneous non-linear differential equations resulted from point (3), for which Lin chose the approximate solution (±10% of the numerical solution) by van Krevelen and Hoftijzer (1947).

The effects of C_M and pH on flux were represented in the resulting models by the interfacial speciation. As it will be discussed below (section V.3), modelling the interfacial speciation is most important because it decides whether models based on adsorption/desorption and reaction can mimic the dependence of fluxes on aqueous composition. Lin (1984) used his measured values of EM to estimate ζ and ψ. Those values of ψ were used to correct aqueous bulk concentrations for electrostatic interactions.

Osseo-Asare and Chaiko (1986) studied the rate of Co(II) extraction by supported liquid membranes of DNNSA in dodecane. A reaction mechanism was proposed by those authors considering that micelles do not adsorb as such, but that they disaggregate near the interface. They however stopped short of suggesting that adsorption of some of the monomers freed by demicellisation may cause the renewal of adsorbed material, thus resulting in metal complexes transferring from interface to organic subphase. That critical step of "concerted" or "triggered" desorption (Carroll, 1981) was apparently not envisaged by Osseo-Asare and Chaiko (1986), who instead proposed, as Danesi et al. (1976) before, that adsorbed, charged complexes were "solubilized" by reversed micelles "right next" to the adsorbed layer.

II.3.3. SYNERGISM IN METAL EXTRACTION BY MIXTURES

Markus and Kertes (1969) reviewed the formation of mixed synergic adducts. Markovitz and Choppin (1973) reviewed two early reports of synergism brought about by mixing DNNSA with other extractants. One of them was due to van Dalen (1971), who used mixtures of DNNSA (1, C_1) and D2EHPA (2, C_2) to extract lanthanides and actinides, and found that the distribution coefficient in the mixture (D_M) peaked at a C_1/C_2 ratio of 0.5. No synergism was observed by that author in the extraction of some M(II) and M(I) cations.

The second work had been presented earlier by Wang and Li (1965), who reported synergic extraction of zinc when the solvating extractants TBP and tri-n-octyl phosphine oxide (TOPO) were added to DNNSA.

When Flett et al. (1973) added LIX63 to LIX65N solutions, the distribution coefficient of copper was found to be independent of [LIX63]. The authors concluded on that evidence that mixed complexes were not formed. The extraction of Cu(II) by LIX63 alone was not studied.

Van Dalen et al. (1974b) observed increases in Am(III) distributions when a second organic acid was added as co-extractant to n-dodecane solutions of DNNSA. There were maxima in the values of D_M at [second acid]/[DNNSA] ratios around 8/2. Water was desolubilized by presaturated reversed DNNSA micelles when D2EHPA was mixed in the organic diluent. The authors thus concluded that D2EHPA was substituted by water in the micellar core. More probable however was the breakage of micelles due to formation of smaller, mixed aggregates as suggested by later work (Keeney and Osseo-Asare, 1982).

Lakshmanan et al. (1975) found no synergism in the extraction of Cu(II) and Fe(III) by mixtures of LIX64N and the carboxylic acid Versatic 911, but Lakshmanan and Lawson (1973) did identify mixed complexes in the extraction of Co(II) by KELEX100 and Versatic 911. The complex stoichiometry was M/KELEX100/Versatic: 1/2/2.

Duyckaerts and Desreux (1977) presented a thorough review of the research on synergism published in the period 1970-77. Those authors discussed the correlation between enhanced extraction and the increasing hydrophobicity of mixed complexes due to the displacement by the ligands of metal hydration water.

Osseo-Asare and Keeney (1980a) found enhanced extraction of Ni(II) by DNNSA-LIX63 mixtures in hexane. At a given [LIX63], D_M increased abruptly at p[DNNSA] $\cong$ 2 to a value around 6 times the values for DNNSA alone (D_D) from a value similar to D_D. Then D_M was almost constant as [DNNSA] was increased further. Comparing metal distribution results with σ data, the authors showed that the sharp increase in the D_M vs log[DNNSA] curve coincided with the CMC of the extractants mixture. That observation suggested a link between aggregation and metal distribution in this chemical system. In more general words one could say that some properties of these mixtures, including their metal extraction ability, depend on aggregation via the speciation.

Osseo-Asare and Renninger (1984) found synergic extraction of Ni(II) and Co(II) by DNNSA-LIX63 mixtures in hexane. In the absence of LIX63, D_D increased linearly with [DNNSA]. However when LIX63 was present at a constant concentration and [DNNSA] was varied in the range 10^{-4} to 0.5M, D_M was found to vary in an irregular pattern, similar at the three values of [LIX63] used. Values of $D_M \cong 10D_D$ were observed at 2. $\leq$ p[DNNSA] $\leq$ 4. D_M peaked and decreased approaching the values of D_D as [DNNSA] was increased further. The peaks were found at higher [DNNSA] as [LIX63] was in-

creased from 0.01, to 0.05, and 0.10kmolm^{-3}, and closely corresponded to [LIX63]/[DNNSA] = 3/2.

Earlier work reporting interactions between DNNSA and LIX63 to form mixed aggregates (Osseo-Asare and Keeney, 1980a; b) and the previous conclusion that the extraction behaviour of mixtures followed the same patterns as the organic phase speciation (Osseo-Asare et al., 1983a), coupled to their results, lead Osseo-Asare and Renninger (1984) to conclude that mixed micelles of stoichiometry $\overline{(HD)_d . jLIX63}$ were responsible for the observed synergic effects. Such micelles would originate from the incorporation of the oxime into the micellar palisade. Although it could be j=1,2,3, ..., only micelles with j≥3 would have synergic properties. Demicellisation resulting in *sub-micellar aggregates* (**SMA**) was not considered by those authors, nor they suggested any correlation between the peaks in the D_M vs log [DNNSA] curves and the CMC values of the mixtures.

Based on the facts that DNNSA is a strong acid which readily deprotonates (Markovitz and Choppin, 1973) and that LIX63 can form metal complexes at relatively low pH without deprotonating (Renninger and Osseo-Asare, 1983; later confirmed by Zapatero et al., 1987), Osseo-Asare and Renninger (1984) assumed that protons from DNNSA were those exchanged by the mixed extractant. Log D_M (Ni(II)) varied as 2.0pH, and log D_M (Co(II)) as 2.2pH in the range 0.2 ≤ pH ≤ 1.6. D_D for both metals depended on C_H raised to a varying exponent, as expected from the K^+-H^+ exchange between DNNSA and the supporting electrolyte, 1.0M KNO_3 (Högfeldt et al., 1978). LIX63 is selective in the sense that loads negligible K^+ under those conditions. The variation of D_M as $C_H^{\cong -2}$ thus suggests that the (K-H)DNNS balance was not responsible for the observed pH effect on D_M as it apparently was for the effect on D_D. The possibility that H^+ from LIX63 instead of from (K,H)DNNS be exchanged for Ni(II) is intriguing.

Mixtures of Kelex 100 and D2EHPA in kerosene have been shown to extract iron from sulphate media. Depending on acidity, iron was extracted selectively over copper (Demopoulos and Gefvaert, 1984). Isodecanol was required as a modifier to improve coalescence and phase separation.

LIX63 and DNNSA *per se* show rather poor selectivity. When mixed in ratios LIX63/DNNSA = (2 to 3)/1, however, high selectivities to copper over iron in the pH range 0.5 to 3 were reported (Gallacher, 1982). That author found that upon addition of LIX63, water was desolubilized by presaturated DNNSA reversed micelles. Van Dalen's treatment (1974a) of a set of Cu(II) extraction data estimated an aggregation number m=9.5, although with considerable deviations. Gallacher (1982) concluded from the value of m that LIX63 displaced water from the micellar cores, but it did not destroy micelles.

The selectivity of DNNSA-LIX63 mixtures was investigated by Zheng and Osseo-Asare (1985). Compared to DNNSA alone, the mixture performed synergic extraction of Fe(III) at pH $\geq$ 1.4, and showed antagonism at pH < 1.4. Because no antagonism was observed in the extraction of Ni(II) or Co(II) (Osseo-Asare and Renninger, 1984), this extracting system offers a way to selectively recover these divalent metals from acidic leach liquors. A question on the feasibility of such separation had earlier been posed by van der Zeeuw and Kok (1977). Large selectivity for Ni^{2+} over Fe^{3+} was observed at pH=1, whereas the selectivity over $Fe(OH)^{2+}$ at pH=2.5 was low.

The analysis of extraction by mixtures is in general more involved than that of extraction by single reagents due to the variety of organic and organo-metallic species to be considered. The relatively simple data-treatment techniques of *slope analysis* and *continuous variation* do not suffice to elucidate the stoichiometry of complexes formed by some mixed extractants. There are

reports in the literature on the use of statistical computer packages to rationalize extraction equilibrium data.

Baes et al. recently reported (1987) attempts to identify the species extracted in the system Mn^{++}-didodecyl naphthalenesulphonic acid (DDNSA)-crown ether-toluene. The mixture was synergic with respect to DDNSA alone. Various reaction schemes leading to alternative metal complexes were proposed and a computer program was let to single out that scheme that fitted the data best. The authors reached the important conclusion that further information was needed in order to uniquely characterize the complexes. Besides distribution data, an insight into the **aggregation** in the organic phase was required.

II.3.4. RATE ENHANCEMENTS BY EXTRACTANT MIXTURES

Van der Zeeuw and Kok listed the types of extraction accelerating reagents identified until then (1977). Cox and Flett (1977) agreed with the former authors in respect of the causes of rate enhancements, and added that the pK_a value of the acidic extractant determines the acceleration effect via dictating the protonation equilibrium of the adsorbed reagent. One could add that pK_a^i instead of pK_a could have that significance. The latter authors stated that "even the presence of small amounts of DNNSA totally displaces" hydroxyoximes from the interface, and discussed some synergic and accelerated extractant systems in the light of their interfacial parameters.

Van der Zeeuw and Kok (1977) discussed the chemistry related to the acceleration phenomena in pairs of oximes and other extractants. The authors recalled that "the only commercial" chelating accelerator "known" then, LIX63, and the accelerated β-hydroxyaryl oximes form rings of five and six members, respectively, in the metal chelate. Thermodynamics, they concluded, thus favours the β-

aryloximes, and the rate enhancement due to the aliphatic oxime must be of kinetic origin.

Osseo-Asare (1984) has critically reviewed most of the reaction schemes mentioned in this section, and Whewell and Hanson (1981) had previously reviewed the most relevant (experimental) work in the area.

Flett et al. (1973) investigated the rate of copper extraction (R) by LIX65N-LIX63 mixtures. The proposed stoichiometry of the equilibrated complex excluded LIX63. Additions of LIX63 to LIX65N increased R, however. In view of such rate enhancements and the smaller value of the activation energy for extraction (E_a) by LIX64N (a mixture of LIX65N with small amounts of LIX63) than by LIX65N, those authors proposed LIX63 to play a catalytic rôle. The rate enhancements would be due to an effect of the mixed interfacial complex formed when LIX63 was present in the adsorbed film.

About two years later than the report by Flett et al. (1973), a number of investigations conducted with the single drop contacting technique were communicated. For LIX64N in the dispersed phase, Whewell et al. (1975) discovered that the "rate of mass transfer per unit area" (i.e. the interfacial flux) was independent of the drop size over the narrow size range allowed by that technique. The authors did not identify the locale of the rate controlling reaction step, but they "felt" that there was a link between the observed concentration dependences and interfacial phenomena. Because the drop hydrodynamics cannot be externally varied, the nature of the rate-determining phenomenon, whether diffusional or chemical, could not be ascertained. Whewell et al. (1975) correctly avoided assigning to the observed concentration dependences the character of reaction orders. It is not possible to change drop volumes independently of drop areas, thus it does not seem easy to design experiments using drop techniques wherein the area be changed while the volume remains constant.

The value of E_a determined by Whewell et al. (1975) was 3 times higher than the estimate by Flett et al. (1973). It has been stated however that the value of E_a is not a direct indication of whether mass transfer or chemical kinetics controls the rate of metal extraction (Danesi and Chiarizia, 1980). Another conclusion of Whewell et al. (1975) relevant to the present work is that the effect of reverse reactions could be safely ignored when initial rates of a moderately slow reaction were studied, even when the initial conversion of the extractant was substantial.

That last opinion was not shared by Miller and Atwood (1975) when they re-interpreted the data of Flett et al. (1973) for LIX 65N/LIX63 mixtures. The former authors proposed a model for the reversible extraction of copper by LIX64N which included a term accounting for stripping. The model was based on an interfacial reaction, on the similar adsorption of two reagents (LIX65N and LIX63) of different adsorption efficiency (A_o=0.85 and 1.01 nm^2 $molec^{-1}$, respectively; Al-Diwan et al., 1977), and a proton donor-acceptor interaction between both extractants.

Because of the different interfacial activity of LIX65N (RH) and LIX63 (BH), Osseo-Asare (1984) doubted that LIX63 be able to populate the interface with a density high enough to promote an effective proton donor-acceptor interplay. The data shown by Al-Diwan et al. (1977) do not prove that LIX65N be more surface active than LIX63, because although σ_{RH} was about 5 mNm^{-1} lower than σ_{BH} at equal pH and I, the hydroxyoximes were at different concentrations. In mixtures, however, σ reflects σ_{RH} exclusively (Cox and Flett, 1977).

Atwood et al. (1975) underlined the need to quantify the interfacial area when they reported their studies on copper extraction rates by LIX64N in xylenes using the, then, "noteworthy experimental technique" of the single falling drop. The effect on

rates of the independently varied concentrations of LIX65N and LIX63 was also investigated. The authors calculated metal ion fluxes (J) from their results, which were obtained under initial conditions as fresh dispersed phase was introduced with each drop. The conversion of the continuous (organic) phase was usually less than 5%. Probably the main advantage of single drop techniques is that the o/w interface is renewed with every drop, thereby minimizing the accumulation of surface active impurities. That renewal of the interface, however, increases the sensitivity to end effects. J depended as $[LIX63]^{0.5}$ at constant [LIX65N], and a zero order dependence of J on pH in the pH range 2.2 to 5 was reported.

The rate of Cu(II) extraction by LIX65N, LIX63 and their mixtures was investigated by Fleming (1976) using a non-dispersive contactor as that employed by Lewis (1954) in physical mass transfer work. Fleming's interpretation of the catalytic rôle of LIX63 was as an inhibitor of the formation of an adduct that blocked the interface. The mixed complex would thus desorb more readily than the single-reagent complex. The fractional flux dependence on [LIX63] was attributed to the dimerization of the oxime. Data presented by Hummelstedt (1977) on the aggregation of LIX65N and LIX63 support the last hypothesis.

Paatero and Golding (1983) used a modified Lewis cell for their rate experiments. The effect of impurities on rates was underlined by the observation that purified LIX65N alone extracted copper faster than mixtures of technical grade LIX63 and LIX65N. Those authors proposed the formation of a mixed LIX65N-LIX63 copper complex as the reason for the observed rate enhancements in mixtures. Their model is thus similar to that by Flett et al. (1973) in that they envisage LIX63 in a mixed interfacial film playing a catalytic rôle, as it was not included in the final complex .

Rod et al. (1985) argued that the catalytic action of various reagents is not due to specific chemical interactions, but rather to a general mechanism of phasetransfer catalysis. The authors extended the model previously presented by Hughes and Rod (1983; 1984a; b) for a single reagent to include a second, *accelerating* reagent. As in the former model, Rod et al. (1985) considered a reaction zone in the aqueous diffusion film. Catalysis would only be observed according to the authors if:

a) mass transfer resistences are negligible compared to kinetic rates, and

b) kinetics favours metal complexation by the accelerating reagent (A) while thermodynamics favours the equilibrium of extraction by the accelerated reagent (B).

The scheme included fast metal complexation by A (but also by B) in the aqueous reaction zone, partition of complexes, ligand exchange in the organic phase, and partition of freed A back into the aqueous phase to continue the cycle. No mixed complex needed be considered.

Such a mechanism would be expected to depend on the aqueous solubility of the reagents. Rod et al. (1985), as Hughes and Rod before (1984a; b), did not consider the concentration dependence of the partition coefficient (P) and clustered it together with $\mathcal{D}$, the kinetic constant, and the equilibrium constant in lumped "kinetic parameters" for both extractants. The thickness of the reaction zone was said to depend on the ratio of the kinetic rate constant to P (Hughes and Rod, 1983), as in the classical models of gas absorption with reaction in the liquid (Sherwood et al., 1975) which the former authors extrapolated to liquid-liquid systems (P is replaced by Henry's constant in the gas-liquid case). However, Rod et al. (1985) stated that "the effect of catalysis is not dependent on the reaction zone thickness", thus it is not

dependent on P. It seems contradictory that a rate "more or less controlled on the aqueous side of the interface" be independent of the extractants aqueous solubilities.

Lin (1984) extended his rate studies with the rising drop (RD) technique to mixtures of DNNSA-LIX63 in hexane. The same approach considering diffusion and chemical reaction in the organic film followed for DNNSA alone applied to mixtures. From his speciation analysis, Lin concluded that the "active micelle" $D_m.3HL$ was the main species which reacted with metal complexes desorbed into the organic film, and set up his equations accordingly.

Using Lin's speciation analysis, Savastano et al. (1986) presented numerical simulations by models based on various possible rate-controlling interfacial reactions. The effect of [DNNSA] and [LIX63] on fluxes was approximated by the predictions. The correlation between the inflexions observed in the flux vs [DNNSA] curves with [LIX63] as the parameter and the CAC, CMC values of the mixtures was recently pointed out by Savastano et al. (1987).

II.3.5. MICROEMULSIONS AS METAL EXTRACTANTS.

Wu et al. (1980) suggested that w/o microemulsions mediated in the extraction of lanthanides and some divalent metal ions by naphthenic acid, D2EHPA, and Aliquat336. According to their model, additions of octyl alcohol stabilize large reversed micelles able to solubilize raffinate. The ensuing cation exchange between the reagent in the palisade and the metal ions in the core would result in complexation of the latter, followed by demicellisation and the loss of solubilizate back to the aqueous bulk.

Bauer and Komornicki (1983) noticed that liquid-liquid extraction systems where reversed micelles form are comparable to those microemulsions used in enhanced oil recovery. Those authors

reported dramatic increases in the rates of Ge(IV) extraction by KELEX 100 in kerosene when the micelle-forming surfactant Na-dodecyl benzene sulphonate and n-butanol as co-surfactant were mixed in the organic diluent. Equilibria were reached after 15h when the surfactants were present, whereas days were required otherwise (Bauer and Komornicki, 1987). The authors concluded (1987) that the catalytic effect was due to changes in phase structure rather than to chemical reasons.

When n-butanol was added as a modifier to DNNSA solutions in kerosene, the distribution coefficient of some metals decreased (Blumberg and Gai, 1977). A chemical reason was suggested for this effect, namely that the modifier increased $[H^+]$, thus favouring the stripping. But it is also expected that alcohols stabilize larger reversed micelles. Assuming that the stoichiometric ratio micelle/metal:1/1 is maintained, it follows that *larger* micelles in *smaller* concentrations will load less metal at a given [DNNSA]. Aggregation thus offers also in this case a plausible, alternative explanation.

Tondre and Xenakis (1984) studied the transfer of alkali-metal picrates between two aqueous phases through a w/o microemulsion behaving like a liquid membrane (Li, 1971). Non-ionic surfactants and hexanol were used to form the microemulsions. The rate enhancements were 5-fold with respect to the performance of the extractant (a crown ether) alone in the diluent. An excellent correlation was observed between the metal flux and the water concentration in the organic phase, mostly as "water pools". The microemulsions were less selective than conventional extractants. The results were represented by a model of facilitated, diffusionally controlled carrier mediated transport.

CHAPTER III. EXPERIMENTAL

III.1 REAGENTS

III.1.1. DNNSA

DNNSA was received as the NH_4^+- salt. It was purified and converted into the acidic form following the method proposed by Danesi et al. (1973). The procedure is detailed in Appendix A. Elemental analysis of purified and as-received DNNSA was performed with a Carlo Erba Instrumentazione Elemental Analyzer 1106, which automatically evaluated the area under the peaks resulting from the combustion in an oxygen stream of N, C, and H in the samples. The as-received product was evaporated to a gelly consistency before the analysis. The composition of the purified reagent was within 7% of the theoretical, whereas deviations of up to 35% were found for the impure extractant. The results listed below are averages of three determinations. The formula weight is 460 (Danesi et al., 1973).

ELEMENTAL ANALYSIS OF PURIFIED DNNSA

	measured	theoretical	variation
	%	%	%
N	0.7	0.	—
C	67.8	73.0	7.
H	9.94	9.57	4.

The concentration of purified stock solutions in hexane was determined by two methods: organic-phase titration and ultimate loading. Tetra-n-butyl-NH_4OH standard in xylene (BDH) was used to titrate dilutions (typically 1/10) of the stock, with thymol-blue or phenolphthalein as indicator. Sharper end points were obtained

with the latter. The organic base was standardized with 1/10 N H_2SO_4. The titration was followed with a Phillips PW 9409 digital pH-meter in potentiometric mode connected to a chart recorder. The end point was confirmed by the position of the peak in the d(voltage)/d(volume of base) vs volume of base plot.

Any HCl residue left in the DNNSA after the purification would be titrated, resulting in concentrations erroneously high. Ultimate loading tests of the extractants were made to confirm the titrations. Equal volumes (5 cm^3) of $\bar{C}_{DT}$ =1.45.10^{-2} or 5.10^{-3}M were shaken with [Ni(II)]=1. at pH=1.6 (to avoid hydrolysis) and no other added salt during 3h. Equal volumes (2 cm^3) of the extract and 4N HNO_3 were shaken for one hour. Nickel concentrations in the strippates were measured as detailed in section III. 6, and showed that the stoichiometry of the nickel complex under ultimate loading conditions was metal/sulphonate: 1/2.

$\bar{C}_{DT}$ values found from ultimate loading were around 7% lower than those titrated, suggesting that mineral or other acids with no extracting ability were present in the extractant. The tests were run in triplicate and the results are listed in table III.1.

III.1.2. LIX63

This extractant was purified as proposed by Tammi (1976), with the modifications introduced by Lin (1984). Details are given in Appendix B. Elemental analysis of purified LIX63 was done as described above for DNNSA. The following results are the averages of three determinations.

ELEMENTAL ANALYSIS OF PURIFIED LIX63

	measured %	theoretical %	variation %
N	5.03	5.17	2.6
C	72.2	70.8	2.
H	13.3	12.2	8.6

The concentration of stock solutions was measured by ultimate loading as explained in section II.1.1. Duplicate tests lead to [LIX63]=0.324±0.003 in the main batch of purified reagent, based on the 1/2 stoichiometry. Acid-base titration in non-aqueous media yielded values of concentration around 16 times lower, underlining the reagent ability to extract nickel without exchanging protons (Zapatero et al., 1987). The theoretical formula weight is 271 (Lin, 1984; Keeney and Osseo-Asare, 1984, Tammi, 1976).

III.1.3. OTHER REAGENTS AND CHEMICALS

Hexane 95%+ pure (Aldrich Chemicals Co.) was used for nickel extraction equilibria and rate work. Hexane 99%+ (Hypersolve, BDH) was used in the reagent partition and transfer, interfacial tension, and water solubilization work. Ethanol, ethyl ether and acetone were BDH general reagent quality. The salts and acids were BDH AR grade. All these chemicals were used as-received. Singly distilled water was used, of the best quality available.

III.2. SURFACE TENSION MEASUREMENTS.

The organic solutions were presaturated by shaking with aqueous blanks of appropiate ionic strength (I) and pH. The phases were separated by centrifugation. Longer centrifugation times were required to break down macroemulsions that formed at $\bar{C}_{DT}$ above 5.10^{-3}M. Such emulsification was favoured by lower values of I.

A Krüss K10 digital tensiometer was used and the Du Nuoy ring method (Adamson, 1967) was followed. The aqueous phase was first run into the cell, then the ring was immersed in it and the organic solution was slowly added on top. The ring was automatically drawn by the instrument at a controlled speed and the interfacial tension was read in an LCD. The work was done in the "clean room" of the department, at ambient temperature (about 21°C). The refractory glass cell and the ring were washed with hexane and acetone then flamed between measurements.

III.3. WATER ANALYSIS IN MICELLAR SOLUTIONS.

Water was directly analyzed in hexane-DNNSA solutions by gas-phase chromatography (GC) with a Pye Unicam instrument. Porapack N and Q columns were found satisfactory to resolve the peaks corresponding to water, ethanol and hexane. Most of the work was done with a Porapack N column 5 foot (around 1.5m) long, 2 mm diameter, packed with 80-100 mesh beads. The column was kept at 150°C, the thermal conductivity detector at 150°C, and the injector at 200°C. Injection volumes varied between 0.5 µl to 10µl. Helium flowing at 45 psia, and at 60 $cm^3 min^{-1}$ was the carrier gas. The filament no.2 in the thermal conductivity detector was usually chosen to increase its sensitivity.

The elution times of water, ethanol, and hexane were found to be approximately proportional to the respective formula weights

(Table III.2). DNNSA was slowly eluted from the column and no peak was identified attributable to this reagent. Noise starting around 25 min after injection could have been due to DNNSA or a product from its pyrolytic decomposition reaching the detector.

Distilled water alone and ternary water-ethanol-hexane solutions were used for calibration. The latter standards (Table F.1; Seidell, 1941) were preferred because their low water concentrations allowed to set the instrument at the high sensitivities required for the analysis (i.e. attenuation between 1 and 4). Water as standard instead required a large attenuation. Injections of 1.0µl water produced around 65 chart divisions with an attenuation of 1024, whereas injecting an equal volume of $\bar{C}_{DT}$ =0.12 M stock solution translated into only 3 chart divisions at attenuation 128. The water concentration in this organic sample (C_W) was estimated as follows

$$C_W = \frac{3}{65} \quad \frac{128}{1024} 55.5M = 0.32M$$

where 55.5M is the concentration of neat water. Thus the ratio of water concentration in the stock solution to DNNSA concentration was W=0.32/0.12 ≅ 2.7 in this case. The solubility of water in hexane was measured as 0.006M. An attenuation of 4 was sensitive enough to measure changes in the water content of $\bar{C}_{DT}=5.10^{-3}M$ samples taken in dynamic water transfer experiments at 1 min intervals.

Table III.1. Ultimate loading of DNNSA. [Ni(II)]=1.,pH=1.6.

$\bar{C}_{DT}$ (1)	$\frac{C_M}{\bar{C}_{DT}}$	$\bar{C}_{M,equil}$	$\bar{C}_{DT,u.l}$	$\cong 2x\bar{C}_{M,equil}$	$\frac{(\bar{C}_{DT,u.l.} - \bar{C}_{DT})}{\bar{C}_{DT,avge}}$
10^3M	-	ppm	10^3M	10^3M	%
14.5	69	409.3	6.97	13.9	-4.2
		395.3	6.70	13.4	-7.1
5.	200	135.6	2.32	4.64	-7.8
		135.1	2.31	4.62	-8.2

(1) titrated

Table III.2 Gas phase chromatography of wet hexane solutions of DNNSA.

Fluid	F.W.	Elution time (min)	$\frac{F.W}{F.W.\ H_2O}$	$\frac{\text{Elution time}}{\text{Elut. time } H_2O}$
H_2O	18	1.0	1.0	1.0
Ethanol	46	2.5	2.55	2.5
Hexane	86	5.0	4.8	5.5

III.4. WATER SOLUBILIZATION EXPERIMENTS.

The extent and rate of solubilization of aqueous phases by DNNSA micelles have been measured. Values of saturation loading (C_W^s) were determined by shaking equal volumes of aqueous KNO_3-HNO_3 at varying pH and I and DNNSA solutions for 30 min, and sampling the organic phase after centrifugation. Water concentrations were measured directly by GC as described in section III.3.

Once the dependence of C_W^s on $\bar{C}_{DT}$ was found from this GC work, the solubilization of radioactive tracer was studied. Carrier-free ^{32}P orthophosphate (Amersham International plc), a soft β-emitter, was used in this work. The tracer specifications are listed in Table F.2. About 10 cm^3 of DNNSA solutions at varying $\bar{C}_{DT}$ were shaken for 30 min with a volume of as-received tracer solution (370M Bq/ml) large enough to saturate the organic phase but avoiding excesses. A few drops were usually enough. After centrifugation, 0.1 and 0.5 cm^3 of the organic phases were placed on planchettes and the diluent was allowed to evaporate. The radioactivity from the solid residue on the planchettes was counted during 30s by a Scintillation Counter 663 (Isotope Development Ltd.), connected to a Scaler-Ratemeter SR3 (Nuclear Enterprises) counter. The results are shown in section IV.3. All the work was duplicated. Relative errors at one standard deviation did not exceed 3%. From these countings and the previous GC measurements, the following calibration line was found:

$$C_{WP}^s = 0.0079 + 1.2.10^{-7} \text{ (counts/cm}^3\text{30s)}$$

where C_{WP}^s is the concentration at saturation of ^{32}P-spiked water. The radioactive decay factors listed in Table F.2 were used to correct the countings.

The solubilization rates of aqueous phases spiked with ^{32}P were measured in a 2.5 cm i.d. glass beaker, into which a thin

layer of 1/100 tracer dilution (3.7M Bq/ml) was placed first and 25 ml of hexane were poured next. Stirring at 250 rpm was provided by a flat 2-blade glass stirrer of 1 cm diameter. Higher speeds were found to disturb the free, unsupported interface. At time zero, the required volume of dry or presaturated DNNSA solution was mixed in and the stopwatch was started. The 'wet' DNNSA used in core-exchange experiments was presaturated with water the day before. Samples of 100 μl were removed, evaporated on planchettes, and the radioactivity was counted. A sample of diluent was removed before the DNNSA injection. No electrolytes were added to the ^{32}P solutions.

The effects of $\bar{C}_{DT}$ and of Re on the initial solubilization rates were investigated in the non-dispersive, stirred cell (NDSC) shown in figure III.1a. The operative routine is detailed in appendix C. Samples of typically 2 cm^3 were removed for direct analysis of water by GC.

The hydrophilic dye fluoresceine was originally believed useful to this work. The main reason for trying to use dyes is that on-line recording of absorbances read by a UV-VIS spectrophotometer is an attractive alternative to the discrete withdrawal of samples followed by time-consuming GC analysis. DNNSA however may associate with the dye beyond physical solubilization capacity, probably through chemical bonding with the molecules. Dyes were not further used once the possibility of chemical interaction with DNNSA was suspected.

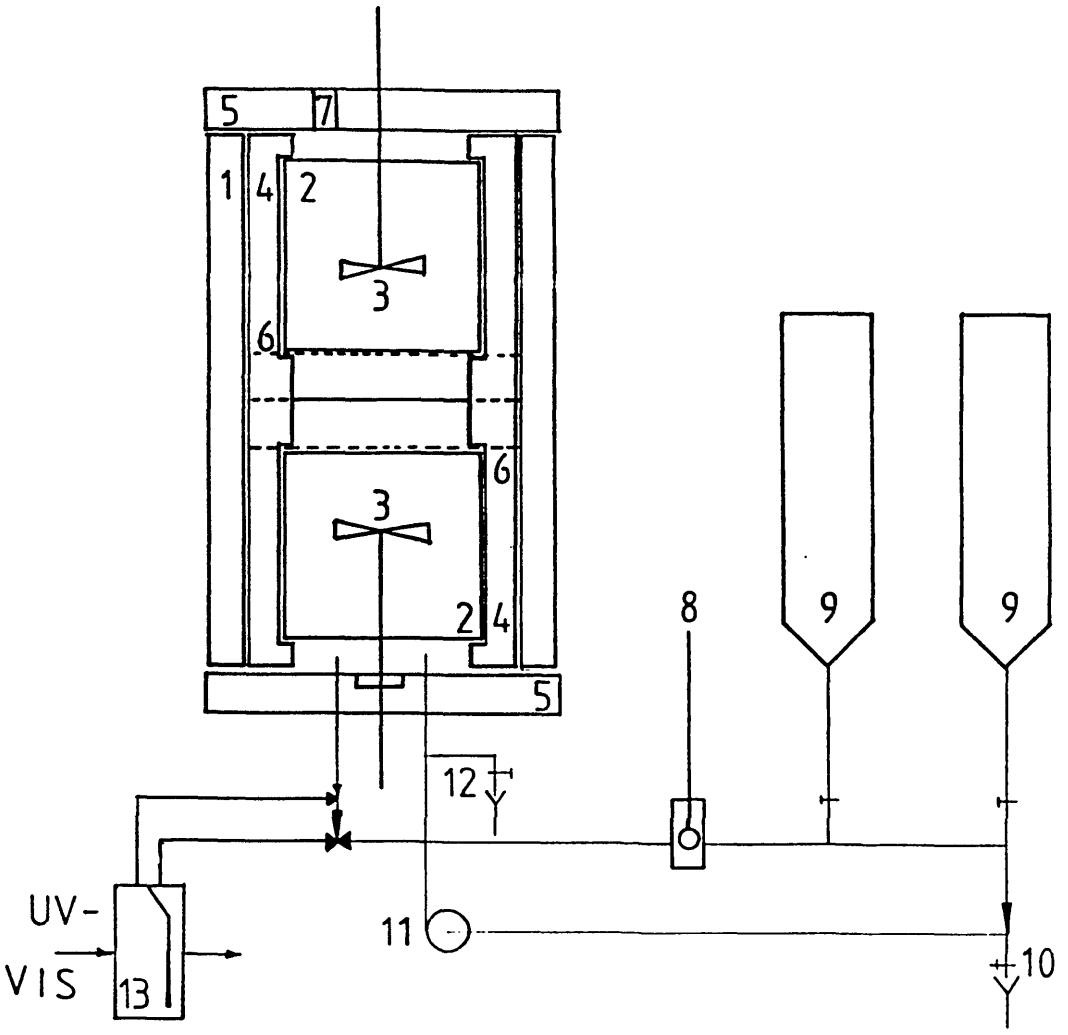


Figure III.1.a Contactor and Auxiliary Flow Circuit.

1. Glass body and water jacket.
2. Glass cylindrical baffles.
3. Glass stirrers.
4. 6 PTFE baffles.
5. PTFE top and bottom.
6. Wire mesh.
7. Loading-sampling orifice.
8. pH-meter electrode.
9. Feed reservoirs.
10. Drain.
11. Peristaltic pump.
12. Sampling valve.
13. Flow-through cell

Water transfer rates across hydrophilic membranes were measured as follows. The organic diluent (typically 20 cm^3) was loaded into a 25mm i.d. PTFE hollow cylinder fitted with a membrane at the base (figure III.1.b). The membranes used were disks cut off Visking cellullose nitrate dialysis tubing, previously impregnated with water with the purpose of forming the interface on the organic side. The cell was covered to avoid evaporation and was placed in a beaker containing the aqueous phase. Both phases were stirred independently. The temperature was 25°C. Samples of the organic phase (of about 200μl) were removed for water analysis by GC.

Alternative membrane arrangements were tried out without success. A filter paper sleeve soaked in water was supported onto a glass cylindrical rod rotating coaxially within a beaker containing the organic diluent. The hydrodynamics of such a system, and its mass transfer characteristics are described in the literature (Eisenberg et al., 1955). It was not possible however to strike a satisfactory balance between the soaking of the paper with enough water to promote appreciable transfer and the overloading of the paper which resulted in the detachment of water droplets. Similar problems were found when soaked disks of filter paper were placed at the bottom of the beaker.

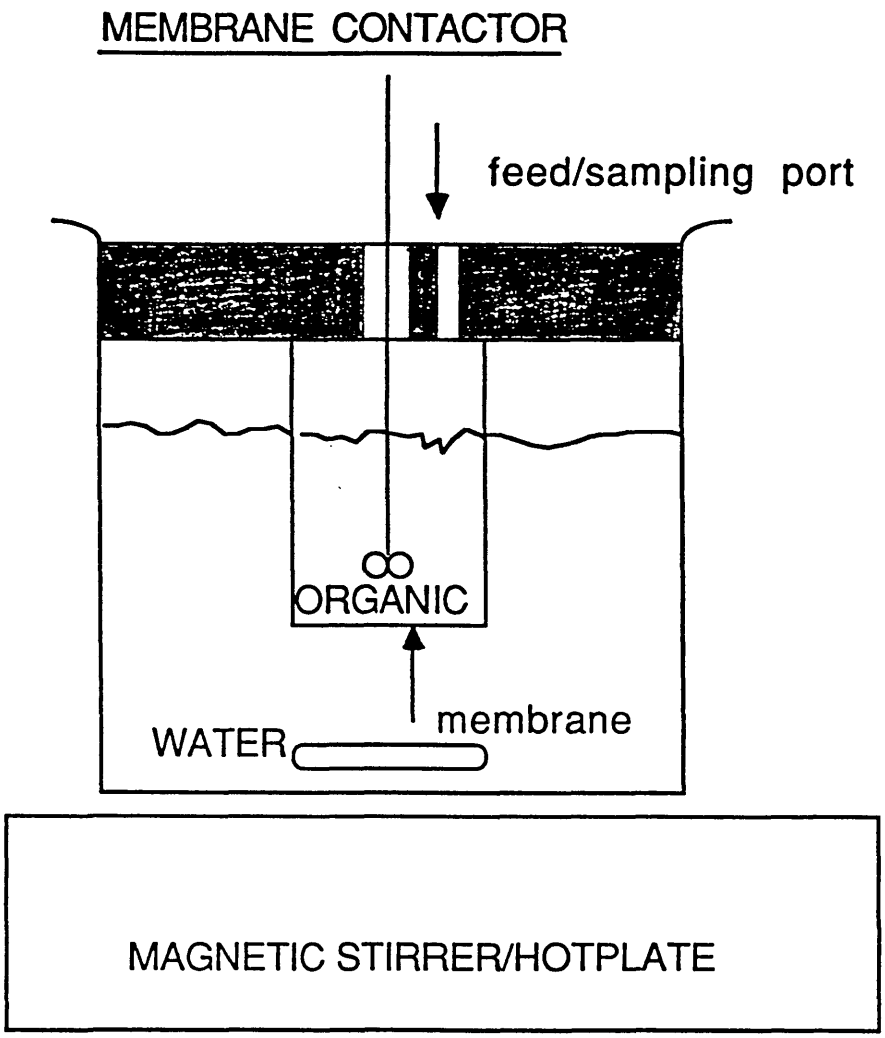


Figure III.1.b. Arrangement used in experiments of water solubilization by DNNSA micelles across membranes.

III.5. DNNSA SOLUBILIZATION EXPERIMENTS.

The partition coefficient of DNNSA and its K-salt between hexane and aqueous phases at varying I and pH was investigated by shaking together $10cm^3$ of each phase of the desired composition in $30cm^3$ flasks. The phases were separated by centrifugation during typically one hour. The emulsions that formed at high $\bar{C}_{DT}$ and low I required aging overnight (in a refrigerator at 4^oC) before centrifugation.

Light absorbances by (H,K)DNNS in aqueous media were measured in a Perkin-Elmer 554 UV-VIS spectrophotometer using a 10x10 mm Hellma Blue Quartz cell and a blank aqueous of similar composition in the reference cell. Due to its double aryl group, it was expected that DNNSA absorbs UV radiation. This assumption was confirmed by the intense absorption observed as sharp peaks at 280 and 230 nm. The latter peak was more intense (figure III.2). The peak at 280nm was used most. The absorption by KNO_3 at relatively high concentrations obliterates the peak at 230nm. At $\bar{C}_{DT}=1.10^{-3}$ with hexane as reference, the peak at 230nm exceeded the detection limit of the instrument, thus 10x1 mm cells were used for analyses of organic solutions.

The absorbance by aqueous DNNSA did not change whether the shaking time was 1, 2, 3, or 4 hours. It was thus decided that 1h was enough to reach physical equilibration.

Particularly careful preparation of standards was necessary. Calibrations for two sets of standards are shown in figure III.3. One set of standards consisted of organic DNNSA dilutions with hexane as reference. The second set was prepared in water-ethanol mixtures, and a hexane-water-ethanol blank was the reference. The ternary diluent solutions were prepared as indicated in Table F.1 (Seidell, 1941). There is a fair agreement between both sets. The aqueous-ethanolic standards were preferred in this work.

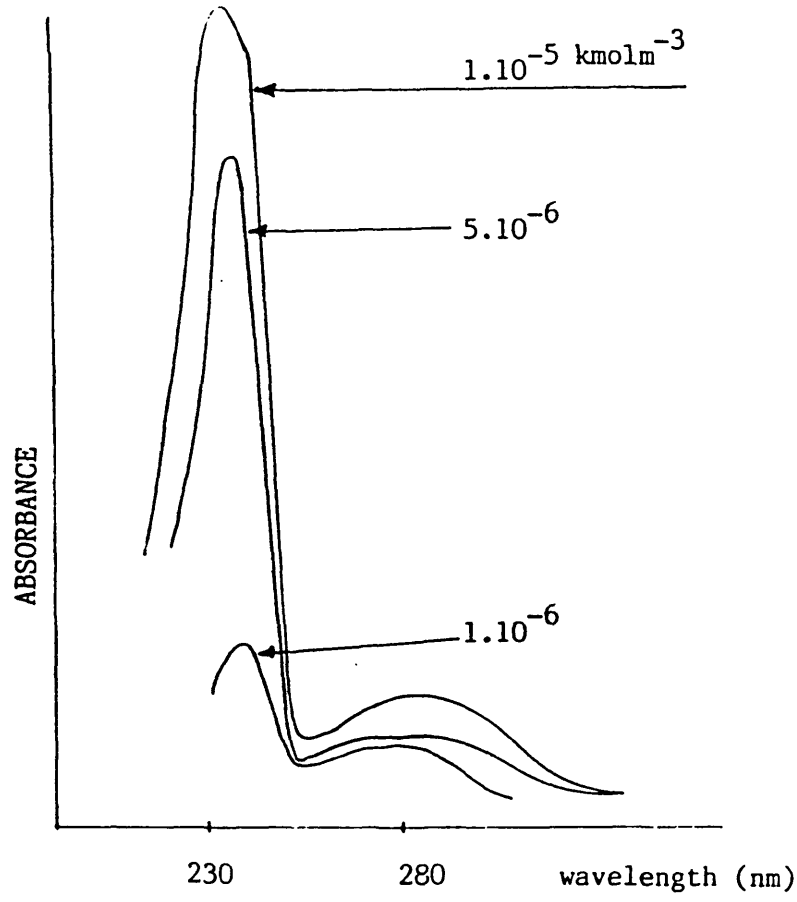


Figure III.2 UV-Vis. spectrophotometry absorption charts for DNNSA in hexane. Main peak at 230nm, secondary peak at 280nm. Parameter is DNNSA concentration in hexane.

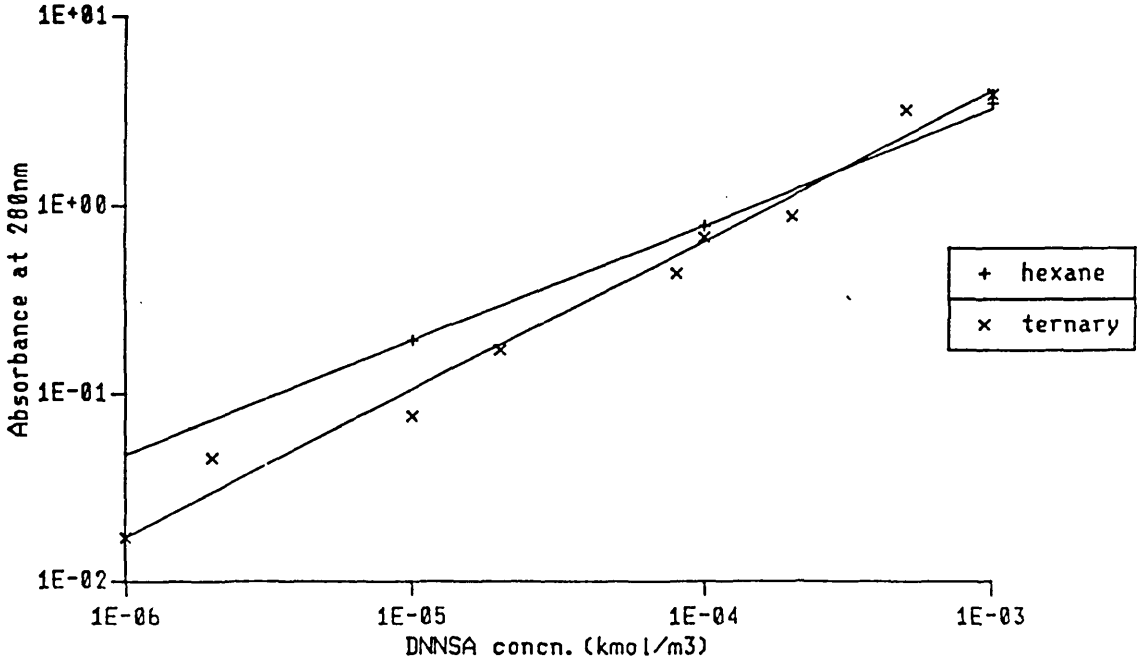


Figure III.3 UV-VIS absorbance by DNNSA hexane and ternary ethanol-water-hexane solutions. Absorbances at 280nm in 10mm cell.

The rates of (K-H)DNNS dissolution into aqueous phases of varying composition were measured in the NDSC shown in figure III .1.a. A 10x10mm Hellma Blue Quartz flow-through cell was inserted in the external flow circuit. The peristaltic pump was fitted with a piece of Viton rubber tubing, and 0.5mm i.d.PTFE tubing was used to connect the flow-through cell. Absorbance and pH were measured and recorded continously. The experimental routine was similar to that described in Appendix C for nickel extraction rate work. Samples of the aqueous phase were removed at intervals to correct the continuous absorbance readings for surfactant adsorption at the cell walls normal to the light beam. The corrections needed were small. Some experiments were extended longer than a day with the purpose of reaching a plateau indicating the end of DNNSA transfer.

III.6. NICKEL EXTRACTION EQUILIBRIUM EXPERIMENTS

The extraction equilibria of Ni^{2+} from I=0.5N (KNO_3+ HNO_3) by hexane solutions of DNNSA, LIX63, and DNNSA-LIX63 mixtures were studied by shaking equal volumes (5 cm^{-3}) of both phases together during one hour, followed by stripping the extracts by shaking with 4N HNO_3 during another hour at room temperature. Estimating the loadings *a priori* from the work of Renninger and Osseo -Asare (1983), the extract /strippate volume ratios were chosen in such a way that the metal concentrations fell within the linearity limit of the instrument without further dilutions. Aqueous nickel concentrations were measured by atomic absorption spectrophotometry (AAS) in an Instrumentation Laboratories instrument, at 232nm. AAS/AES nickel standard solution (BDH, 1000 mg/l) was volumetrically diluted to calibrate the instrument. Typically three standards were prepared after every experiment.

The loading of HNO_3/NO^-_3 by LIX63 was investigated qualitatively by high performance liquid chromatography analysis (HPLC). A Perkin Elmer Series 4 instrument fitted with a VYDAC 302 IC column and a Perkin Elmer LC21 conductivity detector was used. The eluant ("mobile phase") was 2mM acid potassium phthalate, pH-adjusted to 4.9 with saturated sodium tetraborate. Hexane solutions of LIX63 equilibrated with HNO_3 were injected. Two peaks were resolved in the eluate of heights that changed consistently as [LIX63] was changed. The first peak was at around 1min after injection, and the second peak at around 3 min.

III.7. (K-H)DNNS EXCHANGE EQUILIBRIUM

The equilibrium of potassium extraction from I=0.5N (KNO_3 + HNO_3) by DNNSA in hexane was investigated using shaken-flasks experiments. Equal volumes ($5cm^3$) of both phases were shaken together during one hour at room temperature. Aqueous feeds in the pH range 0.5 to 4.0 were prepared at constant I, by dilution of 1N KNO_3. The following relationship was used to prepare the feeds:

$$I= 1/2\ \Sigma(z_i^2 C_i) = 1/2\ (C_{Hf} + C_{Kf} + C_{NO_3}) = C_{Hf} + C_{Kf} = 0.5$$

where z was the charge of each ion i. The organic feed was $\bar{C}_{DT}$ = $0.1 kmol m^{-3}$. After separating the phases, the extracts were stripped by shaking with 4N HNO_3 during one hour at room temperature. The extract/strippate volume ratios were chosen so to dilute the strippate to below 50ppm K. The acidity of raffinates and feeds was measured by titration with NaOH and phenolphthalein. The aqueous feeds and the raffinates were diluted like the strippates. Aqueous potassium concentrations were measured by atomic emission spectrophotometry (AES) in an Instrumentation Laboratories instrument at 404.4 nm. KNO_3 AAS/AES standard (BDH, 1000 mg/l) was volumetrically diluted. Straight calibration lines up to 90ppm K^+ were obtained. A typical calibration follows:

Data:

[K], (ppm)	20	40	70	80	90
Emmission	0.35	0.49	1.24	1.34	1.50

Calibration:

ppm K= 6.19 + 54.7 Emission (correlation coeff.=0.9856)

III.8. NICKEL EXTRACTION RATE EXPERIMENTS.

These experiments were run in the NDSC shown in figure III.1 a. The reactor was operated as described in Appendix C. It is a variation of the original design by Nitsch (1978). Six PTFE baffles 1mm thick and 10mm wide run the full height of the cell and support the two coaxial glass cylindrical baffles in position in each half of the body. The impellers are also made of glass, with the blades welded to the hub at a small angle with the horizontal. The full length baffles and the small angle of attack of the impellers serve the purpose of reducing the tangential component of momentum imparted to the liquid and to favour the toroidal circulation that more effectively sweeps the liquid layer between the mesh and the interface (Nitsch and Kruis, 1978).

The only metallic elements in the NDSC in contact with the liquids were stainless steel meshes which broke large eddies down, thus allowing the interface to be stagnant under intense turbulence on the far side. No leaching of nickel out of the meshes was observed in week-long tests using electrolytes of similar composition as the aqueous feeds.

It was decided to run the experiments under hydrodynamic similarity. The independent control of both stirring speeds and consideration of the diluents physical properties enabled to obtain similar values of Re in both phases (section IV.1). The temperature (T) was controlled by circulating water from a thermostatic bath through the reactor jacket. Except in those experiments done to investigate the effect of T on the rate, T was mantained at 25±0.5°C.

The phases were physically equilibrated before loading into the reactor. A volume of aqueous blank at full I was shaken with a small volume of DNNSA solution at the concentration of the experiment. After separating the organic residue, the appropiate volume of stock nickel was diluted into the preequilibrated aqueous solution. The stock DNNSA was shaken with a small volume of nickel-free blank at full I to saturate the reversed micelles. DNNSA converted partially to KDNNS in the process (section IV.4.1).

Initial transfer fluxes were measured. Samples of typically $2cm^3$ were removed from the organic phase at time zero and at intervals thereafter. The samples were stripped of nickel with 4N HNO_3. The volume ratios were chosen such that the resulting strippate concentrations fell within linearity limit (5ppm) of the AAS. The instrument setting and the standards used to calibrate it are described in section III.6.

The reason why the rate of extraction was followed in the organic phase becomes obvious from the following example. When the aqueous concentration of nickel fell from 300 ppm ($\cong 5.10^{-3}$ $kmolm^{-3}$) to, say, 297 ppm at the end of an experiment, the latter was 99% of the feed concentration. The experimental errors were higher than 5%, thus 1% change in concentration could not be accurately measured. Instead, the concentration in the organic phase increased from 0 to 3 ppm, a change that is readily measured. Eight to ten samples were drawn in every experiment.

Direct AAS of the organic samples was attempted with unsatisfactory results. Due to the high volatility of the diluent, the nebulization rate had to be reduced to levels which prevented even combustion of the sample and caused large reading drifts. AAS analysis of iron-Kelex 100 complexes in xylene has been successfully done before (Savastano, 1984).

III.9. MISCELLANEOUS MEASUREMENTS

Densities (ρ) of hexane solutions of DNNSA and LIX63-DNNSA mixtures were measured with a hydrometer at 25°C.

Viscosities of those organic solutions were measured with a Technico 317 capillary viscometer of the Ostwald type, using hexane as reference fluid.

CHAPTER IV. RESULTS AND DISCUSSION OF RESULTS

Experimental results obtained in this work are presented and discussed in this chapter. Measurements of physical properties of solutions and calculations of derived quantities are reported in section IV.1. Data and calculations concerning the partition and dynamic solubilization of DNNSA are included in section IV.2. The results from work related to the solubilization of aqueous substrata by reversed micelles are grouped in section IV.3. In section IV.4, the equilibria of metal ion exchange and extraction by DNNSA is dealt with. Data on the equilibrium of nickel extraction by LIX 63 and by DNNSA-LIX63 mixtures are presented in sections IV.5 and IV.6, respectively. An attempt to explain the origins of the observed synergism from thermodynamic principles is also presented in the latter section. The last three sections of the chapter are concerned with rates of nickel extraction by DNNSA and LIX63, alone and in mixtures.

IV.1. CHARACTERIZATION OF DNNSA SOLUTIONS AND DNNSA-LIX63 MIXTURES[1]

The work reported in this section was done with the aim to evaluate parameters to be incorporated in rate and equilibrium models. Results on the following subjects are presented:

1) physical properties of diluents,
2) interfacial tensions and adsorption (π-A) isotherms,
3) correction of literature values of ψ due to ionic strength changes, and
4) direct measurement of reversed micelles

---

[1]I thank Mark Sadler for his help with the interfacial tension measurements.

Tables numbered IV.- are interspersed with the text, whereas those coded F.- have been collected in appendix F.

IV.1.1. PHYSICAL PROPERTIES OF SOLUTIONS

The density (ρ) of hexane solutions of DNNSA and LIX63-DNNSA mixtures was measured as described in section III.9. The results are listed in table F.3. The largest variation across the space investigated was about 1.5%.

Viscosities of those organic solutions were measured as detailed in section III.9. Hexane was the reference fluid (1). Viscosity values of hexane (μ_1) were found in the literature (CRC Handbook of Chemistry and Physics, 23rd. ed., p.1326) to be as follows:

Table IV.a Viscosity of hexane.

T (°C)	0	20	40	50
T (°K)	273	293	313	323
μ_1 (mPa.s)	0.401	0.326	0.271	0.248

The value of μ_1 at 25°C was interpolated from the above values using the Andrade correlation (Reid et al., 1977):

$$\mu = A \exp(B/T) \qquad (IV.1)$$

The following values for the parameters in eqn.IV.1 were estimated by regression of the literature values:

$$\ln A = -4.025$$

$$B = 850.8$$

At 25°C the resulting value was μ_1=0.310mPa.s, thus the kinematic viscosity was

$$\nu_1 = \frac{\mu_1}{\rho_1} = \frac{0.310 \text{ mPa.s}}{0.654 \text{ g/cc}} = 0.474 \text{ cS}$$

The kinematic viscosity of reagent solutions (ν_2) was evaluated from the times measured (t_1 and t_2) and the Hagen-Poiseuille formula, from ratio IV.2

$$\nu_2 = \nu_1 \frac{t_2}{t_1} \qquad \text{(IV.2)}$$

Measurements and calculations are listed in table F.4. The times listed are the average of three readings. As shown in figure IV.1, μ_2 increased fast as $\bar{C}_{DT}$ was increased from 1.10^{-3} to 1.10^{-2}M, and $\bar{C}_{LT}$ was 1.10^{-2} or 2.10^{-2}M. Similar increases in μ_2 with $\bar{C}_{DT}$ were reported by Osseo-Asare and Chaiko (1986). At $\bar{C}_{DT} \cong 1$M, μ_2 reached 100 mPas. The physical properties of aqueous phases were found similar to those of water, i.e. $\rho_a \cong 1 \text{kgdm}^{-3}$, $\mu_a \cong 1$ mPa.s.

Viscosities and densities were measured with the aim to estimate the ratio of stirring speeds which generated the same value of Reynolds numbers (Re) in both phases in the NDSC. This condition required, on average, that

$$N_{aqueous} = 2N_{organic} \qquad \text{(IV.3)}$$

IV.1.2. INTERFACIAL TENSIONS AND π-A ISOTHERMS.

The values of interfacial tension (σ) measured as detailed in section III.2 are plotted versus log $\bar{C}_{DT}$ and log $\bar{C}_{LT}$ in figure IV.2. The three curves for the mixtures at $\bar{C}_{LT} = 1.10^{-3}$, 5.10^{-3},

and 1.10^{-2}M and varying values of $\bar{C}_{DT}$ are shown between the curves corresponding to DNNSA and LIX63 alone (table F.6). With DNNSA alone, the $\bar{C}_{DT}$ range spanned from 1.10^{-6} to 1.10^{-2}M. For hexane -water interfaces σ^{o}=51 mNm^{-1} was measured, in agreement with the literature (CRC, 1983-4). From the plots, CACs and CMCs could be estimated in all cases. These values are listed in table IV.1 and agree with values in the literature (Keeney and Osseo-Asare, 1982). The CMC of DNNSA was confirmed by solubilizing fluorescein in micellar solutions of varying concentrations and extrapolating to zero the absorbance read by the spectrophotometer, as shown in figure IV.3 as a straight line in arbitrary absorbance units.

The shape of the σ vs $\bar{C}_{LT}$ curve resembled the others in the sense that showed an inflexion suggesting a CMC. This was an unexpected finding because there is no reported evidence of LIX63 micelles (Zheng and Osseo-Asare, 1987). The data (in table F.7) can be compared with values from the literature (Al-Diwan et al., 1977), which are also shown in figure IV.2. At low values of $\bar{C}_{LT}$ both sets of data closely agree, but the curves diverge as $\bar{C}_{LT}$ was increased. No inflexions are seen in the literature data. The lower values of σ measured in this work were possibly due to contamination of the glassware by the strongly surface-active DNNSA. As shown below, calculations with the data presented here for LIX63 lead to values of interfacial excesses or adsorption densities (Γ_L) apparently too high, but to an estimate of the limiting area of the adsorbed molecule (A_o) and a shape of the π-A isotherm in better agreement with literature reports than the results derived from the data by Al- Diwan et al. (1977).

The adsorption or "π-A" isotherm of a surfactant adsorbed at an interface (where A is the area of interface covered by a molecule at interfacial pressure π) is a useful source of information because it provides a link between bulk and interfacial concentrations (or adsorption densities, Γ) via experimentally determined interfacial pressures. The isotherms are found by application of the Gibbs equation of adsorbed state to the σ–formal bulk concentration data, eqn IV.4.

$$\Gamma_D = \frac{1}{A} = -\frac{1}{RT}\ \frac{d\sigma}{d\ln(\gamma\ \bar{C}_{DT})} \qquad \text{(IV.4)}$$

where Γ_D is the adsorption density of DNNSA in this particular case and γ is the activity coefficient in the organic phase.

For DNNSA alone at $\bar{C}_{DT}$<CMC, $\bar{C}_{DT} \cong \bar{C}_{monomer}$ (herefrom called $\bar{C}_D$), thus in this range $\gamma\bar{C}_{DT}$ can be approximated by $\bar{C}_D$. A and Γ_D were evaluated from the σ data presented in table F.5. The statistical package MINITAB available in the College's CDC computer library was used to fit the data as a third degree polynomial in $\ln(\bar{C}_{DT})$. From its first derivative Γ_D was then obtained via equation IV.4.

Results are plotted as Γ_D versus $\log\bar{C}_{DT}$ in figure IV.4. Γ_D increased fast as $\bar{C}_{DT}$ was increased up to about the CAC, then Γ_D increased more slowly and it was almost constant as $\bar{C}_{DT}$ exceeded the CMC. Rate experiments are usually done in that range where $\Gamma_D \cong$ constant (Danesi et al., 1976), thus modellists are allowed to consider Γ_D as a constant without introducing large errors. The kinetic experiments done here (at $\bar{C}_{DT} \geq 5.10^{-5}$M) were also at $\Gamma_D \cong 9.5.10^{9}$ kmolm^{-2} ($\cong$ constant). The shape of the curves in figure IV.4. are typically described by the Langmuir adsorption isotherm:

$$\Gamma_D = \frac{a\ \bar{C}_{DT}}{1 + b\ \bar{C}_{DT}} \qquad \text{(IV.5)}$$

where the constants a and b are solute-specific. For mixtures of DNNSA and LIX63, π, Γ_M (interfacial adsorption density for mixtures), and A were similarly estimated from the corresponding data (table F.6). The results are shown as Γ_M versus $\bar{C}_{DT}$ with $\bar{C}_{LT}$ as the parameter in figure IV.4. All the curves follow a similar pattern, and higher values of $\bar{C}_{DT}$ were required to reach constant values of Γ_M as $\bar{C}_{LT}$ was increased. Higher values of $\bar{C}_{LT}$ produced less dense films.

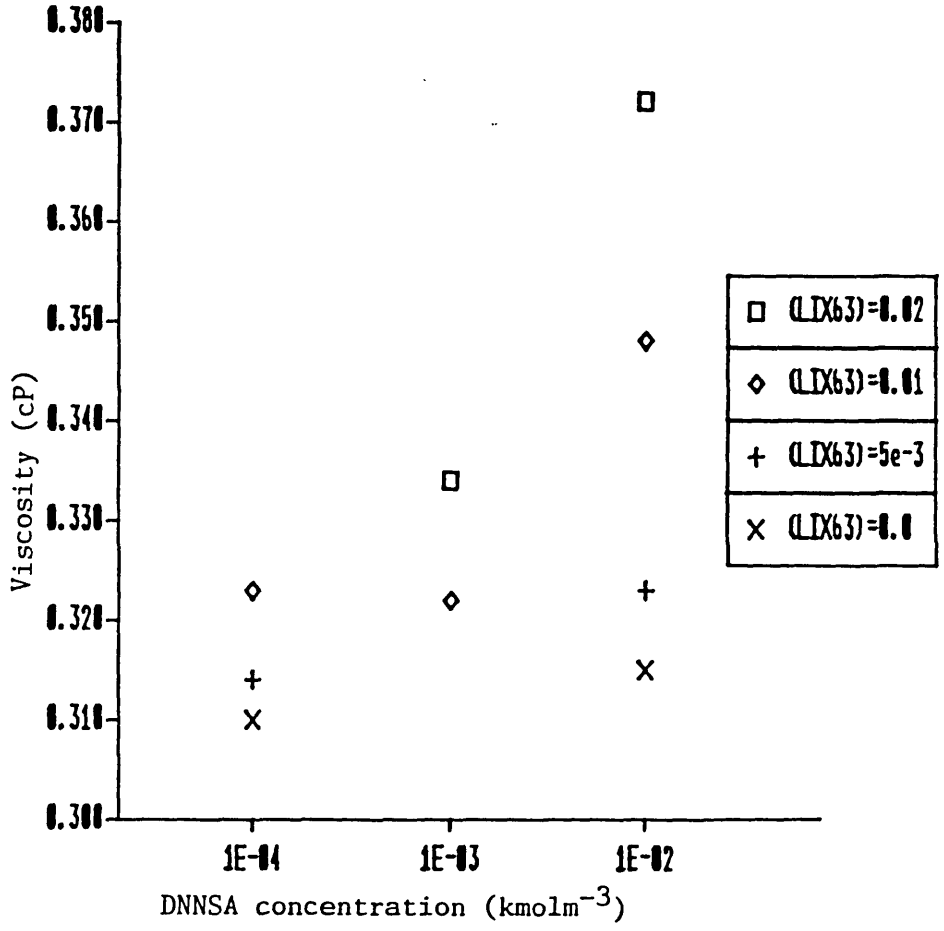
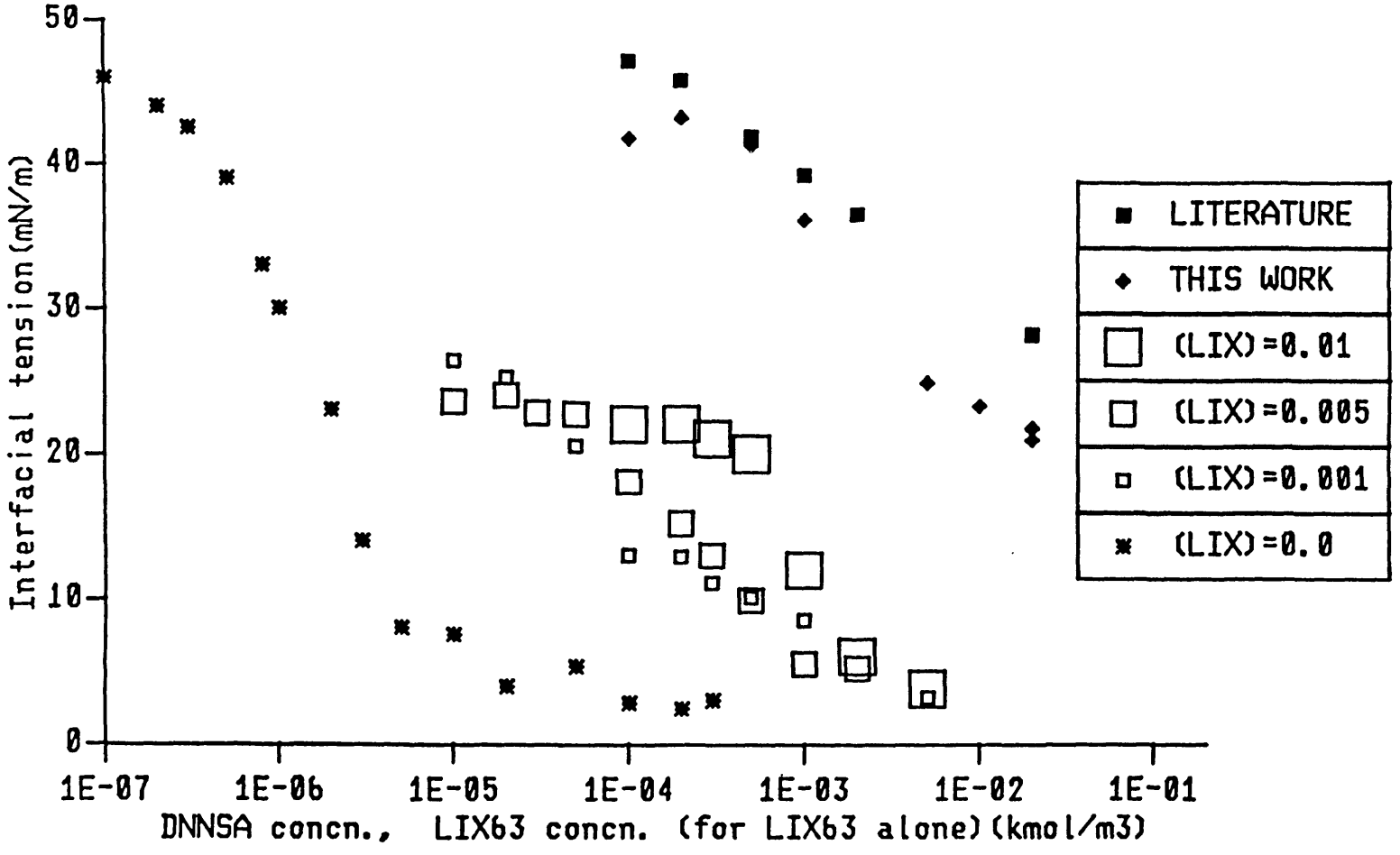


Figure IV.1. Viscosity of DNNSA solutions in hexane at varying LIX63 concs.



FigureIV.2. Interfacial tension of DNNSA, LIX63 and mixtures
LITERATURE and THIS WORK values are for LIX63 alone.
LITERATURE values by Al-Diwan et al. (1977).

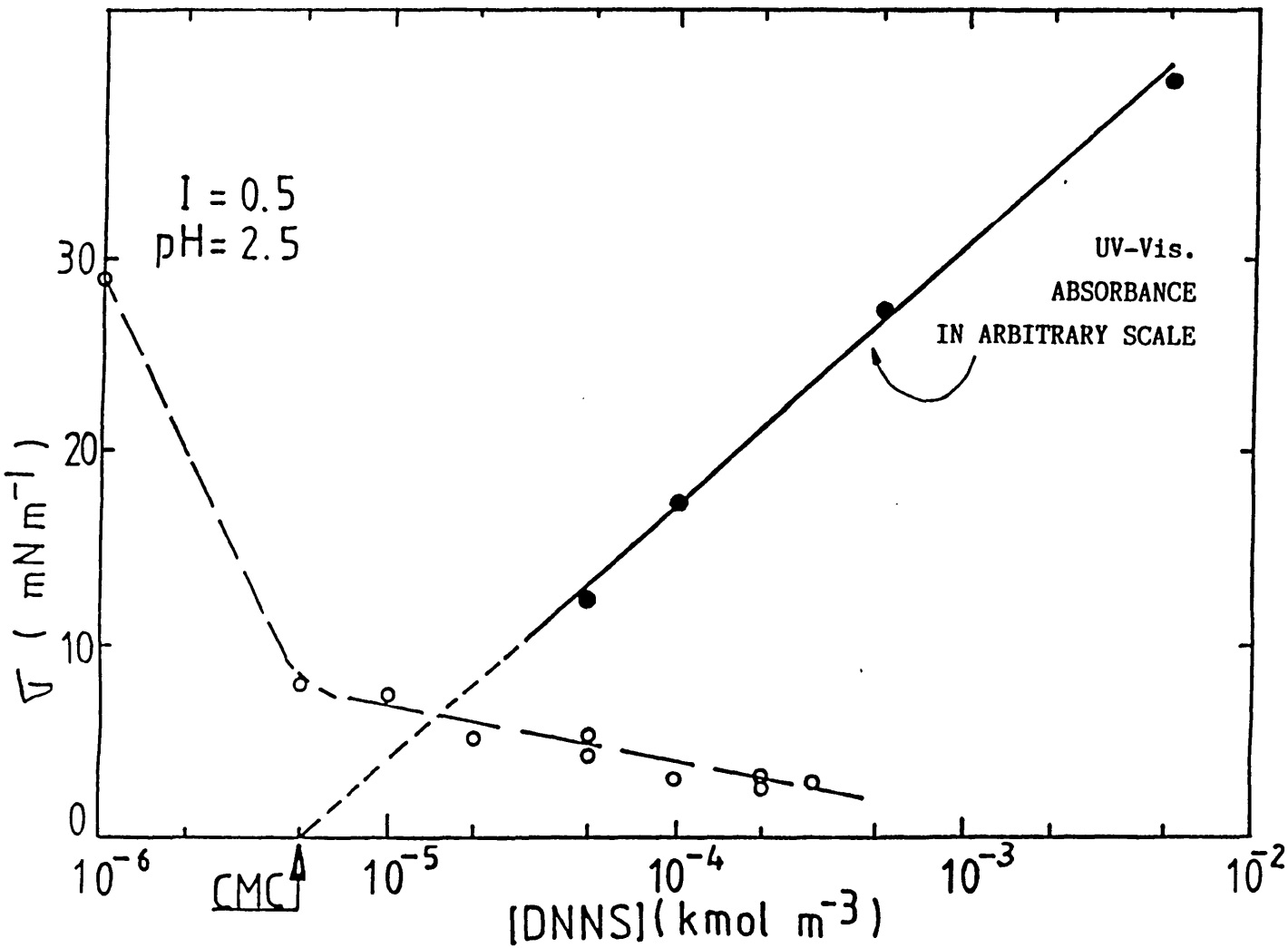


Figure IV.3. CMC of DNNSA found by interfacial tension and UV absorbance measurements

The same procedure was applied to data for LIX63 obtained in this work (table F.7) and previously by Al-Diwan et al. (1977, table F.8).Results are shown in figure IV.4. The values of interfacial excess for LIX63 (Γ_L) estimated from literature data were roughly constant at $\bar{C}_{LT}>1.10^{-3}$M, whereas Γ_L estimated from the data obtained in this work increased in that region.

The π-A isotherms are shown in figure IV.5. In general the films compressed readily below the respective CAC, at π between 24 and 30 mNm^{-1}. The limiting area (A_o) of adsorbed DNNSA was estimated as 0.40 nm^2molec^{-1} by extrapolating to π=0 the straight section of the curve. Preston and Whewell (1977) reported A_o=0.27 nm^2molec^{-1} for 2-(n-tetradecyl) naphthalenesulphonate. Values of A_o between 1.01 and 1.21 nm^2molec^{-1} were reported by Chaiko and Osseo-Asare (1983), who suggested that impurities could prevent a denser packing of their films.

The limiting area for LIX63 was estimated from figure IV.5 as 1.15 nm^2molec^{-1}, thus it was larger than A_o for DNNSA. Osseo-Asare and Chaiko (1983) found the opposite. They reported A_o=0.99 nm^2molec^{-1} for LIX63. Al-Diwan et al. (1977) estimated A_o=1.01 nm^2 $molec^{-1}$ for the same chemical system, although a larger value may be estimated from their data (figure IV.5). Thus the value of A_o estimated from the results obtained in this work was within 15% of previous reports. Limiting areas for mixtures were around 1.4 nm^2 $molec^{-1}$.

Chaiko and Osseo-Asare (1983) presented an isotherm for DNNSA of the liquid-condensed type (Lucassen-Reynders, 1981) whereas a liquid-expanded type isotherm corresponded to LIX63. The same conclusion is reached from the shape of the isotherms in figure IV.5, which resemble the shapes shown by the former authors. Like the interfacial excess variations shown in figure IV.4, the curves for the mixtures (figure IV.5) fell between that for DNNSA and that for LIX63 calculated from the data of Al-Diwan et al. (1977). Two further points can be discussed concerning these results:

1) Figures IV.2, IV.3, IV.4 indicate that DNNSA is more surface active than LIX63, as expected from the comparison of the CAC values of both reagents. In hexane, the ratio of CAC values can be expressed as follows (Osseo-Asare, 1984):

$$pCAC^{DNNSA} - pCAC^{LIX63} = 6.5 - 3.7 = 2.8$$

This ratio suggests that DNNSA adsorbs around 600 times more strongly than LIX63. It seems thus consistent that a $\bar{C}_{LT}/\bar{C}_{DT}$ ratio of around 100 was needed to obtain similar packing densities at interfaces of single reagent solutions (figure IV.4). Concentration ratios of around 100 were used in some rate experiments with mixtures in this work, thus the exclusion of LIX63 from the adsorbed film was probably not complete. Although DNNSA adsorbs preferentially, it seems reasonable to expect that a fraction of the interfacial mosaic be covered by adsorbed hydroxyoximes.

2) For mixtures, the adsorbed films were less dense than those of DNNSA alone at a given value of π. The aggregation of DNNSA and LIX63 apparently reduces the DNNSA monomer activity (Keeney and Osseo-Asare, 1982) but does not readily explain the decreases in Γ_M as more LIX63 was added to the mixture, shown in figure IV.4. Such effect may in part be due to the increasing adsorption of oxime, or of oxime-sulphonate aggregates, which decreases the interfacial packing.

Now the discussion aims at estimating what fraction of the mixed adsorbed film is made up of sulphonates (θ_D). The balance (θ_L) will be assumed covered by the oxime. This assumption means neglecting the fractional interfacial coverage by the diluent which is in general small (Lucassen -Reynders, 1981), and it seems justified considering for example that toluene covered only around 6% when LIX65N adsorbed at the o/w interface (Freeman and Tavlarides, 1982). Adsorption of aggregates is also neglected. Abstraction is made here of the fact that adsorbed species deprotonize and exchange cations to various extents. The further assumption of no specific interactions between adsorbed species is made, in fact

assuming the ideal behaviour of these species. Lucassen-Reynders (1981) presented an analysis for non-ideal surfactant mixtures, wherein a fugacity coefficient was included in the adsorption isotherm to account for non-idealities. The following relationships between fractional coverages and adsorption densities apply to ideal films (Lucassen-Reynders, 1981):

$$\theta_D = \frac{\Gamma_D}{\Gamma_D + \Gamma_L}$$

$$\theta_L = \frac{\Gamma_L}{\Gamma_D + \Gamma_L}$$

Thus

$$\frac{\theta_D}{\theta_L} = \frac{\Gamma_D}{\Gamma_L} \qquad \text{(IV.6)}$$

From the assumption that only extractant monomers adsorb, the balance about adsorbed species is

$$1 = \theta_D + \theta_L \qquad \text{(IV.7)}$$

The fractional coverages are related to Γ_M as follows

$$\theta_D = \frac{\Sigma\, C_{Dj}^{ad}}{\Gamma_M/\lambda} \quad ; \quad \theta_L = \frac{\Sigma\, C_{Lj}^{ad}}{\Gamma_M/\lambda} \qquad \text{(IV.8)}$$

where λ is the thickness of the adsorbed layer (included for dimensional consistency) and the summations are respectively over the sulphonates and oximates of all types and ionization status. The concentrations in eqns. IV.8 are not known, but estimates of θ_D, θ_L may be obtained from figure IV.4 and equations IV.6, IV.7. From the data by Al-Diwan et al. (1977), θ_L around 14% was estimated in the concentration range of interest. The higher values of Γ_L calculated from the values of σ measured in this work translated into

Table IV.1 CMC and CAC values for DNNSA and DNNSA-LIX63 solutions in hexane. I=0.5M (HNO_3 + KNO_3), pH=2.5

$\bar{C}_{LT}$	THIS WORK		from: Keeney and Osseo-Asare (1982)	
kmolm^{-3}	CAC	CMC	CAC	CMC
0.0	3.10^{-7}	5.10^{-6}		
1.10^{-3}	3.10^{-5}	2.10^{-4}	3.10^{-5}	2.10^{-4}
5.10^{-3}	1.10^{-4}	5.10^{-4}		
1.10^{-2}	3.10^{-4}	5.10^{-3}	3.10^{-4}	2.10^{-3}

Table IV.2 Fractional interfacial coverages (mixed reagents)

$\bar{C}_{LT}$	This work			Al-Diwan et al. (1977)		
kmolm^{-3}	Γ_L	θ_L	θ_D	Γ_L	θ_L	θ_D
1.10^{-3}	2.3	0.19	0.81	1.5	0.140	0.86
5.10^{-3}	6.0	0.39	0.61	1.6	0.145	0.855
1.10^{-2}	9.1	0.49	0.51	1.7	0.15	0.85

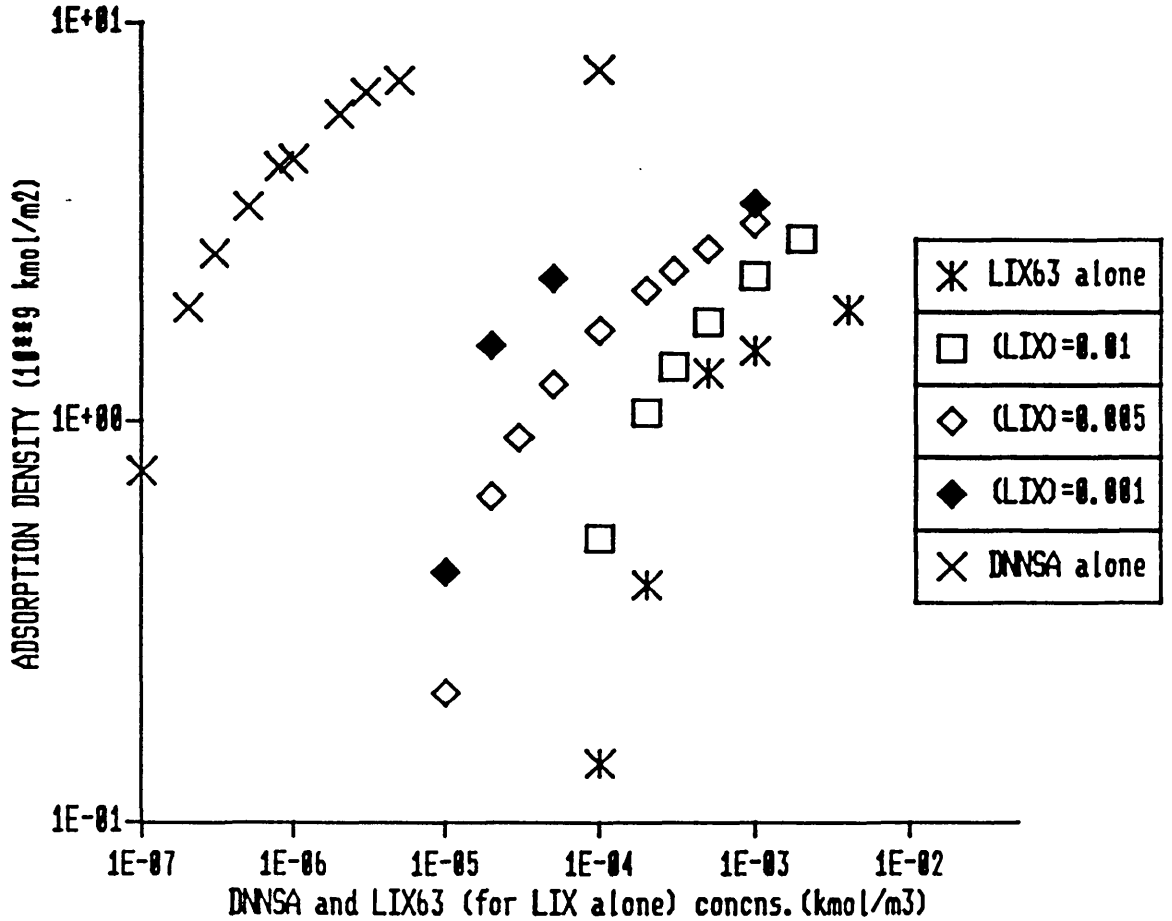


Figure IV.4 .Interfacial adsorption density of DNNSA, LIX63 and mixtures. X axis is (LIX) for LIX63 alone.

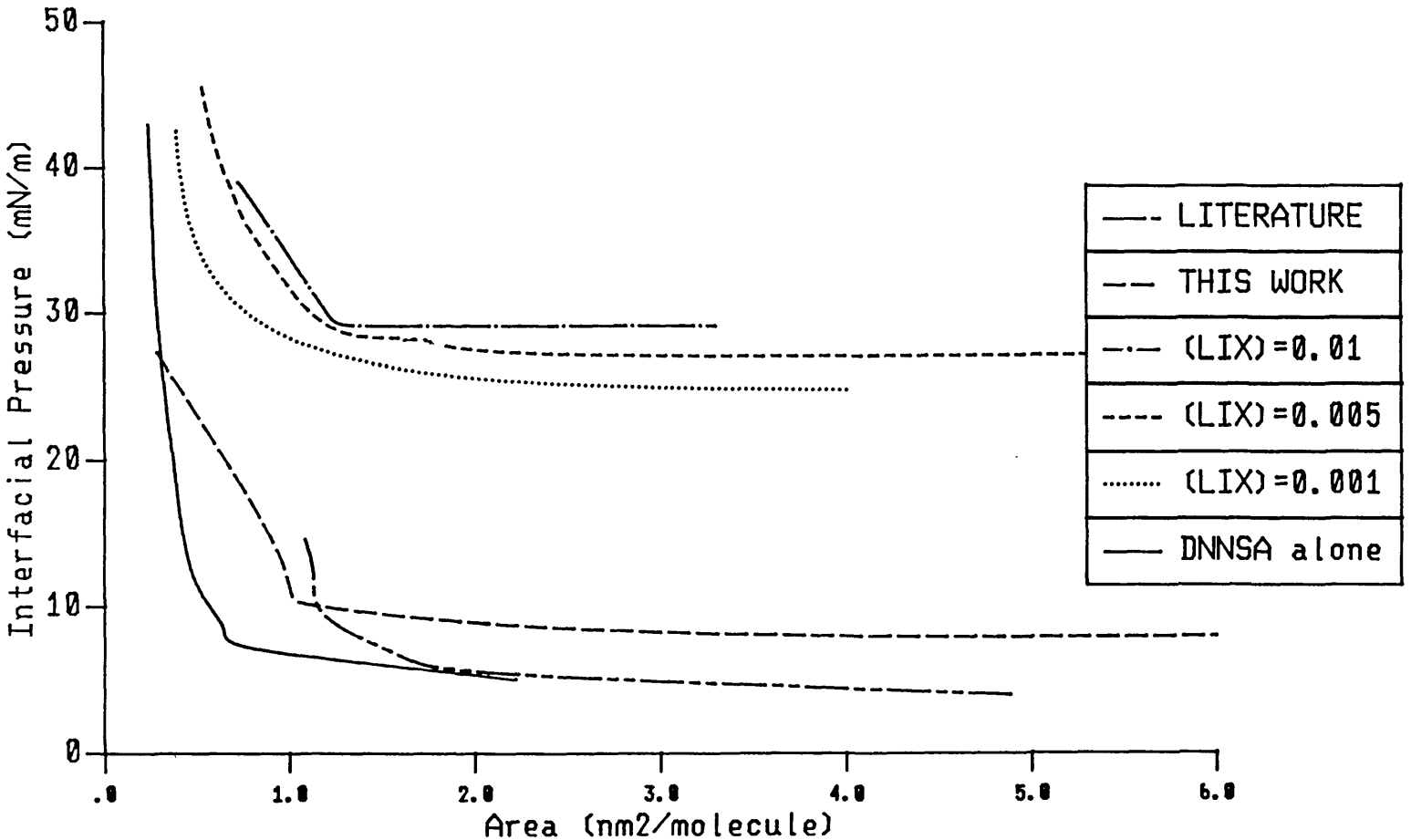


Figure IV.5 Adsorption isotherms for DNNSA, LIX63, and mixtures. THIS WORK and LITERATURE (Al-Diwan et al., 1977) for LIX63 alone.

values of θ_L between 19% and 49% (table IV.2). These predictions seem too high and were not used in the calculations presented in this and in next chapter. The estimates for θ_L and θ_D obtained from the literature data were used instead.

IV.1.3 CORRECTION OF INTERFACIAL POTENTIALS.

Lin (1984) measured the EM of droplets of hexane solutions of DNNSA, LIX63, and mixtures in aqueous media at $I=4.10^{-3}M$. That author calculated zeta potentials (ζ) from the EM data using the Smoluchowski equation. By fitting his cobalt and nickel extraction rate data, Lin found that consistent flux dependences on concentrations were predicted when ζ and ψ were equated as in eqn. IV.9:

$$\frac{\psi\ (mV)}{\zeta\ (V)} \cong 1000 \qquad (IV.9)$$

Lin's data are listed in table F.9 and shown in figure IV.6 as $-\psi$ versus log $\bar{C}_{DT}$. The rate experiments were done at I=0.5 in this work. The Guoy equation, as presented by Ortiz (1978), was used to correct ψ as follows:

$$\psi = 50.4 \sinh^{-1} \frac{134}{A\ C_j^{1/2}}$$

where A is the area of the adsorbed ion and C_j is the electrolyte concentration (assumed here equal to I). The area A depends on $\bar{C}_{DT}$, $\bar{C}_{LT}$ via the π–A isotherm. A also depends on I, which affects the adsorption density. Only the dependency of A on $\bar{C}_{DT}$, $\bar{C}_{LT}$ was considered here. Values of π and A are listed in table F.9 (section IV.1.2). These parameters varied little in the concentration range of rate experiments. Equation IV.10 was used to correct ψ as I was changed from a value I_1 to another value I_2.

$$\frac{\psi_1}{\psi_2} = \frac{\sinh^{-1}\dfrac{134}{A\ I_1^{1/2}}}{\sinh^{-1}\dfrac{134}{A\ I_2^{1/2}}} \qquad \text{(IV.10)}$$

The ratio IV.10 is around 0.42 for $I_1=4.10^{-3}$M, $I_2=0.5$M. Values of ψ at $\bar{C}_{LT}=0$ are listed in table F.9. The last column in the table are concentration correction factors at I=0.5, as proposed by Hartley and Roe (1940, eqn. II.2). The exponent in eqn II.2 is -0.039ψ for ψ given in mV. Presented in table F.10 are the values of ψ estimated as above from Lin's data (1984) at $\bar{C}_{LT}=1.10^{-3}$M. and 1.10^{-2}M, I=0.5. The conversion ratio from EM to ψ (mV) was 5.2.

IV.1.4. DIRECT MEASUREMENT OF REVERSED MICELLES.

Three samples of DNNSA solutions in hexane (99%+ pure) were sent to Malvern Instruments (Malvern, Worcs., England) for measurement of micellar sizes by photon correlation spectroscopy (PCS) with an Autosizer 700 IIc instrument. The samples were prepared as follows:

Sample	[DNNSA]	Notes
A	0.27	dry
B	0.27	equilibrated with 0.5N KNO_3, pH=2.5
C	0.081	dry

Sample A was too polydisperse for the analysis to yield useful information. At the same reagent concentration, sample B was substantially less polydisperse. The narrower size range of micelles equilibrated with aqueous phase (i.e. microemulsions) suggests a redestribution of surfactant between aggregates. It has been argued that moisture is a requirement for extensive micellisation (Eicke and Christen, 1978).

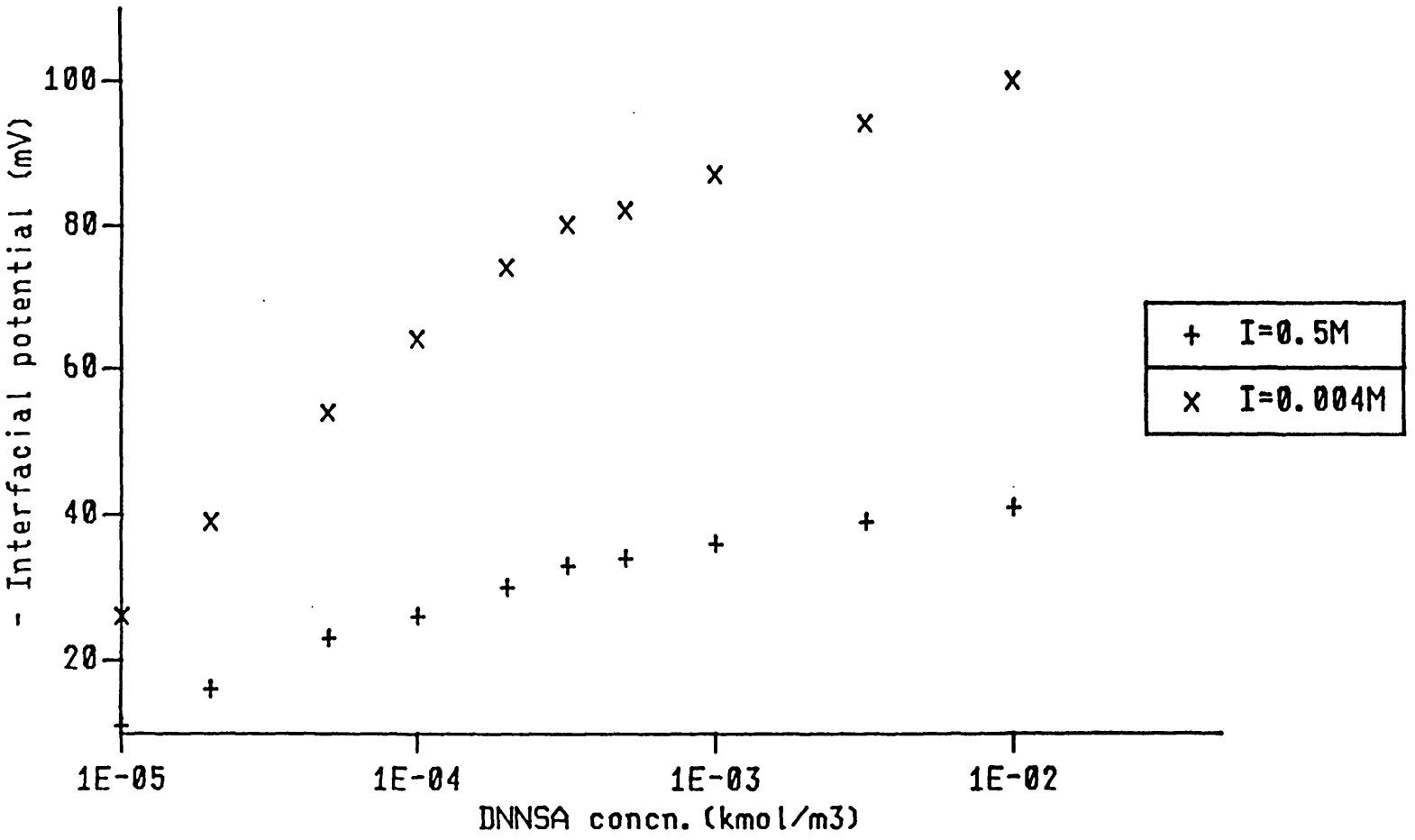


Figure IV.6 Effect of ionic strength on interfacialpotential of DNNSA solutions (data at I=0.004M from Lin, 1984)

The histograms F.11.a to F.11.c correspond to sample B. The micellar diameters distributed in the range 2.2 to 21.7 nm, with an arithmetic mean of 4.5 nm. The dry micelles in sample C spanned the same size range, but their mean diameter was 3.0nm (histograms F.11.d to F.11.f). Thus saturation of micelles translated in a 50% increase in the mean diameter. Similar treatment in previous work caused the size to nearly double (Högfeldt et al., 1981). Marcus and Kertes (1969) reviewed reported micellar radii around 1.3nm, and conceded that "solubilized water may increase the size of micelles somewhat". Van Dalen et al. (1977) estimated a diameter of 3.2 nm for DNNSA micelles saturated with 1N $HClO_4$.

IV.2. AQUEOUS SOLUBILITY OF (K-H)DNNS[2]

IV.2.1. PARTITION EQUILIBRIUM RESULTS

The partition of (K-H)DNNS between aqueous media and hexane was experimentally studied as detailed in section III.5. The partition coefficient (P) dependence on $\bar{C}_{DT}$, I, and pH was investigated. The aqueous sulphonate concentration at equilibrium (C_{DT}, *solubility*, or *S*) at varying I and $\bar{C}_{DT}$ listed in table F.12 were measured with no KNO_3 in the aqueous phase (i.e. the ionic strength was regulated with HNO_3 only). The effect of I on solubility is shown in figure IV.7 as log C_{DT} versus I, with $\bar{C}_{DT}$ as the parameter. The data are more scattered at lower values of $\bar{C}_{DT}$, where the measurements were more difficult. A marginal effect of I on solubility was found as I was increased to around 1.10^{-3}kmol m^{-3}. As I was increased further, C_{DT} fell at constant organic bulk concentration. Aqueous solubilities of high molecular weight quaternary ammonium extractants were also reduced by added electrolytes (Markus and Kertes, 1969).

[2] I thank my colleague Filomena Pinto for her help with the experiments reported in sections IV.2 and IV.3. Elios Jorisi ran some of the experiments reported in subsection IV.2.2.

These results suggest that ionization of aqueous sulphonates was hindered at higher I, resulting in a salting-out effect. DNNSA is a strong acid (pK_a=0.57) and it would fully deprotonize at I around 1.10^{-3} $kmolm^{-3}$. This forecast is readily substantiated as follows. With no other electrolytes but acids, the sulphonate balance about the aqueous phase is given by:

$$C_{DT} = C_{HD} + C_D + n\,(C_P + C_P^{ionized}) \qquad (IV.11)$$

where n is the aggregation number of the aqueous micelle, HD stands for the acidic monomer, D for the sulphonate, and P for the micelle. The ionization of HD molecules in the micelles is accounted for by the last term in eqn. IV.11. Neglecting micelles at low values of $\bar{C}_{DT}$ and high values of I for simplicity, and substituting balance IV.11 into the law of mass action (LMA) applied to the ionization IV.12,

$$HD \Leftrightarrow H^+ + D^- \quad ; \quad K_a = \frac{C_H\, C_D}{C_{HD}} \cong 0.27 \qquad (IV.12)$$

eqn. IV.13 is obtained:

$$\frac{C_{DT}}{C_D} = \frac{C_H}{K_a} + 1 \qquad (V.13)$$

Arbitrarily choosing to define full ionization as that condition where C_D=0.99 C_{DT}, the value $I=C_H=2.7.10^{-3}M$ is found.

Partition cofficients calculated as follows:

$$P = \frac{\bar{C}_{DT}}{C_{DT}}$$

are shown in figure IV.8 as log P vs log $\bar{C}_{DT}$ with I as the parameter. The values of P are seen to increase as $\bar{C}_{DT}$ was increased, the effect being most marked at higher values of I. The results

clustered on a single curve when I was 1.10^{-3}kmol m^{-3} and lower. At I=0.5 and $\bar{C}_{DT} \geq 10^{-3}$M, P depended as $\bar{C}_{DT}^{\cong 0.41}$ (with R = 0.9824), whereas P varied as $\bar{C}_{DT}^{0.21}$ at I=1.10^{-5} to 1.10^{-3}kmol m^{-3}. From the former, it follows that $C_{DT} \alpha \bar{C}_{DT}^{(1-0.41) \cong 0.6}$. Coleman and Roddy (1971) reviewed data on partition of alkylphosphoric acids that show similar variations of P. From the work of Inoue et al. (1985) on partition of hydroxyoximes, a smaller than one dependence (exponent $\cong$ 0.39) can also be estimated.

It is believed that the dependence of P on concentrations has implications in metal extraction rate modelling. Hughes and Rod (1984a; b) presented a model based on the reaction between the cation and the aqueous extractant in the *aqueous film* adjacent to the interface as the rate-determining step (RDS). The dependence of P on $\bar{C}_{DT}$ shown in figure IV.8 supplies a criterion to assess the possibility of the diffusion film as the locale of the RDS. The criterion is implemented in section IV.7.

The effect on P of adding KNO_3 to the aqueous phase was investigated. The results presented in table F.13 were obtained at constant value of I=0.5N(HNO_3+KNO_3) and varying electrolyte composition. These results show that P decreased as the ratio C_H/C_K was increased at constant I, suggesting that HDNNS is more soluble than KDNNS. No data have been found in the literature to corroborate this observation. The literature on carboxylic acids however suggests that metal carboxylates dissolve more in aqueous media than carboxylic acids, in increasing order of basicity (Marcus and Kertes, 1969).

IV.2.2. DYNAMIC SOLUBILIZATION

The NDSC shown in figure III.1.a was used to investigate the rates of DNNSA solubilization into aqueous phases of varying composition under controlled hydrodynamic conditions. The effect of several variables on solubilization dynamics was studied. The effect of changing bulk organic concentrations ($\bar{C}_{DT}$) and stirring

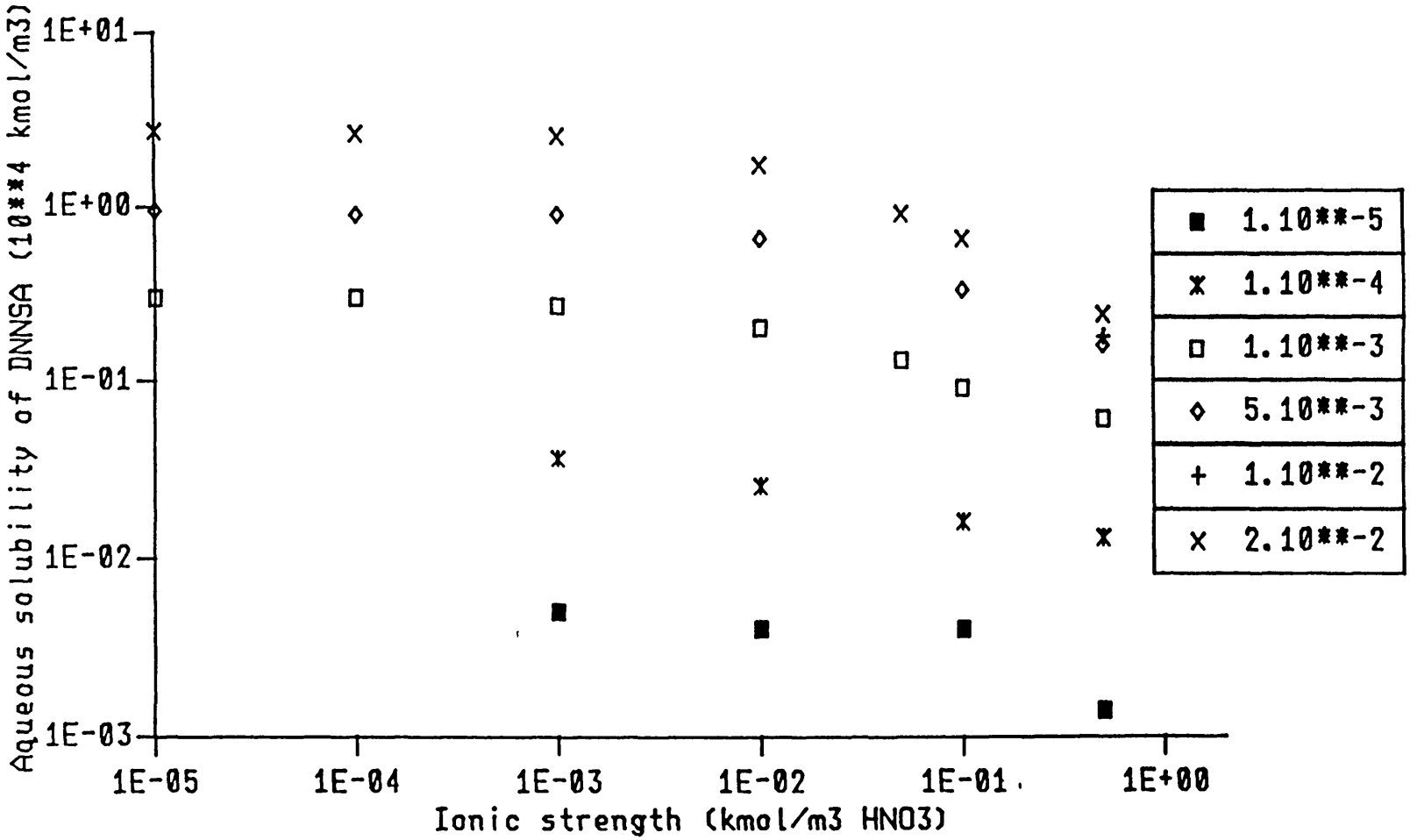


Figure IV.7 Effect of ionic strength on the aqueous solubility of DNNSA. Organic concentrations are parameters (kmol/m3)

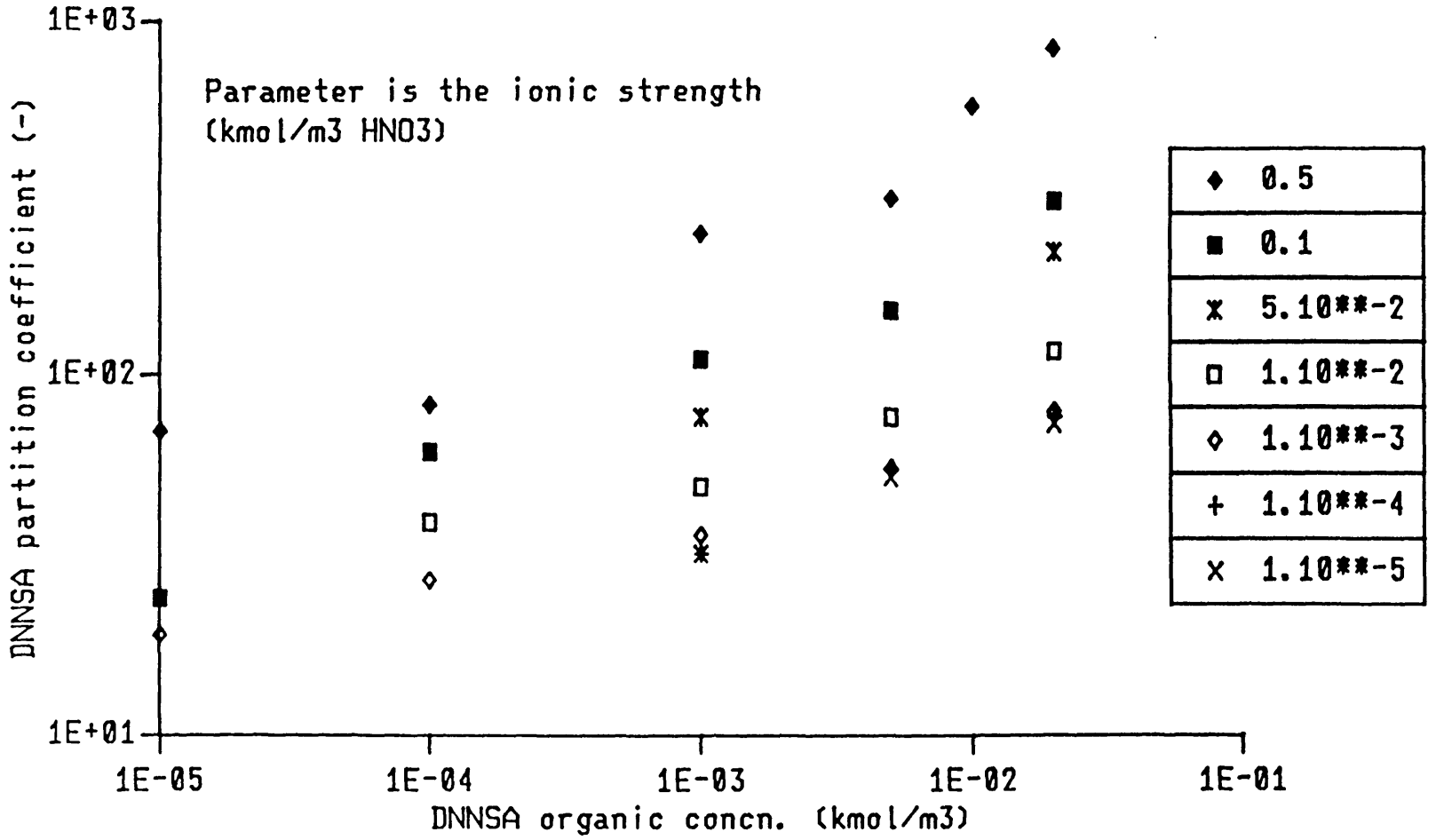


Figure IV.8 Effect of organic DNNSA concentration and ionic strength on the partition coefficient of DNNSA.

speeds (N) on dissolution rates is shown in figure IV.9. Aqueous concentrations (C_{DT}) are plotted versus time as three sets of data, each set corresponding to one value of $\bar{C}_{DT}$. Variations within each set are due to changing values of N, which in these experiments was set at 200, 250, and 300 rpm. The organic phase was usually stirred as N/2 rpm. The calibrations in figure III.3 were used to translate absorbances at 280nm into values of C_{DT}.

The transfer rate is seen from the slopes to increase as $\bar{C}_{DT}$ was increased. The results are thus consistent with the partition data shown in figures IV.7, IV.8, and the fact that partition (of monomers) at the interface must supply the driving force for the physical transfer. Unexpectedly, in some experiments C_{DT} was found to exceed up to four times the aqueous solubility values after around 20 to 30 minutes of contacting the phases. This large variation cannot be wholly attributed to experimental errors, and it is believed in part due to the differences in size and shape between diffusing and stabilized surfactant aggregates like those earlier reported by Carroll et al. (1982). By the change in micellar sizes, the authors could justify dissolution rates double of those expected from equilibrium. The combination of size and shape changes could account for differences of up to one order of magnitude. Transport mechanisms involving dissaggregation, diffusion of monomers and aggregation (Evans et al., 1983) cannot substantiate the apparent breaches of partition equilibrium entailed by the supersaturation observed. Centrifugation of aqueous phase samples at the end of the runs did not change the UV-VIS absorbance in a consistent way. Thus microemulsions originated by dispersion of liquid crystalline phases sheared off the interface (Shaiewitz et al.1981; Raterman and Shaiewitz, 1984) are not a likely explanation to these observations.

Good straight lines were charted continuously in real time and allowed precise slope calculations. From those continuous lines the points shown in figure IV.9 were culled.

The effect on solubilization rates of changing I is shown in

figure IV.10 as C_{DT} vs time at $\bar{C}_{DT}=5.10^{-3}$kmolm^{-3} and N=300 rpm, with I as the parameter. The rates are seen to decrease as I was increased from 0.004 to 0.5, following the trend expected from the partition data in figure IV.7.

It was found that nickel added to the aqueous phase resulted in decreased DNNSA transfer rates. A similar effect on the rate had the preequilibration of the organic feed with a KNO_3 blank. The effect of nickel on the rate is shown in figure IV.11. It seems straightforward to explain this effect. As DNNSA desorbed and transferred, it was complexed by the metal. The distribution coefficient of the nickel complex is larger than that of KD or HD (Marcus and Kertes, 1969), which favoured the transfer of metal complexes back into the organic phase. The composition of the interfacial mosaic also varied when nickel was present in solution (section V.5). Then a fraction of the interface was covered by adsorbed nickel sulphonates, which preferentially desorbed into the organic phase.

An example of the rate reductions observed when the organic feed was preequilibrated with an aqueous blank is shown in figure IV.12. The causes behind these observations are less obvious than in the case of nickel in solution. One possible reason is the lower aqueous solubility of KD compared to HD (table F.13). Another possibility is the slower interfacial dynamics resulting from interactions with the interface of saturated reversed micelles instead of relatively dry reversed micelles. Similar rate decreases were observed when K-free blanks were used to preequilibrate the organic feeds, thus supporting the latter hypothesis.

Because micelles are able to solubilize lipophiles, the possible simultaneous transfer of hexane and HD was explored. Negative results are to be reported. No hexane in the aqueous phase could be detected by GC or by changes in refractive index (η). For hexane η=1.375 (CRC, 1983-4). For water, η varies from 1.309 to 1.313, and η=1.332 was measured. The values of η for DNNSA solutions in hexane were found to depend slightly on $\bar{C}_{DT}$ as follows:

$\bar{C}_{DT}$ (M)	0.00	1.10^{-4}	5.10^{-3}	1.10^{-2}	0.27
η	1.372	1.372	1.373	1.373	1.391

In the dynamic experiments η changed no more than two thousandths between start and end, and the typical change was from 1.3325 at t=0 to 1.333 at $t \longrightarrow \infty$.

The rates per unit volume of sulphonate transfer into the aqueous phase (r_a) listed in table F.14 were calculated from the raw data (i.e. C_{DT} vs time) using eqn. IV.14.

$$r_a = \frac{dC_{DT}}{dt} \quad (\text{gmol dm}^{-3}\text{min}^{-1}) \qquad (IV.14)$$

The interfacial flux (J_a) was then evaluated from the balance IV.15, where V=0.300dm^3 was the aqueous phase volume, and A $\cong$ 0.42 dm^2 was the area of the interface. The fluxes are also listed in table F.14.

$$J_a = \frac{V}{A} r_a \quad (\text{kmol m}^{-2}\text{s}^{-1}) \qquad (IV.15)$$

At I=4.10^{-3} in the range $1.10^{-3}M \leq \bar{C}_{DT} \leq 1.10^{-2}M$, J_a increased as $\bar{C}_{DT}$ raised to an exponent ranging from 1.02 at N=300rpm to 1.08 at N=200rpm. Some fluxes are shown in figure IV.13 vs I, with $\bar{C}_{DT}$ as the parameter. It is shown in the figure that J_a depended strongly on $\bar{C}_{DT}$ at low values of I, whereas the dependence was slight at I=0.5. Such a variation pattern was expected from the shape of the solubility curves in figure IV.7. The tenfold increase in J_a at I=4.10^{-3} closely corresponds to the increase in solubility under identical conditions.

The simultaneous effects of I, N, and $\bar{C}_{DT}$ on J_a are shown in figure IV.14. The J_a dependence on $\bar{C}_{DT}$, averaged over the three values of I was $\bar{C}_{DT}^{1.04}$, with the exponent ranging from 0.97 to 1.07. The effects on the flux of presaturating the organic feed

(A) and of adding nickel (5.10^{-3}M) to the aqueous phase (B) are summarized below (Table IV.b). With non-preequilibrated feeds, J_a was around 11% higher than the value observed when the micelles were initially saturated (J_{as}). At I=0.1, J_a was around 1.75 times the value of the flux with nickel in solution (J_{aNi}). At I=0.5, that ratio was only 1.18. The faster complexation of nickel by the sulphonate at the lower value of I is the proposed reason for this observation.

Table IV.b

	N rpm	I M	J_a ($\times 10^9$ kmol $m^{-2}s^{-1}$)	J_{as}	J_{aNi}	J_a/J_{as} —	J_a/J_{aNi} —
(A)	200	0.1	1.9	1.7		1.12	
	300	0.1	2.2	2.0		1.10	
(B)	200	0.1	1.9		1.1		1.73
	300	0.5	0.91		0.77		1.18

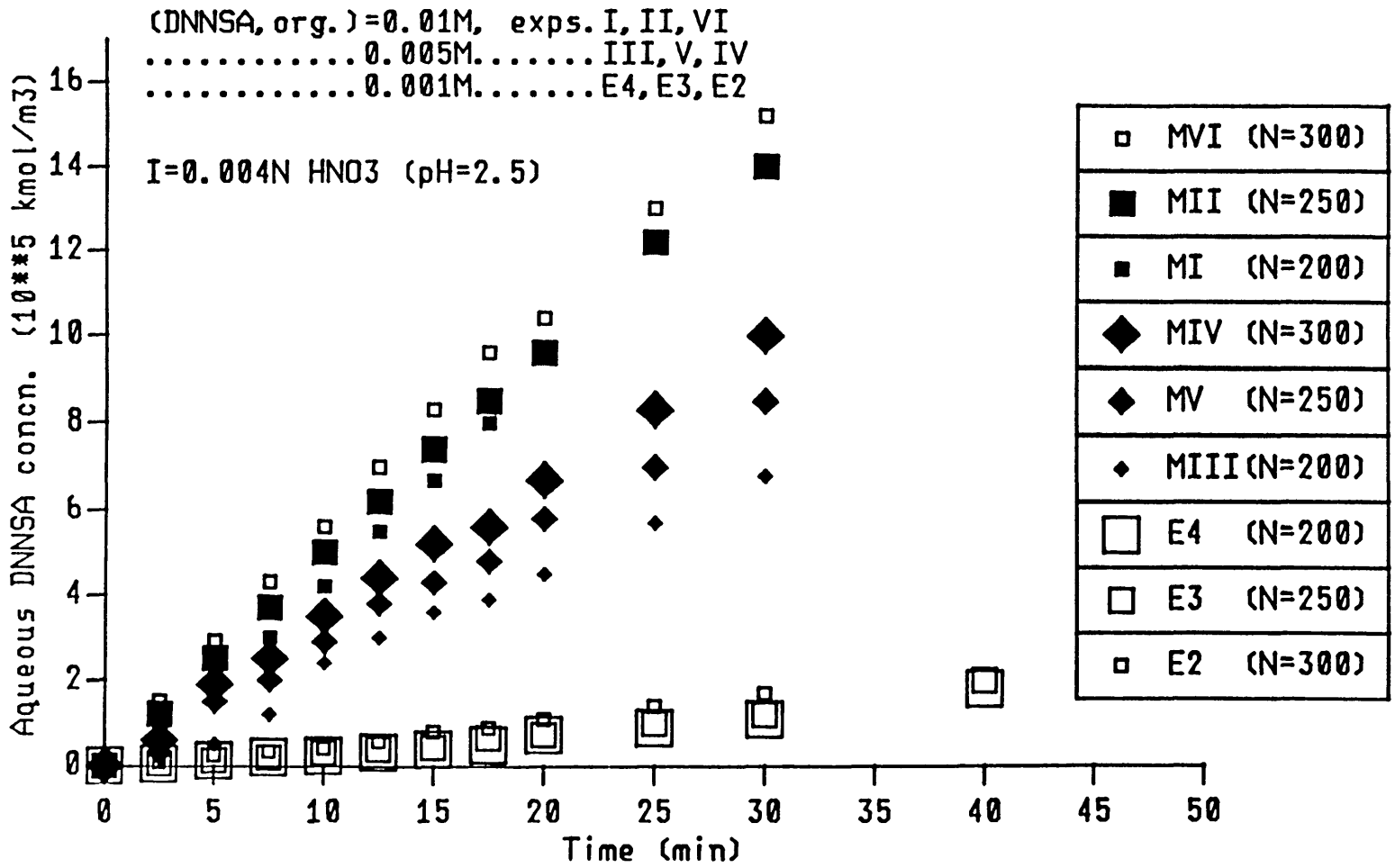


Figure IV.9 Effect of stirring speed and organic DNNSA concentration on the dynamic dissolution of DNNSA.

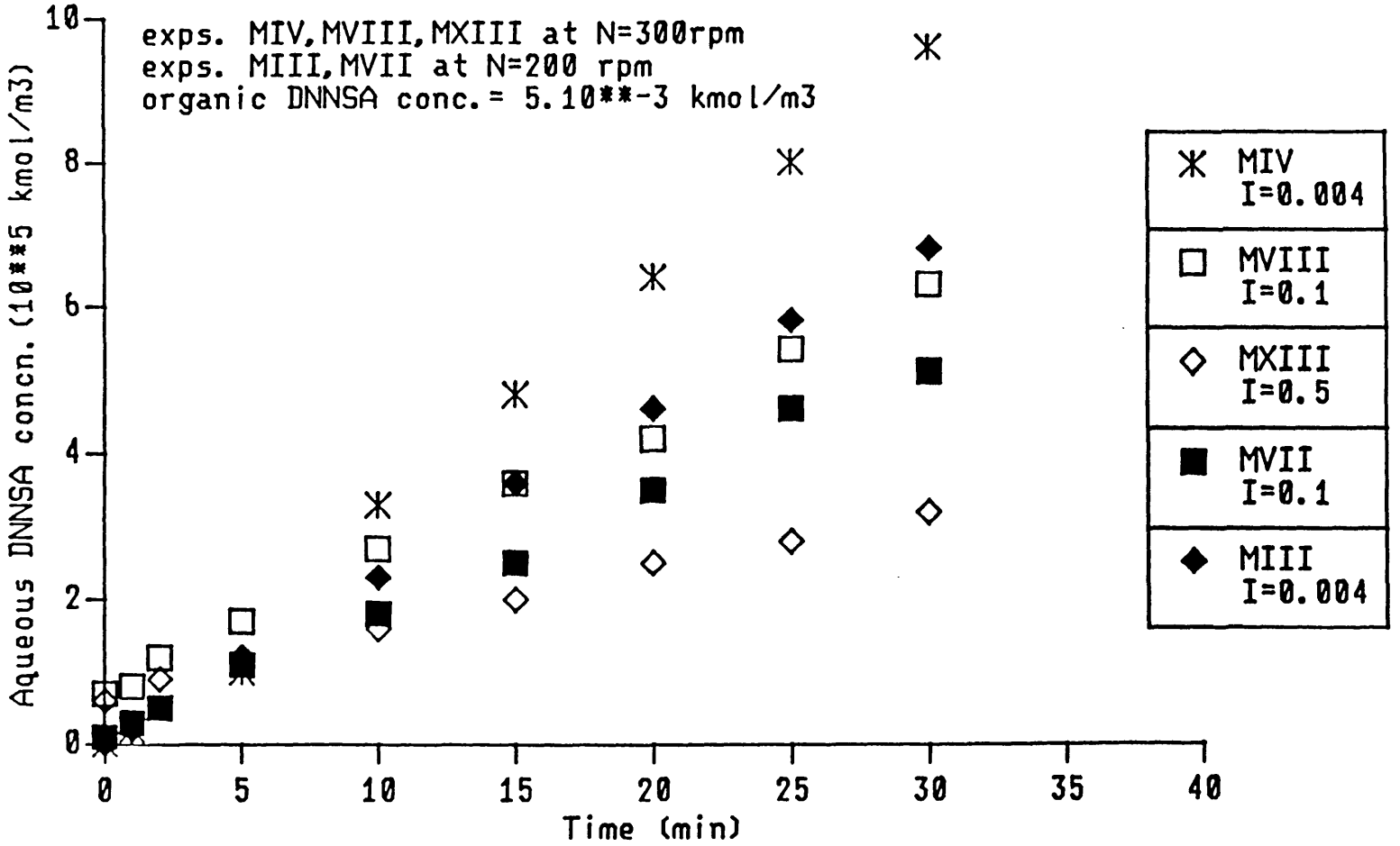


Figure IV.10 Effect of ionic strength and stirring speed on the dynamic dissolution of DNNSA.

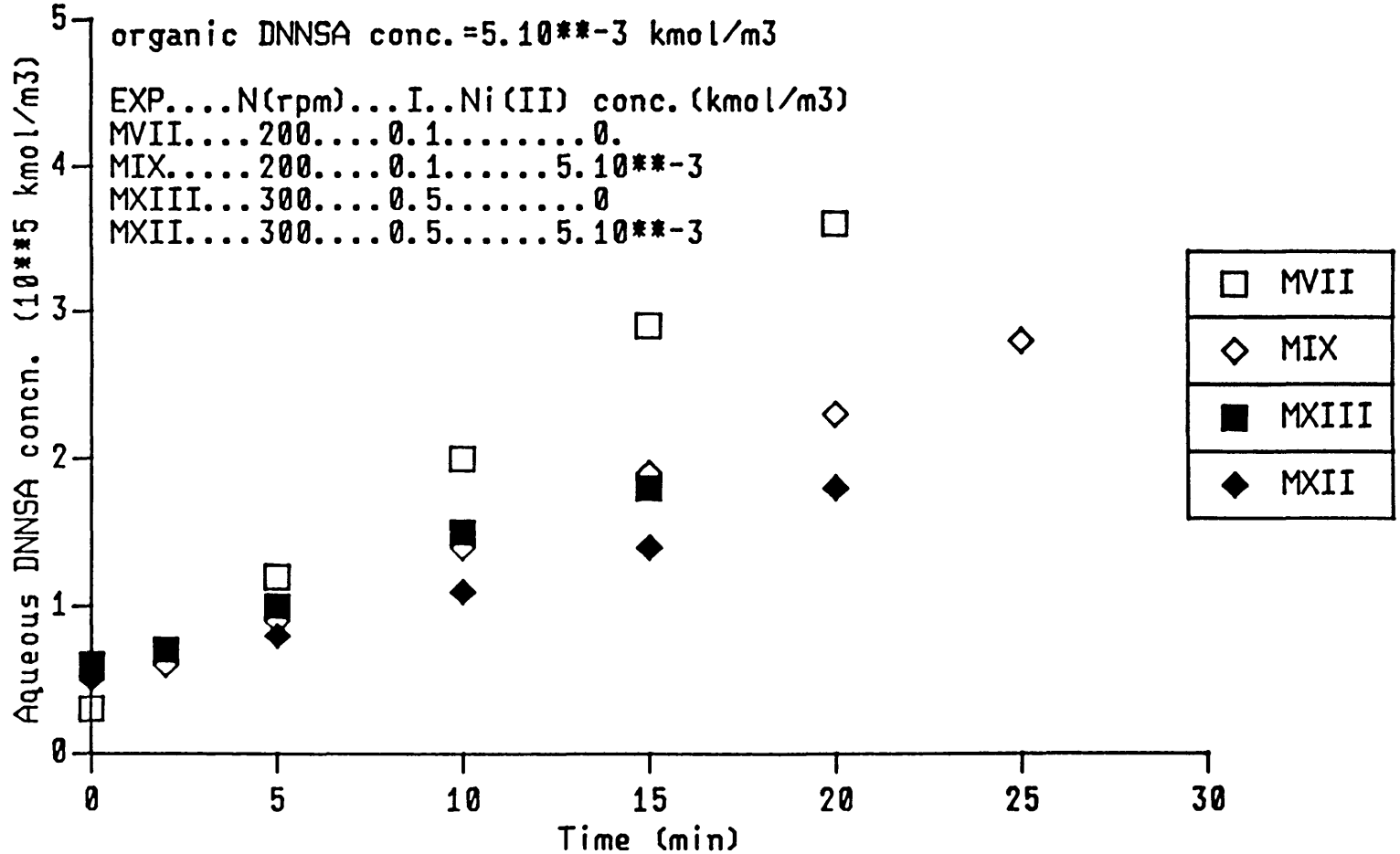


Figure IV.11 Effect of aqueous nickel on the dynamic dissolution of DNNSA.

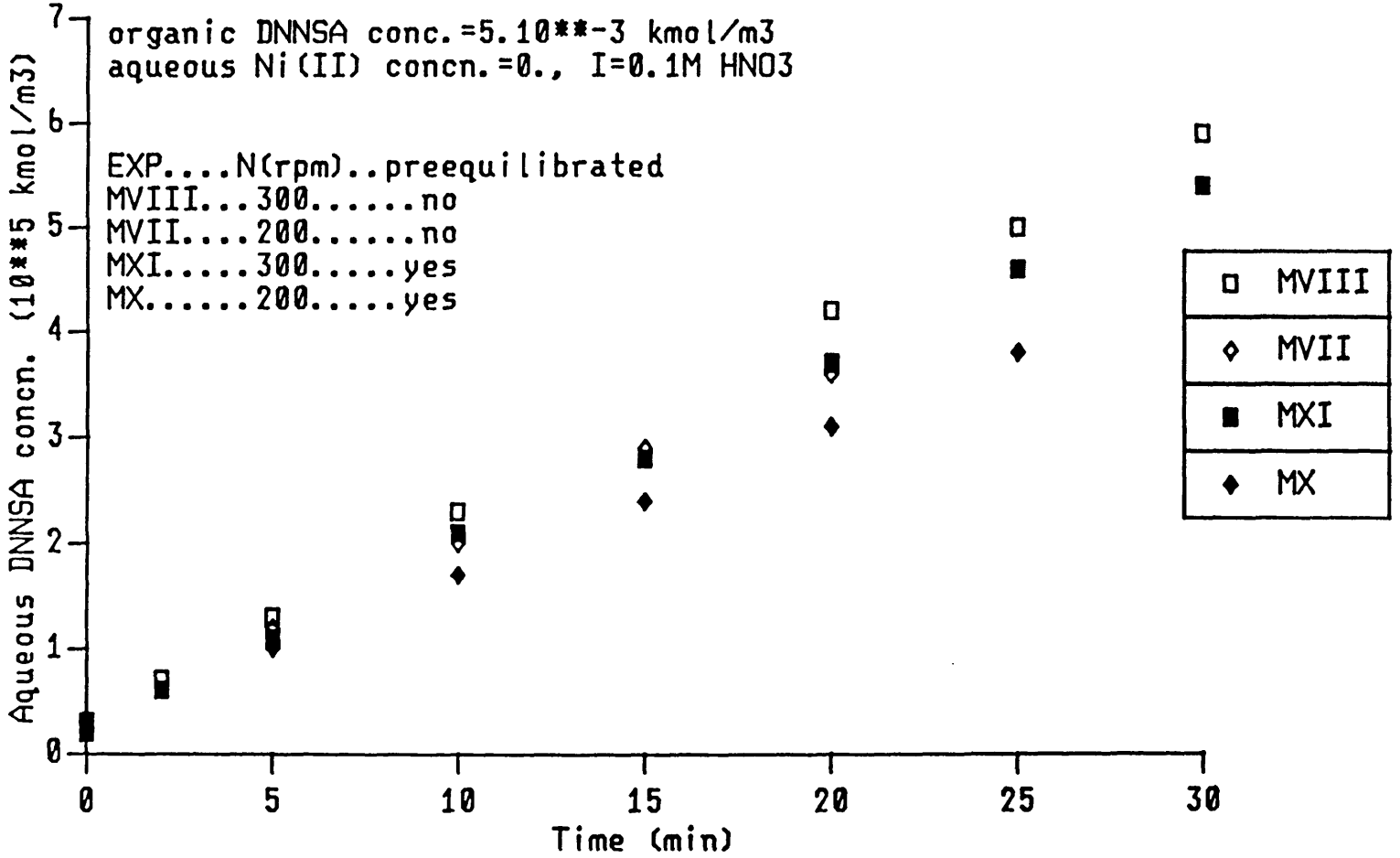


Figure IV.12 Effect of physically preequilibrating the organic feed on the dynamic dissolution of DNNSA.

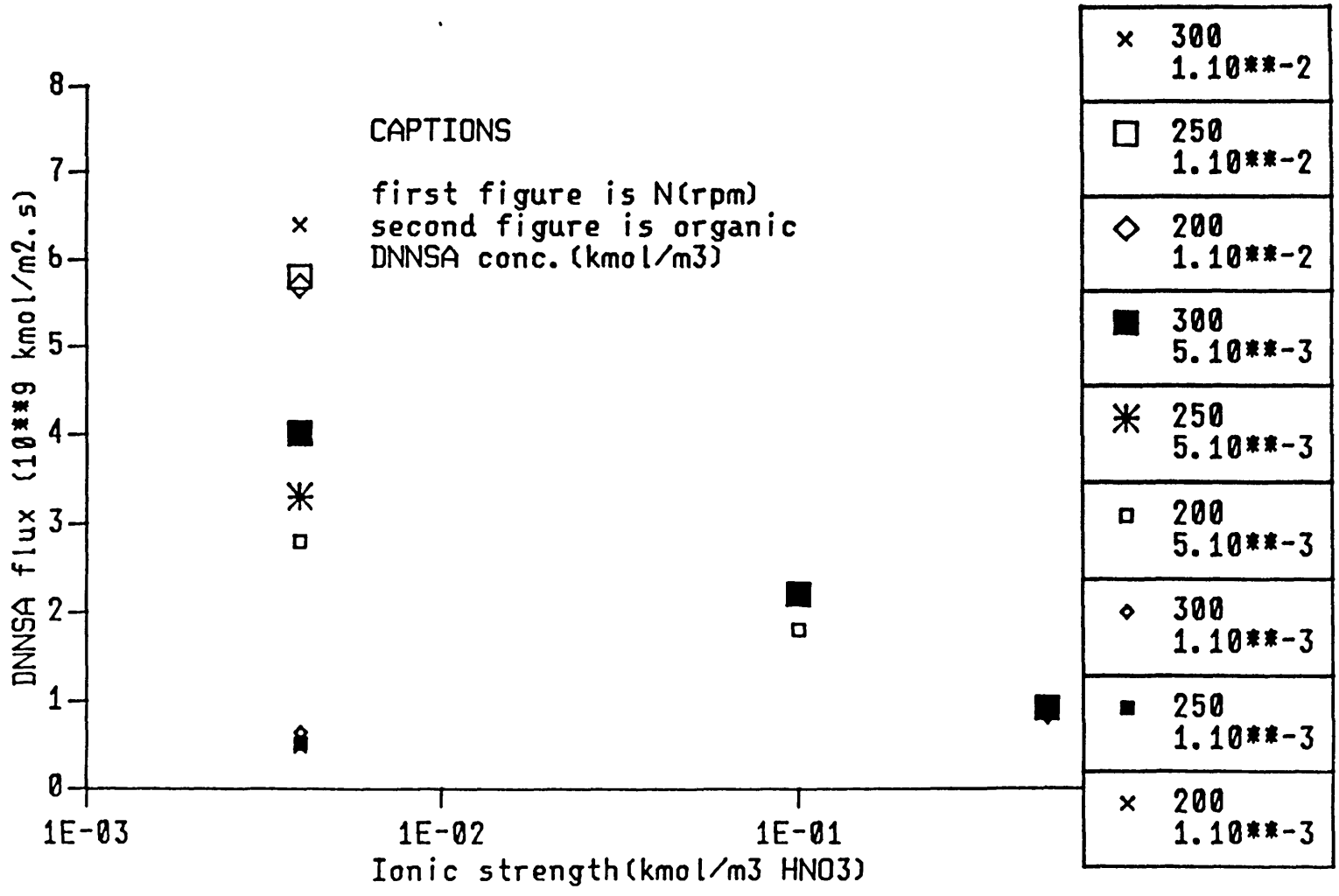


Figure IV.13 Effect of organic DNNSA conc., ionic strength and stirring speed on DNNSA dissolution fluxes

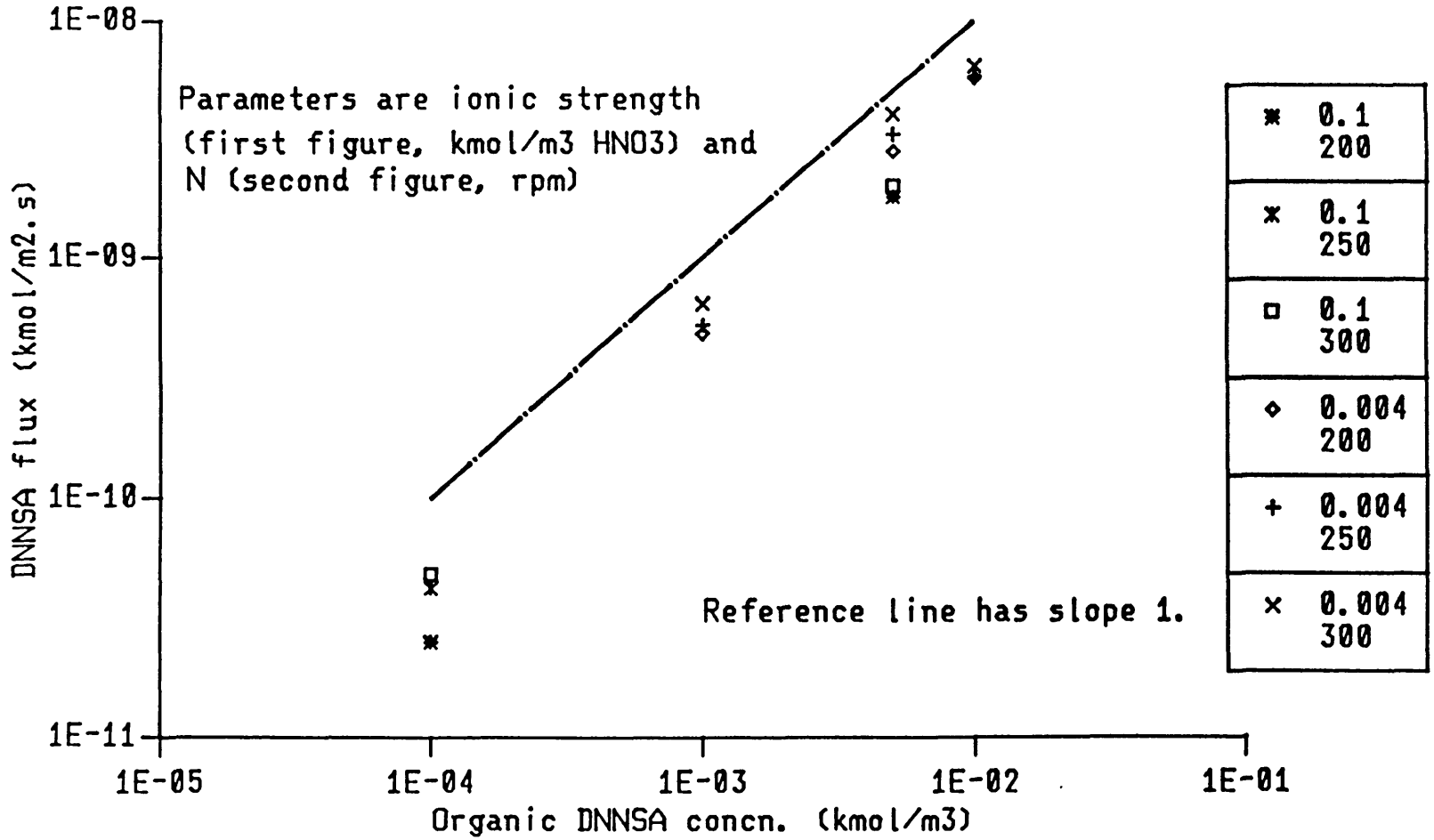


Figure IV.14 Effect of organic DNNSA conc., ionic strength and stirring speed on DNNSA dissolution fluxes.

IV.3. ELECTROLYTE SOLUBILIZATION BY DNNSA MICELLES[3]

The results presented in this section are concentrations of water measured in reversed micellar solutions and the quantities computed therefrom.

The solubilizing capacities of DNNSA-hexane solutions are presented in subsection IV.3.1. Dynamic transfer raw data, rates and fluxes are reported in the following three subsections. In subsection IV.3.2 the work on solubilization across hydrophilic membranes is covered. Experiments in the NDSC are dealt with in subsection IV.3.3. The rates of solubilization of the radioactive tracer ^{32}P by initially dry reversed micelles and by preequilibrated micelles are compared in subsection IV.3.4.

IV.3.1. SOLUBILIZATION CAPACITY

The concentrations of water (C_W) and ethanol (C_E) in DNNSA -hexane solutions were measured by GC as detailed in section III.3. Moisture contents in hexane 95%+ and 99%+ pure were measured similarly. The values found were respectively C_W^h=0.057kmolm^{-3} (0.16% w/w) and $C_W^h \cong$0.004 kmolm^{-3}($\cong$0.01% w/w).

The HD purification process was ended by drying the product at 65°C under 1mm Hg residual pressure. In DNNSA aliquots removed from the oven after variable numbers of days it was found that the ethanol content was reduced by vacuum drying, whereas the moisture was unaffected. The data and the calculations are listed in table

---

[3] Philippe Alinat helped me with the experiments of water transfer through membranes and Christophe Haunold with the solubilization of dyes and alternative experimental devices. Mark Sadler and Elios Jorisi did a thorough and cheerful job helping in the analysis of samples by GC. Elios also run core exchange experiments. For their efforts I owe them many thanks.

F.15 and shown in figure IV.15 as W_1, W_2, and E versus time. W_1 is the total number of water molecules in the organic phase per DNNSA mo lecule in the micelle, i.e.

$$W_1 = C_W/\bar{C}_{DT} \qquad \text{(kmol water / kmol DNNSA)}$$

W_2 results from correcting W_1 for water in the diluent, i.e.

$$W_2 = (C_W - C_W^h)/\bar{C}_{DT}$$

The ratio E is similarly defined as the number of ethanol molecules per DNNSA molecule in the micelle,

$$E = C_{ethanol}/\bar{C}_{DT}$$

Vacuum drying was thus effective to remove residual ethanol, but not to remove residual water. At the end of the drying period each micelle was associated on average with:

$$m\ (W_2+E) \cong 7(2.7+0.7) \cong 24$$

solubilizate molecules. Based on the residual water content in "dry" DNNSA of around 3 molecules per DNNSA molecule and assuming spherical geometry for micelles in dilutions of the product, the core volume of "dry" micelles was estimated as 920 $Å^3$. Thus the "dry" core diameter resulted of 12 $Å^3$. When the length of two DNNSA molecules (2 x 8Å; van Dalen et al., 1974a) was added, a "dry" micellar diameter of 28 Å was estimated. The average from the PCS results shown in sub-section IV.1.4. was 30 Å. In the following paragraphs the ratio W_2 will be called W (and W^s, at saturation) and "dry" micelles will be called dry micelles.

The effect of I and of $\bar{C}_{DT}$ on water loading at saturation (C_W^s) was investigated. C_W^s and W^s are plotted versus I in figure IV.16 at $\bar{C}_{DT}$=0.1kmol m^{-3}. W^s fell from around 14 to about 10 as I was increased to 0.1N (HNO_3) from zero. The electrochemical sublayer surrounding the polar heads becomes more dense as I is increased and improves the screening of electrostatic repulsions among DNNSA molecules heads. The reversed micelles therefore shrink as I is increased, and their cores accommodate less water. The effect was less pronounced at higher value of I. W^s was around 4 at I=0.5, and approached 3 at higher values of I. This limiting value of 3 agrees with the residual water after vacuum drying and it is believed due to water of hydration strongly bound to the polar heads. Thus micellar solutions have an approximate water concentration of $(W^s-3)\bar{C}_{DT}$ as loosely bound "water pools". Water of hydration accounted for 21% total water at I≅ 0, and to 30% at I≅ 0.1. A limiting value of 6 for DNNSA was suggested by the work of Högfeldt et al. (1981), although Högfeldt had previously reported (1966) a value around 1. The estimate of hydration water as 30% of total water agrees closely with the 33% estimated by Balasubramanian (1981) for Triton X-100 in cyclohexane.

The dependence of C_W^s on $\bar{C}_{DT}$ at I=0.1 is shown as the upper line in figure IV.17. The ordinates were corrected for C_W^h. The relatively high value of C_W^h in the hexane 95%+ used in these experiments did not allow to reduce $\bar{C}_{DT}$ below $2.5.10^{-3}$kmolm^{-3}. C_W^s varied approximately as 9 $\bar{C}_{DT}$, suggesting that I increased somewhat on equilibration from the initial value of 0.1 due to DNNSA ionization and dissolution.

Besides the direct water measurements reported above, the solubilizing ability of micelles was explored by two other techniques. The data from ^{32}P tracer solubilization in the concentration range $5.10^{-3}\leq\bar{C}_{DT}\leq$0.1kmol$m^{-3}$ are listed in table F.16 and are shown in figure IV.18. The data tend to diverge from the straight line at lower values of $\bar{C}_{DT}$ and thus they are not amenable to extrapolation to zero concentration.

The green hydrophilic dye fluorescein dissolved in 0.5N (HNO_3+ KNO_3), pH=2.5, was also solubilized. The light absorbances of the extracts at 445nm are shown in an arbitrary scale versus $\bar{C}_{DT}$ in figure IV.3. The absorbances clustered on a straight line which on extrapolation agreed with the CMC as indicated by the σ data. This observation suggests that the dye was transferred mainly by micellar solubilization, which becomes significant around the CMC. The possibility of a reaction between DNNSA and the dye however could not be excluded. Thus dyes were not used in solubilization rate experiments.

IV.3.2. TRANSFER ACROSS HYDROPHILIC MEMBRANES.

The data shown in figure IV.19 were obtained from the experiments described in section III.4. The values of C_w (Table F.17) uncorrected for C_w^h were plotted versus time with $\bar{C}_{DT}$ in the range $2.5.10^{-3}$ to 2.10^{-2}M as the parameter. The initial moisture in the organic phase was that left in DNNSA after purification plus C_w^h. There was a fast uptake of water followed by a plateau as the micelles reached saturation. The plateaux values of C_w^s are in good agreement with the equilibrium loading shown in figure IV.16. The initial rates were higher as $\bar{C}_{DT}$ was increased. The plateaux were reached around 5 min. after starting the experiment.

Volumetric initial transfer rates (r_w) were computed for each value of $\bar{C}_{DT}$ as follows

$$r_w = V \left[\frac{d\,(C_w - C_w(0))}{dt} \right]_{t=0} \qquad (IV.16)$$

where V was the volume of the organic phase. The concentrations at time zero were computed from the water analysis of hexane and of the micellar stock solution, and they were included in the calculations. The results are listed in table F.18 and are shown in

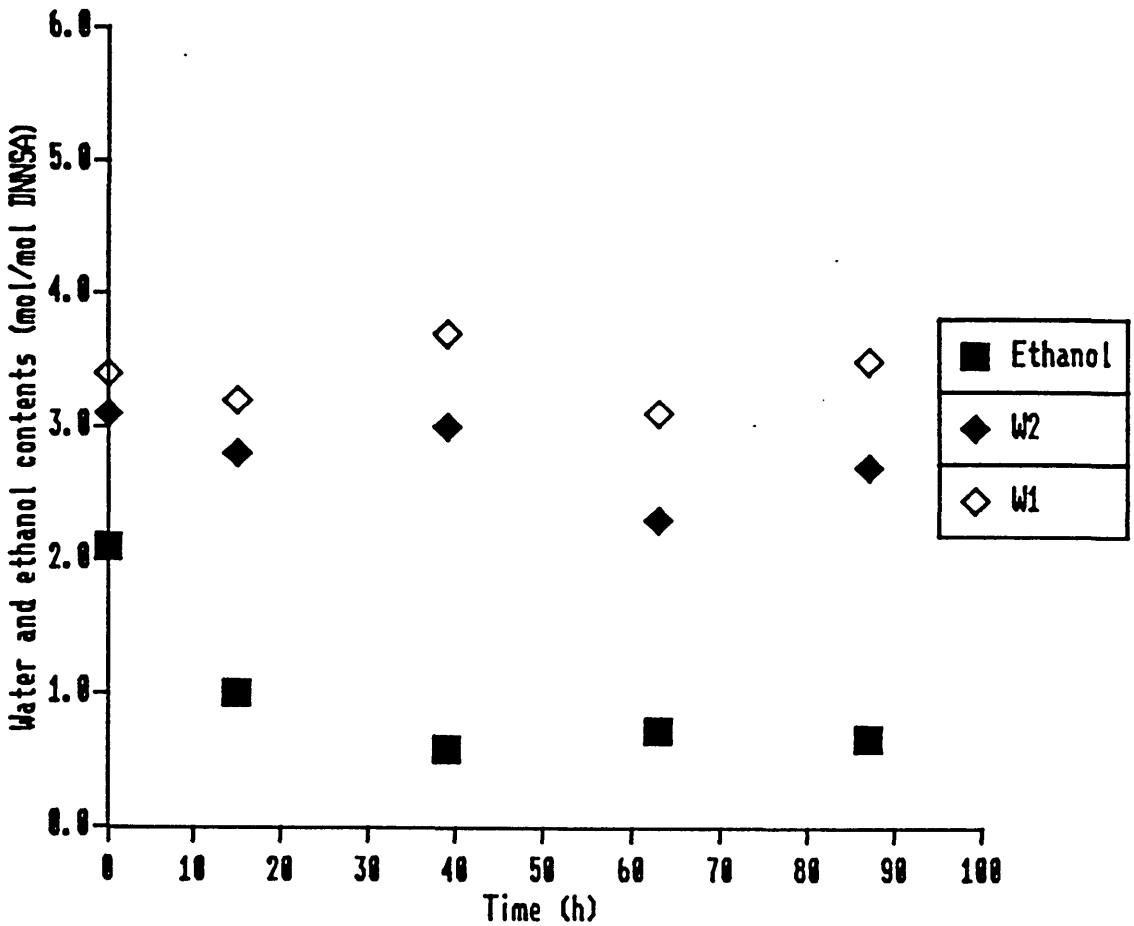


Figure IV.15 Drying of purified DNNSA.

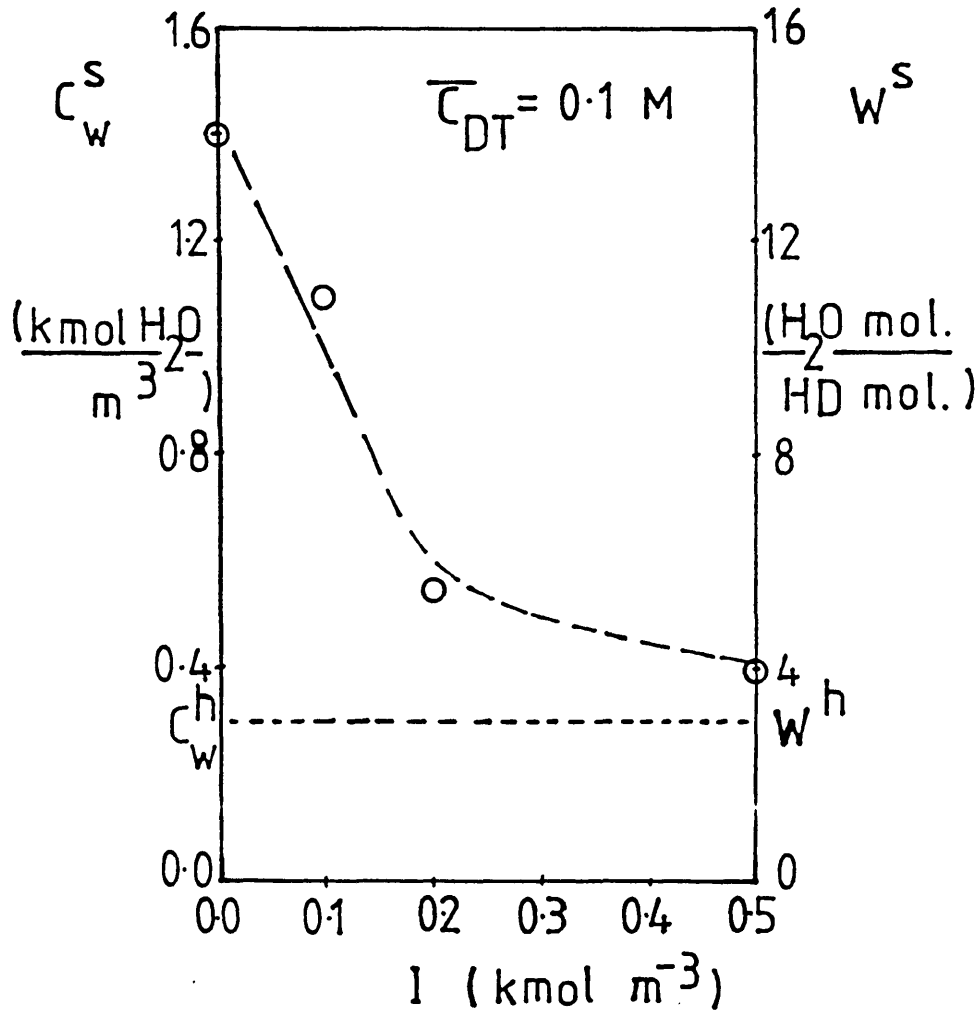


Figure IV.16 Saturation water loading by reversed micelles of DNNSA in hexane and water to DNNSA ratio as function of I (N, KNO_3+ HNO_3). pH=2.5, 20°C.

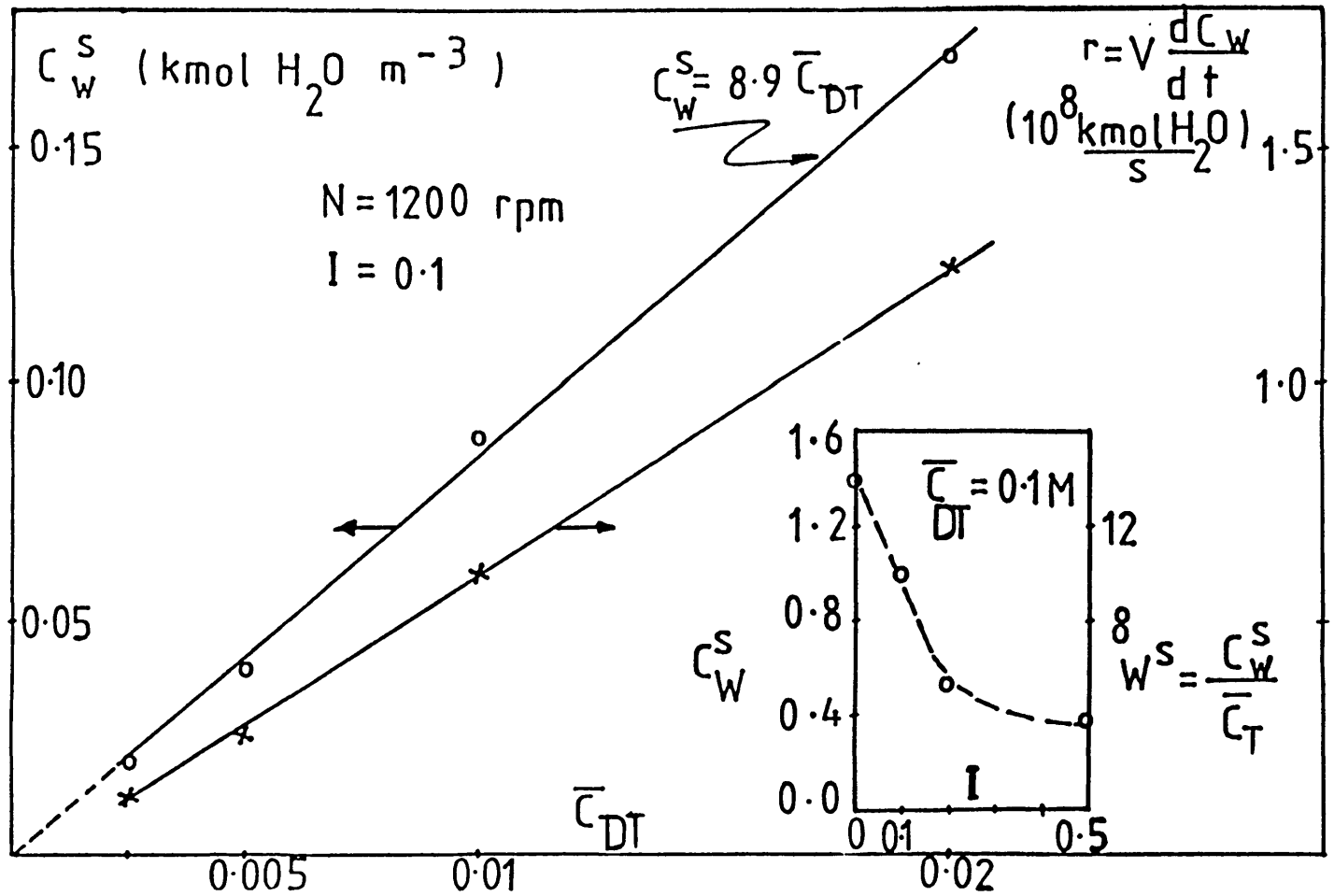


Figure IV.17. Water loading at saturation and rates of water solubilization by initially "dry" micelles. Transfer across hydrophylic membrane. Conditions as for Table F.17.

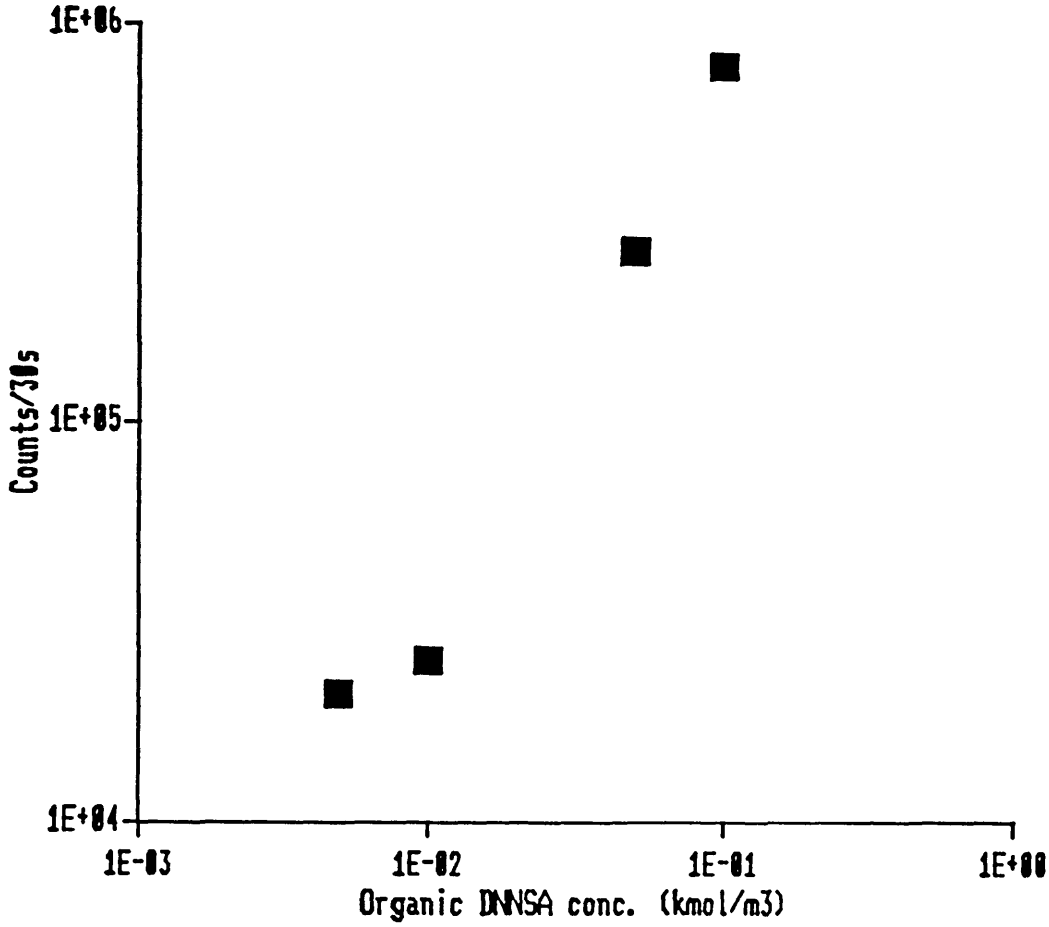


Figure IV.18 Equilibrium solubilization of P-32 tracer by DNNSA solutions.

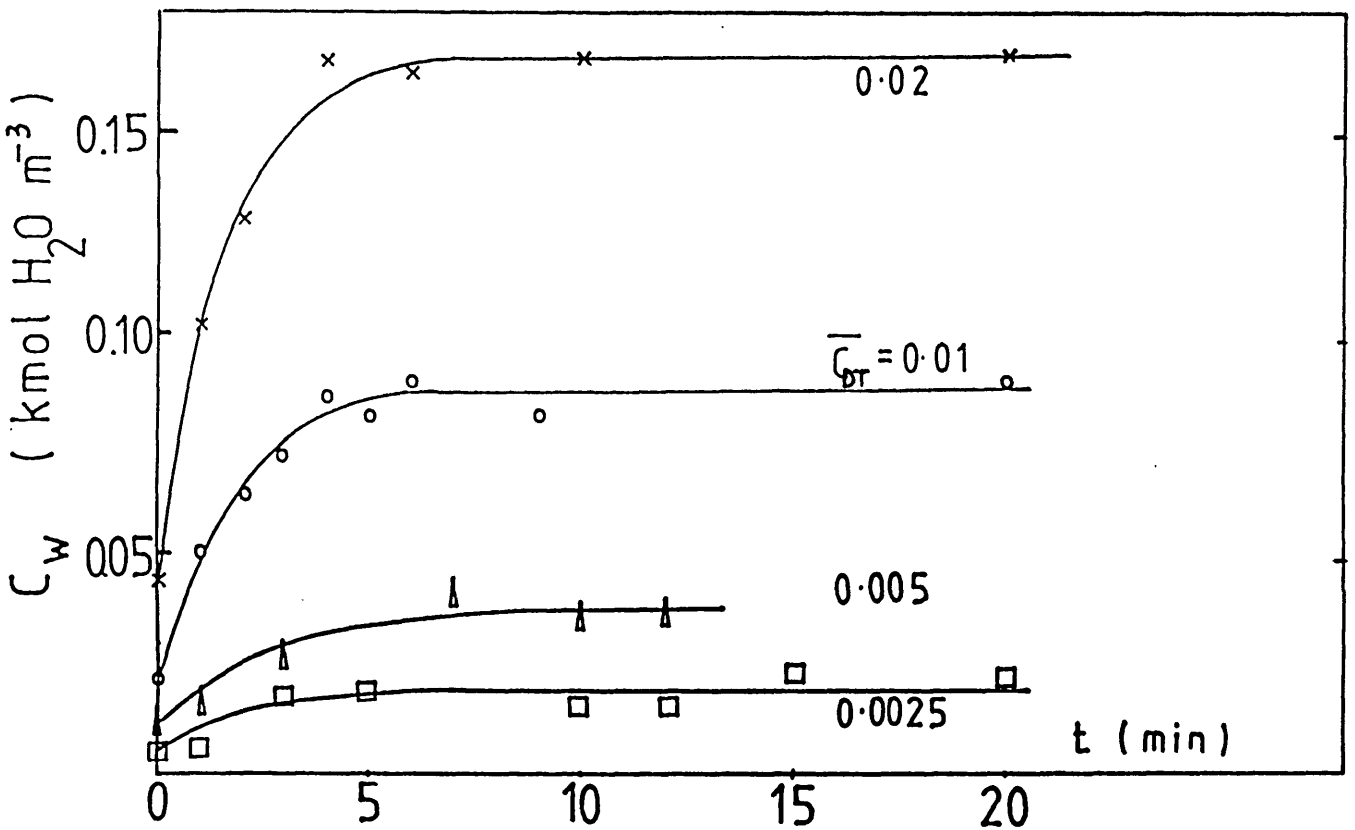


Figure IV.19 Data from experiments of dynamic water solubilization across a hydrophilic membrane.Conditions as in Table H.15.

figure IV.17. Linear regression of the results suggested that the rate depended linearly on DNNSA concentration.

To search for the possible effect of changing hydrodynamic conditions on the transfer rate, an experiment at $\bar{C}_{DT}=1.10^{-2}M$ was conducted at 780 rpm. The data were plotted in figure IV.20, showing that C_W^s was reached sooner at 1200rpm than at 780rpm.

IV.3.3. TRANSFER IN THE NON-DISPERSIVE, STIRRED CONTACTOR

The solubilization rate experiments were aimed at identifying the transport characteristics of the NDSC used in nickel extraction rate experiments. Analyzing the effect of changing stirring velocity on electrolyte transfer rate (r_W) was thus the prime objective. The effect on r_W of varying $\bar{C}_{DT}$ was also studied.

The solubilizate ionic strength (I) affects the micellar loading, thus a dependence of rates on I was expected. Changing the value of I has a two-fold effect. The loading capacity decreases as I is increased (figure IV.16) thus reducing the net solubilizate concentration in the subphase. Drawing a parallel with the physical transfer of surface-inactive solutes, the loaded subphase would be equilibrated with the interface provided that mass transfer resistances exerted global control. It follows that lower subphase loadings would reduce the driving force available to dynamic solubilization. The second effect is that the smaller micelles forming at higher values of I have a larger diffusion coefficient ($\mathcal{D}$, appendix G). This effect may in part compensate for the former. In other words, independently changing the factors in the equation:

$$\text{flux} = \text{transfer coefficient} \times \text{driving force}$$

may result in an invariant product (i.e. the value of the flux).

Data are listed in table F.19 and shown in figure IV.21. C_W is shown to rise as time proceeded, at given values of the parameters (N, $\bar{C}_{DT}$, and I).

At given values of $\bar{C}_{DT}$ and I, the rate increased as N was increased (experiments I,VI,II). This dependence of rate on N is indicative of a mass transfer controlled process. At given values of I and N, the rate increased as $\bar{C}_{DT}$ was increased (experiments I, II, and V, VI). This observation indicates that DNNSA is involved in the solubilization mechanism. Under the condition $\bar{C}_{DT}$ >> CMC used, and considering the experimental finding that significant micellisation is required for appreciable solubilization (figure IV.3), it follows that reversed DNNSA micelles are the most probable agents in this transfer mechanism, as opposed to diffusion of water through hexane. This hypothesis is quantitatively substantiated in section V.1.2.

The aqueous phase pH was continuosly monitored and recorded. The initial pH≅2.5 fell gradually as DNNSA dissolved and deprotonated. When initial pH=1 was chosen the value was steady through the duration of the experiment. The changes in W^s were however not substantial as I increased little, and they were neglected in the calculation of transfer coefficients. Initial transfer fluxes were calculated as follows:

$$J_W = \frac{V}{A}\left[\frac{d(C_W - C_W(0))}{dt}\right]_{t=0} \qquad \text{(IV.17)}$$

from the polynomial fitting of the data. The values of J_W are listed in table F.19 and are shown in figure IV.22 versus Re with $\bar{C}_{DT}$ as the parameter. J_W depended linearly on Re, and the slope of J_W versus Re increased as $\bar{C}_{DT}$ was increased.

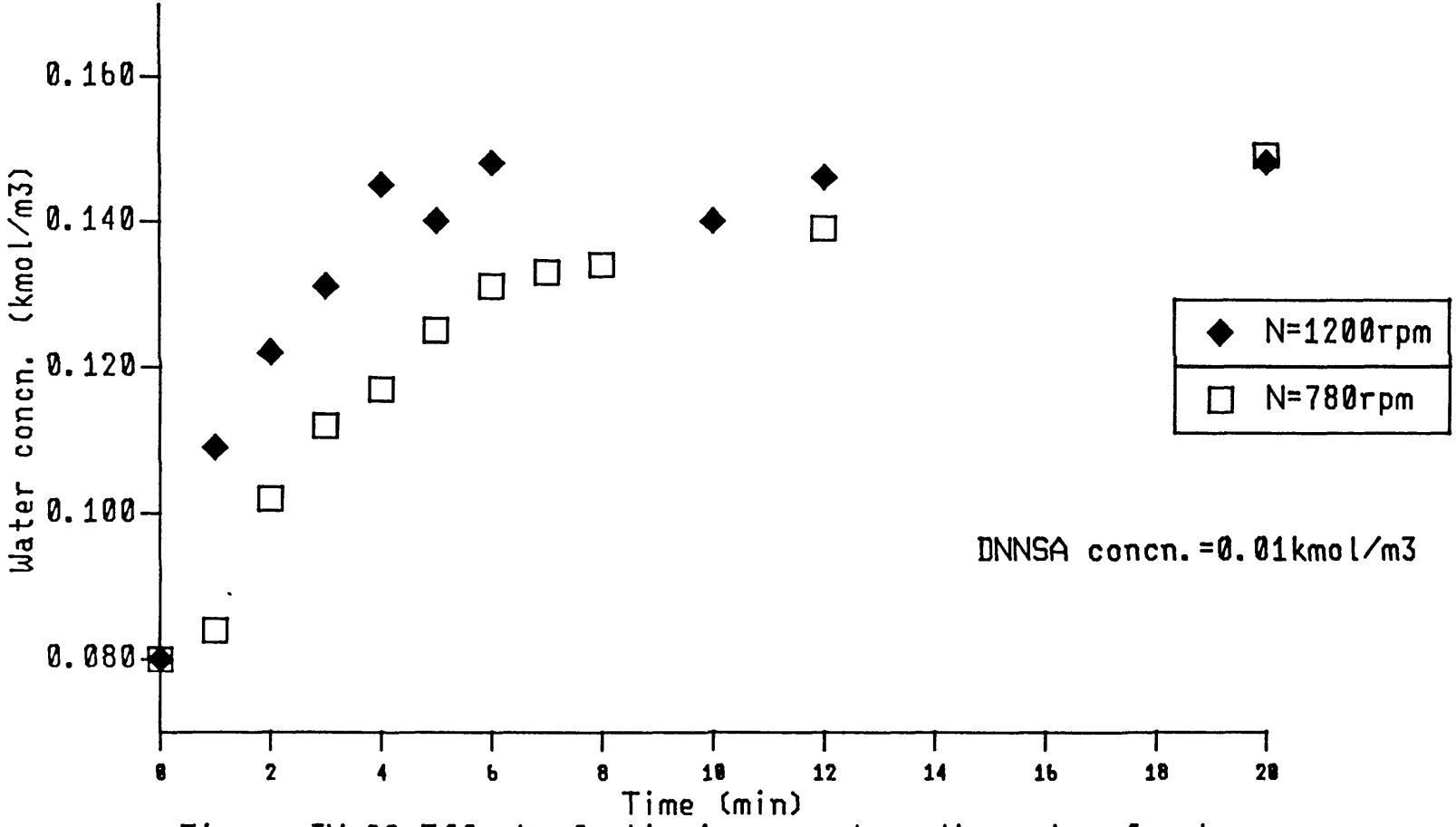


Figure IV.20 Effect of stirring speed on the rate of water solubilization across membranes.

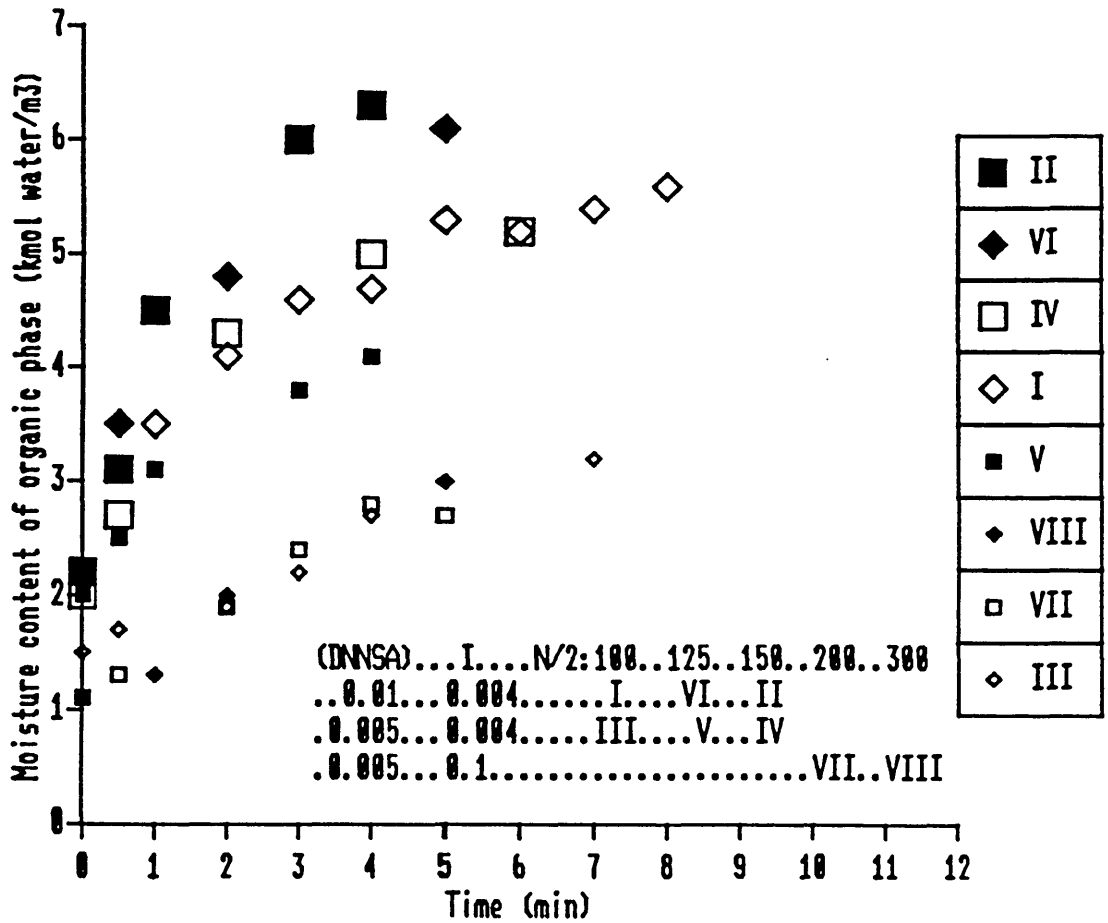


Figure IV.21 Dynamic water solubilization in the NDSC

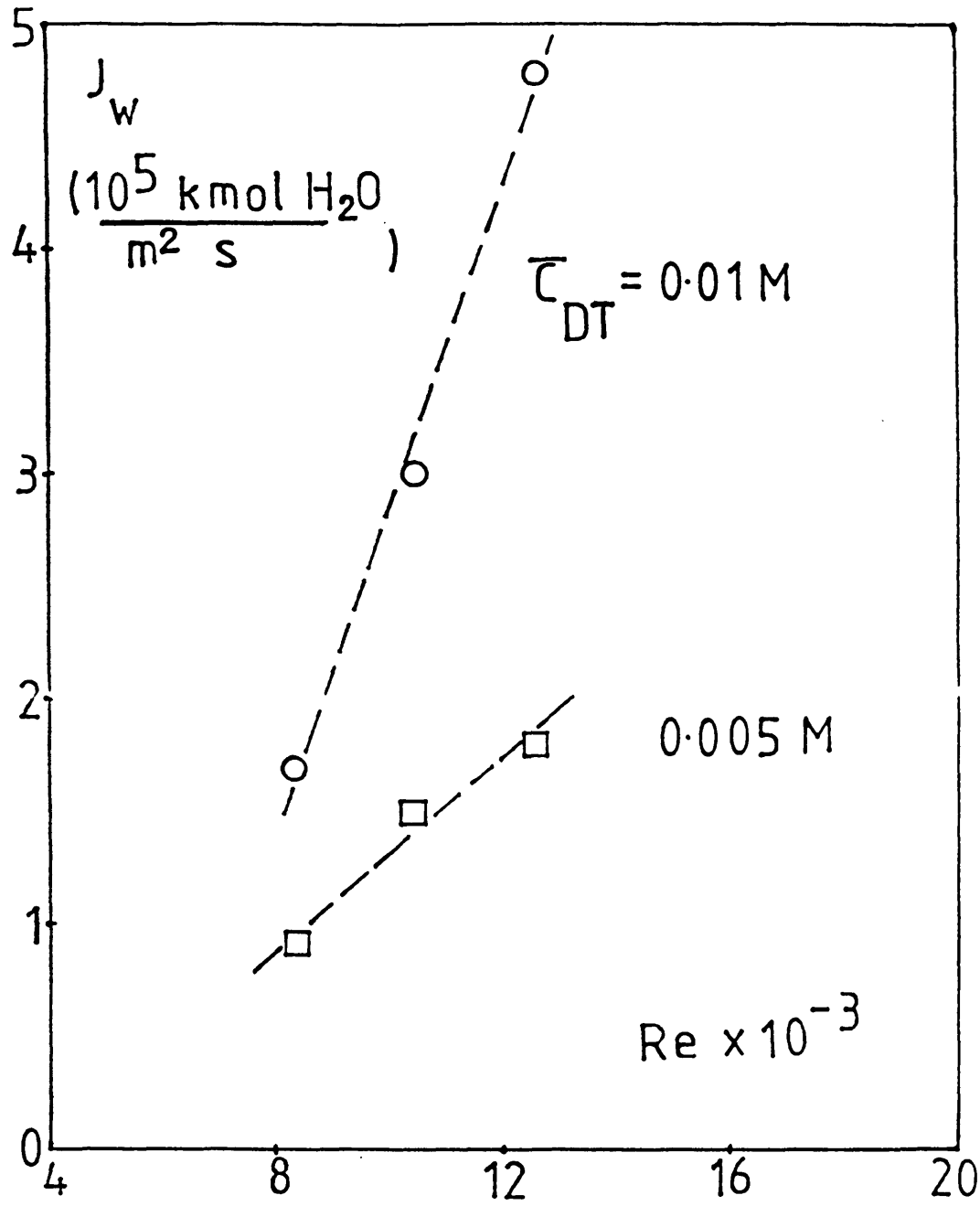


Figure IV.22 Effect of changing hydrodynamic conditions on the flux of water solubilized by reversed DNNSA micelles in the NDSC.

IV.3.4. INITIAL SOLUBILIZATION AND CORE EXCHANGE

These experiments were conducted as described in section III .4, using ^{32}P as a tracer. The countings obtained at $\bar{C}_{DT}$ in the range 0.5 to 5.10^{-2}M are listed in tables F.20.a through F.20.d. The data are the average of four countings corrected for background (typically 80 to 85 counts /30s). The calibration line used to interpret the results was that shown as figure IV.18, plotted from the data in table F.16. The following correlation was chosen:

$$C_{WP} = 0.00786 + 1.2.10^{-7} \text{ counts/30s.cm}^3$$

The increase with time in water concentration (C_{WP}) in the organic phase in initial solubilization experiments is plotted in figure IV.23. It is apparent from the slopes of the lines in the figure that the rate of solubilization at a given value of $\bar{C}_{DT}$ decreased from an initial value as the mechanism of core exchange became more important than that of initial solubilization by dry micelles. The initial rate (r_i) depended on $\bar{C}_{DT}^{\cong 1}$ as concluded from the decreases in slopes at t=0 as $\bar{C}_{DT}$ was reduced from 5.10^{-2} to 5.10^{-3}M.

The rate of core exchange results are shown in figure IV.24 as C_W^e vs time. They were obtained with organic feeds preequilibrated with a tracer-free blank. The data are also listed in tables F.20.a to F.20.d. The transfer of radioactivity observed was in this case due to the exchange of micellar cores. The data followed a pattern similar to that in figure IV.23. There was an initial transient state after which the slopes fell to steady values. There is no obvious reasons for the transient period bar end effects in the form of mixing and adsorption lag-times. No correlation was observed between the extent of the transient and the initial transfer of tracer during it. Once the slopes became constant, their values depended as $\bar{C}_{DT}^{\cong 1}$. Because the core exchange mechanism was always operative, straight lines were expected for C_W^e vs time as that observed at $\bar{C}_{DT}=5.10^{-2}$M.

The treatment applied by Chan et al. (1976) to the rates of solubilization by aqueous micelles was used here in the limiting cases of initial solubilization by dry micelles and core exchange by presaturated micelles. From the raw data corrected for initial contaminations, the initial rate (r_i) was calculated by eqn. IV.16 and the initial flux (J_i) by eqn. IV.17. The results are presented in table IV.4. J_i increased from $1.1.10^{-5}$ kmol water $m^{-2}s^{-1}$ at $\bar{C}_{DT}$ = 5.10^{-3}M to $9.1.10^{-5}$ kmol water $m^{-2}s^{-1}$ at $\bar{C}_{DT}$ = 5.10^{-2}M. and depended as $\bar{C}_{DT}^{\cong 1}$.

The rates of core exchange (r_e) listed in table IV.3 were estimated from the straight portion of the C_w^e vs time lines. The ratio r_i/r_e was independent of $\bar{C}_{DT}$ at 35±6.

IV.4. Ni(II)-K(I)-H(I)-DNNS EXCHANGE EQUILIBRIA.

IV.4.1. (K-H)DNNS EXCHANGE EQUILIBRIUM.

Unlike most liquid ion exchangers that feature tailor-made selectivity toward di- or tri-valent cations, DNNSA readily exchanges H^+ by alkali metal cations. Because the organic feeds used in this experimental work were preequilibrated with 0.5 M (HNO_3 + KNO_3) at the required pH, and in the experiments the raffinates had high K^+ concentrations, the following K^+-H^+ exchange by DNNSA is relevant to the analysis of Ni^{+2} extraction equilibrium and rate results.

$$\overline{HD} + K^+ \leftrightarrow \overline{KD} + H^+ \qquad \text{(IV.18)}$$

Estimates by a literature correlation of the K^+-H^+ exchange balance are first presented in this section, then the results from these experiments are introduced.

Högfeldt et al. (1978) investigated the thermodynamics of the K^+-H^+ exchange at I=0.1 M(KNO_3+HNO_3). The authors defined the fraction of K-sulphonate to total sulphonate as the factor X,

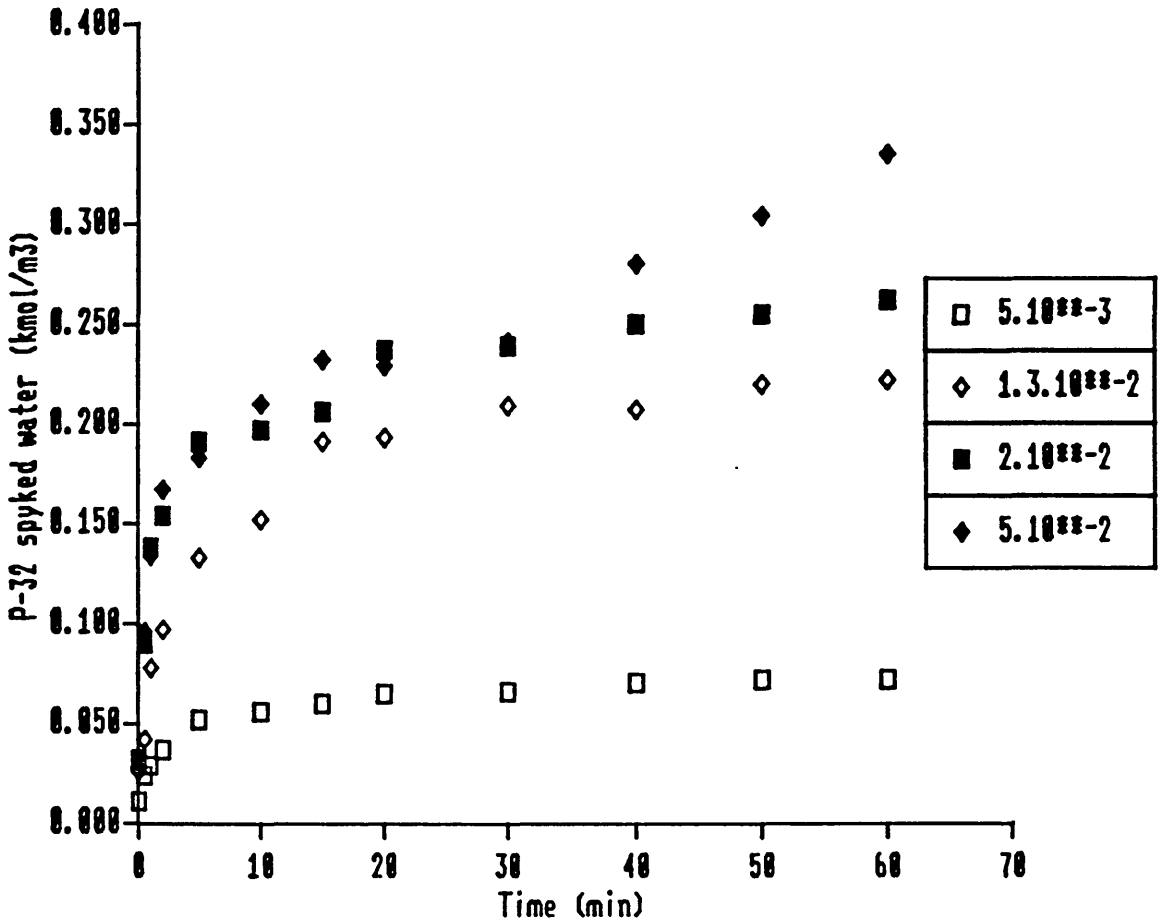


Figure IV.23 Initial solubilization of P-32 tracer. Parameter is organic DNNSA concentration (kmol/m3)

Table IV.3 Rates and Fluxes in initial solubilization and micellar core exchange.

$\bar{C}_{DT}$	r_i	$J_i \times 10^5$	$r_e \times 10^{-2}$	r_i/r_e
kmolm^{-3}	kmolm^{-3}min^{-1}	kmolm^{-2}s^{-1}	kmolm^{-3}min^{-1}	-
0.05	0.108	9.1	0.33	33
0.02	0.061	5.1	0.18	34
0.013	0.033	2.7	0.11	30
0.005	0.013	1.1	0.03	43

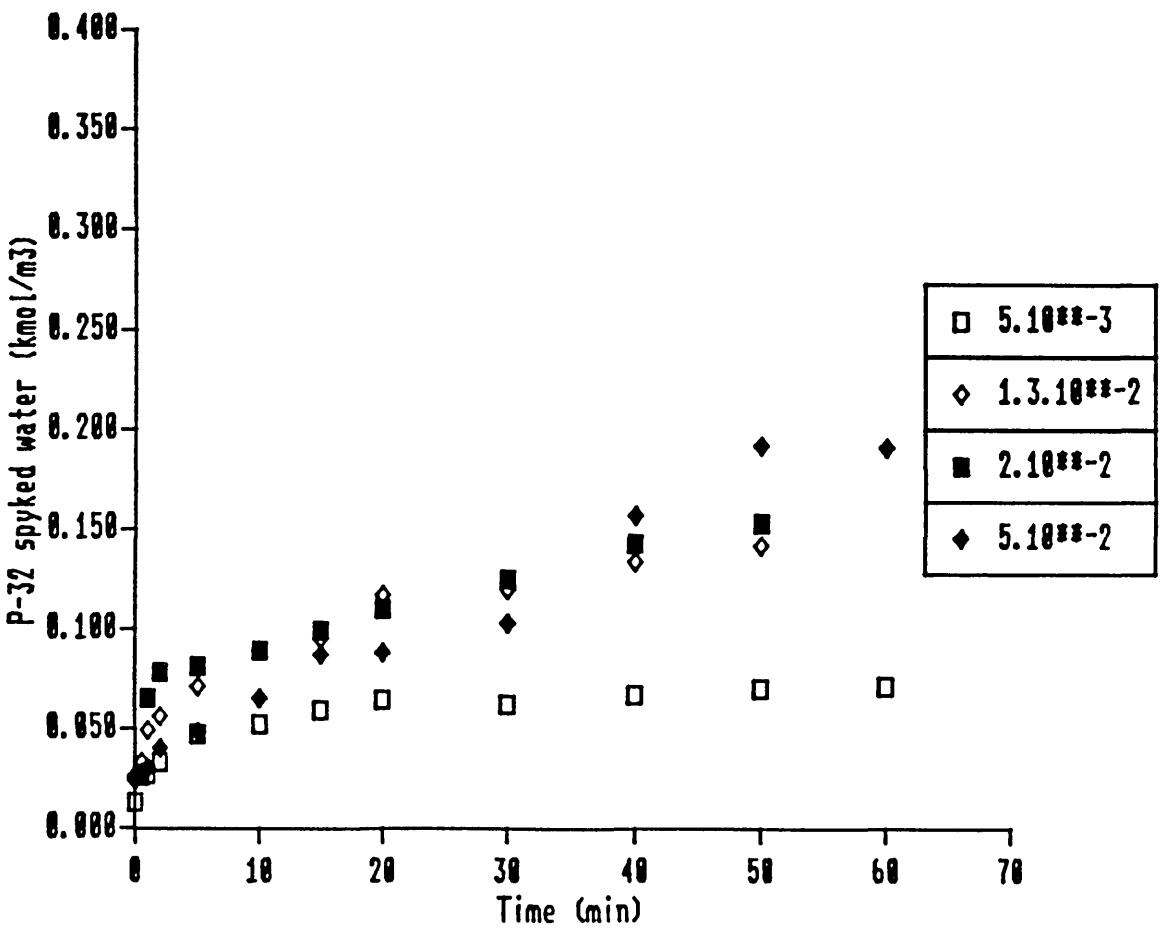


Figure IV.24 Solubilization of ^{32}P tracer due to micellar core exchange . Parameter is organic DNNSA concentration

$$X = \frac{\bar{C}_{KD}}{\bar{C}_{KD} + \bar{C}_{HD}} \qquad \text{(IV.19)}$$

and did not differentiate monomers from micelles. Instead, they gave the concentrations in eqn. IV.19 the meaning of *formal* concentrations. The LMA was applied to the exchange reaction IV.18:

$$K = \frac{X}{1 - X} \frac{C_H \ \gamma_H}{C_K \ \gamma_K} \qquad \text{(IV.20)}$$

where γs are activity coefficients of aqueous species. At 25°C, K was correlated to X as eqn. IV.21

$$\log K = -0.515\ X + 0.099\ (1-X) + 0.258\ X\ (1-X) \qquad \text{(IV.21)}$$

The three constants in eqn. IV.21 were evaluated at I=0.1 by Högfeldt et al. (1978). The same value of those constants will be used here to estimate X at I=0.5M(HNO_3+KNO_3) and pH in the range 0.5 to 4.0. Eqn. IV.21 was derived on the assumption that three types of micelles form due to aggregation of HD monomers alone (first term in eqn. IV.21), KD monomers alone (second term), and mixed monomers. The dependence of X on pH can be made explicit by substituting eqn. IV.20 into eqn. IV.21, and assuming that at constant value of I,

$$\frac{\gamma_H \ C_H}{\gamma_K \ C_K} \cong \frac{C_H}{C_K} \qquad \text{(IV.22)}$$

Using the bisection method implemented by the routine ML-08 in the master library of a TI-59 calculator, X was evaluated (±0.001) in the domain [0,1) from the following expression:

$$\log X-\log(1-X)+\log(C_H/C_K)+0.515X-0.099(1-X)-0.258X(1-X)=0.$$

The values of X found in this way are listed in table F.21 and are plotted versus pH in figure IV.25.

The experimental results are also presented in table F.21. The cation exchange resulted in acidification of the raffinate, lowering the pH from feed values of 2.0 to 4.0 down to equilibrium values of about 1.2. The factor X was calculated from titrations of the raffinates and from measured K^+ concentrations in the strippates. Both sets of values agreed well. Average values were plotted in figure IV. 25 together with the predictions by the model of Högfeldt et al. (1978). The predictions are somewhat higher than the experimental results.

Most of the extractant was in the acidic form (i.e. HD) below pH ≅ 0.3. X increased fast as pH was raised to about 2.0. From pH ≅ 2.5 upward, 98%+ of the reagent was as the K-soap (i.e. KD). It was thus expected that pH would not affect much the distribution of nickel above pH≅2.5, as observed by Osseo-Asare and Renninger (1984) and as shown in figure IV.25, where distribution coefficients are seen to increase as pH was increased then reach a plateau at pH≅2.5.

When dry solutions of DNNSA were equilibrated with the aqueous phase in these experiments, w molecules of water and its associated solutes were solubilized by each micelle (section IV.3). Such solubilization accounted for a secondary mechanism of metal transfer into the organic phase. The overall reaction can be written in micellar terms as follows:

$$\overline{(HD)}_m+(mX+\frac{w}{55.5})K^++wH_2O \Leftrightarrow mX\ H^++\overline{(K^+_X,H^+_{(1-X)})_m D_m}\cdot wH_2O(\frac{w\ C_K}{55.5})K^+ \quad \text{(IV.23)}$$

It is probable that the solubilized electrolyte had a different composition from that in the aqueous bulk. The choice of $C_{K,eq}$ as representative of the micellar core conditions is therefore only an approximation.

The measured organic potassium concentrations used above to estimate X comprised the complexed metal plus the metal solubilized in the aqueous micellar cores. It was possible to refine the above estimates by decoupling both effects. Eqn. IV.24 is the overall potassium balance at equilibrium:

$$\begin{pmatrix} K^+\text{left in} \\ \text{raffinate, (A)} \end{pmatrix} = \begin{pmatrix} K^+\text{in aqueous} \\ \text{feed, (B)} \end{pmatrix} - \begin{pmatrix} K^+\text{exchanged} \\ \text{by } H^+\text{, (C)} \end{pmatrix} + \begin{pmatrix} K^+\text{solubilized} \\ \text{by micelles, (D)} \end{pmatrix} \qquad \text{(IV.24)}$$

The terms in eqn. IV.24 were calculated as follows:

i) $A = V_a C_{K,eq}$ (where V_a = volume of the aqueous phase, and $C_{K,eq}$ was the potassium concentration in the raffinate after equilibration) (IV.25)

ii) $B = V_a C_{K,f}$ (where $C_{K,f}$ was the potassium concentration in the aqueous feed) (IV.26)

iii) $C = V_o m X_e \frac{\overline{C}_{DT}}{m}$ (where V_o was the volume of the extract) (IV.27)

and

iv) $D = V_o \frac{\overline{C}_{DT}}{m} \left(w \frac{C_{K,eq}}{55.5}\right)$ (IV.28)

The value of m was known from the literature, and the values of w, $C_{K,eq}$ and $C_{K,f}$ were estimated from experiments, thus the terms A, B, and D could be computed. The factor X_e in term C (the subscript means *exchange only*) could be evaluated from the balance IV.24 and

eqns.IV.25 to IV.28. When $V_a=V_o$, then

$$X_e = \frac{C_{K,f} - C_{K,eq}\left(1 + \frac{W}{55.5}\frac{\bar{C}_{DT}}{m}\right)}{\bar{C}_{DT}}$$

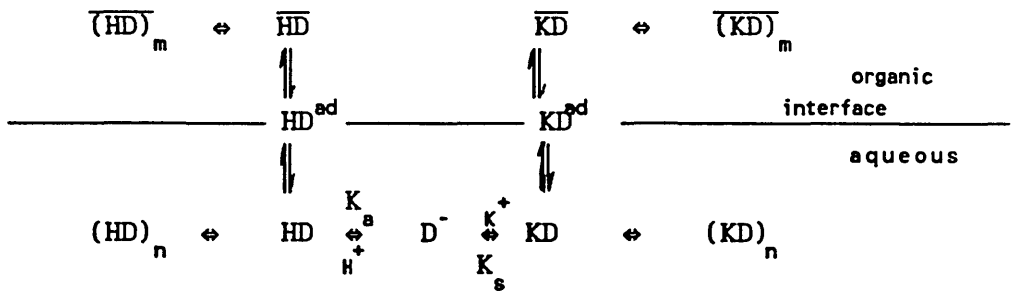
The values of X estimated above and listed in table F.21 differ from X_e by a factor given by:

$$\left(1 + \frac{W}{55.5}\frac{\bar{C}_{DT}}{m}\right) = 1.007$$

when m=7 is chosen, and recalling that $w=7xW^s \cong 7x4=28$ at I= 0.5 (figure IV.16). The refinement accounting for the solubilization of K^+ was therefore beyond the accuracy of these experiments, estimated at 10%. Analysis of K^+ by AES, in particular, showed around 15% deviations. These rather large errors were of similar order as the ratio of solubilization to exchange, estimated as follows

$$\frac{V_o \frac{\bar{C}_{DT}}{m}\frac{W}{55.5} C_{K,eq}}{V_o X \bar{C}_{DT}} = \frac{w C_{K,eq}}{55.5 m X}$$

On average, this ratio was around 6%. The results presented in this section were used together with the partition data reported in subsection IV.2.1 to estimate the K^+-sulphonate bulk ionization constant (K_s). The analysis was based on the following scheme. It included aggregation in the organic and the aqueous phases, ionization of the acid and the salt, and conversion between both. Adsorbed species were not considered as their concentrations were negligible in this context.



The ionization of both types of aqueous micelles is needed to complete the figure, and is presented below as eqns. IV.31, IV.32. The experiments were conducted at I=0.5M (HNO_3+ KNO_3) and at $\bar{C}_{DT,feed}$=0.1 $kmolm^{-3}$. From the following correlation of the partition data in subsection IV.2.1

$$\log P = 3.56 + 0.42 \log \bar{C}_{DT,feed} \quad (R=0.9859)$$

and the sulphonate balance about the system (eqn.IV.39), the aqueous solubility under these conditions was evaluated as follows

$$P = 1383 = \frac{\bar{C}_{DT}}{C_{DT}} = \frac{0.1 - C_{DT}}{C_{DT}}$$

The solubility was $C_{DT}=7.2.10^{-5} kmolm^{-3}$, higher than the CMC by more than one order of magnitude. The aqueous micellisation numbers (n) are generally much larger than those in organic diluents (m). The value of n for (K,H)DNNS was not found in the literature, and it was estimated as n≅100 from the data collected by Rosen (1978). The formula of DNNSA is $(C_9H_{19})\ C_{10}H_5SO_3H$. The most similar surfactants in Rosen's book (they however lack the naphthalenic group) follow:

Formula	n
$(C_{12}H_{25}SO_3^-)\ Mg^{++}$	107
$(C_{10}H_{21}SO_3^-)\ Mg^{++}$	103

In view of the relatively large value of n it seems justified to treat the aqueous micelles as a separate pseudo-phase. Thus the aqueous monomers may be assumed at a constant concentration similar to the CMC (Cussler, 1986), which is neglected in the balance IV.30 about the aqueous phase:

$$C_{DT} \cong n\,(C_{KP} + C_{HP}) + n\,(C^{-}_{KP} + C^{-}_{HP}) \qquad \text{(IV.30)}$$

The assumption was made that HD and KD aggregated in micelles of the same size, excluding one another from their respective micelles. The concentrations in the first term in eqn. IV.30 are those of K-salt micelles and acid micelles, respectively. The concentrations in the second term are those of *ionized* micelles, i.e. those pertaining to the species resulting from the pseudo-dissociations IV.31, IV.32:

$$(KD)_n \Leftrightarrow K^{+} + (KD)^{-}_n \;;\; K_s = \frac{C_K\, C_{KP}^{-}}{C_{KP}} \qquad \text{(IV.31)}$$

$$(HD)_n \Leftrightarrow H^{+} + (HD)^{-}_n \;;\; K_a = \frac{C_H\, C_{HP}^{-}}{C_{HP}} \qquad \text{(IV.32)}$$

Substitution of eqns. IV.31, IV.32 into eqn. IV.30 leads to

$$C_{DT} = n\,[C_{KP}(1 + K_s/C_K) + C_{HP}(1 + K_a/C_H)] \qquad \text{(IV.33)}$$

Monomeric organic concentrations can be safely neglected at $\overline{C}_{DT}$ = 0.1M, and micellar concentrations only are included in the sulphonate balance about the organic phase:

$$\overline{C}_{DT} \cong m\,(\overline{C}_{KP} + \overline{C}_{HP}) \qquad \text{(IV.34)}$$

Micellar concentrations relate to $\bar{C}_{DT}$ through the factor X evaluated above, thus

$$X = \frac{m\,\bar{C}_{KP}}{\bar{C}_{DT}}$$

$$1-X = \frac{m\,\bar{C}_{HP}}{\bar{C}_{DT}} \quad ; \qquad \text{(IV.35)}$$

and

$$\bar{C}_{KP} = \frac{X}{1-X}\,\bar{C}_{HP}$$

It was also assumed that X described the selectivity of the reagent in the aqueous phase as well as in the organic phase, thus the following equation applies to the former:

$$X = \frac{n\,(C_{KP} + \bar{C}_{KP})}{C_{DT}} \qquad \text{(IV.36)}$$

which upon substitution of eqn. IV.31 leads to eqn. IV.37

$$C_{DT} = \frac{n\,C_{KP}}{X}\,(1 + K_s/C_K) \qquad \text{(IV.37)}$$

Substitution of eqns. IV.35 and IV.37 into IV.34 leads to:

$$P = \frac{m\,\bar{C}_{HP}}{n(1+K_s/C_K)C_{KP}}\;\frac{X}{1-X} \qquad \text{(IV.38)}$$

The values of $\bar{C}_{DT}$ and C_{DT} after equilibration were not known, but they were related as follows:

$$\bar{C}_{DT,feed} = \bar{C}_{DT} + C_{DT} \qquad \text{(IV.39)}$$

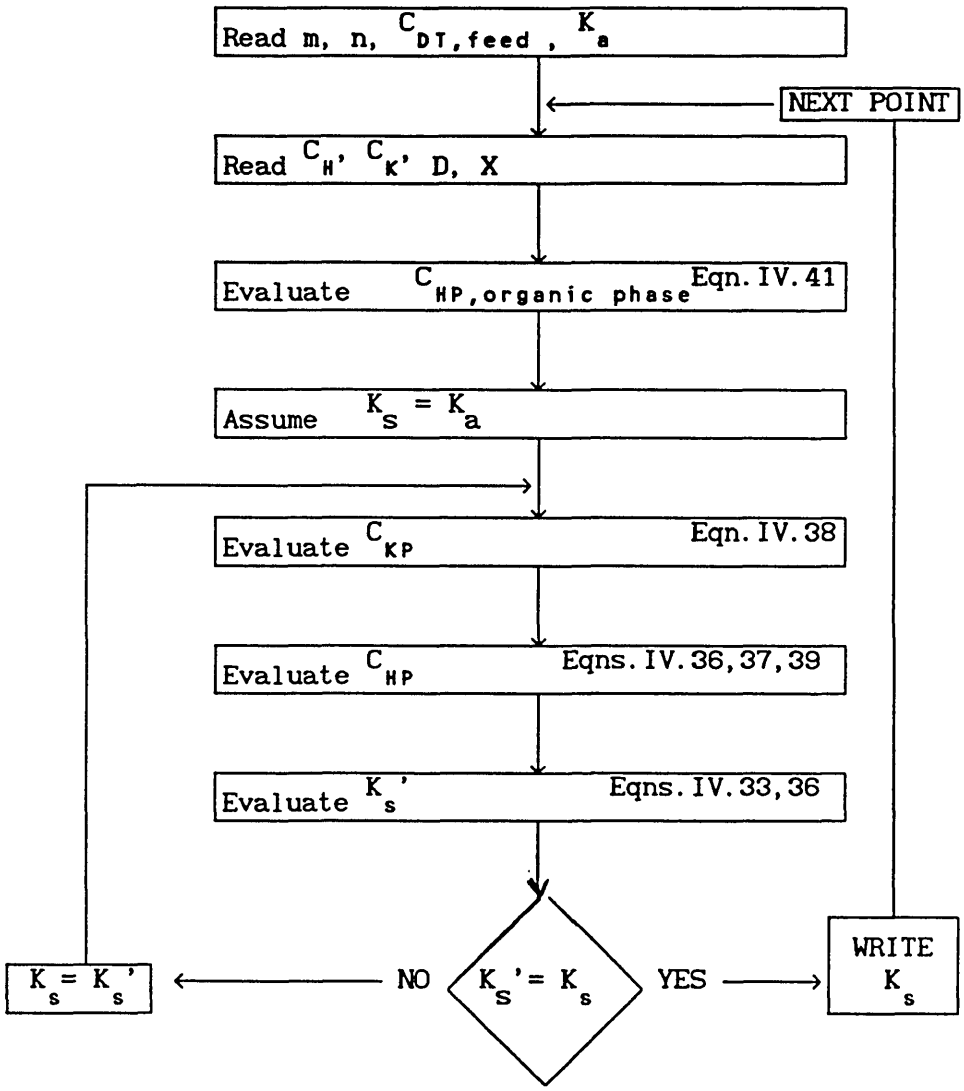
One more equation was needed for a complete set. It was provided by the cation exchange equilibrium. Defining the distribution coefficient of potassium as the ratio of total organic metal to total aqueous metal as follows:

$$D = \frac{m\,\bar{C}_{KP}+\bar{C}_{KD}}{C_K + n\,C_{KP} + C_{KD}} \cong \frac{m\,\bar{C}_{KP}}{C_K} \qquad \text{(IV.40)}$$

which, upon substitution of eqn. IV.35 leads to eqn. IV.41

$$D = \frac{m\,X}{1-X}\,\frac{\bar{C}_{HP}}{C_K} \qquad \text{(IV.41)}$$

The problem is now completely determined as 4 unknowns ($\bar{C}_{HP}$, C_{KP}, C_{HP}, and K_s) can be computed from the data via 4 independent equations (i.e. IV.41, IV.38, IV.36+IV.37+IV.39, and IV.33+IV.36). The preferred computational order is shown below. An average value of K_s = 0.31kmolm^{-3} was found for K_a =0.27 (i.e. pK_a=0.57; CRC, 1983-4), m=7, n=100, and $\bar{C}_{DT,feed}$ =0.1 kmolm^{-3}. The validity of the approach is however limited by the assumption made that dissociation constants K_a and K_s have the same value for both monomers and micelles (eqns. IV.31, IV.32). A more rigorous analysis requires consideration of aggregation parameters in the aqueous phase which were not available.


Read m, n, $C_{DT,feed}$, K_a
NEXT POINT
Read C_H, C_K, D, X
Evaluate $C_{HP,organic\ phase}$ Eqn. IV.41
Assume $K_s = K_a$
Evaluate C_{KP} Eqn. IV.38
Evaluate C_{HP} Eqns. IV.36,37,39
Evaluate K_s' Eqns. IV.33,36
$K_s'= K_s$
NO
YES
$K_s = K_s'$
WRITE K_s

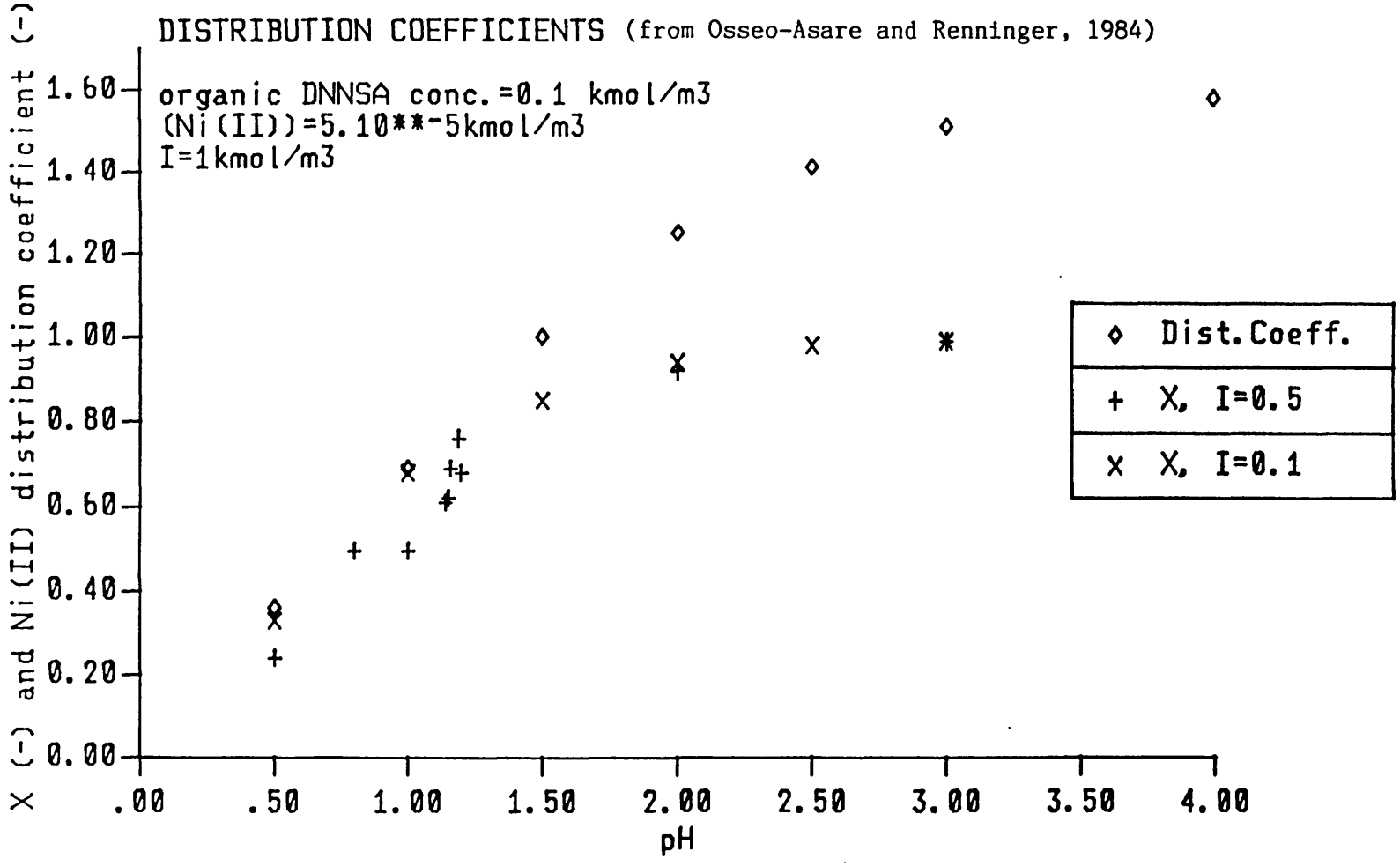


Figure IV.25 Effect of pH on the nickel loading and the K-H exchange by DNNSA. X at I=0.1 from Hogfeldt et al. (1978)

IV.4.2. (Ni-K-H)DNNS EXCHANGE EQUILIBRIUM

The Ni^{+2} extraction experiments presented in this section were planned in such a way that the results were amenable to treatment following van Dalen's method (1974a), which requires low loadings of the organic phase and a constant value of I. There was negligible demicellisation and the micelles extracted metal in 1/1 ratio under low loading conditions (van Dalen et al., 1974a; b; Danesi et al., 1976; Osseo-Asare and Renninger, 1984) thus the mean aggregation number (**m**) of reversed micelles can be estimated from the data. The following conditions were chosen:

i) $\bar{C}_{DT}$= 0.0667, 0.0813, 0.135, and 0.236 $kmolm^{-3}$,

ii) $[Ni^{2+}]= C_M = 1.10^{-4}$ to 5.10^{-2} $kmolm^{-3}$,

iii) $[H^+]= C_H$= 0.3 $kmolm^{-3}$, I=1.0 M(HNO_3+KNO_3)

Around 2/3 of the extractant was in the acidic form as indicated by X≅0.33 at this high acidity (subsection IV. 4.1). The results are listed in table F.22 and are shown as the distribution coefficient D_D vs $\bar{C}_{DT}$, with C_M as the parameter, in figure IV.26. The values listed are the average of duplicate experiments. From the regression of D_D on $\bar{C}_{DT}$ (column (e) in the table) it was found that D_D depended as $\bar{C}_{DT}^{1.03\pm0.13}$, with a relative error for the exponent of 12.6% at one standard deviation (*sd*). The low loadings generated under the conditions of these experiments ensured micelle/cation stoichiometries=1/1. The same D_D dependence on total micellar concentration and on $\bar{C}_{DT}$ was expected, because most DNNSA aggregated at $\bar{C}_{DT}$>>CMC. Lin (1984) presented data from which a D_D dependence as $\bar{C}_{DT}^{1.09}$ can be estimated.

When the loading increased, complexes with metal/DNNS monomer ratios larger than 1/7 occurred, and, at ultimate loading the ratio was 1/2 corresponding to $\overline{MD}_2$. Row (f) in table F.22 includes average values of D_D plus or minus one *sd* at each value of $\bar{C}_{DT}$ used. D_D did not follow any trend as C_M was changed at a given $\bar{C}_{DT}$. The largest dispersion of the data was around 15% D_D. Thus only mononuclear complexes of metal cation and micelles formed in

the concentration space investigated.

The global reaction of nickel extraction by (K,H)DNNS micelles is represented by eqn. IV.42, where physical solubilization was neglected. Mixed micelles are assumed to account for the split between HD and KD, quantified by the ratio X.

$$Ni(H_2O)_6^{++} + \overline{[K_X H_{(1-x)} D]_m} \Leftrightarrow 6\ H_2O + \overline{NiD_2[K_X H_{(1-X)} D]_{(m-2)}}$$

$$+ 2(1-X)\ H^+ + 2X\ K^+ \qquad \text{(IV.42)}$$

Using stability constants (K_h) from the literature (Smith and Martell, 1976) it was verified that hydrolysis of the nickel cation was negligible at the high acidity used in these experiments. Assuming full dissociation of $Ni(NO_3)_2$, the following balance applies to the aqueous feed

$$C_{M,feed} = C_M + C_{MOH}$$

where MOH^+ is the complex formed by hydrolysis:

$$M^{2+} + HO^- \Leftrightarrow MOH^+ \quad ; \quad K_h = \frac{C_{MOH}}{C_M C_{HO}} = 10^{3.7}$$

Using the ionic product of water it is found that:

$$C_M = \frac{C_{M,feed}}{1 + \frac{10^{-10.3}}{C_H}}$$

thus $C_M \cong C_{M,feed}$ in the range $0.5 \leq pH \leq 8$, $C_M \cong 0.95 C_{M,feed}$ at pH=9, and $C_M \cong 0.67 C_{M,feed}$ at pH=10. It was assumed for simplicity in eqn. IV.42 that K- and H-sulphonates were in the micelles in the same ratio as the monomers. This is only an approximation because the counterion type alters the hydrophobicity of the sulphonate, hence the adsorption efficiency and the aggregation status vary

(section II.1). The distribution coefficient was defined in the usual way as eqn. IV.43

$$D_D = \left(\frac{\bar{C}_M}{\gamma_M C_M} \right)_{equilibrium} \qquad (IV.43)$$

The LMA applied to reaction IV.42 is eqn. IV.44

$$K = \frac{\bar{C}_M \; C_H^{2(1-X)} \; C_K^{2X}}{\bar{C}_P \; C_M} \; \frac{\gamma_H^{2(1-X)} \; \gamma_K^{2X}}{\gamma_M} \qquad (IV.44)$$

The free micellar concentration at equilibrium ($\bar{C}_P$) is related to the formal sulphonate concentration by the balance IV.45

$$C_P \cong \frac{\bar{C}_{DT}}{m} - \bar{C}_M \quad ; \text{ at } \bar{C}_{DT} >> CMC \qquad (IV.45)$$

Combination of eqns. IV.43 through IV.45 leads to eqn. IV.46

$$D_D = \frac{1}{\gamma_H^{2(1-X)} \gamma_K^{2X}} \; \frac{K}{C_H^{2(1-X)} C_K^{2X}} \left(\frac{\bar{C}_{DT}}{m} - \bar{C}_M \right) \qquad (IV.46)$$

The factor grouping aqueous activities and K is a constant at given values of I and pH, thus eqn. IV.46 can be rewritten as eqn. IV.47.

$$\frac{D_D}{\bar{C}_{DT}} = \frac{\alpha}{m} - \alpha \frac{\bar{C}_M}{\bar{C}_{DT}} \qquad (IV.47)$$

Thus plots of $D_D/\bar{C}_{DT}$ versus $\bar{C}_M/\bar{C}_{DT}$ have slope of α, and m can be estimated from the y-intercept. The assumed constancy of α must

be verified after equilibration, because that condition will only be met when $\bar{C}_M << C_{H,feed}$ (eqn. IV.48)

$$C_{H,eq} = C_{H,feed} + 2(1-X)\,\bar{C}_M \qquad \text{(IV.48)}$$

The calculations are plotted as eqn. IV.47 in figure IV.26 and are listed in table F.23. The results at lowest loadings were omitted due to the rather large experimental errors involved in measuring very low metal complex concentrations. Linear regression of the data returned the following parameters:

$$\frac{\alpha}{m} = 3.32$$

$$\alpha = 0.434.10^{-3}\text{ppm}\ \frac{58690\text{g kmol}^{-1}}{\text{ppm}} = 25.48$$

$$\text{thus } m = \frac{25.48}{3.32} \cong 7.7$$

This estimate of the aggregation number agrees well with the findings of van Dalen et al. (1974a), Chiarizia et al. (1976), and Zheng and Osseo-Asare (1987). It was verified with eqn. IV.48 that α was indeed almost constant. At the highest loadings, $C_{H,eq}$ varied within 8% of the feed value.

The complexation equilibrium constant (K) was estimated from the value of α. The activity coefficients in eqn. IV.46 were estimated from the Davies correlation (Robinson and Stockes, 1959):

$$-\log \gamma = \frac{1}{2} z_1 z_2 \left(\frac{\sqrt{I}}{1+\sqrt{I}} - 0.20\ I \right) \qquad \text{(IV.49)}$$

The value of the constant resulted K=0.195. Lin (1984) estimated double this value. The effect of pH on D_D in this chemical system has been reported in the literature (Osseo-Asare and Renninger, 1984) hence it was not investigated in this work. This effect is discussed in section V.3.

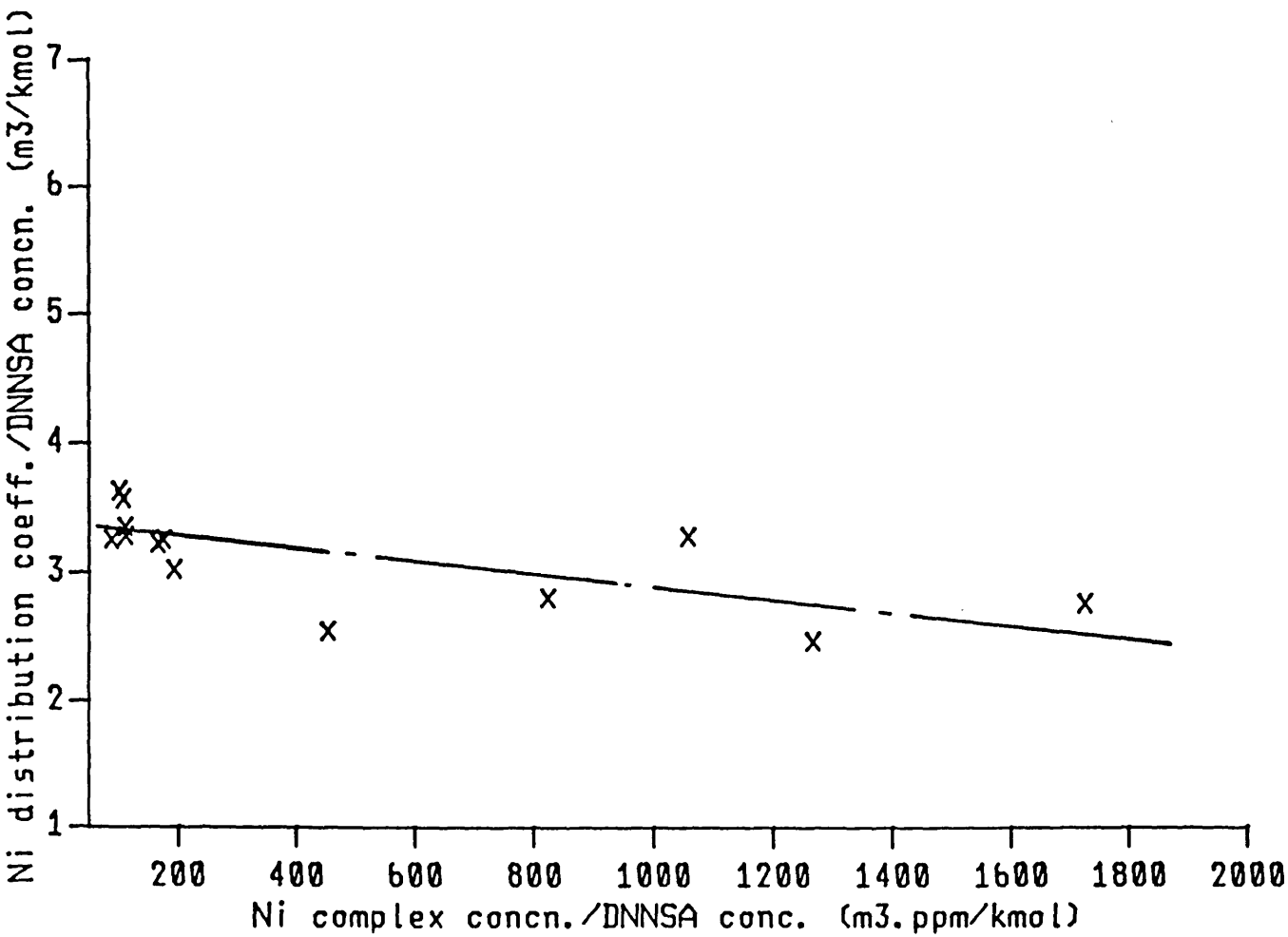


Figure IV.26 Ni(II) distribution data fitting to estimate the aggregation number of DNNSA.

IV.5. EQUILIBRIUM OF Ni(II) EXTRACTION BY LIX63.

The effect of changing pH and LIX63 concentrations in hexane ($\bar{C}_{LT}$) on the equilibrium distribution of metal between 0.5M KNO_3 and organic phases was investigated. The experimental details were presented in section III.6. The distribution coefficients (D_L) were calculated from the metal analysis in both phases in the usual way. The dependency of D_L on $\bar{C}_{LT}$ is shown in figure IV.27 from the data listed in table F.24. The values of D_L were in the range 1.10^{-3} to 1.10^{-2}, similar to those values for the distribution of copper (Zapatero et al., 1987) and of nickel (Renninger and Osseo-Asare, 1983).

Linear regression of the data showed that D_L depended as $\bar{C}_{LT}^{0.48}$, with R=0.9669. The points shown in figure IV.27 aligned almost parallel to the reference line drawn with slope=0.5.

The effect of changing acidity on D_L is shown in figure IV.28 from the data listed in table F.25. D_L was found to rise slightly as pH was increased from 0.5 to 2.5.

The possible simultaneous extraction of potassium was investigated, but no traces of this metal were detected in the strippates.

The dependence of D_L as $\bar{C}_{LT}^{0.48}$ suggests an exponent 0.5, and that most LIX63 was as dimers, in agreement with the VPO work of Zheng and Osseo-Asare (1987). Eqn. IV.50 describes the dimerization

$$2\ \overline{H_2L} \Leftrightarrow (\overline{H_2L})_2 \quad ; \qquad K_d = \frac{\bar{C}_2}{\bar{C}_1^{\,2}} \qquad \text{(IV.50)}$$

Thus the oxime balance about the organic phase is

$$\bar{C}_{LT} = \bar{C}_1 + 2\,\bar{C}_2 = 2\,\bar{C}_2 + (\bar{C}_2/K_d)^{1/2} \cong 2\,\bar{C}_2 \qquad \text{(IV.51)}$$

where the approximation is only valid at relatively high values of

$\bar{C}_{LT}$ and for large values of the dimerization constant. It follows from considering the aggregates as a miscible pseudo-phase, thus it is a good approximation for larger aggregates as discussed above. It provides however a facile explanation to the half order dependency of D_L on $\bar{C}_{LT}$ observed and it will be used in the analysis leading to eqn. IV.60.

The oxime partitions between organic and aqueous phases with partition coefficient P_L. Aqueous solubilities of LIX63, however, have not been measured in this work. Further, it is not known whether the oxime dimerizes in the aqueous phase. The aqueous solubility was considered extremely low under the chosen conditions of low $\bar{C}_{LT}$ and high I, thus reactions in the aqueous phase will not be included in the analysis.

The σ measurements shown in subsection IV.1.2 indicate adsorption at the o/w interface. Calculations with the data of Al-Diwan et al. (1977) lead to the conclusion that Γ_L was approximately constant in the concentration range used (figure IV.4). The interfacial concentration of extractant (C_1^{ad}) was thus taken as a constant, given by eqn IV. 52 at large values of $\bar{C}_{LT}$:

$$\overline{H_2L} \Leftrightarrow H_2L^{ad} \quad ; \qquad C_1^{ad} = \frac{a\,\bar{C}_{LT}}{1 + b\,\bar{C}_{LT}} \qquad \text{(IV.52)}$$

The EM work of Lin and Osseo-Asare (1984) allows the dissociation of the adsorbed oxime to be safely neglected under the present conditions of pH and I. The pH dependence of D_L suggested that Ni^{2+} was not extracted by cation exchange only, but also by solvation. Both types of mechanisms were proposed for the extraction of Cu^{2+} by LIX63 (Zapatero et al., 1987). There is experimental evidence that LIX63 loads H_2SO_4 (Hummelstedt, 1977). This uptake was found highest for LIX63 and SME529 among six hydroxyoxime -based extractants used as-received by Al-Diwan et al. (1977). Those authors hypothesized that the species $H_3R^+HSO_4^-$ resulted from the interaction between extractant and acid. H_2SO_4 was also extracted by KELEX 100 (Bauer and Chapman, 1976). It seemed therefore reasonable to assume that other mineral acids are likewise

extracted by hydroxyoximes. This assumption was confirmed by HPLC analysis of LIX63 solutions equilibrated with 0.1N HNO_3. The following qualitative data (chart divisions vs concentrations, Table IV.c) indicates a linear relationship between NO_3^- concentration in the organic phase and $\overline{C}_{LT}$. Duplicates are sometimes listed.

Table IV.c

$\overline{C}_{LT} \times 10^3 kmol\,m^{-3}$	20	10	7	5	1
1^{st} peak	20/29	21	18/14	16	3
2^{nd} peak	9/9	5	4/3	2.5	0.5

Two reaction schemes are proposed based on the above discussion, one consisting of half-neutralization by aqueous anions and cation exchange (A), and the other consisting of neutralization and solvation (B).

(A) EXCHANGE.

$$NO_3^- + H_2L^{ad} \Leftrightarrow NO_3^-.H_2L^{ad} \qquad \text{(IV.53a)}$$

$$M^{2+} + NO_3^-.H_2L^{ad} \Leftrightarrow M(NO_3).HL^{ad} + H^+ \qquad \text{(IV.53b)}$$

$$M(NO_3).HL^{ad} + (\overline{H_2L})_2 \Leftrightarrow \overline{M(NO_3).HL\,(H_2L)_2} \qquad \text{(IV.53c)}$$

A disproportionation follows to yield the 1:2 complex:

$$\overline{M(NO_3).HL\,(H_2L)_2} \Leftrightarrow \overline{M(NO_3).HL\,(H_2L)} + \overline{H_2L} \qquad \text{(IV.53d)}$$

The superscript "ad" identifies species adsorbed at the o/w interface, M^{2+} is the Ni(II) cation where the six molecules of hydration water were not shown for clarity, and the bar over a species has the usual meaning. The LMA constant for the 4-step reaction IV.53a,b,c,d is K_e, defined as follows

$$K_e = \frac{\bar{C}_{Me}\ C_H\ \bar{C}_1}{C_M\ C_a\ C_1^{ad}\ \bar{C}_2} = K_a K_b K_c K_d \qquad \text{(IV.54)}$$

where C_a is the concentration of the main aqueous anion (i. e. nitrate). Substitution of eqns. IV.50, IV.51 into eqn. IV. 54 leads to the distribution coefficient due to exchange:

$$D_e = \frac{\bar{C}_{Me}}{C_M} = \frac{K_d^{1/2}\ K_e\ C_1^{ad}}{\sqrt{2}} \frac{C_a\ \bar{C}_{LT}^{1/2}}{C_H} \qquad \text{(IV.55)}$$

(B) SOLVATION

$$2\ NO_3^- + H_2L^{ad} \Leftrightarrow (NO_3^-)_2.H_2L^{ad} \qquad \text{(IV.56a)}$$

$$M^{2+} + (NO_3^-)_2.H_2L^{ad} \Leftrightarrow M(NO_3)_2.H_2L^{ad} \qquad \text{(IV.56b)}$$

$$M(NO_3)_2.H_2L^{ad} + (\overline{H_2L})_2 \Leftrightarrow \overline{M(NO_3)_2(H_2L)_3} \qquad \text{(IV.56c)}$$

$$\overline{M(NO_3)_2(H_2L)_3} \Leftrightarrow \overline{M(NO_3)_2(H_2L)_2} + \overline{H_2L} \qquad \text{(IV.56d)}$$

The equilibrium constant for the global reaction IV.56 is K_{so}:

$$K_{so} = \frac{\bar{C}_{Ms}\ \bar{C}_1}{C_M\ C_a^2\ C_1^{ad}\ \bar{C}_2} = K'_a\ K'_b\ K'_c\ K'_d \qquad \text{(IV.57)}$$

The distribution coefficient due to solvation is defined similarly as before:

$$D_{so} = \frac{\bar{C}_M^s}{C_M} \qquad \text{(IV.58)}$$

$$= \frac{K_d^{1/2} \quad K_{so} C_1^{ad} \quad C_a^2 \, \bar{C}_{LT}^{1/2}}{\sqrt{2}} \qquad \text{(IV.59)}$$

We note on passing that the same metal/oxime ratio (1:2) is proposed for both types of complexes, the concentration of which are $\bar{C}_{Me}$ and $\bar{C}_{Ms}$, respectively. The neutralization (eqn. IV.56a) or half-neutralization (eqn. IV.53a) of Ni^{2+} charges by NO_3^- has the same effect on the observed pH dependences as the hydrolysis of the cation. Hydrolysis changes the net charge, thereby it alters the apparent reaction orders (Danesi and Chiarizia, 1980) and also the pH dependence of D_L. At pH ≤ 3 and $I=[NO_3^-]=0.5$ as used in this work, NO_3^- will coordinate with Ni(II) in preference to HO^-, as the above calculations with the hydrolysis stability constant prove. The EM experiments of Lin and Osseo-Asare (1983) indicated that the interfacial charge of LIX63 solutions drops was negligible. Thus the proportions $K_a/K_b/K_c/K_d$ and $K'_a/K'_b/K'_c/K'_d$ must be such that the concentration of adsorbed anionic species be low.

The total (observed) distribution coefficient was the sum from both effects, i.e.:

$$D_L = D_e + D_{so}$$

which can be rewritten using eqns. IV.55 and IV.59 as follows

$$D_L = \frac{(2 K_d)^{1/2}}{2} \; C_a \, C_1^{ad} \left[\frac{K_e}{C_H} + C_a K_{so} \right] \bar{C}_{LT}^{1/2} \qquad \text{(IV.60)}$$

Figure IV.28 and eqn. IV.60 suggest that as pH was increased solvation became a less important and exchange a more important extraction mechanism. The $\bar{C}_{LT}^{1/2}$ dependence of D_L predicted by eqn. IV.60 derives from the experimental evidence of LIX63 dimerization and agrees well with the dependence shown in figure IV.27: $D_L=0.103 \; \bar{C}_{LT}^{0.48}$. The constants in eqn. IV.60 were lumped in the coefficient 0.103. They are evaluated below. The pH dependence of D_L can be approximated by a line of equation:

$$D_L = a + \frac{b}{x} \qquad \text{(IV.61)}$$

where $x = C_H$,

$$a = \frac{(2 K_d)^{1/2}}{2} K_{so} a_1^2 C_1^{ad} \bar{C}_{LT}^{1/2}, \text{ and}$$

$$b = \frac{(2 K_d)^{1/2}}{2} K_e C_a C_1^{ad} \bar{C}_{LT}^{1/2}$$

The parameters a=0.005 and b=0.0001 in eqn. IV.61 gave a good fit of the data, as shown by the solid line in figure IV.28. From these values, the constants were evaluated as follows:

$$K_{so}/K_e = 100 \qquad \text{(IV.62)}$$

$$K_d^{1/2} K_e C_1^{ad} = 28.2.10^{-4} \text{ kmol}^{-1}\text{m}^{3/2}$$

for $C_a = I = 0.5$. These estimated values are free from the approximation error introduced in eqn. IV.51. From the ratio of the equilibrium constants IV.62 one can estimate that the concentrations of both types of complexes are similar (i.e. $\bar{C}_{Ms} = \bar{C}_{Me}$) at pH ≅ 1.7. The values of the ratio $\bar{C}_{Me}/\bar{C}_{Ms}$ are listed in table F.25. The approximation in eqn. IV.51 leads to eqn. IV.64

$$\frac{2 D_L}{C_a C_1^{ad} \left[\frac{K_e}{C_H} + C_a K_{so}\right]} \equiv \alpha \equiv (2\bar{C}_{LT} K_d)^{1/2} \cong 2\bar{C}_2/\bar{C}_1 \qquad \text{(IV.64)}$$

$$\equiv \beta \equiv (\bar{C}_{LT}/\bar{C}_1 - 1) = \left(\bar{C}_2/\bar{C}_1\right) 2 \qquad \text{(IV.65)}$$

whereas eqn. IV.65 results when no approximation is made when replacing $\bar{C}_2/\bar{C}_1$ in eqn. IV.54. From both RHS's, $K_d \cong 5000$ was estimated by minimizing the ratio α/β.

The ratios α/β are shown in figure IV.29 versus $\bar{C}_{LT}$. The deviation from 1 was around 10% as $\bar{C}_{LT}$ was reduced down to 0.002M. The monomer concentrations predicted by K_d=5000 are also shown vs $\bar{C}_{LT}$ in the figure. $\bar{C}_1$ was 7% $\bar{C}_{LT}$ at the upper end of the range.

The values of $\bar{C}_2/\bar{C}_1$ are also shown in figure IV.29. The results cluster on the same line (in a different scale) as the $\bar{C}_1$ values, with slope 0.5. D_L depends on $\bar{C}_2/\bar{C}_1$, therefore the slope 0.5 is consistent with the results shown in figure IV.27.

An attempt was made to estimate K_d from the distribution data without making assumptions concerning the speciation. In eqn. IV .60, rewritten as eqn. IV.66:

$$D_L = C_a \, C_1^{ad} \left[\frac{K_e}{C_H} + C_a K_{so} \right] \bar{C}_2/\bar{C}_1 \qquad \text{(IV.66)}$$

$\bar{C}_2$ was replaced by $K_d \bar{C}_1^2$, and $\bar{C}_1$ by eqn. IV.67, which results from eqn. IV.50 and the balance IV.51 when the assumption of complete dimerization is relaxed.

$$\bar{C}_1 = \frac{-1 \pm \sqrt{1 + 8 K_d \bar{C}_{LT}}}{4 K_d} \qquad \text{(IV.67)}$$

Only the positive root of eqn. IV.67 was used. Eqns. IV.66 and IV.67 are non-linear in K_d. They were solved using Newton's iteration for the data listed in tables F.24 and F.25 The average value of K_d was 158, much lower than that estimated above from the assumption of complete dimerization. For LIX65N, $K_d \cong 126$ was reported by Akiba and Freiser, in acceptable agreement with the estimate obtained from this approach. (1982).

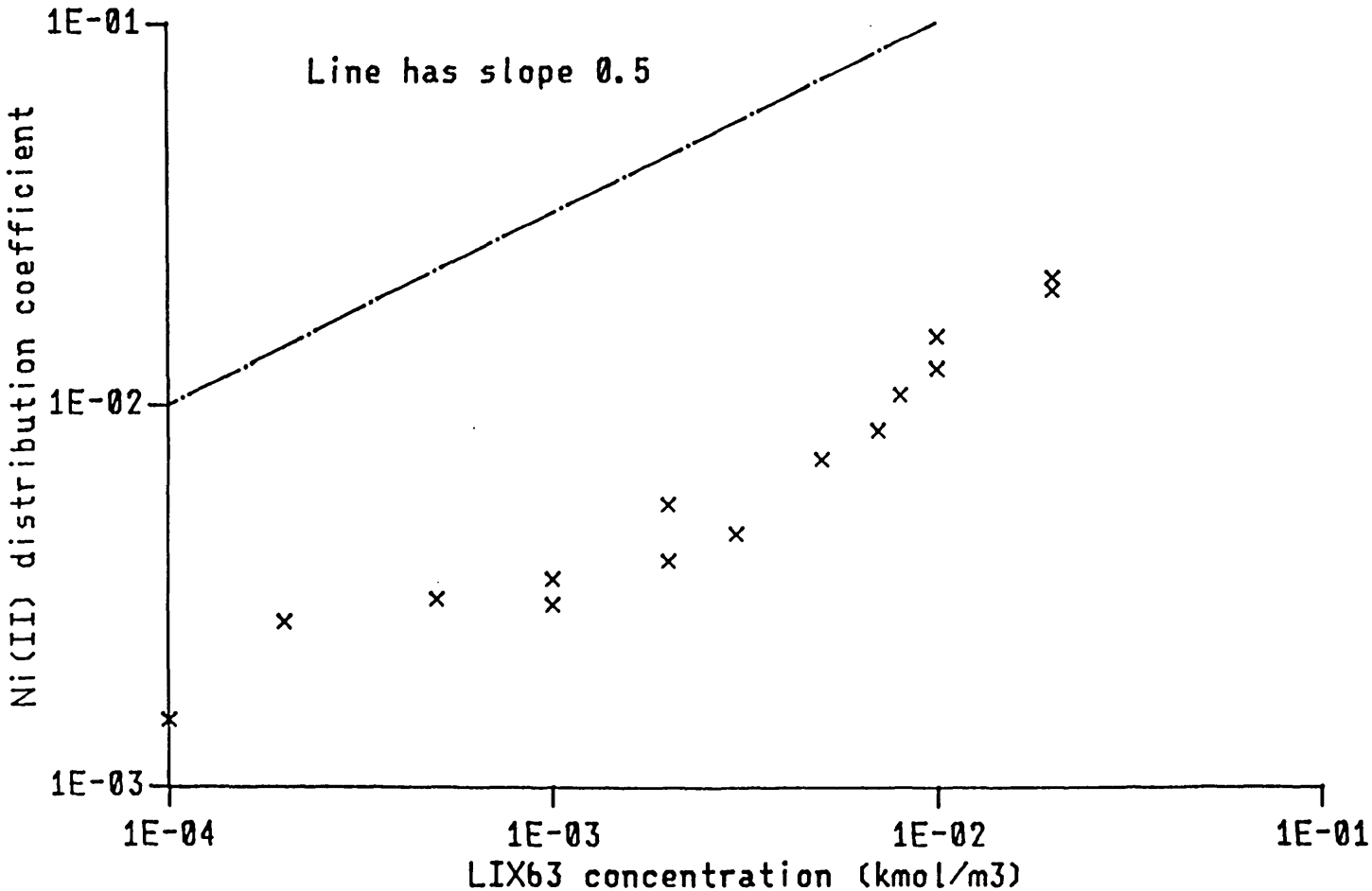


Figure IV.27 Distribution coefficients of Ni(II) with LIX63.
Feed Ni(II) conc.=0.005M, I=0.5M(HNO3+KNO3), pH=2.5

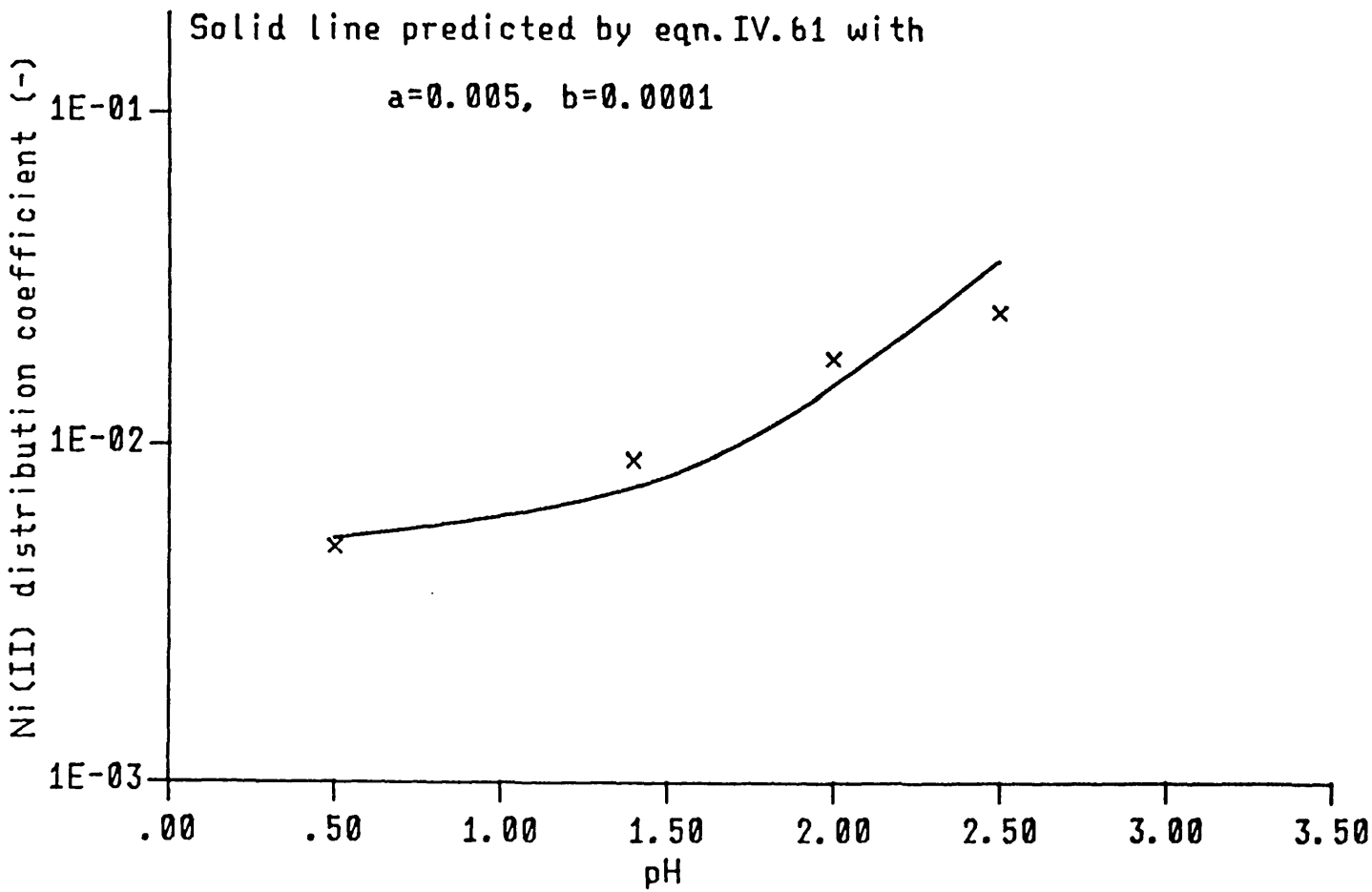


Figure IV.28 Effect of pH on Ni(II) loading by LIX63
(Ni(II)=5.10**-3kmol/m3, I=0.5M(HNO3+KNO3), (LIX)=1.10**-2kmol/m3.

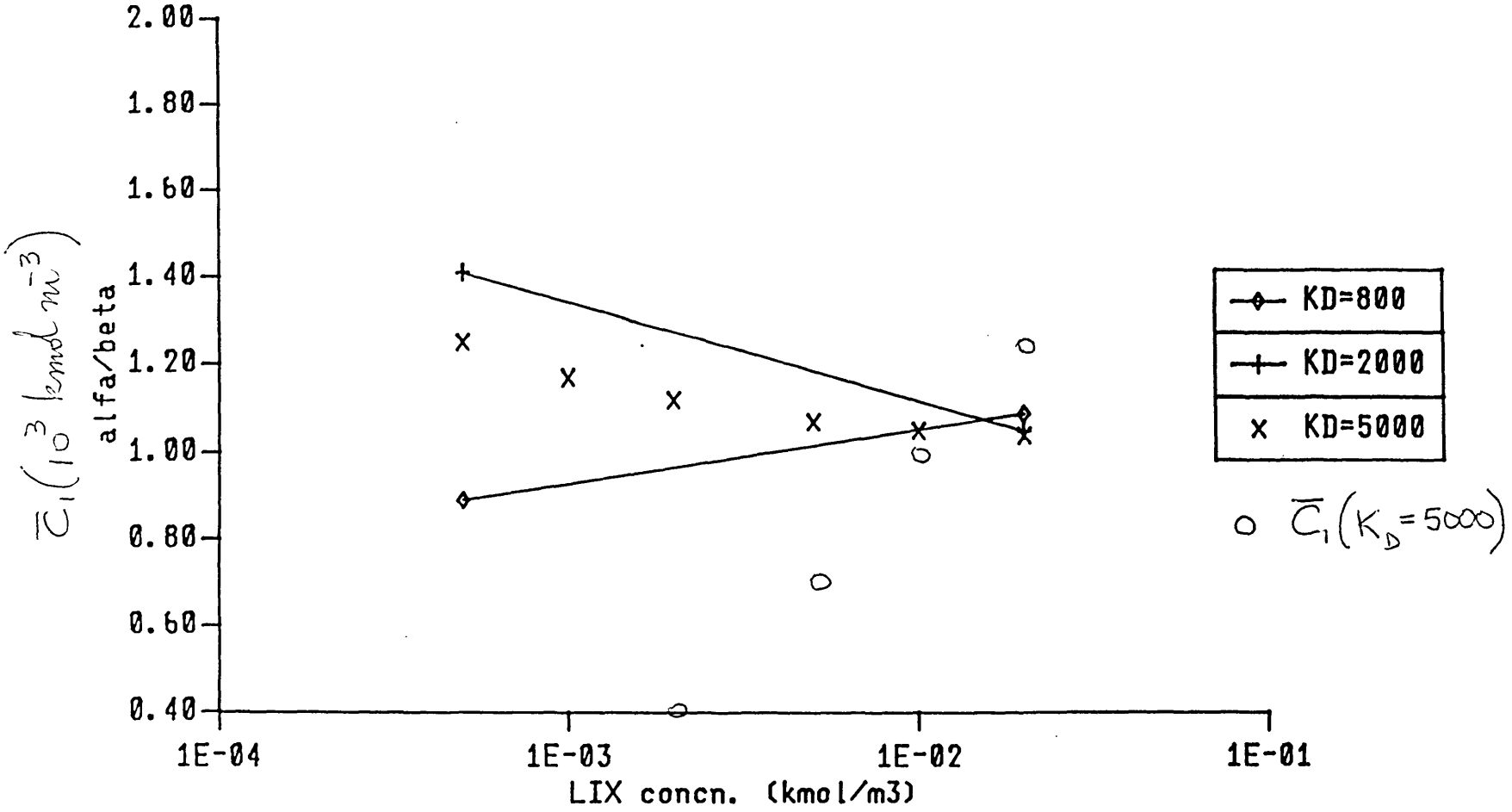


Figure IV.29 Estimation of LIX63 dimerization constant by minimizing the error in the species balance approximation.

IV.6. EQUILIBRIUM OF Ni(II) EXTRACTION BY DNNSA-LIX63 MIXTURES

The distribution coefficients (D_M) shown in figure IV. 30 vs $\bar{C}_{DT}$ were determined at $\bar{C}_{LT}=5.10^{-3}$kmolm^{-3} and 1.10^{-3} kmolm^{-3}. For comparison, the values of D_D (i.e. the coefficients with DNNSA alone) are also shown. The σ vs $\bar{C}_{DT}$ curve shown corresponds to $\bar{C}_{LT}=5.10^{-3}$kmolm^{-3}, and it was included in the graph to indicate that the sudden increase in the observed values of D_M roughly corresponded to the CMC of the reagents mixture. A similar agreement was previously reported by Asseo-Asare and Keeney (1980 b).The data are listed in table F.26.

Unlike the complexation of Ni(II) by KD, where the stoichiometric reaction is as follows (Chiarizia et al., 1976; counter-ions are sometimes omitted for simplicity):

$$M^{z+} + \bar{D}_7 \Leftrightarrow \overline{MD_z.D_{(7-z)}} + zK^+$$

the complex extracted by mixtures could not have seven sulphonates associated with one metal nucleus. This conclusion follows from the data in tables IV.4, IV.5. The concentration of complex at equilibrium ($\bar{C}_{M,eq}$) was always higher than the concentration of DNNSA micelles at the same $\bar{C}_{DT}$ levels but with no LIX63 in solution (i.e. $\bar{C}_{DT}/7$).

The average stoichiometry determined by Osseo-Asare and Renninger (1984) using the Method of Continuous Variation was M/D/L =1/2/3 (eqn. IV.68) at $\bar{C}_{DT}+\bar{C}_{LT}$=constant=0.01 kmolm^{-3} and I=1.0 M KNO_3. Those authors found that D_M peaked at $\bar{C}_{DT} \cong 4.10^{-3}$ kmolm^{-3}. In this work, D_M was seen to increase without peaking up to $\bar{C}_{DT}=5.10^{-3}$kmolm^{-3} at $\bar{C}_{LT}=5.10^{-3}$kmolm^{-3}.

$$M^{2+} + \overline{D_2.3L} \Leftrightarrow \overline{MD_2.3L} + 2\,(H^+,K^+) \qquad \text{(IV.68)}$$

It was noted that $\bar{C}_{M,eq}$ was higher than $\bar{C}_{DT}/2$ at low values of $\bar{C}_{DT}$ and $\bar{C}_{LT}=1.10^{-3}$ kmolm^{-3} and at all values of $\bar{C}_{DT}$ at $\bar{C}_{LT}=5.10^{-3}$kmolm^{-3}. This observation indicates that there were complexes with M/D ratios higher than 0.5, such as $\overline{MDL}$, and possibly $\overline{ML_2}$, or $\overline{ML_2.L}$. The speciation analysis (section V.7) indicates

that L and DL are the two chief species at $\bar{C}_{DT} < 1.10^{-3}$ kmolm^{-3}. Such possible sulphonate-free complexes were not considered by Zheng and Osseo-Asare (1987) in their speciation analysis, nor by Osseo-Asare and Renninger earlier (1984). The latter authors worked at higher values of $\bar{C}_{DT}$, where the values of M/D were closer to 0.5.

The average 1/2/3 stoichiometry of the complex (Osseo- Asare and Renninger, 1984) suggests that added LIX63 breaks down the DNNSA micelles, possibly through aggregation as $\overline{D.L}$ oligomers as proposed by Keeney and Osseo-Asare (1982), or due to solubilization of LIX63 into the micellar palisade followed by chelation of the metal solubilized in the micellar core and the subsequent destruction of the micelle (Osseo-Asare and Keeney, 1980). This argument seems important because it can explain why D_M increases abruptly as shown in figure IV.30. Help from thermodynamics will be summoned below in an attempt to describe with more rigour these effects. The organic phase speciation was estimated using the model by Zheng and Osseo-Asare (1987) as detailed in section V.7.

Metal complexation with simultaneous micelle breakage may be represented by eqns. IV.69, IV.70

$$\bar{D}_7 + 3\,\bar{L} \Leftrightarrow \overline{D_2.3L} + 5\,\bar{D}\ ; \qquad K_A = \frac{\bar{C}_{D23L}\,\bar{C}_D^{\,5}}{\bar{C}_{D7}\,\bar{C}_L^{\,3}} \qquad \text{(IV.69)}$$

$$M^{2+} + \overline{D_2.3L} \Leftrightarrow \overline{MD_2.3L} + 2\,K^+\ ; \qquad K_e = \frac{\bar{C}_M\,\bar{C}_K^{\,2}}{C\bar{C}_{M\,D23L}} \qquad \text{(IV.70)}$$

It was assumed in eqn.IV.70 that all the extractant was as the K-soap, a good approximation at pH≥2.5. Zheng and Osseo-Asare (1987) evaluated the constants as $K_A \cong 1.27 \cdot 10^{-13}$ and $K_e \cong 284$. Adding reactions IV.69 plus IV.70 leads to:

$$M^{2+} + \bar{D}_7 + 3\,\bar{L} \Leftrightarrow \overline{MD_2.3L} + 5\,\bar{D} + 2\,K^+ \qquad \text{(IV.71)}$$

Table IV.4 Equilibrium distribution of Ni(II) at $\bar{C}_{LT}=1.10^{-3}$ kmolm^{-3}, I=0.5, pH_{feed}=2.5.

$\bar{C}_{DT}x10^3$	$\frac{\bar{C}_{DT}}{2}x10^3$	$\frac{\bar{C}_{DT}}{7}x10^3$	D_M	$\bar{C}_{M,eq}\ x10^3$
kmolm^{-3}	kmolm^{-3}	kmolm^{-3}		kmolm^{-3}
0.1	0.005	0.0014	0.0034	0.017
0.5	0.025	0.0071	0.012	0.060
1.	0.05	0.014	0.035	0.17
2.	0.1	0.029	0.018	0.09
3.	0.15	0.043	0.031	0.15
5.	0.25	0.071	0.080	0.37
10.	0.5	0.14	0.114	0.51
50.	2.5	0.71	0.52	1.7

Table IV.5 Equilibrium distribution of Ni(II) at $\bar{C}_{LT}=5.10^{-3}$ kmolm^{-3}, I=0.5, pH_{feed}=2.5.

$\bar{C}_{DT}x10^3$	$\frac{\bar{C}_{DT}}{2}x10^3$	$\frac{\bar{C}_{DT}}{7}x10^3$	D_M	$\bar{C}_{M,eq}\ x10^3$
kmolm^{-3}	kmolm^{-3}	kmolm^{-3}		kmolm^{-3}
0.1	0.005	0.0014	0.0062	0.031
0.5	0.025	0.0071	0.0138	0.068
1.	0.05	0.014	0.0225	0.11
2.	0.1	0.029	0.033	0.158
3.	0.15	0.043	0.052	0.246
5.	0.25	0.071	0.054	0.256
10.	0.5	0.14	0.44	1.53
50.	2.5	0.71	1.38	2.9

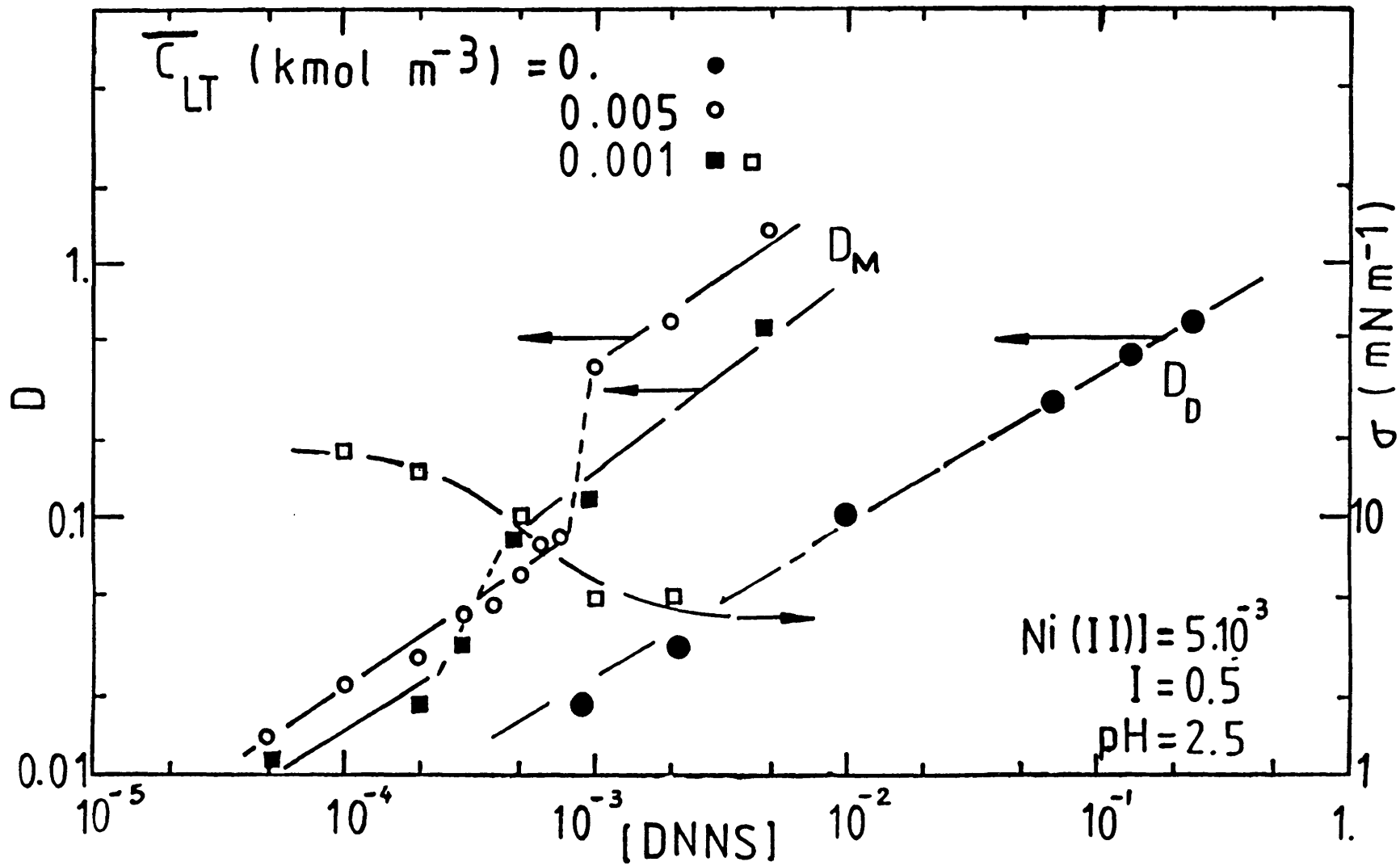


Figure IV.30 Synergic extraction of nickel by DNNSA-LIX63 mixtures.

The equilibrium constant for this global reaction is

$$K_2 = D_M \frac{C_K^2}{K_p \bar{C}_D^{\,2} \bar{C}_L^{\,3}} = K_A K_e \qquad \text{(IV.72)}$$

where the distribution coefficient is $D_M = \bar{C}_M / C_M$ and K_p is the aggregation constant of the DNNSA micelle ($\bar{D}_7$), $6.47.10^{26}$ (Zheng and Osseo-Asare, 1987). Micelles are involved in reaction IV.69 because the region considered now is that at $\bar{C}_{DT} \geq$CMC. From the speciation analysis it is expected that $\bar{C}_D$ and $\bar{C}_L$ will not vary much as $\bar{C}_{DT}$ is changed, and that their respective changes be in opposite directions (section V.7), thus a *pseudo* distribution coefficient K_2' may be defined as follows

$$K_2' = K_2 K_p \bar{C}_D^{\,2} \bar{C}_L^{\,3} = D_2 C_K^2 \qquad (\bar{C}_{DT} > \text{CMC}) \qquad \text{(IV.73)}$$

where $D_2 = D_M$ in this region. There are few micelles at $\bar{C}_{DT}$<CMC, thus in that region only reaction IV.70 need be considered, and a pseudo distribution coefficient may be similarly defined in this case as follows:

$$K_1' = K_e \bar{C}_{D23L} = D_1 C_K^2 \qquad (\bar{C}_{DT} < \text{CMC}) \qquad \text{(IV.74)}$$

In this region D_M is named D_1, and $\bar{C}_{D23L}$ increases appreciable as $\bar{C}_{DT}$ is increased (section V.7) thus K_1' will vary accordingly. Pairs of D_1, D_2 values need be compared at given values of $\bar{C}_{DT}$ thus the D_1 vs $\bar{C}_{DT}$ line was projected beyond the CMC and the extrapolated values were used to calculate K_1'. The results are listed in table F.27 at $\bar{C}_{LT} = 5.10^{-3}$kmolm^{-3}. The ratio K_2'/K_1' was almost constant because the slope of the D_M vs $\bar{C}_{DT}$ graph was roughly the same below (i.e. D_1) and above (i.e. D_2) the CMC. The Gibbs free energy change involved in reaction IV.70 is given by:

$$\Delta G_1 = \Delta G_1^o + RT \ln K_e \qquad \text{(IV.75)}$$

At equilibrium, it is expected that

$$\Delta G_1^\circ = -RT \ln K_1 = \Delta H_r^\circ - T\Delta S_r^\circ \qquad \text{(IV.76)}$$

No demicellisation or water desolubilization are involved in reaction IV.70, thus only heats and entropies of chemical reaction are included in eqn. IV.76. When eqns. IV.69, IV.70 are combined and the water solubilized within the micellar cores is considered, then reaction IV.77 applies

$$M^{2+} + \overline{D_7.3L.xH_2O} \Leftrightarrow \overline{MD_2.3L} + \overline{D_5.yH_2O} + (x-y)H_2O + 2\,K^+ \qquad \text{(IV.77)}$$

Two additional terms must be included in this case in the expression for the standard free energy, one that corresponds to the (x-y) water molecules desolubilized by a micelle (ΔG_d°), and the other due to the removal of two DNNSA monomers from the micelle (ΔG_{75}°). Thus

$$\Delta G_2^\circ = -RT \ln K_2 = \Delta H_r^\circ - T\Delta S_r^\circ + \Delta G_d^\circ + \Delta G_{75}^\circ \qquad \text{(IV.78)}$$

ΔG_d° depends on the work done by the system to loose core interfacial area (Aveyard, 1987) and on the *decrease* in entropy resulting from the solubilized water returning to the bulk aqueous phase. In other words,

$$\Delta G_d^\circ = \Delta H_d^\circ + T\,\Delta S_d^\circ$$

Subtracting eqn. IV.76 from eqn. IV.78 leads to

$$\Delta G^\circ = \Delta G_2^\circ - \Delta G_1^\circ = \Delta G_d^\circ + \Delta G_{75}^\circ = -RT \ln \frac{K_2}{K_1} \qquad \text{(IV.79)}$$

The thermodynamic parameters ΔH_d°, ΔS_d°, and ΔG_{75}° need be evaluated to allow predictions of the synergic ratio K_2/K_1 in eqn. IV.79. The interfacial tension σ is the work required to form a unit area of interface (Aveyard, 1987), thus

$$\sigma = \left(\frac{\partial \Delta H_d^o}{\partial A} \right)_{T,P,composition} \qquad (IV.81)$$

where A is the palisade-micellar core interfacial area. Eqn. IV.81 can be used to estimate the work required to increase the interfacial area within micelles by ΔA, i.e.

$$\Delta H_d^o = \sigma \Delta A \qquad (IV.82)$$

It is noted that $\Delta A<0$ on water desolubilization. ΔA can be evaluated in two ways. One way is from the direct measurement of micelles. The hydraulic radius (r_h) of a water saturated (at $I \cong 0$) reversed DNNSA micelle was on average 45/2Å (subsection IV.1.4.). Subtracting from that value the length of a DNNSA monomer, d=8Å (van Dalen et al., 1974a), the core radius is

$$r_c = r_h - d = 45/2 - 8 = 14.5Å$$

The water desolubilized due to reaction IV.77 is given by

$$x - y = W^s \bar{C}_{DT} (7-5) = 2 W^s \bar{C}_{DT} \qquad (IV.83)$$

Thus the ratio of water core volume in D_5 to that in D_7 is approximately 5/7 ≅ 0.7. The core volume of D_7 was 12770Å^3, thus the core volume of D_5 was 8939Å^3, and r_c=12.8Å. The area change is ΔA= -583 Å^2/micelle. It must be recalled that this result was based on solubilized water at $I \cong 0$.

The core radius can also be estimated from the volume of the water molecule (v), the ratio $C_w/\bar{C}_{DT}$ in the organic phase (i.e., W^s), and the area of core interface occupied by the polar head of one DNNSA monomer (a). The variables are related as in eqn. IV.84 (Aveyard, 1987)

$$r_c = \frac{3 W^s v}{a} \qquad (IV.84)$$

It was shown above that at $I \cong 0.5$, $W^s \cong 4$ (figure IV.16). Assu-

ming that macroscopic conditions extrapolate to micellar scale, the data shown in figure IV.5 can be used to estimate $a \cong 0.40$ nm^2 molec^{-1}. Using the molecular volume of water $v = 0.03$ nm^{3}molec^{-1} (Aveyard, 1987) in eqn. IV.84, r_c results of 9Å.

The value $r_c = 14.5$Å measured directly at $I \cong 0$. can be corrected considering that $W^s \cong 14$ under these conditions (figure IV.16) and using elementary geometry as follows (V_c is the volume of the core, numerical subindexes refer to I)

$$\frac{r_{c,0.0}}{r_{c,0.5}} = \left[\frac{V_{c,0.0}}{V_{c,0.5}}\right]^{1/3} \cong \left[\frac{W^s_{0.0}}{W^s_{0.5}}\right]^{1/3} = \left[\frac{14}{4}\right]^{1/3} = 1.52$$

Thus $r_{c,0.5} = 14.5/1.52 \cong 9.6$Å, which compares very well with the value estimated via eqn. IV.84 (9Å). Now ΔA must be estimated at $I = 0.5$. The core area of D_7 at $I = 0.5$ is:

$$A_{0.5,7} \cong \pi(2 \times 10)^2 = 1256 \text{ Å}^2$$

The core radius of D_5 at $I = 0.5$ is given by:

$$r_{c,0.5,5} = (r_{c,0.5,7}) \left[\frac{0.7\ V_c}{V_c}\right]^{1/3} \cong 10 \text{ Å} \times 0.89 = 8.9 \text{ Å}.$$

Thus $A_{0.5,5} = 995$ Å^2, $\Delta A = -260$ Å^2, and $\dfrac{\sigma\ \Delta A}{RT} \cong -0.64\ \sigma$.

The value of σ at the core interface cannot be known *a priori* and it is probably different from those values of σ measured at the planar macro-interface. Furthermore, σ depends on the core size as eqn. IV.85.

$$\sigma = \frac{K}{2\ r_c^2} \qquad \text{(IV.85)}$$

where K is the rigidity modulus of the surfactant monolayer. Eqn. IV.85 means that work is needed to bend as well as to stretch an adsorbed monolayer, and strictly applies to micelles with large cores, where $r_c \cong r_h$ (Aveyard, 1987). It is therefore a good model

for AOT, for instances, with values of W^s around 50, but it is probably not as good for the smaller DNNSA micelle. For AOT, K varies between 0.5kT and 2.0kT, where k is the Boltzmann constant ($1.38.10^{-23}$ JK^{-1}). For K=0.5kT, then σ=1.75 mNm^{-1}.

The value of ΔS_d^o may be roughly approximated assuming the water lost by micelles as water lost by DNNSA hydrates, for which data are available in the literature. Some values of ΔS^o of hydration in the DNNSA/heptane system are listed below (Högfeldt et al., 1981)

	ΔS^o (cal $K^{-1}gmol^{-1}$)
$HD(H_2O)_6$	-36.1
$HD(H_2O)_4$	-22.7

The entropy changes associated with the loss of two water molecules per monomer is therefore $\Delta S_d^o \cong -13 calK^{-1}gmol^{-1}$, and $\Delta S_d^o/R$= -6.50. The value of ΔG_{75} may be approximated from the free energies of micellisation collected by Kertes and Gutman (1976) for alkylammonium salts in organic diluents at 25°C. From those data, an average value $\Delta G^o \cong$ -2.8 $calgmol^{-1}$ was estimated, thus $\Delta G_{75}^o \cong$ 5.6 $calgmol^{-1}$ for the loss of two monomers, a positive value meaning that the D_5 micelle is less stable than the D_7 micelle.

We are now ready to estimate ΔG^o. From Eqn. IV.79,

$$\frac{\Delta G^o}{RT} = -0.64\sigma - 6.5 + 5.6 = -\ln \frac{K_2}{K_1}$$

Thus the following equation is eventually obtained. It predicts that the synergic ratio increases exponentially with σ:

$$\frac{K_2}{K_1} = \exp (0.9 + 0.64\ \sigma) \qquad \text{(IV.85)}$$

Additions of LIX63 at a given $\bar{C}_{DT}$ indeed resulted both in increasing σ as well as increased synergism. The synergic effect was constant as σ became constant. Thus the result IV.85, obtained from thermodynamic principles, is qualitatively verified. Values

of the ratio calculated with eqn. IV.86 for some values of σ are listed in Table IV.d. A ratio K_2/K_1=7.5, about double the experimental values of K_2'/K_1' listed in table F.27, corresponds to the value of σ=1.75 estimated from eqn. IV.85. Taking in account the assumptions done along this derivation, the predictions are considered satisfactory.

Table IV.d

σ (mNm^{-1})	10	8	6	4	2	1	0.5	0
K_2/K_1	1480	411	114	32	9	4.7	3.4	2.5

IV.7. KINETICS OF Ni(II) EXTRACTION BY DNNSA.

The observed effects of changing concentrations, interfacial area, hydrodynamic conditions, and temperature on the rate of nickel extraction by (K,H)DNNS are reported and discussed in this section. The experiments were conducted as detailed in section III.8, in the NDSC shown in figure III.1.a operated as described in Appendix C.

The time variation of organic nickel concentration was always measured under initial conditions. Data from a typical series of experiments are shown in figure IV.31 as nickel complex concentrations ($\bar{C}_M$) versus time, with the formal extractant concentration as the parameter. The straight lines shown are typical of a system reacting under initial conditions, thus far from equilibrium.

It is known that most reactions resulting in metal extraction are reversible. Considering that the experiments were ended at or before 5% conversion of the limiting reagent, it seems reasonable to neglect the reverse reaction ("stripping", or "back-extraction") in this discussion and in the models derived in section V.5. The stripping rate usually depends on the metal complex con-

centration (Danesi and Chiarizia, 1980), which was low under these conditions. Interfacial nickel fluxes (J_D) were calculated from the data as follows:

$$J_D = \frac{V}{A} \frac{d \bar{C}_M}{dt} \qquad (IV.87)$$

where V was the mean volume of the organic phase averaged over the duration of the experiment and A was the (geometric) interfacial area. The value of the derivative in eqn. IV.87 was found by linear regression of the data. Before the intrinsic kinetics of the reaction could be investigated it was necessary to identify the minimun level of turbulence in the reactor at which the *chemical regime* existed. This regime is attained when the resistance to mass transfer of reactants and products across their respective diffusion layer is negligible with respect to the intrinsic resistance of the chemical reaction (Astarita, 1967). The thickness of the diffusion layer adjacent to the interface depends on the turbulence in the bulk phase. Thus a purely diffusional process shows transfer rates which strongly depend on the rotational speed of the stirrers, whereas the rate at which a process proceeds in chemical regime is independent of the stirring speed. The effect of mass transfer resistances on the overall rate of extraction is analyzed in sections V.4 and V.5.

All experiments reported here were conducted at equal Re in both phases. The variables in the series of experiments aimed to identify the chemical regime were as follows:

i) rotational speed of the aqueous phase stirrer, N=150 to 350rpm.
ii) initial nickel concentration in the aqueous feed, $C_M = 5.10^{-3}$ $kmolm^{-3}$,
iii) pH=2.5, I=0.5M (HNO_3+ KNO_3),
iv) Formal (H,K)DNNS concentration, $\bar{C}_{DT} = 5.10^{-4}$ to $1.10^{-2} kmolm^{-3}$.

The effect of changing stirring speeds on J_D is shown in figure IV.32, with $\bar{C}_{DT}$ as the parameter. Lines are predictions by the Penetration-Surface Renewal model V.50. The shape of the curves is typical of processes controlled by resistances in series due to

diffusion and heterogeneous reaction (Danesi, 1983; 1984; Cussler, 1986). The top curve in the figure corresponds to the concentration vector yielding the fastest kinetics. Under those conditions there was a mixed chemical-mass transfer control at intermediate values of N. A plateau started at N ≅ 300 rpm indicating a shift into chemical kinetic regime. Expectedly, the plateaux started at lower values of N as the reaction was slowed down by reducing $\bar{C}_{DT}$.

Under moderate stirring of the phases, interfacial turbulence due to Marangoni instabilities may result in fluxes independent of macroscopic agitation. No Marangoni-type instabilities were however found when this chemical system was observed in a Schlieren field as described by Sawistowski (1971).

Danesi has argued (1984) that plateaux as those found here may result from losses in stirring efficiency which mimic a chemical control. It is demonstrated next, and in section V.4, however, that that was not the case in this work. Comparison of the effect of stirring speeds in the NDSC on the flux of nickel (J_D, figure IV.32) and of DNNSA (J_a, figure IV.36) reveals that J_a increased as N was increased in regions where J_D was in a plateau. Such increases in J_a can only be attributed to MTCs of increasing value, which however did not affect J_D. The plateaux shown in figure IV.32 were therefore attributed to a mechanism under kinetic control. Consequently all rate experiments were conducted at 300rpm, at $\bar{C}_{DT} \leq 0.01$ kmolm^{-3}, and at other concentrations such that the resulting fluxes did not exceed the plateau value at the corresponding value of $\bar{C}_{DT}$.

Indications of a locale for the RDS in the interfacial region as opposed to the bulk phases were obtained from the results of two series of experiments under kinetic regime in which the contact area and the temperature were independently varied. The effect of changing A on the rate of nickel complex accumulation per unit volume of extract ($r=J_D A/V$) is shown in figure IV.33. A was changed by inserting (at the interface) PTFE rings of varying internal diameter while V was kept constant. Under plateau conditions, r is expected to remain constant when V and composition are constant and the extraction rate is determined by reactions in the

bulk. If the process is rate-controlled by mechanisms operative in the interfacial region, however, one expects J_D to be constant under those conditions. In the latter case the value of r must therefore increase, as shown in the figure, with a slope of J_D/V.

The value of the apparent activation energy (E_a) provides another criterion to weight in the question of whether a phase-transfer process is rate-limited by mass transfer or by chemistry. According to Caldin (1964) "for small molecules in ordinary solvents, diffusion control gives rise to (values of) E_a in the region of 1 to 3 $kcalmol^{-1}$ (i.e. 4.2 to 12.6 $kJmol^{-1}$). Diffusion rates will not, however, contribute to the values of E_a when $E_a \geq 6$ $kcalmol^{-1}$(24.6 $kJmol^{-1}$)". E_a is usually evaluated from an Arrhenius plot of rates at changing temperatures as those data listed in table IV.6, obtained under plateau conditions at two sets of compositions. The mean E_a value was 25.2 $kJmol^{-1}$, just above Caldin's limit for a fully chemical regime, but around half the value found by Lin (1984) from single rising drop experiments. However it has also been argued that the value of E_a is not a conclusive criterion regarding the site of the rate-controlling mechanism in heterogeneous systems as those found in hydrometallurgical liquid-liquid extraction (Danesi and Chiarizia, 1980).

The effect on J_D of changing C_M and $\bar{C}_{DT}$ individually under all other conditions constant is shown in figures IV.34 and IV.37, respectively. The fluxes are listed in table F.29. Replicate results are shown as average values with an error band of one *sd*. The J_D vs $\bar{C}_{DT}$ results align as a straight line in the range 1.10^{-5} $M \leq \bar{C}_{DT} \leq 1.10^{-2}M$. Linear regression of the data returned a first order dependence as the following correlation:

$$J_D = 0.34.10^{-6}\bar{C}_{DT}^{1.01} \qquad (R=0.9967)$$

Experiments made from a single batch of purified DNNSA were reproducible within 5%. When experiments were done with extractant from separate purification batches, the reproducibility deteriorated to average global errors around 14%, underlining the effect that purity and characterization of reagents have on the results from rate investigations.

In the range 5.10^{-4}kmolm^{-3} $\leq C_M \leq$ 5.10^{-3}kmolm^{-3}, the J_D vs C_M data at constant $\bar{C}_{DT}$ fell on the following straight (in log-log coordinates) line:

$$J_D = 0.45.10^{-7} C_M^{0.96} \text{ (kmolm}^{-2}\text{s}^{-1}\text{)} \qquad (R=0.9980).$$

The values of J_D fell below the straight line as C_M was increased above 5.10^{-3}kmolm^{-3}. Additional experiments at higher values of N and at C_M=0.01kmolm^{-3} did not indicate departures from plateau conditions, thus the observed effect at higher C_M is believed due to chemical rather than to transport effects.

The effect on J_D of changing pH at constant I, $\bar{C}_{DT}$ and C_M is shown in figure IV.35. J_D increased as pH was increased from 0.5 to around 2.5, and varied as $C_H^{-0.43}$. A fractional pH dependence (0.81) was also found by Lin (1984) for the same chemical system from rising drop experiments. The hydrodynamics of the phases cannot be externally varied in single drop experiments, thus the locale of the rate-controlling step cannot be conclusively ascertained. It follows that the observed rate dependences on concentrations may or may not be equal to the true orders of chemical reaction. The uncertainties associated with the single drop technique as a tool for hydrometallurgical extraction rate investigations have been pointed out by Ortiz (1985).

The dependence on pH of J_D (figure IV.35), and of X and D_D (figure IV.25) were very similar. Such consistency suggests that the K^+-H^+ exchange equilibrium was responsible for the pH effect on D_D and J_D. J_D was essentially constant above pH $\cong$ 2.5, where X $\cong$ 0.99. To verify that the observed fluxes at high pH values were not the product of mass transfer resistances, experiments were conducted at stirring speeds ranging from 200 to 350 rpm at pH=3. No effect on J_D of varying N was observed, confirming the permanence under chemical regime.

Locale of the rate-controlling reaction/s

The process studied involves mass transfer and chemical reactions, which are usually assumed to be sequential steps each having an intrinsic resistance (Astarita, 1967; Sherwood et al., 1975; Danesi et al., 1977; Danesi, 1984; Smith, 1981). The overall (observed) resistance is thus determined by the largest individual resistance in the series. Conclusive location of the slowest step is therefore needed to characterize the rate control.

It is only when the extraction rate is controlled by chemical mechanisms that the observed flux dependences on concentrations can be related to partial reaction orders (Ortiz et al., 1977). It follows that diffusional effects must be decoupled from chemical effects in order to formulate reaction schemes which accurately describe the intrinsic kinetics of the system. The mass transfer characteristics vary from one experimental device to another, and authors choose to decouple mass transfer from chemistry using phenomenological transfer coefficients (Ortiz et al., 1977, for three different reactor types; Danesi et al., 1976, and Komasawa et al., 1980b, for a NDSC; Komasawa et al., 1980a, for the single drop) or microscopic continuity equations involving diffusion coefficients (Freeman and Tavlarides, 1982, for a laminar jet in a continuum).

Concentrations vary between bulk and boundary of a phase (Ortiz et al., 1977) therefore the site of the controlling step must be identified prior to the formulation of meaningful rate models. Three possible locations:

i) bulk aqueous phase,

ii) aqueous interfacial film, and

iii)o/w interface

are discussed in the following paragraphs in view of the results presented in this chapter. Several criteria are instrumented to discriminate possible sites for the RDS, as advised by Danesi (1984).

i) **Bulk aqueous phase.** Under plateau conditions, control by a bulk reaction should render a value of r independent of A (Astarita, 1967). The experiments however showed a linear dependence of r on A (figure IV.33).

A second criterion to discriminate against a RDS in the bulk was provided by the relative values of DNNSA solubilization fluxes (J_a) with respect to J_D under similar conditions. The results are shown in figure IV.36. Fluxes at I other than 0.5 were corrected to the equivalent value at 0.5 using the ratio of partition coefficients at both values of I. Comparing $J_a/2$ with J_D clearly shows that the rate of supply of extractant to the aqueous bulk was insufficient to yield the observed nickel fluxes. This fact becomes more evident by recalling that the complex stoichiometry was 1:7 instead of 1:2 under those conditions. The ratio $(J_a/2)/J_D$ was around 0.5. No other application of this criterion has been found in the literature, with exception of the comparison between rates of monolayer dissolution and of metal extraction done by Chaiko and Osseo-Asare (1986a).

ii) **Aqueous interfacial film.** The observed linear variation of the extraction rate with A would be the same for controls located either at a stagnant aqueous film adjacent to the interface or at an interfacial *plane* of molecular thickness.

Unequivocal evidence against a control locus at the aqueous film was obtained by comparing the experimental results with well established theories of mass transfer with simultaneous chemical reaction (van Krevelen and Hofjitzer, 1947; Astarita, 1967). The aqueous solubility of DNNSA is relevant to this analysis. Metal fluxes are proportional to aqueous extractant concentrations in rate models based on controlling reactions in the aqueous film and simultaneous diffusion (Hughes and Rod, 1984a; b). However, due to the dependence on $\bar{C}_{DT}$ of P found in this work (subsection IV.2 .1) the formal aqueous extractant concentration (C_{DT}) did not vary linearly with $\bar{C}_{DT}$, nor would J_D in the case of first reaction order in DNNSA. At I=0.5, J_D was found to vary as $\bar{C}_{DT}^{\cong 1.0}$ whereas the variation predicted by a model based on a control at the for-

mation of the 1:1 complex in the aqueous film would be $\bar{C}_{DT}^{\cong 0.6}$, as given by

$$J_D \alpha C_{DT} \equiv \frac{\bar{C}_{DT}}{P}$$

and $P \alpha \bar{C}_{DT}^{\cong 0.4}$.

The dependence of P on $\bar{C}_{DT}$ just discussed supplies a definitive argument against a control in the aqueous film in these rate experiments, and, although its significance has long been emphasized (Coleman and Roddy, 1971), it was neglected by authors who proposed extraction rate models based on reactions in the aqueous film (Hughes and Rod, 1984a; b).

The latter authors (1984a) let their model fit three sets of rate data for the extraction of Cu(II) by hydroxyoximes. However, in the only fit shown of the flux dependence on extractant concentration (that of the data by Albery and Fisk (1981) from rotary disk experiments), the RDS was **not** in the aqueous film. As discussed in section II.1, Akiba and Freiser (1982) have shown that the extent of extractant aggregation affects P. Constant values of P corresponded to non-aggregating reagents in solvating diluents, whereas P increased as the reagent concentration in non-polar, less solvating diluents was increased. The variation of P with changing I observed in this work thus may in part be due to a changing extent of aggregation. Larger micelles favoured by lower values of I result in increased aqueous solubility. It is somewhat surprising that such variations in P were not considered by Hughes and Rod (1984a; b) in view of the earlier studies on the partition of one of their case-study reagents (Acorga P5000) reported by one of the authors (Whewell et al., 1977). The validity of the approach by Hughes and Rod (1984a; b) therefore seems limited to non-aggregating extractants, able to partition at constant P values.

Due to the rather low solubility of DNNSA at high values of I, in the aqueous film it was $C_M(5.10^{-4}$ to 5.10^{-3}kmolm$^{-3}) \gg \bar{C}_{DT}/P=C_{DT}$ ($\cong 1.10^{-5}$kmolm^{-3}) and the reaction would be pseudo first order in metal (Sherwood et al.1975; Astarita, 1967). Thus the

square root of C_M would appear in models derived from placing the control at the 1:1 complex formation step. J_D varied as $C_M^{\cong 1.0}$ in this work, thus a controlling reaction could have taken place in the aqueous film only if it was second order in metal. Most of the work on metal extraction however indicates first order in metal (Danesi and Chiarizia, 1980).

The fact that the overall process is not controlled by steps sited at the aqueous film does not exclude reaction in that region. DNNSA molecules desorbed and diffused through the film, reacting with metal ions on their way. Due to the nickel complexes being less soluble than H- or K- sulphonates, one would expect the complexes to diffuse back toward the interface. The net effect of this hypothesis would be a lower value of J_a. This prediction was verified by the experiments (subsection IV.2.2).

iii)**Interface.** The combination of the observed effects of changing stirring speed, interfacial area, and temperature on J_D, and the equilibrium and dynamic transfer of DNNSA unequivocally identify the interface as the locale of the rate-determining step. The curves shown in figure IV.32 are typical of a process controlled by mass transfer and heterogeneous chemical reaction in series (Cussler, 1986). Under plateau conditions, the diffusive resistances were relatively small and the observed resistance was due to interfacial phenomena. The observed flux dependences on concentrations thus corresponded to partial reaction orders, summarized as follows:

$$J_D \propto \bar{C}_{DT}\, C_M \frac{(1-X)}{C_H} \; ; \; pH \leq 2.3 \qquad (IV.88)$$

It is apparent from figures IV.25, IV.35 that the variation of the parameter X with pH mimics that of J_D. Mechanistic models incorporating concentration dependences similar to eqn. IV.88 are derived in section V.3. In those models, the interfacial speciation is estimated from the bulk selectivity parameter X.

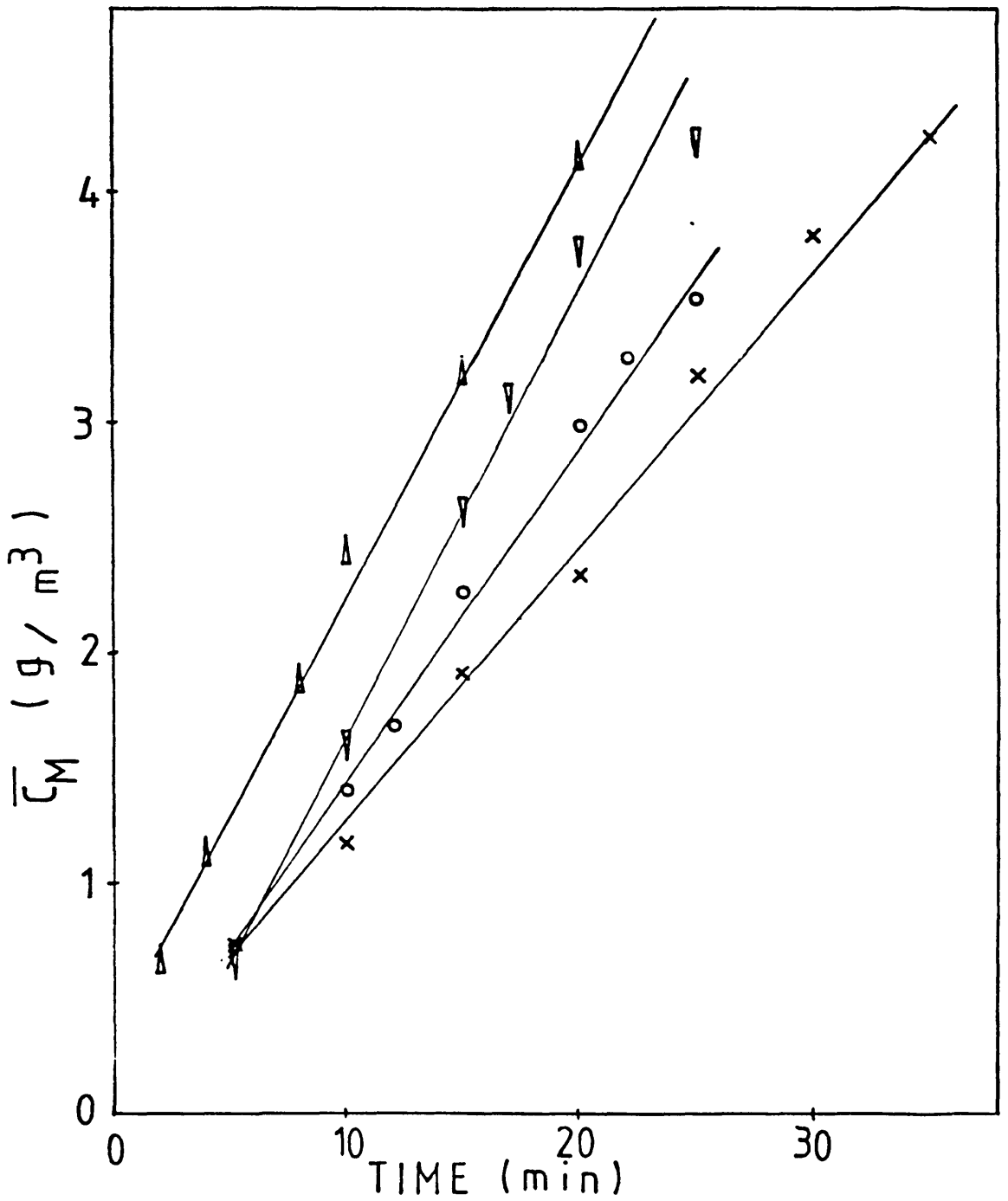


Figure IV.31 Typical sets of data from experiments of initial rate of nickel extraction by DNNSA in the NDSC. Parameter is DNNSA concentration.

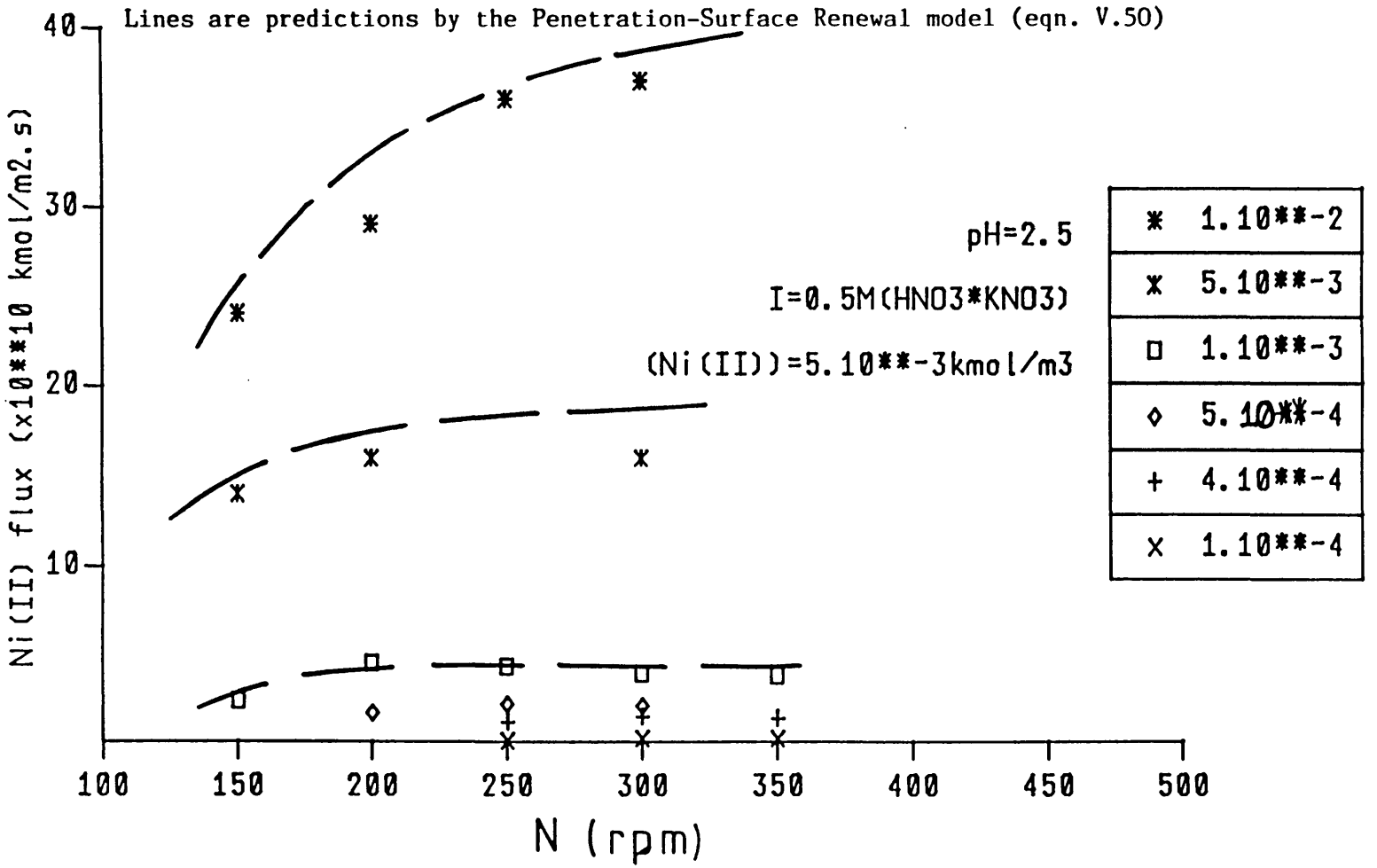


Figure IV.32 Effect of stirring speed on the extraction flux in the NDSC. Parameter is organic DNNSA concn. (kmol/m3).

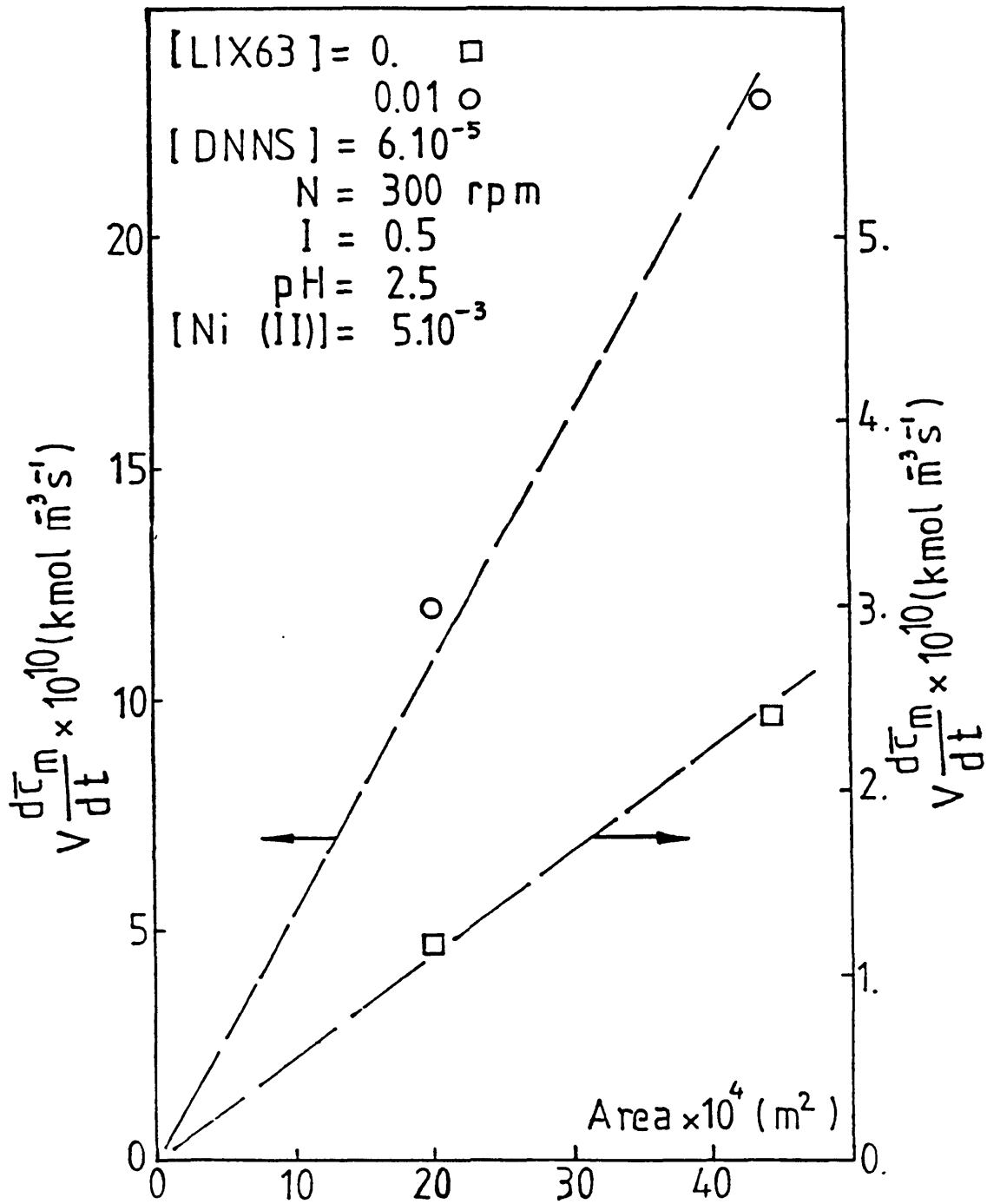


Figure IV.33 Effect of the interfacial area on the rate of nickel extraction by DNNSA and DNNSA-LIX63 mixtures in the NDSC.

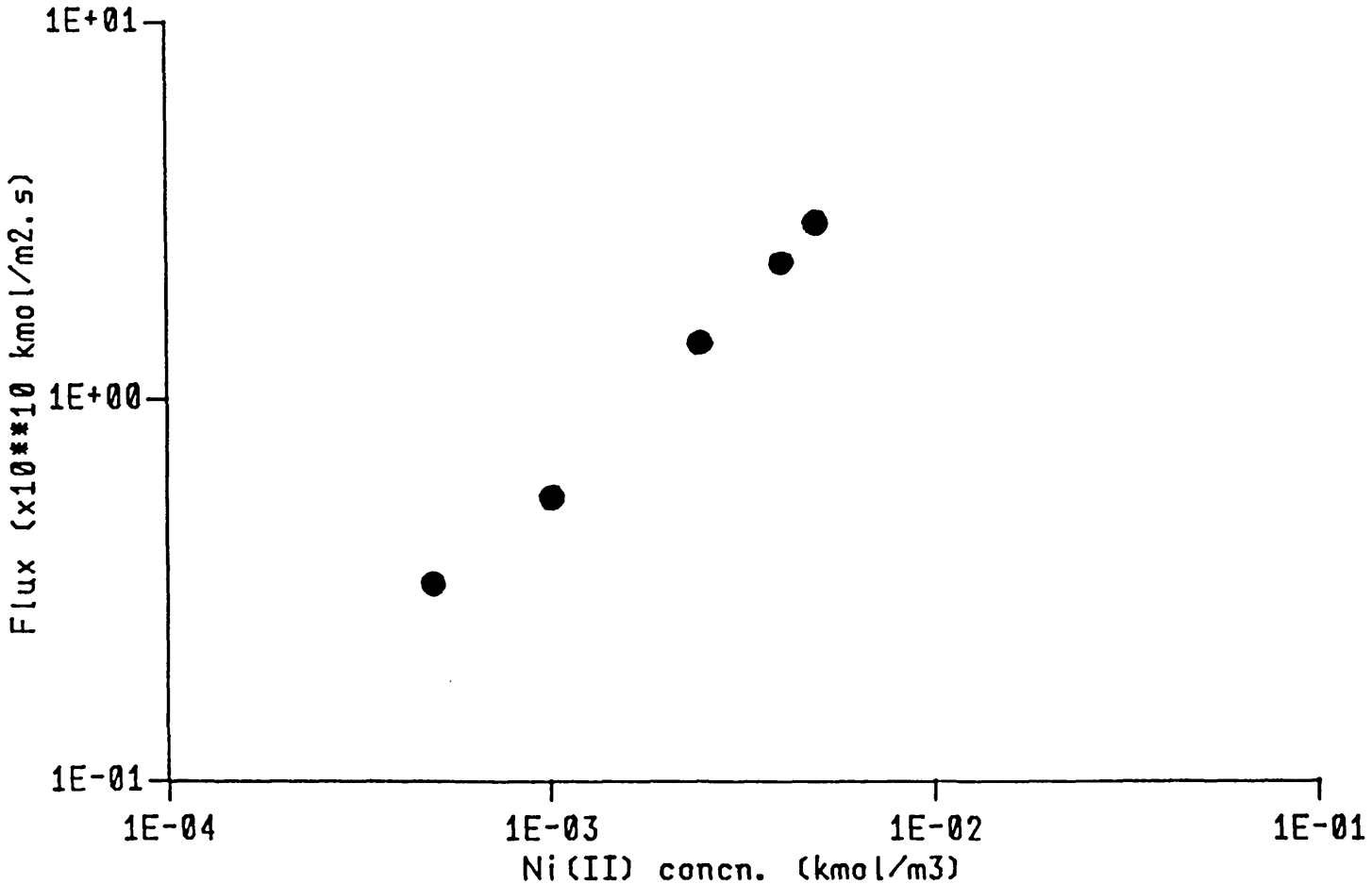


Figure IV.34 Effect of Ni(II) concn. on extraction fluxes.
(DNNSA)=1.10**-3kmol/m3, I=0.5M(KNO3), pH=2.5

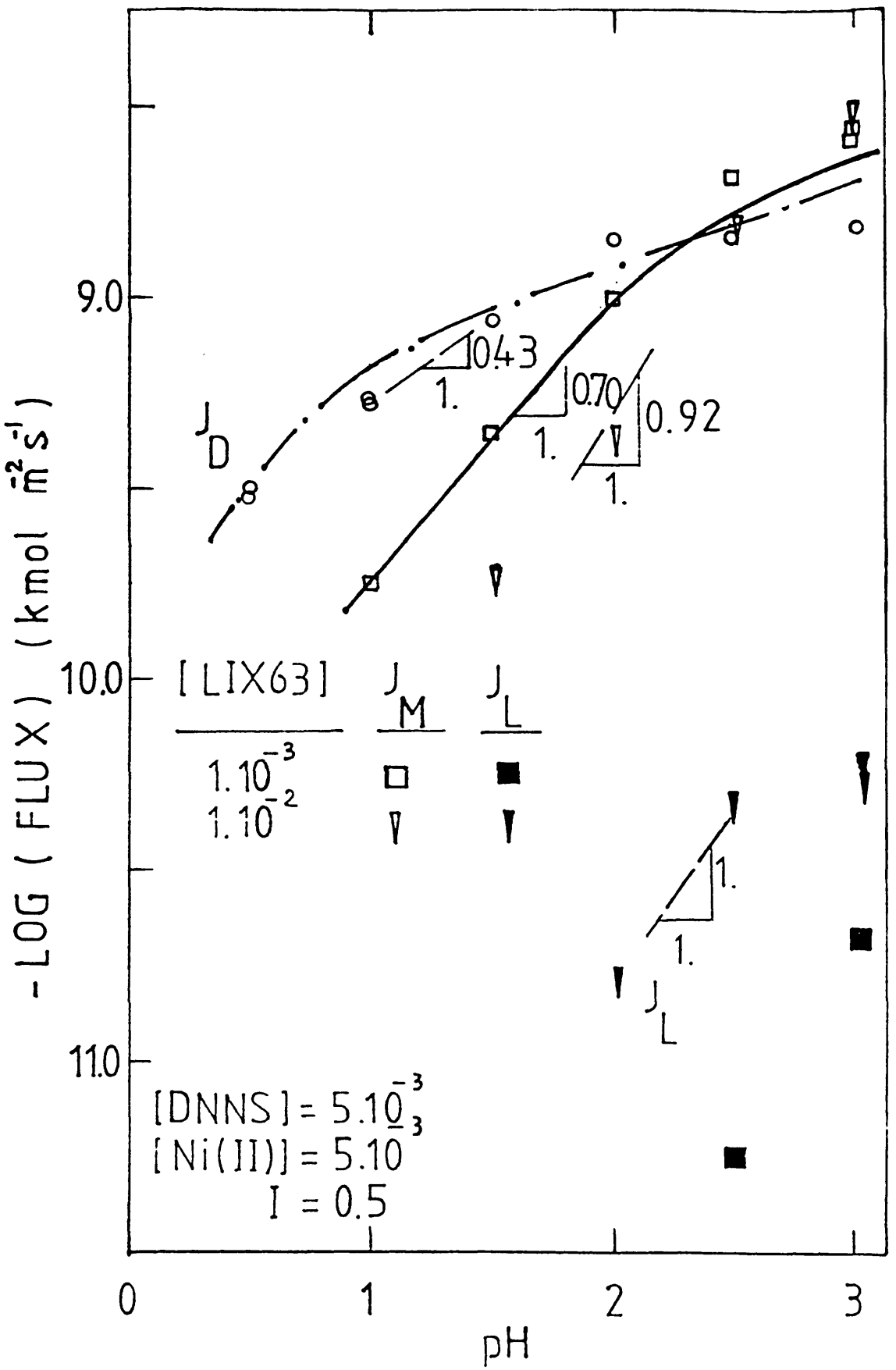


Figure IV.35 Effect of pH on nickel fluxes in the NDSC.

Experimental J_D, o; J_D predicted by Model C, _.-._.-._; J_M predicted by Model V.93, _____.

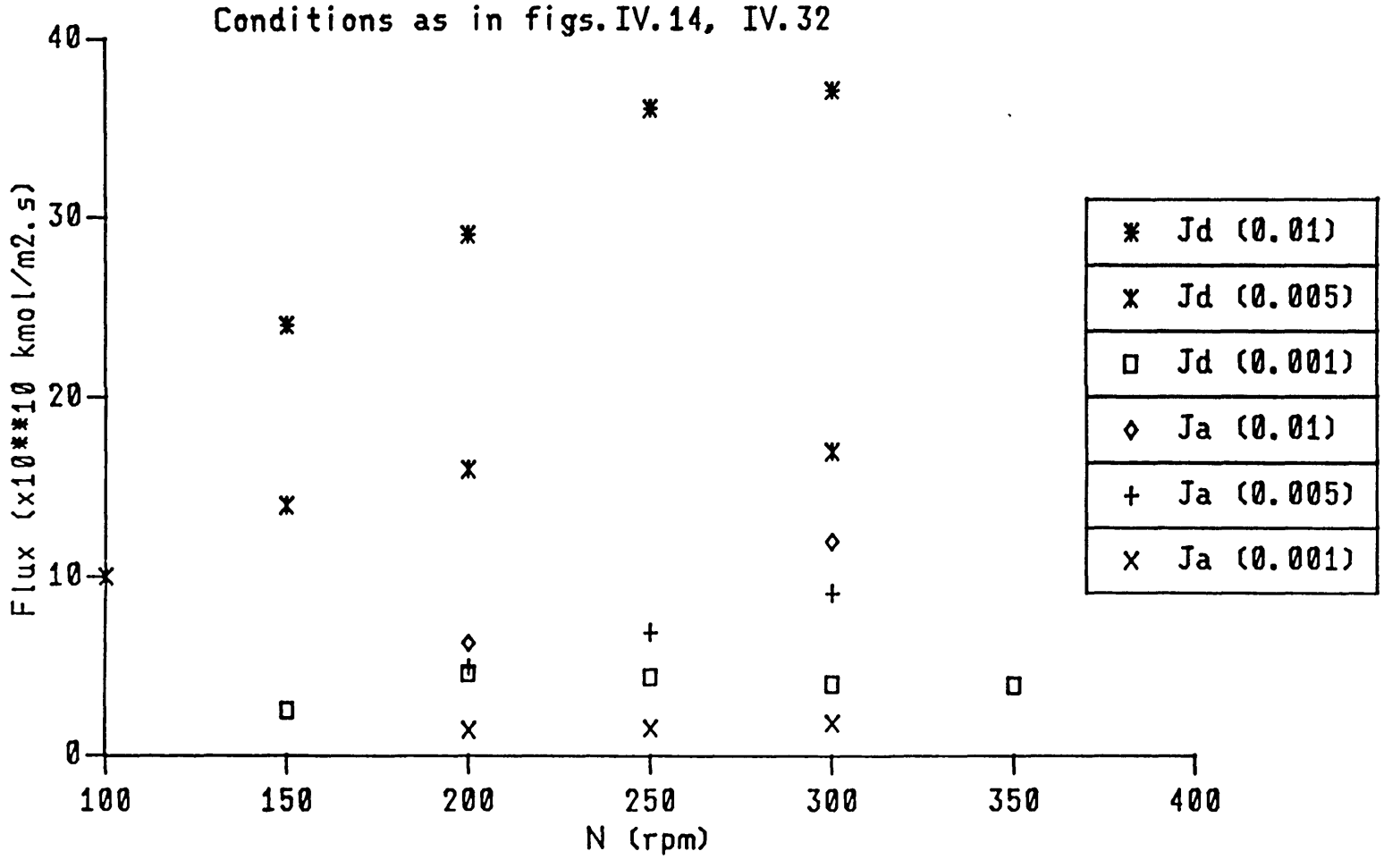


Figure IV.36 Comparison of nickel extraction flux and DNNSA dissolution flux in the NDSC. Parameter is DNNSA organic concn.

Table IV.6 Nickel fluxes for the calculations of activation energy (E_a), $J_D x10^{10}$ kmolm^{-2}s^{-1}. I=0.5, pH=2.5, N=300 rpm.

T (°C)	30	40	50	E_a
T (K)	303.5	313.5	323.5	
1/T (x10^3 K^{-1})	3.29	3.19	3.09	kJmol^{-1}
$\bar{C}_{DT}$=5.10^{-3}kmolm^{-3}				
C_M=5.10^{-3}kmolm^{-3}		19.9	26.2	22.9
$\bar{C}_{DT}$=1.10^{-3}kmolm^{-3}				
C_M=5.10^{-3}kmolm^{-3}	2.46	2.79	4.77	27.5

IV.8. KINETICS OF Ni(II) EXTRACTION BY LIX63

The effect of changing formal LIX63 concentration ($\bar{C}_{LT}$) on the value of the extraction flux (J_L) is shown in the lower part of figure IV.37. The following correlation is the equation of the line through the points and was returned by linear regression:

$$\log J_L = -8.42 + 0.96 \log \bar{C}_{LT} \quad (R = 0.9992)$$

The data are listed in table F.30. It can be concluded from the regression of the data that J_L varied as $\bar{C}_{LT}^{1}$, within experimental error.

The effect of pH on J_L is shown in figure IV.35 at $\bar{C}_{LT}=1.10^{-3}$ and 1.10^{-2}. Within error, J_L depended as C_H^{-1} below pH≅2.5. The curve flattened above that pH value and J_L became independent of pH above pH ≅ 3. The data are listed in table F.31.

Higher extraction fluxes by DNNSA alone were observed under similar hydrodynamic conditions. The extraction rate by DNNSA was found to be under chemical control (section IV.7). It is therefore believed that a chemical control was also operative during the experiments reported here with LIX63. It follows that observed dependences on concentrations are actual reaction orders. The controlling reaction in the ranges chosen was first order in LIX63, and reciprocal first order in H^+. The kinetics of extraction by LIX63 was roughly ten times slower than by DNNSA.

IV.9. KINETICS OF Ni(II) EXTRACTION BY MIXED REAGENTS

Results from kinetic experiments using DNNSA-LIX63 mixtures are presented in this section. The experiments were conducted as described in section III.8, similarly as the single-reagent experiments.

The effect of changing A on the transfer rate per unit volume (r_M) was similar as that with DNNSA alone (figure IV.33). As A was increased, r_M was found to increase, suggesting also here the interfacial character of the rate-determining step.

The effect of changing organic composition ($\bar{C}_{DT}$, $\bar{C}_{LT}$) and aqueous composition (C_M, pH) on the extraction flux (J_M) was investigated. When the organic composition was the variable, experiments were done in the range $1.10^{-5} \leq \bar{C}_{DT} \leq 5.10^{-3}$ kmolm^{-3}, and at $\bar{C}_{LT}$ = 1.10^{-3}, 5.10^{-3}, and 1.10^{-2} kmolm^{-3}. The results are shown in figure IV.37 as $\log J_M$ vs $\log \bar{C}_{DT}$ with $\bar{C}_{LT}$ as the parameter. Fluxes by single extractants are also shown for comparison. The lines shown have the only meaning of joining the experimental points.

It was found that $J_L < J_D < J_M$ throughout the range investigated. Also the condition for catalysis (i.e. $J_M > J_L + J_D$) was verified, except in a narrow band of $\bar{C}_{DT}$ around the CMC of each mixture. The results followed the same pattern of change at all levels of $\bar{C}_{LT}$ investigated, each curve showing two conspicuous inflexions. J_M varied as $\bar{C}_{DT}^{1.0}$ below the shoulder at lower values of $\bar{C}_{DT}$, with little effect of $\bar{C}_{LT}$ on J_M. It was $J_M \cong 10\ J_D$ in this region, where rate enhancements due to the addition of LIX63 were highest. Shoulders appeared at all values of $\bar{C}_{LT}$ as J_M started to vary less when $\bar{C}_{DT}$ was increased toward the CAC of the mixture. J_M became almost constant in the region CAC$< \bar{C}_{DT} <$CMC. A good correlation between the position of the shoulders and the CAC values was noted.

The second break in each data set took place near the respective CMC. There, the slope of the curves changed from essentially zero to around 1 again. Above the CMC, it was found that $J_M \cong 1.1$ to $1.5\ J_D$, thus the rate enhancements there were substantially smaller than those observed below the CAC.

The results just shown gave rise to a hypothesis that attempts to explain (qualitatively) the mechanisms responsible for rate enhancements in mixed extractants systems. It is known from the π-A isotherms that the interfacial adsorption density of mixtures (Γ_M) increased markedly as $\bar{C}_{DT}$ was increased up to the CAC of the mixture. In that region, it was $\Gamma_M < \Gamma_D$. Also in that region there was demicellisation of DNNSA due to sulphonate-oxime aggregation (Keeney and Osseo-Asare, 1980; Lin, 1984; Zheng and Osseo-Asare, 1987). More plentiful, smaller *sub-micellar aggregates* (SMA) resulted from the breakdown of micelles. This argument is substantiated by the speciation analysis included in section V.7.

The rate of interaction between those SMAs and the o/w interface could not be quantified by electrolyte dynamic solubilization experiments because SMAs lack exchangeable core contents. If it is however accepted that SMAs interact with the interface with similar efficiency as reversed micelles, then the following physical scenario is proposed:

- The rate of Ni^{++} complexation is lower than with DNNSA alone, because $\Gamma_M < \Gamma_D$.
- The desorption and renewal of the mixed monolayer that results from the interaction between the o/w interface and particles in its vicinity, however, is faster than the renewal of DNNSA films, because $\bar{C}_{sma} > C_{micelles,DNNSA\ alone}$ (section V.7).
- It was concluded in sections IV.7, IV.8 that interfacial reactions were rate-determining in the extraction by single reagents. In section V.3 such reaction is identified as the interaction between reversed micelles and the adsorbed film, resulting in metal complex desorption.

The above arguments and the results presented here suggest that at $\bar{C}_{DT} < CAC$ the rate was controlled by conversion of the adsorbed film instead of by its desorption. Thus J_M is expected to increase in this region and become nearly constant around the CAC while the former step in the mechanism controls. As $\bar{C}_{DT}$ was increased toward the CMC, the organic speciation results show that the concentration of aggregates able to interact with the film at the o/w interface decreased due to micellisation at the expense of the

SMAs. That decrease must translate in a decreasing rate of film desorption and renewal. This rate equalled the essentially constant rate of film conversion at a critical value of $\bar{C}_{DT}$, near the CMC of the mixture. As $\bar{C}_{DT}$ was increased further, micellar-assisted desorption of complexes again provided the overall rate control, as with DNNSA alone, because it was slower than the conversion of the film.

The effect of pH on J_M is shown in figure IV.35 as log J_M vs pH, in the pH range 0.5 to 3.0, with $\bar{C}_{LT}$ as the parameter and at constant values of C_M and $\bar{C}_{DT}$. The data are listed in table F.33. J_D and J_L are also shown in the figure for comparison. The data were well aligned at low pH as straight lines with slope that depended on the value of $\bar{C}_{LT}$. The J_M dependence on pH increased as α0.43pH (at $\bar{C}_{LT}$= 0.), α0.70pH (at $\bar{C}_{LT}=1.10^{-3}$kmolm^{-3}), α0.92pH (at $\bar{C}_{LT}=1.10^{-2}$ kmolm^{-3}), and α1.0pH at $\bar{C}_{DT}$=0. The pH effect, in other words, varies between the limits that correspond to both reagents alone. This observation is relevant to the modelling of extraction rates as it underlines the involvement of LIX63 in the chemistry of the process.

At pH=2.5, the values of J_M at all values of $\bar{C}_{LT}$ used were close to one another. Also it was $J_M(\bar{C}_{LT}=1.10^{-3}M) > J_M(\bar{C}_{LT}=1.10^{-2}M) > J_D$. This order is consistent with the patterns followed by the curves in figure IV.37. At pH<2, the order was $J_D > J_M(\bar{C}_{LT}=1.10^{-3}M) > J_M(\bar{C}_{LT}=1.10^{-2}M)$. The latter order was reversed at pH $\cong$ 3.

With DNNSA alone, at $\bar{C}_{DT}=5.10^{-3}$kmolm^{-3} and pH=2.5, desorption of nickel complexes is found to be slower than complex formation in section V.3. It is possible that the same situation applies to mixtures. Decreasing pH values affect the complexation rate, but it is not probable that they affect the desorption rate because the latter depends on the organic phase speciation only. The approximate tenfold decrease in J_M values as pH was reduced to 1 from 2.5 may be related to a slowing down of the complexation rate such that the control shifted from desorption to complex formation. The speciation analysis supplied a criterion in this respect and it will be fully discussed in section V.8.

Whether the control shifted or complex desorption controlled throughout the pH range, it is clear from the higher dependence of J_M on pH as $\bar{C}_{LT}$ was increased that the cation exchange by the oxime was involved in the controlling step. In section IV.7, the o/w interface was shown to be the locus of the rate-determining reaction with DNNSA alone. The same conclusion was arrived at by Inoue et al. (1984) for LIX63 as nickel extractant based on aqueous solubility considerations. Thus it is to be expected that the rate-controlling reaction/s in mixed systems be located at the interface. This conclusion is in part substantiated by the results shown in figure IV.33. It follows that the oximes are not totally excluded from adsorbing at the interface by the more active sulphonates. LIX63 monomers, oximates, and possibly sulphonate-oxime binaries may partake in the interfacial mosaic, with fractional coverages varying according to the value of the ratio $\bar{C}_{DT}/\bar{C}_{LT}$ (the results in subsection IV.1.2 substantiate this statement). Should the oxime be completely prevented from adsorbing at the o/w interface, consideration of a control in the aqueous phase would be required to justify the pH dependences observed.

The effect of simultaneously changing C_M and $\bar{C}_{LT}$ on J_M is shown in figure IV.38 as $\log J_M$ vs $\log C_M$ with $\bar{C}_{LT}$ as the parameter at $\bar{C}_{DT}=1.10^{-3}$ and $0.3.10^{-3}$ $kmolm^{-3}$ (table F.34). J_M varied as $C_M^{1.0}$ at both levels of $\bar{C}_{DT}$.

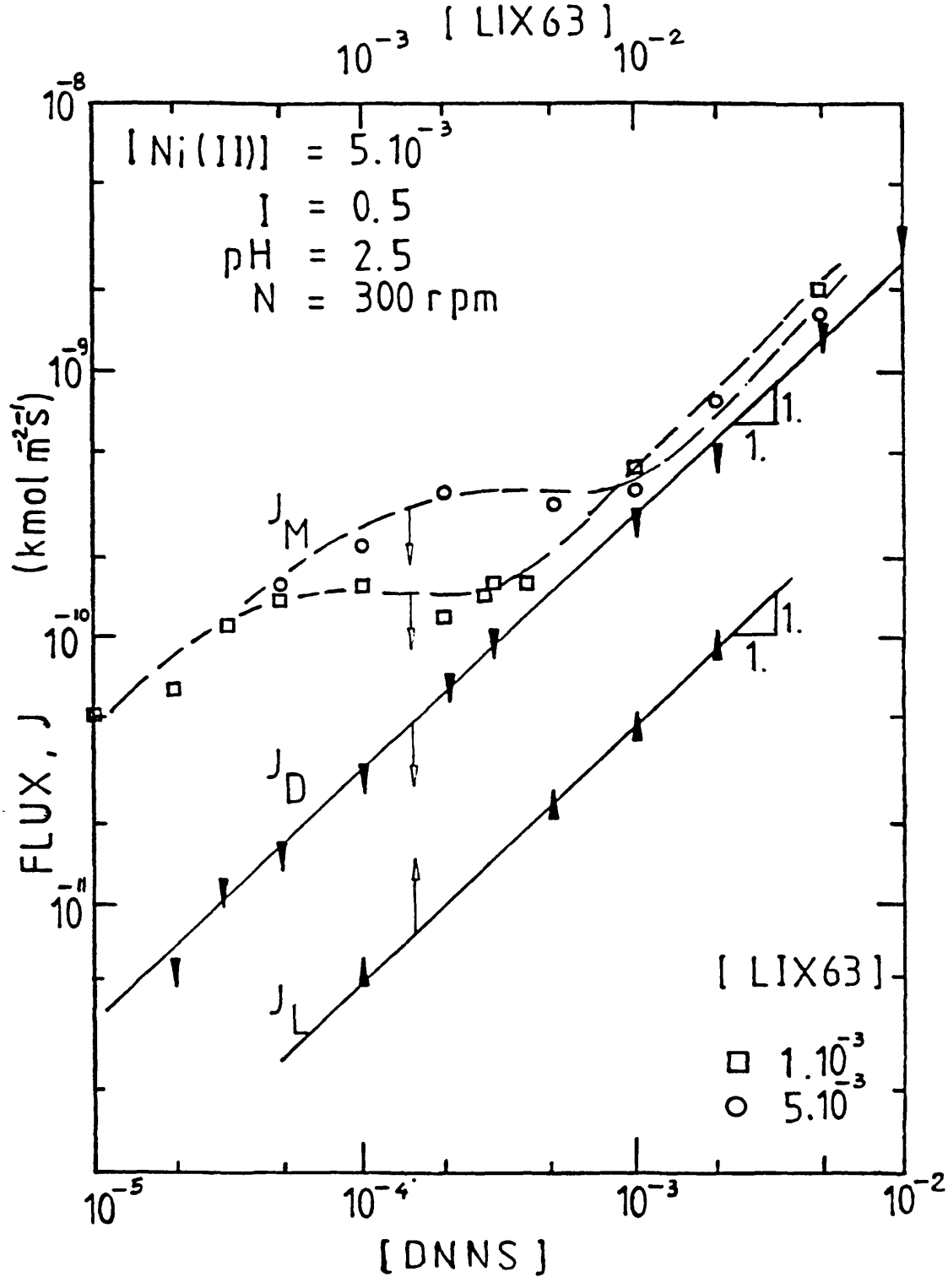


Figure IV.37 Effect of extractants concentration on nickel fluxes in the NDSC.

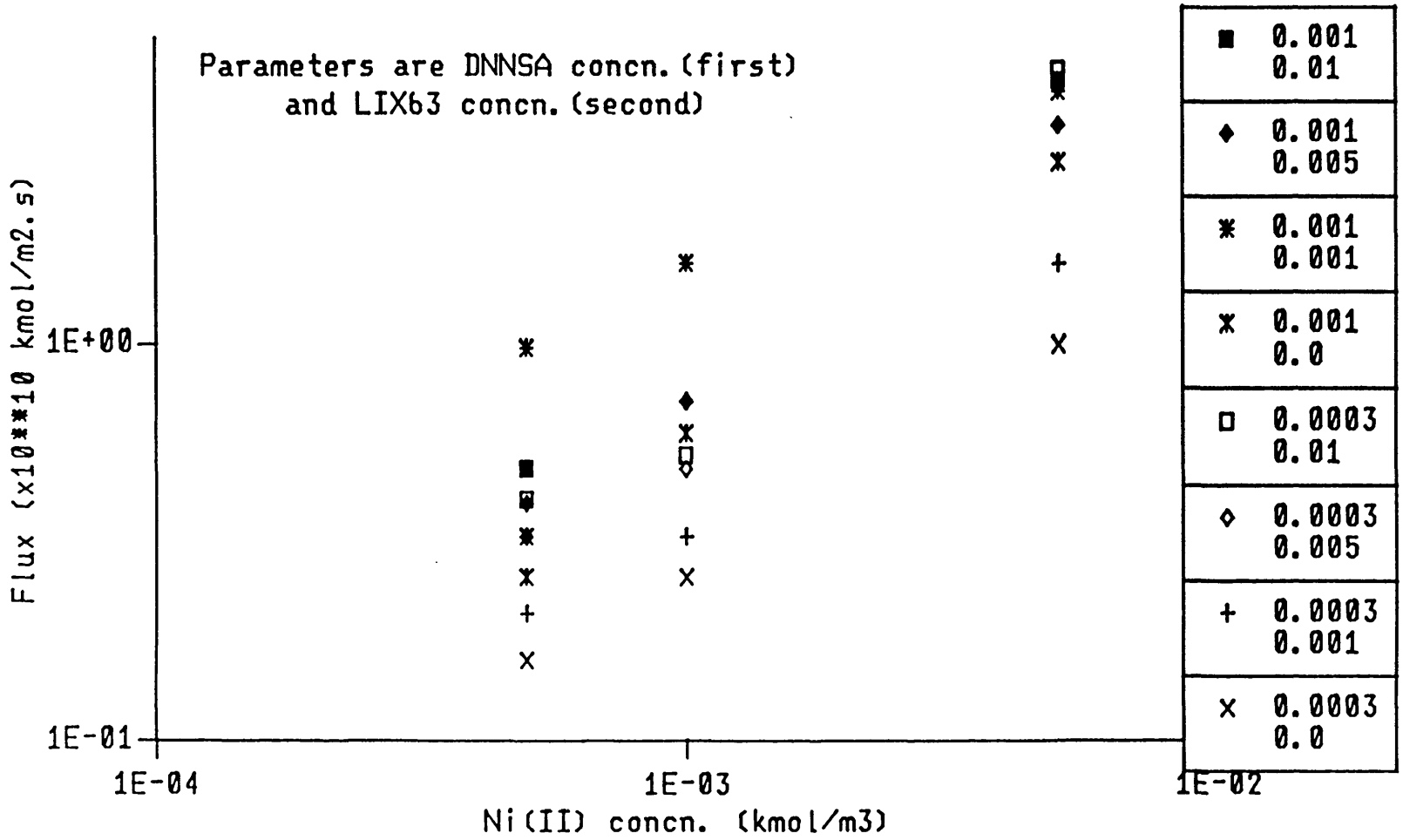


Figure IV.38 Effect of Ni(II) concn. on extraction fluxes by mixtures
I=0.5M (KNO3+HNO3), pH=2.5.

CHAPTER V. MODELLING

V.1. PHYSICAL MASS TRANSFER

V.1.1. DNNSA AQUEOUS SOLUBILIZATION DYNAMICS

It was desired to estimate aqueous phase mass transfer coefficients (MTCs, K_{aq}) in the NDSC, which could be used as inputs in the models of extraction kinetics. Due to aggregation, the dynamic phase transfer of surfactants is more difficult to model than the transfer of non-surface active solutes (Cussler, 1986). Assuming that diffusion of surfactant monomers and micelles be much slower than interfacial adsorption/desorption mechanisms, aggregation equilibrium in the aqueous diffussion film, and simultaneous diffusion of both species, Weinheimer et al. (1981) arrived at the following expression for the surfactant flux:

$$J_a = - \mathfrak{D} \nabla C_{DT} \qquad (V.1)$$

where the apparent diffusion coefficient $\mathfrak{D}$ depends on surfactant concentration as follows:

$$\mathfrak{D} = \mathfrak{D}_m + \frac{\mathfrak{D}_1 (nK_p)^{-1/n}}{n (C_{DT} - CMC)} \qquad (V.2)$$

The analysis applies to the range $\bar{C}_{DT}$>CMC only. Cussler (1986) claimed its validity for non-ionic detergents and presented data showing that for Triton X-100, $\mathfrak{D}$ varied approximately as $(C_{DT} - CMC)^{\cong -0.075}$. The exponent (-0.075) is however much smaller than 1. (in eqn.V.2) thus the goodness of the prediction is only qualitative. The analysis would not be valid for anionic detergents at low values of I (Cussler, 1986). For example, aggregation of SDS was apparently prevented by high values of ψ in that case , and $\mathfrak{D}$ increased as C_{DT} was increased. At high values of I eqn.V.2 was again verified (Cussler, 1986).

Apparent transfer coefficients of DNNSA were computed from the following solute balance about the aqueous phase:

$$J_a = K_{aq} (C^*_{DT} - C_{DT}) = \frac{V}{A} \frac{dC_{DT}}{dt} \qquad (V.3)$$

Integration with the initial condition $C_{DT}(0)=C^0_{DT}$ yields eqn.V.4 from which K_{aq} was computed with the interfacial concentration $C^*_{DT}=\bar{C}_{DT}/P$.

$$\ln \left[\frac{C^*_{DT}-C^o_{DT}}{C^*_{DT}-C_{DT}} \right] = (A/V)\ K_{aq} \qquad (V.4)$$

The values of K_{aq} thus found are listed in table F.35 and shown vs Re in figure V.1. K_{aq} depended on $Re^{\cong 1.1}$ at constant values of $\bar{C}_{DT}$. The coefficients are "film coefficients" as no contribution to the overall resistance to mass transfer was expected from diffusion through the organic film or from adsorption/desorption at the o/w interface. Decreasing values of K_{aq} are shown in the figure as $\bar{C}_{DT}$ was increased at constant Re. According to the film theory of mass transfer (Lewis and Whitman, 1924), the MTC is

$$K_{aq} = \mathcal{D}/\delta$$

where δ is the thickness of the diffusion film. Thus division of eqn.V.2 by δ indicates that K_{aq} must decrease when $\bar{C}_{DT}$ is increased at constant value of Re. The results in figure V.1 show such variation.

V.1.2. SOLUBILIZATION BY REVERSED MICELLES

The purpose of the work presented in this section was to characterize the mass transfer in the NDSC (organic phase), and to gain an insight into the different dynamics of the initial solubilization and core exchange mechanisms. Thus transfer coefficients were estimated from the data presented in section IV.3.

The mechanism of water solubilization is viewed as resulting from the following pseudo-reaction at the o/w interface:

$$\text{dry micelle} + W^s \text{ water molecules} \longrightarrow \text{saturated micelle} \qquad (V.5)$$

Complete saturation of the micelle upon interaction with the interface was thus assumed. Once they diffuse back into the bulk, the loaded micelles pool their cores with drier micelles and the average moisture content increases in the phase as contacting time proceeds. Further, the interfacial interaction V.5 was assumed much faster than diffusion through stagnant films, thus the mechanism was under full mass transfer control. The diffusion coefficient of saturated micelles is around 2/3 that value for dry micelles (appendix G) thus the process was rate-limited by the transfer of the former from the source (the o/w interface) to the bulk. The water balance about the organic phase is eqn.V.6

$$J_w = \frac{V}{A} \frac{dC_w}{dt} \qquad (V.6)$$

A link was needed between the observed rate of water accumulation in eqn.V.6 and the transfer coefficient of saturated micelles, K_o. The following assumption was made:

$$\text{flux of dry micelles} = - \text{flux of saturated micelles } (J_{sm}) = -J_w/(m\ W^s)$$

where J_w was the flux of water into the organic bulk and m is the aggregation number of DNNSA, 7. K_o was defined as

$$J_{sm} = K_o\ (C^*_{sm} - C_{sm}) \qquad (V.7)$$

where $C^*_{sm}=\bar{C}^i_{DT}/m$ and $C_{sm}=(W/W^s)\bar{C}_{DT}/m$ are the concentrations of saturated micelles at the interface and in the bulk, respectively. From the pseudo-stoichiometry of solubilization, and assuming that the moisture initially in the diluent was unaltered after the saturation of micelles, the total water is estimated as:

$$m\ W^s\ (\bar{C}_{DT}/m) + C^h = C^s_w \qquad (V.8)$$

From eqns.V.6 through V.8 an equation was obtained upon integration which allowed the evaluation of K_o from the data as follows:

$$\log\left[\frac{C^s_w - C^0_w}{C^s_w - C_w}\right] = \frac{A\ K_o}{2.3\ V}\ t \qquad (V.9)$$

The values of C^s_w were estimated as $W^s\bar{C}_{DT}$ from the W^s vs I results shown in figure IV.16. The pH of a typical experiment fell to around 2.3 from the initial value around 2.5, thus the corrections to W^s due to changes in I were neglected. The value of C^0_w varied from experiment to experiment and measured values were used in the calculations.

From the data in table F.19 and A=42 cm^2, V=300cm^3 in the NDSC, the values of K_o listed in table F.36 and shown in figure V.1 were evaluated. K_o was found to increase as $Re^{1.1}$ (i.e. with the same dependence as Re_{aq}) up to Re≅12600. The exponent decreased at higher values of Re suggesting a deterioration in the stirring efficiency. Higher values of K_o than of K_{aq} were found at a given value of Re. Unlike K_{aq}, K_o did not depend on the value of $\bar{C}_{DT}$, suggesting that reversed micelles had an invariant size.

The values of K_o thus estimated were of the order expected in the NDSC. The water fluxes listed in table F.19, however, are much higher than the nickel fluxes observed for metal extraction across the quiescent interface. From comparing both sets of results a criterion was derived to decide whether the observed phase transfer of water was micellar-mediated or simply due to molecular diffusion. If water reached the bulk organic phase after having diffused through a stagnant hexane layer, the flux would be:

$$J_w \cong K'^{*}_o \text{ solubility}$$

Water solubility in hexane is around 0.005% (i.e. around 1.10^{-3} $kmolm^{-3}$). Thus values of K'_o in the order:

$$J_w / \text{solubility} \cong 10^{-5} kmolm^{-2}s^{-1} / 10^{-3} kmolm^{-3} = 10^{-2} ms^{-1}$$

would be expected, around 100 times the experimental values. Assuming the film theory of MT to hold, and using a value of diffusion coefficient for water $\mathcal{D}_w = 5.8.10^{-9} m^2 s^{-1}$ (the average of three estimates by the Wilke-Chang, Scheibel, and Reddy-Doraiswami correlations; Reid et al., 1977), a diffusion film thickness $\delta = K'_o / \mathcal{D}_w \cong 10^{-7} m$ would be required for molecular diffusion to justify the values of J_w observed. Diffusion films this thin cannot be realistically expected in a NDSC. Carroll (1981) has used a similar argument when discussing the mechanism of solubilization of hydrophobes by detergent micelles. The observed fluxes can only be substantiated by a mechanism based on reversed micelles interacting with the macro-o/w interface, solubilizing water in their polar cores, then diffusing toward the bulk organic phase.

Based on such a mechanism, the time variation of water concentration was simulated using a solution to the problem of unsteady diffusion and solute accumulation in a boundary layer (Austin, 1966). The problem is briefly described and Austin's solution is shown in appendix D. The value of $\mathcal{D}$ for saturated micelles used to generate the curves (shown in figure V.2 as C_w vs time with δ as the parameter) was estimated in appendix G from literature data (Chaiko and Osseo-Asare, 1986). The simulation was done at chan-

ging values of $\bar{C}_{DT}$. When the data were superimposed, they fell between the curves at $\delta = 0.5.10^{-5}$ to 1.10^{-5}m. Similar values of δ were found by Danesi et al. (1977) to fit their results of extraction by DNNSA with simultaneous mass transfer in a NDSC. Pairs of (δ, $\mathcal{D}$) values that simulated curves comparable to the experimental results are listed in Table V.1.

The mechanisms shown in figure V.3 are therefore proposed for initial solubilization and transfer to pre-saturated micelles, respectively. Micelles reach the organic sublayer, they disaggregate, the freed monomers desorb in a concerted action (Carroll, 1981), forming fresh reversed micelles which encapsulate electrolyte in their polar cores. The micelles diffuse away from the interface, and, as the solubilizate concentration increases, micelles probably pool their core contents in the bulk of the organic phase.

The value of K_o was estimated with eqn.V.9 also for transfer across membranes. The group K_oA/V was found to be independent of $\bar{C}_{DT}$ and it was on average $1.2.10^{-7}s^{-1}$. The effective transfer area of the membrane was estimated following the approach of Albery and Fisk (1981), and the value of K_o resulted around $3.10^{-4}ms^{-1}$, about three times greater than the largest values estimated for the NDSC. It is normally the case that mass transfer at a solid/liquid interface be associated with a MTC of higher value that the coefficient at a liquid/liquid interface.

The initial solubilization of ^{32}P-containing electrolyte and the core exchange mechanisms were modelled as Chan et al. (1976) treated the solubilization of fatty acids by detergent micelles in aqueous media. The coefficients of initial transfer were estimated from the following balance:

$$\frac{A}{V} K_i C_w^s = \left(\frac{dC_{wp}}{dt}\right)_{t=0} = r_i$$

where $C_{wp}^s = C_w^s = 12\ \bar{C}_{DT}$ was assumed, accounting for the fact that I was not zero. The results are listed in table V.2. K_i was found to

be independent of $\bar{C}_{DT}$ at $(15\pm2)10^{-5}$ ms^{-1}, close to the upper end of the coefficients in the NDSC.

During core exchange experiments, the total moisture content of the organic phase was nearly constant, because decreases in tracer-free water concentration (C_w) balanced with increases in tracer-spyked water concentration (C_{wp}). In this case it was

$$C_w^s = C_w^0 + C_{wp}^0 = C_w + C_{wp} = \text{constant}$$

where the zero superscript stands for initial conditions. The coefficients (K_e) were estimated using balances equivalent to V.6, V.7 (Chan et al., 1976), which resulted in an expression similar to V.9. The estimates are listed in table V.2. The MTC's evaluated in this section are **film** coefficients but they are numerically equal to **overall** coefficients because there were no concentration gradients in the aqueous phase. K_e was found to depend on $\bar{C}_{DT}$ in a similar way as K_{aq} did. Thus the ratio K_i/K_e decreased toward 1 as $\bar{C}_{DT}$ was increased in the range chosen.

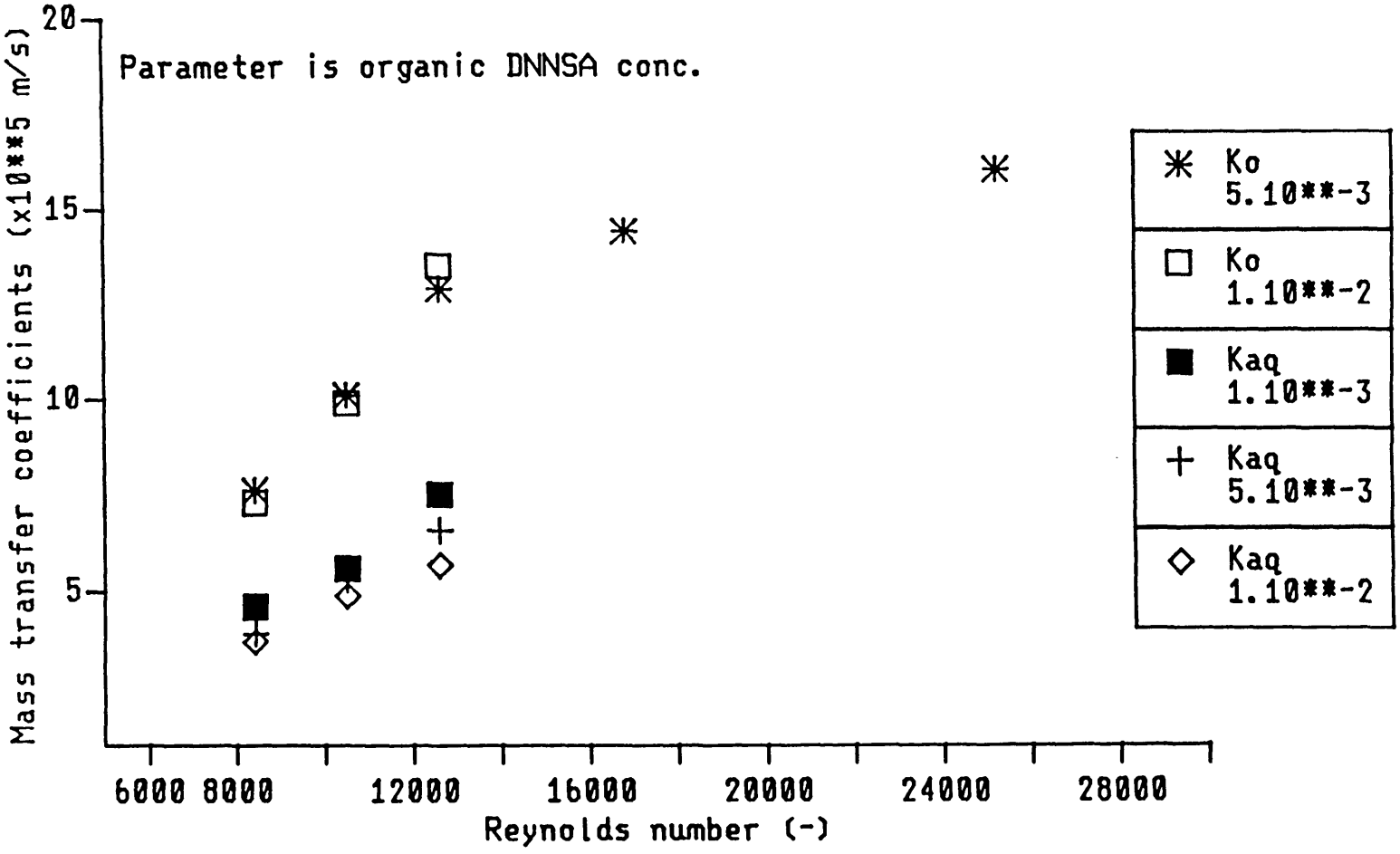


Figure V.1 Mass transfer coefficients in the organic (Ko) and aqueous (Kaq) halves of the NDSC.

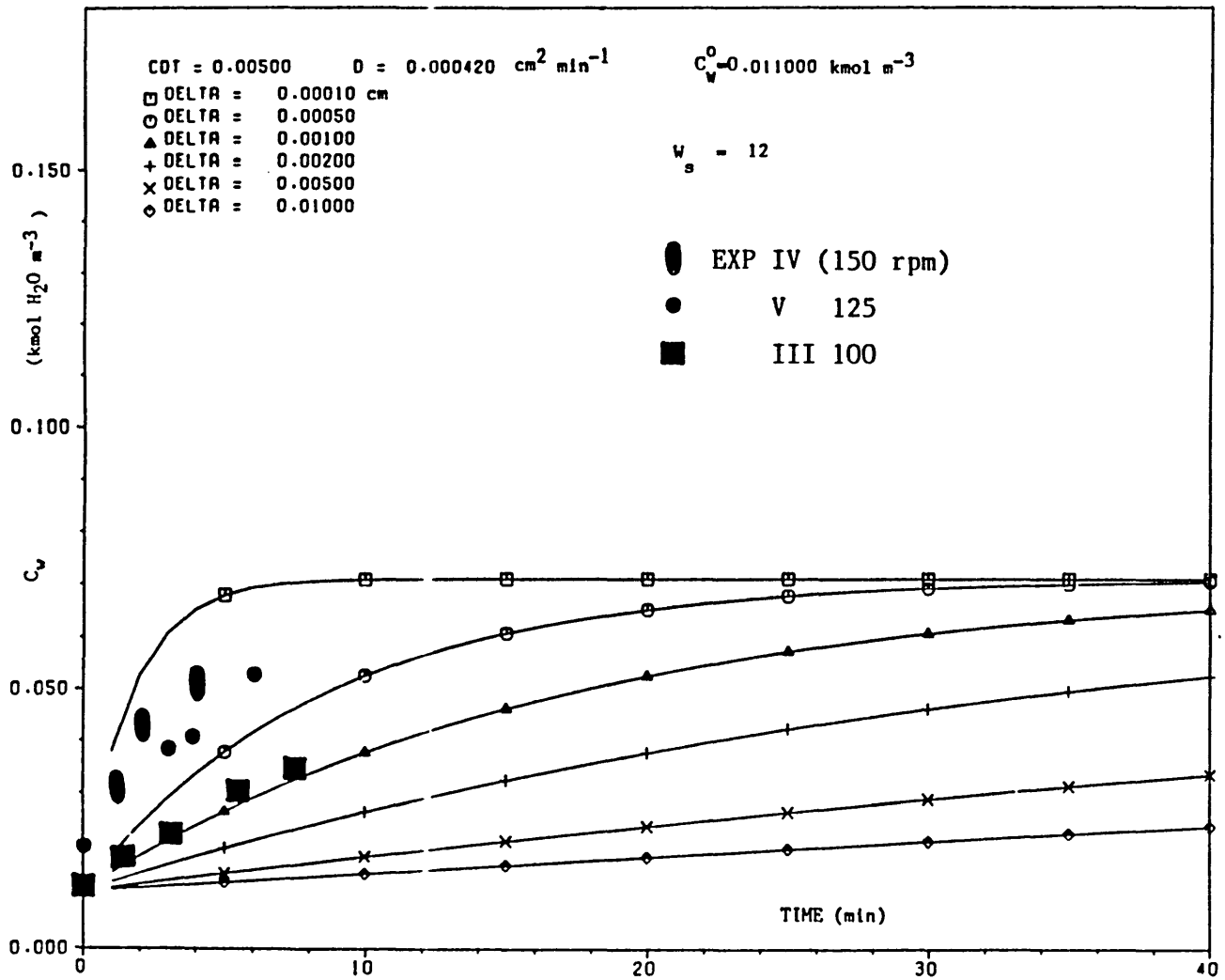
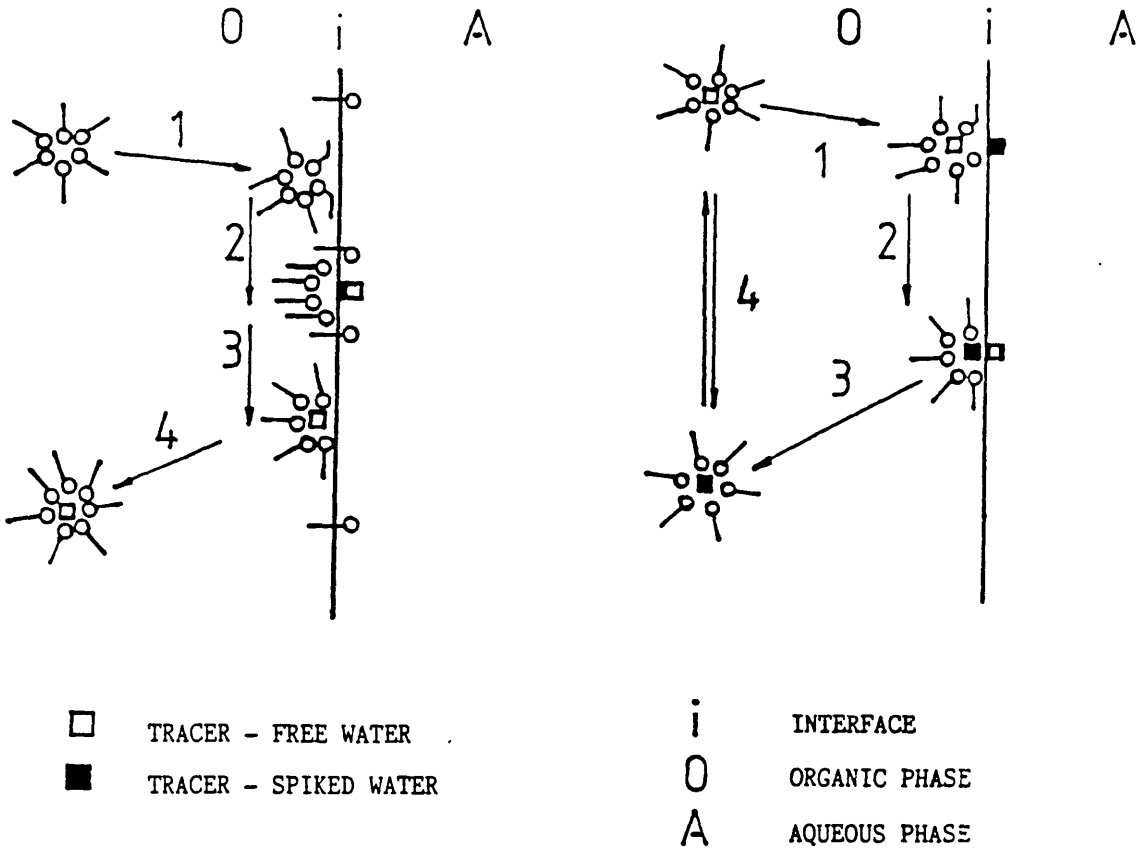


Figure V.2 Dynamic water solubilization by reversed DNNSA micelles in the NDSC. Lines are predictions (Appendix D)..Parameter is the thicness of the diffusion film.



INITIAL SOLUBILIZATION

1- DRY MICELLE DIFFUSES TO INTERFACE
2- MICELLE DISAGGREGATES, MONOMERS ADSORB
3- MONOMERS DESORB, WATER IS SOLUBILIZED
4- SATURATED MICELLE DIFFUSES AWAY FROM INTERFACE

CORE EXCHANGE

1- TRACER-FREE MICELLE DIFFUSES TO INTERFACE
2- MICELLE EXCHANGES CORE WITH AQUEOUS PHASE
3- MICELLE DIFFUSES AWAY FROM INTERFACE
4- MICELLES IN BULK EXCHANGE CORES

Figure V.3 Proposed mechanism of interaction between reversed DNNSA micelles and the o/w interface, resulting in solubilization by initially "dry" micelles and in core exchange.

Table V.1 Fit of (δ, $\mathcal{D}$) pairs in the NDSC from water dynamic solubilization. Listed values are $\delta x10^{6}$m.

$\mathcal{D}x10^{10}$ ms^{-1}	$\bar{C}_{DT}=1.10^{-2}$ kmolm^{-3}	$\bar{C}_{DT}=5.10^{-3}$ kmolm^{-3}	$K_o=\mathcal{D}/\delta$ x10^{4}ms^{-1}
1.7	2	$\cong$ 2	$\cong$1
7.0	5	5 to 7	$\cong$1*
17.	10 to 20	20	$\cong$1

* This row corresponds to $\mathcal{D}=4.2.10^{-4}cm^{2}min^{-1}$.

Table V.2. Transfer coefficients in ^{32}P initial solubilization and core transfer experiments.

$\bar{C}_{DT}$kmolm^{-3}	K_ix 10^{-5}ms^{-1}	K_ex 10^{-5}ms^{-1}	K_i/K_e
0.05	13	0.46	28
0.02	18	1.1	16
0.013	15	2.2	7
0.005	15	9.9	1.5

V.2. SOLUBILIZATION CONTRIBUTION TO INITIAL EXTRACTION FLUXES.

In his rising drop (RD) experiments of Ni(II) extraction rates by DNNSA, Lin (1984) used dry organic feeds, and found that the $\bar{C}_M$ vs time data extrapolated to finite y-intercepts ($\bar{C}_M^0$). That author attributed the observation to end (initial) effects, namely to transfer while the drops formed at the tip of the nozzle. The values of $\bar{C}_M^0$ in that work align vs $\bar{C}_{DT}$ as a straight line of slope close to 1 in a log-log graph. That effect could however be partly ascribed to the physical transfer that took place as aqueous phase saturated the dry micelles in the feed. The linear dependence of $\bar{C}_M^0$ on $\bar{C}_{DT}$ does not help to decide in this respect because kinetics and solubilization are both linear in $\bar{C}_{DT}$. Longer contact times in the NDSC experiments offer a means to decouple the effects of both mechanisms.

Experiments were run under identical conditions except for the physical pre-equilibration of the organic feed. Data from a typical pair of runs are shown in figure V.4 as $\bar{C}_M$ vs time. The data from the conventional ("wet" feed) run pass through the origin. When "dry" feeds were used the data again aligned as straight lines after 1min , but those lines did not intercept the origin. Similar values resulted for the flux from the similar slopes, but the "end effect" was nonexistent in the former case. The observation is most likely due to metal transfer as aqueous phase was solubilized, thus it was physical transfer as opposed to that due to reaction, as substantiated next.

The values of J_W calculated in subsection IV.3.2 and IV.3.3 and the values of J_D found in section IV.7 are listed in table F.37. After correcting J_W for the change in I as follows:

$$\frac{J_W^{I_1}}{J_W^{I_2}} \cong \frac{W^{s,I_1}}{W^{s,I_2}}$$

the contributions to the observed J_D due to solubilization were estimated from the following pseudo-reaction, in which complexation of Ni(II) by DNNSA was neglected for simplicity

$$\overline{\text{micelle}} + mW^s H_2O + (mW^s \frac{C_M}{55})Ni^{++} \Leftrightarrow \overline{\text{micelle}.mW^s H_2O(\frac{mW^s}{55}C_W)Ni^{++}}$$

where 55 $kmolm^{-3}$ is the concentration of water. The stoichiometry of solubilization thus indicates that

$$J_{DS} = \frac{C_M}{55} J_W$$

where J_{DS} is the solubilization contribution to the observed nickel flux. The ratio J_{DS}/J_D was around 30% (table F.37). In figure V.5 values of $1.3J_D$ in the NDSC are plotted vs $\bar{C}_{DT}$, and are compared with the values of J_D found from the RD experiments by Lin (1984). The RD results agree well with the $1.3J_D$ values. This argument seems a good way of explaining the unexpected observation in RD experiments of extraction fluxes higher than in the NDSC. The significance of mutually saturating the feeds in short contact time techniques such as the RD is thus manifest. The physical solubilization of nickel by saturated micelles was however negligible compared to J_D in the NDSC because the rate of core exchange was around 30 times lower than the rate of initial solubilization (table V.2).

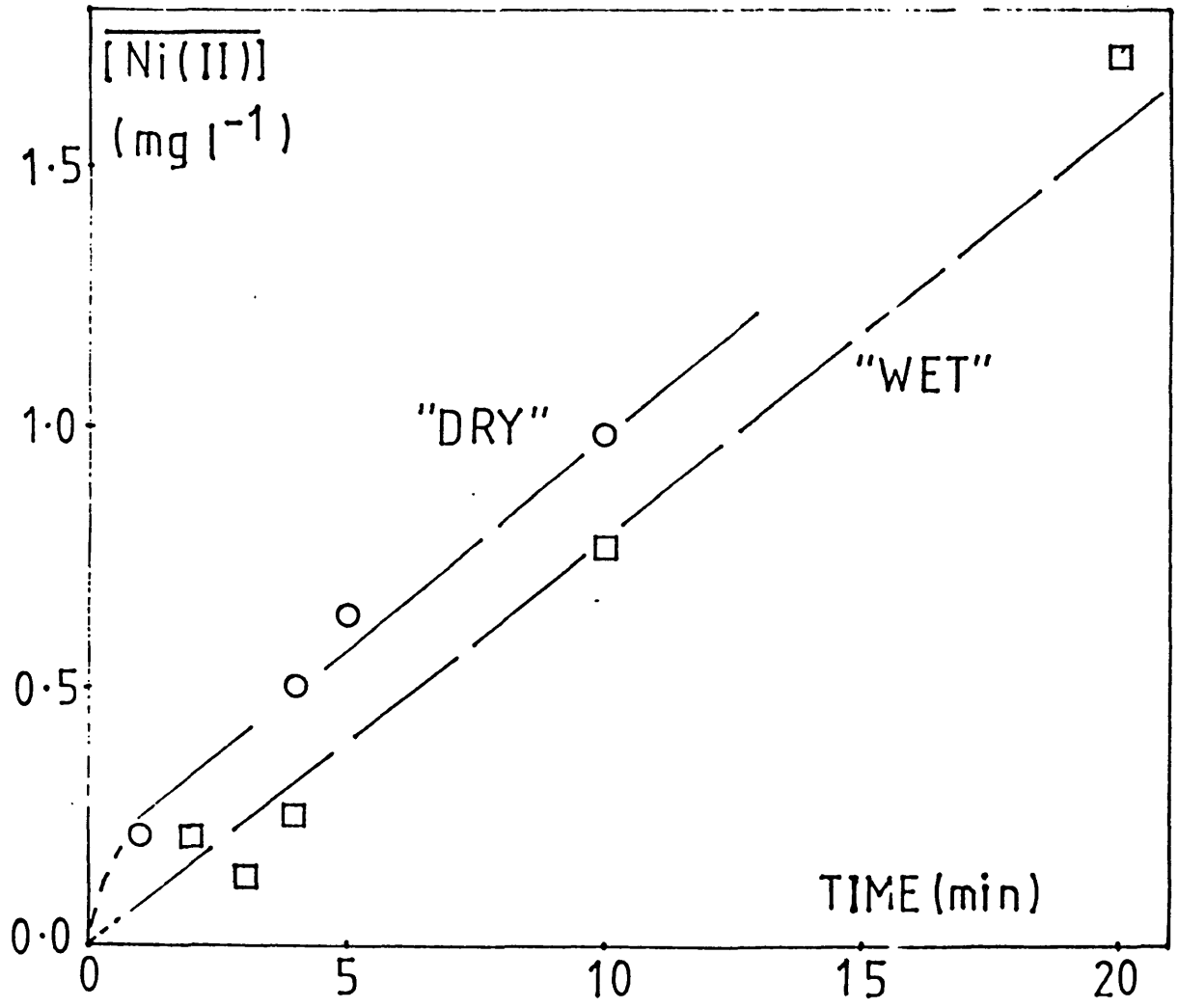


Figure V.4 End effect in the initial extraction of nickel by DNNSA in the NDSC.

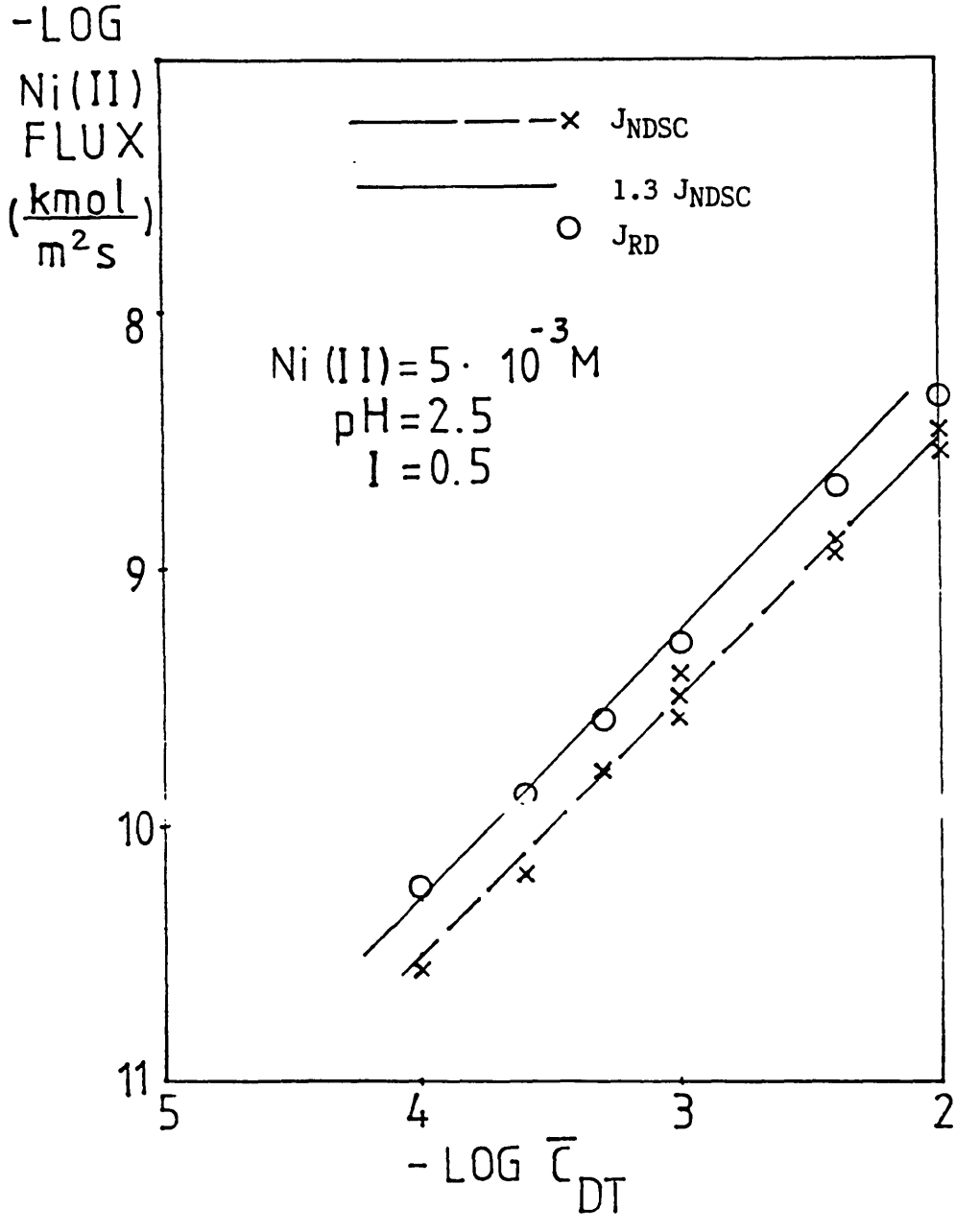


Figure V.5 Nickel fluxes due to chemical and physical transfer by DNNSA micelles in the NDSC and with the RD technique.

V.3. KINETIC MODELS FOR NICKEL EXTRACTION BY DNNSA.

A substantial mumber of kinetic models are available in the solvent extraction literature which can explain the observed effects of the experimental variables (reagents concentrations, flow conditions, interfacial properties, solubilities, etc.) on the rates of metal transfer. Because of the complexities of the mechanisms involved, which usually combine mass transfer with chemical reactions, most models assume a series of steps. Depending on which step is taken as rate-determining, different rate equations result. This is necessarily so because, unlike equilibrium situations where the final state of the system is a function of bulk conditions, the rate of transfer far from equilibration depends on the reaction paths and the locale of the RDS. Besides, the RDS is usually located at or very close to the o/w interface, whose properties may differ from the properties of the bulk phases (Cox and Flett, 1977).

The interfacial character of the RDS in the extraction of nickel by DNNSA has been proved in section IV.7. In this section, rate models are derived that incorporate interfacial parameters (ψ, Γ) in addition to concentrations and the effect of hydrodynamic conditions via the MTCs. In this work the approach has been to build the models mostly on foundations directly gained from experimentation. The following building blocks are used:

1) Observed flux dependences on concentrations are partial reaction orders (section IV.7).

2) The transfer of metal due to physical solubilization can be safely neglected (section V.2), thus it is a good approximation to assume that interfacial complexation is wholly responsible for extraction.

3) MTCs were evaluated from physical mass transport without additions of solutes alien to the system (section V.1). In former investigations MTCs have been estimated:

i) from rate models under conditions of a mixed kinetically-mass transfer (MT) controlled regime where the model was not sensitive to the concentration of one or another reagent (Ajawin, 1980),

ii) using diffusion coefficients ($\mathcal{D}$) calculated from rates of monolayer dissolution into stagnant sublayers (Osseo-Asare and Chaiko, 1986a),

iii) from measurements of dynamic interfacial tensions (Rodríguez de Carvalho and Slater, 1983), or

iv) from transfer rates of interfacially inactive solutes (Tavlarides et al., 1985; Komasawa et al., 1980b).

Of all these approaches, the least realistic was probably that of using non-amphipatic solutes to evaluate transport characteristics of systems involving surfactants. As discussed in section II.2, the transfer properties of surfactants differs in several respects from those of non-surface active solutes.

4) The cation exchange between DNNSA and the supporting electrolyte (section IV.4) provides an insight into the pH effect on J_D.

5) It is believed that models must acknowledge the *sui generis* properties of the interface. Two parameters are particular signicant in this respect. The interfacial population density of the reagent (Γ_D) varied little when the bulk concentration was changed above the CAC (subsection IV.1.2). The concentrative effect of ψ on the cationic population near the interface was underlined in section II.1.

Some authors have recently incorporated interfacial parameters in their models. Fyles (1985) attributed the independence from hydrodynamic conditions of extraction rates to a mechanism controlled by adsorption/desorption, and the selectivity shown by crown ethers to the composition of the mosaic formed by interfacially adsorbed species (1986). Fyles (1985) used estimated interfacial stability constants of the adsorbing complexes to compute the interfacial speciation. That author solved the system of non-

linear equations which relate the total electrical charge density to that charge density intrinsic to the reagent, and to the charge contributed by adsorbed species (Cohen and Cohen, 1981), to compute values of ψ, which were not measured independently.

Harada and Miyake (1986) included ψ in the rate models for metal extraction by chelating agents, as well as a definition of fractional occupancy of the interface by adsorbed species, previously derived (Miyake et al., 1983). Rather dissapointingly, however, Harada and Miyake (1986) assigned zero value to the interfacial potentials due to the difficulties associated with their experimental evaluation.

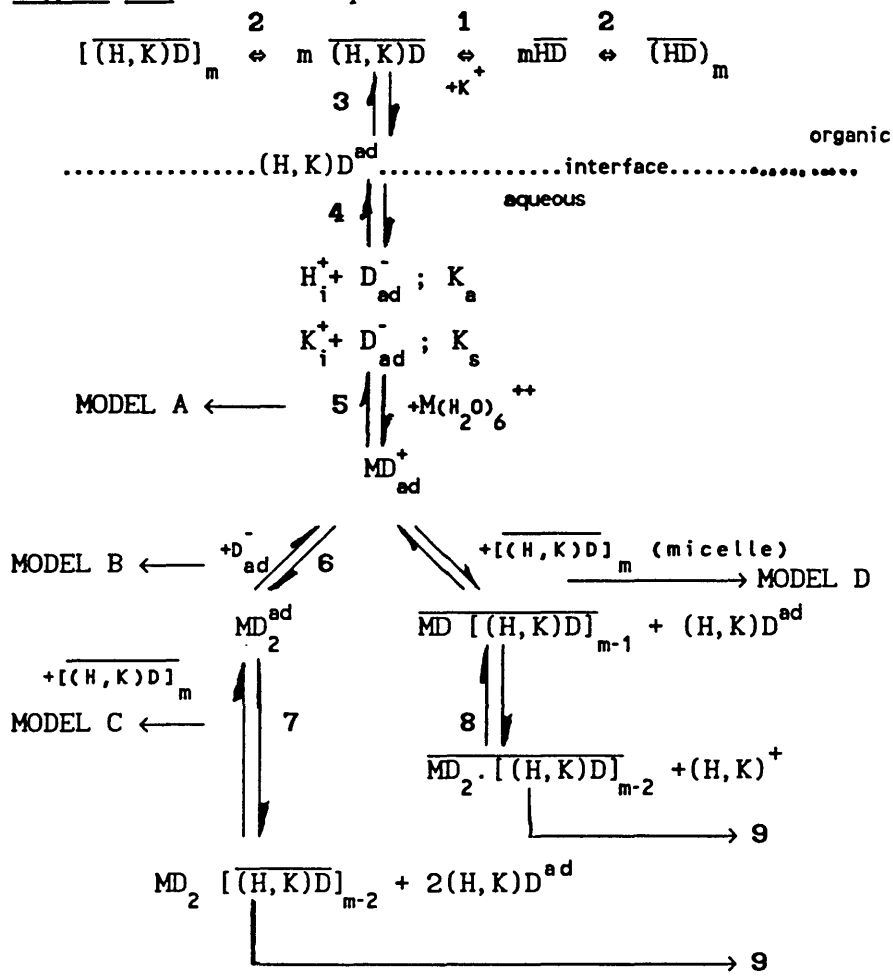
In subsection V.3.1 possible reaction mechanisms are proposed. Rate models are derived in subsection V.3.2. The discrimination of the rate-controlling step is based on the dependence of the interfacial flux on concentrations as discussed in subsection V.3.3.

V.3.1. Reaction mechanism

A reaction mechanism is proposed as shown in figure V.6. With the exception of the complexation steps 5 and 6, all other steps have been substantiated by experiments and are individually discussed next.

1) K^+-H^+ exchange: It takes place during physical equilibration of the organic feed (subsection IV.4.1). The factor X was defined in chapter IV as the ratio of K-sulphonate concentration in the bulk organic phase to formal sulphonate concentration ($\bar{C}_{DT}$).

Figure V.6. Reaction paths in the extraction of nickel by DNNSA.



In terms of monomers, that ratio is given by:

$$X = \frac{\bar{C}_{KD}}{\bar{C}_{KD} + \bar{C}_{HD}} = \frac{1}{1 + \frac{\bar{C}_{HD}}{\bar{C}_{KD}}} \qquad (V.10)$$

For simplicity the assumption is made that KD and HD aggregate to the same extent. In other words, it is assumed that the aggregation number m is independent of the type of counterion. Mixed micelles of KD and HD are assumed. A value m=7 is chosen in agreement with the results obtained in section IV.4.2 and with previous literature reports.

2) Aggregation: it is assumed that the LMA is a good representation of the aggregation equilibrium, thus

$$K_p = \frac{\bar{C}_p}{\bar{C}^m_{mon}} \qquad (V.11)$$

For the values of K_p around 10^{25} reported in the literature (Lin, 1984; Zheng and Osseo-Asare, 1987), it is found that $\bar{C}_{mon} \ll \bar{C}_p$ at $\bar{C}_{DT} \gg$ CAC, thus the solution is very dilute in monomers.

3) Monomer adsorption at the o/w interface. Due to the their low concentrations in the organic bulk, monomers adsorb to extents linearly dependent on their bulk concentrations. Thus

$$C^{ad}_{KD} = a_K \bar{C}_{KD} \qquad (V.12)$$

and

$$C^{ad}_{HD} = a_H \bar{C}_{HD} \qquad (V.13)$$

where a_K and a_H are the adsorption coefficients of the respective species as given for very dilute solutions by, among others, the Langmuir isotherm. The *fractional coverages* (FC, θ) by each species is given by:

$$\theta_K = \frac{C^{ad}_{KD}}{\Gamma_D/\lambda} \qquad \theta_H = \frac{C^{ad}_{HD}}{\Gamma_D/\lambda} \qquad (V.14)$$

The thickness of the adsorbed film (λ) need be considered for dimensional consistency. The interfacial excesses Γ_D were estimated in subsection IV.1.2 from measurements of σ and are listed in table F.5. Substitution of eqns.V.12, V.13 and V.14 in eqn.V.10 and the assumption that the adsorption coefficients of KD and HD be equal lead to the following relationship between bulk and interfacial speciation:

$$X = \frac{1}{1+\frac{\theta_H}{\theta_K}} \qquad (V.15)$$

4) Dissociation of adsorbed monomers: Adsorbed extractant molecules dissociate as discussed in section II.1. The interface is envisaged as a mosaic of adsorbed anions, acid and K-salt before there is any complexation of nickel. Instability constants relate the concentrations of the species involved in step 4 as follows:

$$K_a^i = \frac{C_H^i C_D^{ad}}{C_{HD}^{ad}} \qquad (V.16)$$

$$K_s^i = \frac{C_K^i C_D^{ad}}{C_{KD}^{ad}} \qquad (V.17)$$

Surface dissociation constants have in general different value than bulk constants (Al-Diwan et al., 1977). Unlike bulk constants, the values of interfacial constants change with pH (and possibly with I , too) as concluded by van Voorst-Vader (1961), who found that the ratio C_D^{ad}/C_{HD}^{ad} of adsorbed fatty acids changed less rapidly than the ratio in the bulk, $\bar{C}_D/C_{HD}$, when pH was changed. Evaluating surface dissociation constants resulted similarly difficult to Fyles (1986). The bulk ionization constant of DNNSA (K_a=0.27) is available in the literature (CRC Handbook, 1983 -84). The bulk constant for the K-soap was evaluated in section IV.4 as $K_s \cong 0.31$. The LMA constant for the overall reaction between DNNSA and Ni(II) was estimated in section IV.4.2 as K=0.195. These estimates apply to bulk conditions and may be corrected to interfacial values using eqn.II.5 (Hartley and Roe, 1940).

In the absence of diffusional fields, the interfacial concentration of ions relate to bulk concentrations as follows (Hartley and Roe, 1940):

$$C_j^i = C_j \exp(-z_j F\psi/RT) \qquad (V.18)$$

5,6) Interfacial complex formation: Now Ni(II) is added to the system and extraction starts as the adsorbed sulphonates complex nickel ions at the interface. Charged and 1:2 complexes form, completing the interfacial mosaic. Their dissociation equilibria is described as follows:

$$K_1^i = \frac{C_M^i \, C_D^{ad}}{C_{MD}^{ad}} \qquad (V.19)$$

$$K_2^i = \frac{C_{MD}^{ad} C_D^{ad}}{C_{MD_2}^{ad}} \qquad (V.20)$$

Eqn.V.21 is the species balance about the interfacial film:

$$C_{DT}^{ad} = C_D^{ad} + C_{KD}^{ad} + C_{HD}^{ad} + C_{MD}^{ad} + 2\, C_{MD_2}^{ad} \qquad (V.21)$$

or, in terms of FCs:

$$1 = \theta_s + \theta_K + \theta_H + \theta_{Ni} \qquad (V.22)$$

where θ_s is the FC by the ionized sulphonate as given by:

$$\theta_s = \frac{C_D^{ad}}{\Gamma_D / \lambda} \qquad (V.23)$$

and θ_{Ni} is the FC by both types of nickel complexes. Substitution of eqns.V.16, V.17, V.19, V.20, and V.23 in eqn.V.21 leads to

$$C_{DT}^{ad} = C_D^{ad} \left[1 + \frac{C_K^i}{K_s^i} + \frac{C_H^i}{K_a^i} + \frac{C_M^i}{K_1^i} + 2\, \frac{C_M^i \, C_D^{ad}}{K_2^i} \right] \qquad (V.24)$$

or, in terms of FCs, to

$$1 = \theta_s A + \theta_{Ni} \qquad (V.25)$$

where

$$A = 1 + \frac{C_K^i}{K_s^i} + \frac{C_H^i}{K_a^i} \qquad (V.26)$$

The estimates of ψ listed in table F.9 used together with eqns. II.5, V.18 and V.23, and the values of the constants K_a and K_s allow the evaluation of terms (i.e. the FCs) in the balance V.22, provided that K_1 and K_2 be known. Satisfaction of this requirement is complicated by the fact that the interfacial constants, unlike those in the bulk, relate concentrations of adsorbed species. Further, K_1 and K_2 pertain to two reactions in series, whereas the measurable bulk constant is an overall value. Fyles (1985) faced a similar problem. Two sets of values are tried for K_1 and K_2:

i) K_1, $K_2 \longrightarrow \infty$. In other words, $\theta_{Ni}=0$ (from inspection of eqns. V.19, V.20).

ii) $K_1=K_2=K=0.195$, i.e. the value experimentally found for the global complexation in the bulk.

Case i) In this case, $\theta_{Ni}=0$. θ_s was calculated as 1/A (eqn. V.25) for changing values of $\bar{C}_{DT}$ and pH. θ_s was independent of $\bar{C}_{DT}$ and varied slightly around 0.37 with pH as shown in table 1. The FC by K-soap was evaluated for $\theta_s=0.37$, via the approximate balance V.27, and the ratio V.28 (the exponentials cancel out in the latter). The calculations are listed in table 1. θ_K increased from 0.21 at pH=0.5 to 0.63 at pH= 3. There is no effect of changing values of $\bar{C}_{DT}$ on θ_K because ψ is not involved in this case. The bulk ratio X is also listed for comparison.

$$\theta_K + \theta_H = 1 - \theta_s \qquad (V.27)$$

$$\theta_K/\theta_H = C_{KD}^{ad}/C_{HD}^{ad} = (K_a^i/K_s^i)(C_K^i/C_H^i) = (K_a/K_s)(C_K/C_H) \qquad (V.28)$$

Table 1

pH	0.5	1.	1.5	2.	2.5	3.	4.	Notes
θ_K	0.21	0.49	0.58	0.60	0.62	0.63	0.63	case i
X	0.23	0.59	0.81	0.92	0.97	0.99	≅1	"
θ_s	0.361	0.376	0.380	0.381	0.382	0.383	0.383	"
θ_K	0.19	0.44	0.52	0.55	0.56	0.56	0.56	case ii
θ_H	0.64	0.31	0.12	0.048	0.017	0.0056	-	eqn.V.15
θ_H/C_H	1.99	3.06	3.81	4.78	5.32	5.56		

Case ii) Now $\theta_{Ni} \neq 0$. Values of θ_s were estimated from the quadratic (in C_D^{ad}) eqn.V.24 for changing values of $\bar{C}_{DT}$ at constant I and at changing pH at constant $\bar{C}_{DT}$. Again in this case θ_s showed a slight variation between 0.36 and 0.37. These values are larger than those estimated in the case of adsorbed carboxylic acids, consistent with the fact that the latter are weaker acids than DNNSA. Tanaka and Fukutome (1978) modelled monolayers of carboxylic acids as a lattice of three possible site types: ionized, protonated, or metal-complexed surfactant. From considerations of several possible interactions between sites, those authors concluded that coulombic repulsion between ionized sites effectively supressed the population of adsorbed anions. θ_K was estimated from the balance V.24 and the ratio V.29. It varied from 0.59 at $\bar{C}_{DT}=1.10^{-5}$kmolm^{-3} to 0.53 at $\bar{C}_{DT}$ = 0.01kmolm^{-3}. The values are listed in Table 2.

$$\theta_K/(\theta_H+\theta_{Ni}) = C_{KD}^{ad}/(C_{HD}^{ad}+C_{MD}^{ad}+2C_{MD}^{ad}{}_2) \qquad (V.29)$$

$$= \frac{C_K^i}{C_H^i\left[\frac{K_s^i}{K_a^i}\right]+C_H^i\left[\frac{K_s^i}{K^i}\right]+2C_H^i\left[\frac{K_s^i}{K^i}\right]\theta_s\Gamma_D/\lambda}$$

The pH effect on θ_K was simulated also in this case and the results are listed in Table 1. The values of θ_K are smaller than those of X. θ_H was estimated in a way analogous to that used for θ_K, i.e. using eqns.V.24 and V.29, and also via eqn.V.15. Both

sets of calculations were in acceptable agreement. θ_H was found to be independent of $\bar{C}_{DT}$. Values of θ_H calculated with eqn.V.15 are listed versus pH in table 1. The FC by nickel was not affected by pH changes, and it was around 0.08 at pH=2.5.

Table 2

$\bar{C}_{DT}(10^{-4}kmolm^{-3})$	$-\psi(mV)$	θ_K	θ_{Ni}
0.1	11	0.59	0.036
0.2	16	0.585	0.041
0.5	23	0.57	0.056
1.	26	0.57	0.060
2.	30	0.56	0.066
5.	34	0.55	0.076
10.	36	0.545	0.081
32.	39	0.537	0.089
100.	41	0.53	0.096

A ratio X^{ad} may be defined to describe the interfacial speciation as the parameter X describes the organic bulk speciation:

$$X^{ad} = \frac{C^{ad}_{KD}}{\Gamma_D/\lambda} \equiv \theta_K \qquad (V.30)$$

Equivalent formulae may be obtained in terms of C_H, as follows:

$$\theta_H = \frac{C^{ad}_{HD}}{\Gamma_D/\lambda} \qquad (V.31)$$

and

$$(\Gamma_D/\lambda)(1-X^{ad}-\theta_S-\theta_{Ni}) = C^i_H\, C^{ad}_D/K^i_a \qquad (V.32)$$

The above analysis of the interfacial speciation allows the following conclusions:

i)The bulk ratio X and the interfacial parameter X^{ad} (or the FC θ_K) differ by a value equal to $\theta_s+\theta_{Ni}$, which does not vary appreciably when pH and $\bar{C}_{DT}$ are changed.

ii) The small values of θ_{Ni} (<10%) obtained under the experimental conditions suggest that this FC may be neglected in the formulation of the interfacial speciation without introducing large errors.

iii) Expectedly, the interfacial composition predicted when θ_{Ni} is neglected is more similar to the bulk speciation than when finite values are chosen for K_1, K_2. The former case (case i) is however unrealistic because there must be nickel complexes in the adsorbed film to give rise to the observed nickel fluxes.

iv) In view of the fact that the difference between X and θ_K (or X^{ad}) is essentially constant, it is proposed to use the bulk speciation as an approximation to the interfacial speciation in the models derived in subsection V.3.2.

7) Interaction between micelles and the o/w interface: Micelles interact with the interface, exchanging cores (sections IV.3, V.1, V.2) and triggering the desorption of film material upon adsorption of monomers freed as micelles collapse (Carroll, 1981). Metal complexes are thus transferred from the interface into reversed micelles forming in the organic diffusion film.

8) Complex neutralization: when charged complexes are transferred from the film into micellar palisades, the second charge of Ni(II) is neutralized by a sulphonate.

9) Convective-diffusion: Nickel-loaded micelles diffuse away from the interface.

V.3.2. The rate equations

In order to identify the RDS, some of the reactions above described are chosen systematically as the RDS, and the corresponding rate equation is derived. In each case the other steps are considered very fast, thus the concentrations of the species involved are related by equilibrium conditions. The RDS is assumed *irreversible*, thus no reverse reaction is considered. This assumption is justified by the low conversions of reagents in the experiments and translates into models less involved than those incorporating reverse reactions (Danesi et al., 1976; Freeman and Tavlarides, 1982; Lee and Tavlarides, 1986; Komasawa et al., 1980 a; b; Murthy, 1987)) while as conceptually sound as the latter. Then the rate equations are discussed and evaluated.

Model A

When the RDS is the complexation of Ni(II) by adsorbed sulphonates (reaction 5 in figure V.6), the flux that corresponds to a first order reaction in both reagents is:

$$J_D = v\, k'_5\, C_M^i\, C_D^{ad} \qquad (V.33)$$

where $v=V/A$. Substitution of eqns.V.16, V.18, and V.31 into eqn. V.33 leads to

$$J_D = k_5\, \Gamma_D\, \frac{C_M}{C_H}\, \theta_s\, \exp(-2F\psi/RT) \qquad (A)$$

where $k_5=vk'_5K_a/\lambda$. The correction of K_a to the interfacial value (as in eqn.II.5, $10^{-\psi/60}$) is numerically almost identical to the factor $\exp(-F\psi/RT)$, thus the 2 in model A.

Model B

When the formation of the 1:2 metal complex (reaction 6 in the figure) is assumed the RDS, then

$$J_D = v\, k'_6\, C_{MD}^{ad}\, C_D^{ad} \qquad (V.34)$$

Substitutions similar to those made in model A lead to

$$J_D = k_6 \Gamma_D^2 C_M \frac{\theta_H^2}{C_H^2} \qquad (B)$$

where $k_6 = v\, k'_6 K_a^2 / K_1 \lambda^2$

Model C

The reaction between neutral metal complexes adsorbed at the interface and reversed micelles (number 7 in the figure) is now assumed as the RDS. Athough treated as an elementary reaction, this step involves a series of physical interactions such as collisions at molecular level, aggregation/disaggregation, and adsorption /desorption. All those mechanisms are thus lumped in the single step whereby a micelle hits the o/w interface, lo ses its identity, then regenerates. The rate at which this involved mechanism takes place is assumed proportional to the concentration of micelles. This assumption seems reasonable at low micellar concentrations. The flux is given by:

$$J_D = v k'_8 C_{MD_2}^{ad} \bar{C}_P^i \qquad (V.35)$$

The usual substitutions lead to

$$J_D = k_7 \Gamma_D^2 C_M \frac{\theta_H^2}{C_H^2} \bar{C}_{DT}^i \qquad (C)$$

where $k_7 = (v k'_7 / m) K_a / (K_1 K_2 \lambda^2)$

Model D

If the reaction between charged complexes and reversed micelles (number 8 in the figure) controls, then

$$J_D = v\, k'_8 C_{MD}^{ad} \bar{C}_P^i \qquad (V.36)$$

and

$$J_D = k_8 \Gamma_D \frac{C_M \theta_H}{C_H} \bar{C}_{DT}^i \exp(-F\psi/RT) \qquad (D)$$

where $k_8 = (v k'_8 / m) K_a / K_1 \lambda$.

V.3.3. Discussion of the models.

$\bar{C}_{DT}$ is not explicit in model A. The variation of the group $\Gamma_D \exp(-F\psi/RT)$ is, but this group does not vary as J_D did when $\bar{C}_{DT}$ was changed. Γ_D was almost constant above the CMC, and $\exp(-\psi)$ does not depend linearly on $\bar{C}_{DT}$ at I=0.5. Model A is therefore no further considered. Model B similarly fails to mimic the J_D vs $\bar{C}_{DT}$ data.

$\bar{C}^i_{DT}$ appears in both models C and D. Only the exponential in D makes a difference in the goodness of fitting by both models, as Γ_D was essentially constant throughout the $\bar{C}_{DT}$ range chosen for the rate experiments. The linear dependence of J_D on nickel concentration is granted because ψ was unaffected by changing metal concentrations (Lin, 1984). The main unknown was the response of these two models to changes in pH. The dependence of ψ on pH was estimated as a change of less than 4mV across the pH range by Lin (1984). In Table 1, estimates of θ_s and the ratio θ_H/C_H are listed versus pH. The θ_H/C_H curve increases as pH is increased then flattens in a similar way as the J_D versus pH curve. Such behaviour suggested that models incorporating the ratio θ_H/C_H would be able to simulate the pH effect on J_D.

For data-fitting regressions, $\bar{C}^i_{DT}$ was corrected as eqn.V.37 to account for the effect of mass transfer resistances:

$$\bar{C}^i_{DT} = \bar{C}_{DT} - \frac{7\, J_D}{K_o} \qquad (V.37)$$

The value of K_o used was $1.4.10^{-4} ms^{-1}$. This correction ranged from 0.6% $\bar{C}_{DT}$ at pH=0.3 to 1.5%$\bar{C}_{DT}$ at pH≅2.5 and above. Corrections for aqueous concentrations were estimated in a similar way and resulted of similar values. The correction due to MT in the water phase are however negligible in respect to the concentrative effect due to ψ. The exponential factor in model D is around 4.8 for ψ=-40mV.

The statistical package MINITAB available in the library of the College's CDC computer was used to perform multivariable re-

gression analysis of the experimental results. That analysis showed that model C fits the data better than model D (with correlation coefficients R=0.9955 and 0.9803, respectively). Analysis of variance more clearly indicated the better fit by model C. The F-ratio for this model returned by the package was 2564, whereas F was only 540 for model D. Both values are however larger than the requirement (F=248) for the appropriate number of degrees of freedom and at 5% confidence level (Mickley et al., 1957). The apparent kinetic constant in model C was $k_7=9.68.10^{-7}m^2kmol^{-1}s^{-1}$.

Predictions by model C are shown in figure IV.35 to agree closely with the J_D versus pH results. The J_D versus pH subset of the data were also better fit by model C (correlation coefficient R=0.9579) than by model D (R=0.9356). Some conclusions obtained in this section are summarised next:

1) The interfacial speciation has been simulated based on the organic bulk speciation, on adsorption, dissociation and cation exchange equilibria, and using reasonable values for the constants regulating those equilibria.

2) Relatively simple rate models have been derived assimilating the interfacial speciation to that in the organic bulk. Both models based on the assumption that reactions between the adsorbed extractant and nickel ions or complexes are the RDS under chemical regime were unable to simulate the effect that changing extractant concentrations had on fluxes. The other two models based on the assumption that the rate of interaction between nickel complexes adsorbed at the o/w interface and reversed micelles controls the rate of the overall reaction predict fluxes that fully reflect the effect of varying concentrations.

3) The fact that the mechanism of interactions between adsorbed complexes and micelles be common to both successful models indicates such interactions as the most probable RDS in the extraction of nickel. This mechanism synthesizes the following two previous suggestions:

a) that the adsorption of monomers resulting from micelles disaggregating in the interfacial zone "trigger the concerted desorption" of film material (Carroll, 1981). Nickel complexes are among those desorbed species, thus

b) those desorbed nickel complexes reside in the palisade of reversed micelles (Osseo-Asare and Keeney, 1980a) forming in the interfacial region.

4) Statistical analysis of the successful models showed that the main mechanism responsible for the extraction was the removal of **neutral** nickel complexes from the o/w interface by reversed micelles. Danesi et al. (1976), instead, found that the reaction between charged, 1:2/iron:DNNSA adsorbed complexes and reversed micelles was the RDS.

5) It follows from the previous conclusions that the composition of the interfacially adsorbed film is in chemical equilibrium with the aqueous subphase while the rate is subjected to a kinetic control determined by the combination of interfacial and organic bulk compositions. It is important to point out the possibility that changes in either or both these compositions may lead to a shift in the RDS. Such possibility is explored in section V.8, where the organic bulk speciation of extractant mixtures (section V.7) and the interfacial speciation are implemented in a model able to substantiate the rate enhancements reported in section IV.9.

6) The interaction between micelles and adsorbed complexes results in the depletion of fresh micelles in the organic subphase. More reagent is supplied to and products are removed from the reaction zone by the mechanisms of molecular and convective diffusion. The interplay between the chemical kinetics analyzed in this section and those transfer mechanisms that simultaneously take place is investigated in sections V.4 and V.5.

V.4. INTERFACIAL REACTION AND THE TWO-FILM THEORY

Mechanism and rate investigations of heterogeneous reactions are complicated by the occurrence of simultaneous kinetic and mass transfer phenomena. Convective and molecular diffusion supply reagents to interfacial reactions and remove the reaction products. Depending on the relative rates of reaction and mass transfer, the resistance due to one mechanism may predominate over the other and thus determine the global rate.

When the rates of reaction and mass transfer are comparable the overall rate control is shared by both mechanisms. This is called the *mixed* regime of mass transfer with chemical reaction. Consider the reversible reaction V.38 at the o/w interface:

$$aA + o\bar{O} \underset{k_r}{\overset{k_f}{\Leftrightarrow}} p\bar{P} + hH \qquad (V.38)$$

The rate of product P accumulation in the bulk of the receiving phase equals the rate of reaction at the interface and is also related to the diffusive fluxes of species by the stoichiometric coefficients as follows:

$$J = \frac{V}{A}\frac{dC_p}{dt} = k_f f_1(C_j^{\,i}) - k_r f_2(C_j^{\,i}) \qquad (V.39)$$

and, for both reagents:

$$\frac{J}{p} = \frac{1}{a} K_A(C_A - C_A^{\,i}) \qquad (V.40)$$

$$= \frac{1}{o} K_o(\bar{C}_o - \bar{C}_o^{\,i}) \qquad (V.41)$$

where the MTCs K_j describe the resistance to mass transfer across a boundary layer of thickness δ (Lewis and Whitman, 1924), the set of j interfacial concentrations is denoted by C_j^i, and the functionalities f_1 and f_2 are in general different. Equations like V.40, V.41 can be similarly set up for the reaction products. Concentration profiles are shown in figure V.7 for $\bar{O}$ under one hy-

drodynamic condition and for A at two bulk concentrations under three hydrodynamic conditions (i.e. δ, δ', and δ''). Electrostatic interactions are not considered. The profiles of $\bar{P}$ and H are not shown for clarity. The diffusion layer is assumed to thin from δ to δ'' as Re is increased to Re''.

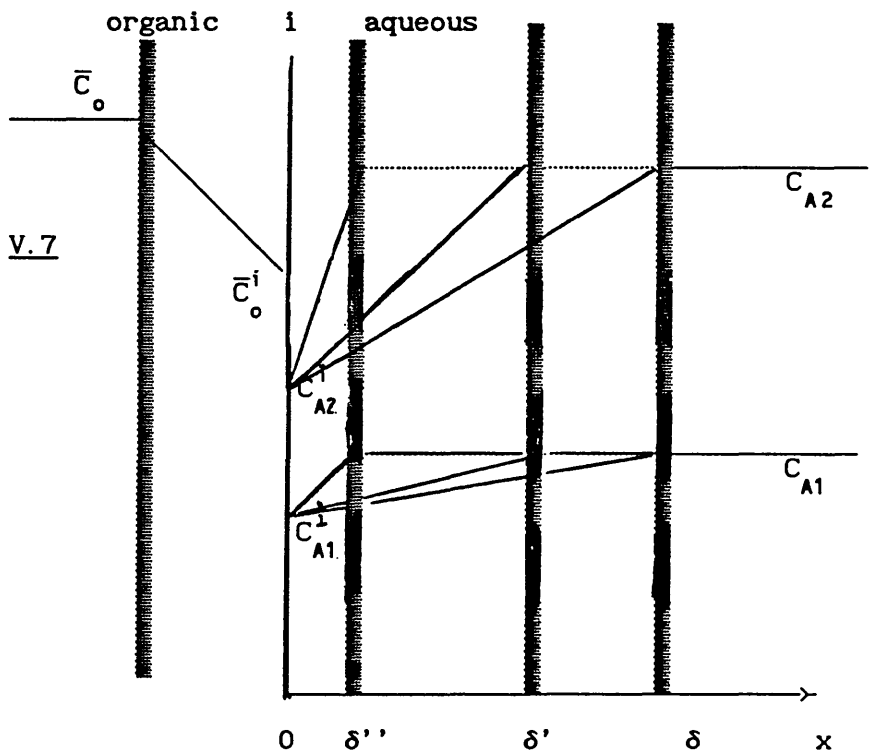


Figure V.7

Under initial conditions, the concentration of products is low and the second term in the RHS of eqn.V.39 may be neglected. The system of eqn.V.39 and the four flux equations can be solved with appropriate values of the mass transfer coefficients (MTCs) for the four interfacial concentrations (C_j^i) and the flux (J).

Assuming first partial order in A and for all other conditions constant, it follows from eqns.V.39, V.40 that

$$K_A(C_A - C_A^i) = (ak/p)\, C_A^i \qquad (V.42)$$

Hence the following proportionality between C_A and C_A^i is obtained:

$$C_A^i = B\, C_A, \text{ where } B = \frac{1}{1+\frac{a\,k}{p\,K_A}} < 1. \qquad (V.43)$$

At constant hydrodynamic conditions B is a constant. When the bulk concentration of A is increased from C_{A1} to C_{A2}, C_{A1}^i increases to C_{A2}^i. The ratio between both pairs of concentrations is a constant given by

$$\frac{C_{A2}^i}{C_{A1}^i} = \frac{C_{A2}^i/B}{C_{A1}^i/B} = \frac{C_{A2}}{C_{A1}}$$

Thus $$C_{A2}-C_{A2}^i = \frac{C_{A2}}{C_{A1}}\,(C_{A1}-C_{A1}^i),$$

and, since we chose that $C_{A2}/C_{A1}>1$, it follows that

$$(C_{A2}-C_{A2}^i) > (C_{A1}-C_{A1}^i) \qquad (V.44)$$

Thus as the bulk concentrations are increased, the concentration profiles are steeper, translating in faster mass transfer and interfacial reaction.

As Re increases, convective-diffusive mechanisms become more efficient (i.e. K increases) whereas kinetic mechanisms do not (i.e. k is constant). The kinetic share of the global control increases as a consequence. When further decreases in δ do not translate into further increases in J the rate is fully controlled by the reaction kinetics, and the system is said to be *chemically* or *kinetically* controlled. Then B approaches 1.

When K is small and the reaction is fast, mass transfer predominates and, in the limit, the observed rate depends fully on the value of the MTCs. The system is then under *diffusional* or *mass transfer* control. Here, the kinetic model V.33 no longer

links concentrations, which are instead related by the LMA, as follows (Bauer and Chapman, 1976):

$$K_e = \frac{k_f}{k_r} = \frac{\bar{C}_{P,e}^{\,p} C_{H,e}^{\,h}}{C_{A,e}^{\,a} C_{O,e}^{-\,o}} \qquad (V.45)$$

In the transfer regime represented by eqns.V.39 to V.41 the dependencies of the extraction rate on bulk concentrations may not be the same as for the interfacial concentrations, thus leading to only apparent orders of reaction (Ortiz et al., 1977). Such obscuring of the true reactions orders is sometimes called "diffusional falsification" (Froment and Bischoff, 1979). It is therefore necessary to ascertain that the reacting system is under chemical control when experiments are made to evaluate those orders.

Experiments run under varying hydrodynamic conditions can help to decide which is the rate determining step (RDS). If the control is diffusional, increases in MTCs and in J are observed when Re is increased. The physical MT results shown in figures IV.14, IV.17, and IV.22 are examples of this case. The nickel flux (J_D) in the NDSC at high [DNNSA] and low stirring speeds (N) depended similarly on N (figure IV.32). When there is chemical control, however, the flux does not change with N, as shown at higher N and lower [DNNSA] in figure IV.32. Higher plateaux are shown at higher values of [DNNSA]. This finding is expected because in this case B->1 and gradients become flatter, thus variations in bulk concentrations are followed at ratios closer to 1 at the interface. The faster the reaction, the more efficient the diffusive mechanism must be to reach kinetic control, thus higher plateaux onset at higher values of N.

Danesi (1983, 1984) has argued that pseudo-kinetic plateaux may result from the lesser stirring efficiency due to slip at interfaces at high speeds. The following discussion however proves that the plateaux shown in figure IV.32 are due to chemical control.

Physical MT fluxes increased as $Re^{\cong 1}$ even above N= 300rpm (figure IV.22, table F.14), where J_D was at plateaux. Thus the

MTCs (K) increased in the plateaux range, i.e. $\partial K/\partial N \neq 0$. The plateau at $\bar{C}_{DT}=5.10^{-3}M$ started at N≅200rpm, whereas J_D at $\bar{C}_{DT}= 1.10^{-2}M$ was found to increase up to N≅300rpm. The shift of the plateaux to higher values of N at faster reaction rates must be due to increases in K because, at a plateau,

$$\partial J_D/\partial N = 0 = \partial J_D/\partial K \; . \; \partial K/\partial N$$

It follows that $\partial J_D/\partial K=0$, which is the condition of kinetic control. Observed flux dependences on concentrations are therefore numerically equal to partial reaction orders, as they were considered in section V.3.

It was said in the previous discussion that the rate of nickel transfer equals the rate of interfacial reaction. It was however found in section V.3 that the reaction rate was controlled by the rate of interaction between the adsorbed film and micelles in the organic subphase. Due to such interaction, unconverted micelles deplete in the organic sub-phase, and its concentration decreases as the FE remains in the interfacial region. Because of turbulence, there is a random replacement of FEs in that region. It follows that the age of FEs and the reaction rate associated to each of them are time-distributed. The two-film theory approach followed in this section does not account for such age distribution. In the next section, the penetration-surface renewal approach is followed in an analysis able to predict fluxes into individual FEs and also average values.

V.5. INTERFACIAL REACTION AND THE PENETRATION-SURFACE RENEWAL THEORY.

The interaction between reversed DNNSA micelles and the macroscopic o/w interface was found in section V.3 to be the RDS in the extraction of nickel by DNNSA. Micelle-interface communications as those shown in figure V.3 are proposed. Such interactions resulted in water solubilization by micelles in the organic subphase (sections IV.1.2, V.1, and V.2) as well as in the transfer of interfacially adsorbed nickel sulphonates.

The mechanisms involved in the solubilization process shown in figure V.3 are: disaggregation, concerted adsorption-desorption (Carroll, 1981), and aggregation, all taking place in a fluid element (FE) in the organic sublayer adjacent to the o/w interface. Similar micellar dynamics must be operative when nickel is present. Changes will then be expected in the composition of the adsorbed film. MTCs calculated from solubilization experiments may thus be used to estimate rates of renewal of the organic sublayer.

It was assumed in section V.3 that, during extraction experiments, the composition of the adsorbed interfacial *mosaic* was that at equilibrium with the aqueous sublayer adjacent to the interface. A micelle contained in a FE next to the interface will be considered **converted** when, due to one interaction with the interface, it has incorporated to its palisade one previously adsorbed nickel sulphonate. The micelle will instead be called **loaded** when it has exchanged its core contents without incorporation of nickel complex to the palisade. Physical solubilization of nickel into the core is neglected. The following non-stoichiometric, irreversible reaction (first order in micelles) is assumed:

$$\overline{D_7.xH_2O} + MD_2^{ad} \longrightarrow \overline{MD_2.D_5.yH_2O} + 2D^{ad}$$

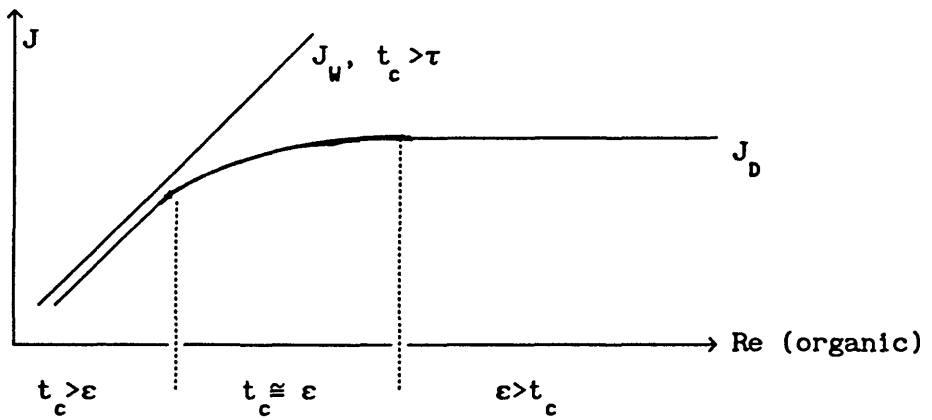
The choice of the 1:2 complex does not imply that the charged 1:1 complex can not be similarly attacked. The FE must remain a critical time ε at the interface to achieve a given conversion, say 99% of the metal loading capacity of the micelles contained in it, $L\bar{C}_{DT}/m$, where L is the equilibrium nickel loading of the ex-

tract. The time required for 99% of the micelles in the FE to load water will instead be called τ. All the interfacial area (A) is available to water solubilization, whereas only the micelles hitting the fraction $A\theta_{Ni}$ covered by Ni-sulphonates transfer nickel from the interface. In other words a micelle loads water the first time it hits the interface, but it requires $1/\theta_{Ni}$ hits to strike upon an adsorbed Ni-sulphonate. It is therefore expected that $\tau<\varepsilon$, and more strictly, that $\varepsilon=\tau/\theta_{Ni}$. It follows from the different rates of conversion and loading that the water transfer flux (J_w) will be largely determined by the rate of FEs renewal (s), whereas the interplay between renewal and conversion due to the above reaction will set the value to the nickel flux (J_D).

The rate of renewal s depends on the level of turbulence in the bulk phase, as confirmed by experiments: the values of J_w increased approximately as $Re^{1.}$ at constant composition (figure IV.22). Thus water solubilization rates were fully under MT control. J_D, instead, increased first as Re was increased, then reached a plateau (figure IV.32).

In the schematic figure V.8, t_c is the time spent by the FE next to the interfacial film. At sufficiently low values of Re, $t_c>\varepsilon$ and the FE adjacent to the interface reaches equilibrium conversion. This is the mass transfer (MT) regime, where J_D depends on s only. When $t_c<\varepsilon$, the FE leaves the interface scantly converted. J_D is then determined by the micelles-film interaction rate, and is independent of the turbulence in the bulk. This is the *chemical* or *kinetic* regime. The height of the plateaux depends on the value of $\overline{C}_{DT}$, as discussed in section V.4.

Figure V.8 . Subphase Conversion and FEs Renewal.



An attempt will now be made to translate the model into mathematical terms. Nickel complex-bearing micelles form by micelle-interface interactions and accum. ulate in the sublayer, giving rise to molecular diffusion into the FE, which is assumed stagnant. The driving force for diffusion is given by the difference between the concentration of complexed micelles at the "surface" of the FE ($\bar{C}_M^s$) and in the bulk ($\bar{C}_M^b$). The second Fick law describes the process in the FE:

$$\frac{\partial \bar{C}_M}{\partial t} = \mathcal{D} \frac{\partial^2 \bar{C}_M}{\partial x^2} \qquad (V.46)$$

$$\bar{C}_M = \bar{C}_M^b \; ; \; t=0, \; x \geq 0$$

$$\bar{C}_M = \bar{C}_M^b \; ; \; t>0; \; x \longrightarrow \infty$$

The remaining boundary condition (BC) is provided by the following balance between reaction and diffusion rates at the interface:

$$- \frac{d\bar{C}_M}{dx} = h(L\bar{C}_{DT}/m - \bar{C}_M) \; ; \; x=0, \; t>0 \qquad (V.47)$$

where $h = \frac{k\theta_{Ni}}{\mathcal{D}}$ and the apparent heterogeneous constant k is $k'\delta\Gamma_D/\lambda$, where k' is the frequency of collisions between micelles and interface. The thickness of the hypothetical reaction film

next to the adsorbed film is δ, and θ_{Ni} is the fractional interfacial coverage by metal complexes. The interfacial excess can be assumed constant at $\bar{C}_{DT}$>>CMC of the reagent.

BC V.47 is equivalent to that found when a solid is heated by radiation (Carslaw and Jaeger, 1959) and also in the case of humidification of a solid in contact with a wet gas stream (Crank, 1979). The solution of eqns.V.46., V.47 is obtained by Laplace tranformation in appendix E. The unsteady flux into each FE is given by:

$$J_i = h\mathcal{D}(L\bar{C}_{DT}/m-\bar{C}_M^b)\exp(h^2\mathcal{D}t)\operatorname{erfc}(h\sqrt{\mathcal{D}t}) \qquad (V.48)$$

where t is the FE residence time at the interface. The average interfacial flux is given by:

$$J_D = \int_0^\infty J_i(t)\ \phi(t)\ dt \qquad (V.49)$$

where $\phi(t)$ is the surface age distribution function. Use of Danckwerts' (1951) random surface renewal model, i.e.

$$\phi(t)=s\ \exp(-st)$$

leads to the following expression of the average flux:

$$J_D = k\theta_{Ni}(L\bar{C}_{DT}/m-\bar{C}_M^b)\left[\frac{s-h\sqrt{\mathcal{D}s}}{s-h^2\mathcal{D}}\right] \qquad (V.50)$$

The integration is detailed in appendix E. The constant k in eqn. V.50 was evaluated from the results shown in figure IV.32 (Table IV.28) using a minimization routine. The computer code (program FIT) is included in Appendix H. The estimates of s obtained in section V.1 and zero bulk complex concentration ($\bar{C}_M^b$) were used. The fractional coverage by nickel complexes and the equilibrium conversion of the extractant were both taken as 10% from the estimates in sections V.3 and in table F.22 (column c), respectively.

The value k=3.27 $.10^{-4}$ ms^{-1} for the apparent heterogeneous constant k fitted the experiments best.

Fletcher et al. (1987) reported intermicellar collision (homogeneous) rate constants in the order of $10^{3}s^{-1}$. Albery et al. (1987) estimated a value of $2.5.10^{-5}ms^{-1}$ for the heterogeneous frequency of collisions between reversed micelles and the macro -o/w interface, thus around one order of magnitude smaller than the result obtained in this work.

Predictions by model V.50 (program REWAL, Appendix H) are compared with the experiments in figure IV.32. The model mimics the plateaux observed at varying heights and onsetting at varying stirring speeds depending on the value of $\bar{C}_{DT}$. No plateaux were observed for physical mass transfer fluxes under similar conditions. It is therefore appropriate to attribute the occurrence of plateaux to the interfacial reaction. The above analysis shows that an integral consideration of:

a) the interfacial resistance due to chemical reaction,
b) molecular diffusion of the reaction product, and
c) renewal of FEs in the organic subphase,
leads to a rate model that correctly simulates the experiments. The finite y-intercepts shown in figure IV.32 at N=0 (hence s=0) are consistent with the fact that, due to natural convection and molecular diffusion, some extraction took place even when there was no forced convection in the phase.

V.6. KINETIC MODEL FOR Ni(II) EXTRACTION BY LIX63.

Two mechanisms in parallel were proposed in section IV.5 for the extraction of nickel by LIX63: exchange and solvation. Depending on pH, one mechanism was found to be thermodynamically more favourable than the other. It is expected that each mechanism be associated with an intrinsic rate of reaction, and that both rates be in general different. Dynamic extraction in the NDSC would thus

follow the reaction path kinetically more favourable. The pH dependence of flux reported in section IV.8 indicates that the extraction proceeded preferentially along the exchange mechanism. Solvation will therefore be neglected in the following rate modelling.

Let us now consider eqns. IV.53a to IV.53c and the fact that $J_L \propto \bar{C}_{LT}^{-1}$. The adsorption density Γ_L is expected to be almost constant as the $\bar{C}_{LT}$ range investigated, (0.5 to 20.) 10^{-3} $kmolm^{-3}$ was above the CAC ($\cong 2.10^{-4}$M; Osseo-Asare, 1984). It was found in section IV.1.2 from the data of Al-Diwan et al. (1977) that $\Gamma_L \cong$ constant around $\bar{C}_{LT}=1.10^{-3}$ $kmolm^{-3}$. Γ_L was found to vary at $\bar{C}_{LT} >$ CAC from σ measured in this work. Γ_L depended on $\bar{C}_{LT}^{\cong 0.7}$ in the range 1.10^{-3} to 1.10^{-2}, wherein J_L depended on $\bar{C}_{LT}^{1}$ (subsection IV.1.2). Thus, according to either set of Γ_L results, reaction IV.53 .b cannot be the RDS.

The constant value of Γ_L plus the rate of copper extraction dependency on bulk concentration of LIX65N prompted Al-Diwan et al. (1977) to conclude that "either the kinetics of extraction are unrelated to the interfacial concentration ...., or that interfacial concentrations have been wrongly estimated". The approach chosen here attempts to demonstrate that minor variations of Γ_L with changes in $\bar{C}_{LT}$ are not irreconcilable with an interfacial RDS.

Reaction IV.53c meets the requirements: it is an interaction between interfacially adsorbed complexes and organic phase aggregates. Constant adsorption densities will reflect in rate models via concentrations of the former species, whereas changes in the concentration of the latter species closely resembles changes in the formal extractant concentration. As shown below, rate equations based on this reaction as the RDS reproduce the effect of changing extractant concentrations on the flux, even though Γ_L be constant in the range of interest. The proposed mechanism is thus similar to that suggested for the extraction by DNNSA alone:

1) The cations are complexed by adsorbed oximes via fast reactions that probably involve the partial loss of hydration water by $Ni(H_2O)_6^{++}$.

2) The interface is a mosaic of adsorbed oximes and nickel oximates at equilibrium with the aqueous phase. The adsorption of K-oximates (known by experimentation) or of ionized species (known from the EM work of Osseo-Asare and Lin, 1983) is negligible. The FC by metal complexes is given by

$$\theta_{Ni} = \frac{C_M^{ad}}{\Gamma_L/\lambda} \qquad (V.56)$$

where λ is the thickness of the adsorbed film, required by dimensional consistency.

3) Thus the monolayer is chemically equilibrated with the aqueous phase, and desorbs upon the interaction between LIX63 aggregates (mostly dimers, $(\overline{H_2L})_2$, or D_2) and the interface, eqns. IV.53c and IV.56c. Thus this interaction controls the rate, and the observed metal flux is given by:

$$J_L = \Gamma_L k_L \theta_{Ni} \bar{C}_2^i \qquad (V.57)$$

where $k_L = k'_L/\lambda$ and $\bar{C}_2^i$ is the concentration of dimers next to the interface. As in section V.3, an expression relating θ_{Ni} to measurable concentrations is needed. Concentrations in both phases adjacent to the interface were estimated by correcting bulk values for mass transfer resistances (as discussed in section V.4). On the organic side the corrections (J_L/K_o) were around 10^{-6}M, thus much smaller than the values of $\bar{C}_{LT}$ used. Substitution of concentrations of adsorbed nickel complexes due to exchange (C_{Me}^{ad}, with stoichiometry Ni^{++}/NO_3^- /oxime=1/1/1) and to solvation (C_{Ms}^{ad}), and the adsorbed oxime (C_1^{ad}) in eqn. V.56 leads to:

$$\theta_{Ni} = \frac{C_{Me}^{ad} + C_{Ms}^{ad}}{C_1^{ad} + C_{Me}^{ad} + C_{Ms}^{ad}} \qquad (V.58)$$

The LMA applied to reactions IV.53a and IV.53b is:

$$K_{53} = \frac{C_{Me}^{ad}\, C_H^i}{C_M^i\, C_a^i\, C_1^{ad}} \qquad (V.59)$$

where C_a^i is the nitrate aqueous concentration close to the interface. The i superscripted refers to the electrostatic correction (Hartley and Roe, 1940) and it will be dropped in view that $\psi \cong 0$ in this case (Osseo-Asare et al., 1983). Equations IV.56 take place simultaneously with eqns.V.53, and from the LMA the following expression is obtained:

$$K_{56} = \frac{C_{Ms}^{ad}}{C_M^i\, C_a^{i2}\, C_1^{ad}} \qquad (V.60)$$

Substitution of eqns.V.59, V.60 into V.58 leads to

$$\theta_{Ni} = \frac{K_{56} C_M\, C_a\, (K_{36}/C_H + C_a)}{1 + K_{56}\, C_M C_a (K_{36}/C_H + C_a)}$$

where $K_{36} = K_{53}/K_{56}$. C_1^{ad} cancels out. Inserting eqn.V.61 into eqn.V.57 leads to

$$J_L = k_L \frac{\Gamma_L\, K_{56} C_M\, C_a\, (K_{36}/C_H + C_a)}{1 + K_{56} C_M\, C_a (K_{36}/C_H + C_a)}\, \bar{C}_2 \qquad (V.62)$$

The constants in eqn.V.62 can be estimated by consideration of the exchange mechanism of extraction alone. At pH=2.5, $\bar{C}_{Me}/\bar{C}_{Ms} > 6$. This approximation simplifies eqn.V.62 into eqn. V.63

$$J_L = k_L/\Gamma_L \frac{K_{53} C_M\, C_a\, \bar{C}_2/C_H}{1 + K_{53}\, C_M\, C_a/C_H} \qquad (V.63)$$

which can be rewritten as follows:

$$\frac{C_M C_a \bar{C}_2 \Gamma_L}{C_H J_L} = \frac{1}{k_L K_{53}} + \frac{C_M C_a}{k_L C_H} \qquad (V.64)$$

The constants in equation V.64 were evaluated by linear regression of the data using the MINITAB package as $k_L K_{53}=28.8 m^6 skmol^{-2}$ and $k_L=14.4\ m^3 s^{-1} kmol^{-1}$, thus $K_{53}=2 m^3 kmol^{-1}$. When $1 \ll K_{53} C_M C_a / C_H$, eqn V.63 reduces to :

$$J_L \cong (k_L)\ \Gamma_L \bar{C}_2 \qquad (V.65)$$

Eqn.V.65 predicts that fluxes be a function of extractant concentrations only. The data at $\bar{C}_{LT}=0.01$ and 0.02M cluster on a straight line up to $C_M C_a \bar{C}_{LT}/2C_H \cong 0.004$; thereafter plateaux at different heights corresponded to each value of $\bar{C}_{LT}$ (figure V.9), in agreement with eqn.V.65.

A second effect of pH on J_L is not explicit in eqn. V.62. As pH was increased from 1 to about 4, σ in the LIX63-Escaid-0.5M (H_2SO_4 +Na_2SO_4) system increased from around 18 to around $22 mNm^{-1}$ (Al-Diwan et al., 1977). Such changes in σ probably reflected changes in the value of Γ_L. No information is available to quantitatively estimate this effect as the dependence of σ on pH and on I has not been investigated in this work.

It seems interesting to note that the concentrations functionality in eqn.V.63 is similar to that found in a rate model proposed by Inoue et al. (1985) for the extraction of nickel by the hydroxyoxime SME 529. That model was based on the reaction between intermediate adsorbed complexes and extractant molecules in the aqueous phase as the RDS. Thus the partition coefficient appeared in the rate model and the authors concluded that it satisfied the correlation between rates and aqueous solubilities found by Akiba and Freiser (1982). Inoue et al. (1985) showed fluxes linearly dependent on organic bulk extractant concentrations at pH<7, consistent with constant partition coefficients under those conditions reported by Inoue and Tsunomachi (1984).

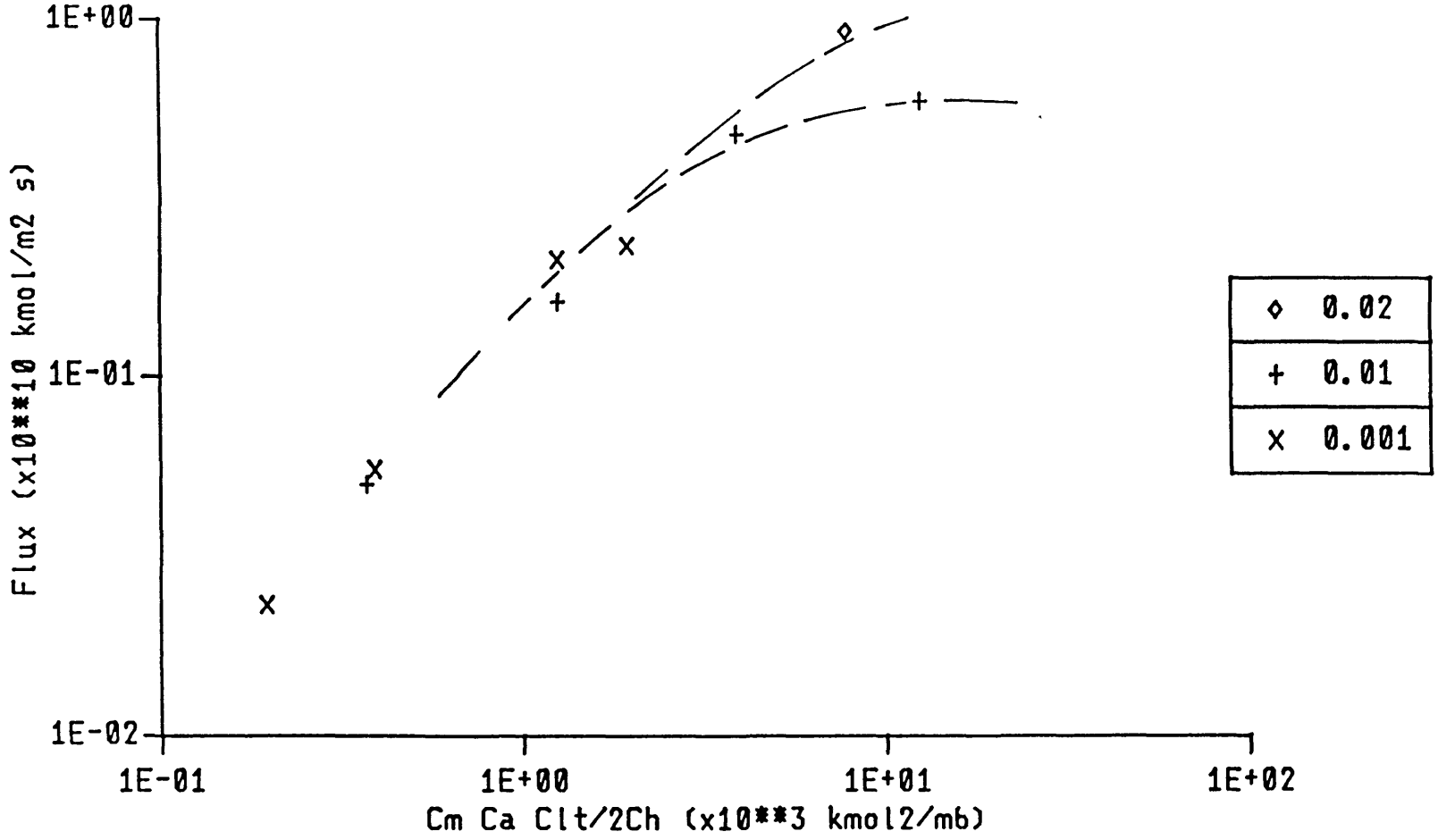


Figure V.9 Ni(II) extraction flux by LIX63. Ni(II) concn.=5.10**-3M
I=0.5M(KNO3+HNO3), pH=2.5. Parameter is LIX63 concn. (kmol/m3)

The fact that similar rate models result from assuming a RDS as a reaction between interfacial films and extractants in the aqueous phase (Inoue et al., 1985) or in the organic phase (this work) is somewhat striking. The model by the former authors could be readily tested by investigating the dependency of fluxes on the bulk concentration of SME 529 at pH>8, where P varied as [SME 529]$^{\cong 0.35}$ (Inoue and Tsunomachi, 1984).

V.7. SPECIATION IN DNNSA-LIX63 MIXTURES

Zheng and Osseo-Asare (1987) proposed that aggregation in DNNSA-LIX63 mixtures result in a number of species and estimated the various constants that relate the concentrations of those species at equilibrium. Here the same species are assumed and the same values of the equilibrium constants are adopted.

The aggregation of DNNSA has been extensively studied (subsection II.1.2). The monomer-micelle equilibrium is described by the LMA:

$$7D \Leftrightarrow D_7 \quad ; \quad K_p = C_{D7}/C_D^7 = 6.47.10^{26} \qquad (V.66)$$

Bars identifying organic species will be omitted in most of this section as all species considered belong in the bulk organic phase. The counterions are likewise omitted for simplicity. Consideration of the aggregation of DNNSA as one-step is substantiated by the abrupt change in aggregation number (m) from nil to around 7 as $\bar{C}_{DT}$ was increased beyond the CMC (Zheng and Osseo-Asare, 1987).

The values of m for LIX63 increased gradually from 1 to around 2.2 at $\bar{C}_{LT} \cong 0.12 kmolm^{-3}$ (Zheng and Osseo-Asare, 1987; Aguilar et al., 1983), thus a stepwise aggregation mechanism is more probable in this case, as follows:

$$2L \Leftrightarrow L_2 \quad ; \quad K_{L2} = C_{L2}/C_L^2 = 2.03 \qquad (V.67)$$

$$L_2 + L \Leftrightarrow L_3 \quad ; \quad K_{L3} = C_{L3}/C_{L2}C_L = 4.68.10^3 \qquad (V.68)$$

A mixture of mono-, di-, and trimers coexist in the range $1.10^{-3} \leq \bar{C}_{LT} \leq 0.1 kmolm^{-3}$ (Osseo-Asare and Zheng, 1987)

The literature on the aggregation of mixed extractants is less rich than that concerning single surfactants. Keeney and Osseo-Asare (1982) proposed the formation of the following mixed binary aggregate as responsible for the shifts in the CAC and the CMC of the mixtures, and for the dissappearance of the IR band of free HO^- in LIX63.

$$L + D \Leftrightarrow DL \; ; \; K_b = C_{DL}/C_D C_L = 4.84.10^4 \qquad (V.69)$$

At $\bar{C}_{LT}$=0.01kmolm^{-3} and at $\bar{C}_{DT}$ within the relatively high range 2.10^{-3} to 0.15kmolm^{-3}, Osseo-Asare and Zheng (1987) concluded that LIX63 was solubilized by DNNSA micelles, to form mixed micelles of variable stoichiometry $D_7.nL$, with n taking values from 0.6 to 7. When $\bar{C}_{LT}$ was increased further to the range 0.01 to 0.09 kmolm^{-3}, the VPO data of those authors showed minima corresponding to the largest extent of aggregation at values of the $\bar{C}_{DT}/\bar{C}_{LT}$ ratio around 2/3. Such ratio was previously found in mixed metal complexes by the Method of Continuous Variation (Osseo-Asare and Renninger, 1984). The following three aggregation equilibria are thus considered, with their relative importance being determined by the value of $\bar{C}_{DT}/\bar{C}_{LT}$.

$$D_7 + L \Leftrightarrow D_7.L \quad ; \quad K_{M1} = C_{D7L}/C_{D7}.C_L = 249 \qquad (V.70)$$

$$D_7 + 2L \Leftrightarrow D_7.2L \; ; \quad K_{M2} = C_{D72L}/C_{D7}.C_L^2 = 1.58 \qquad (V.71)$$

$$D_7 + 3L \Leftrightarrow D_2.3L + 5D; \; K_M = C_{D23L}.C_D^5/C_{D7}.C_L^3 = 1.27.10^{-13} \qquad (V.72)$$

The formal DNNSA balance about the bulk organic phase is:

$$C_{DT} = C_D + C_{DL} + 2\,C_{D23L} + 7\,(C_{D7}+C_{D7L}+C_{D72L}) \qquad (V.73)$$

and the LIX63 balance is

$$C_{LT} = C_L + C_{DL} + C_{D7L} + 2\,(C_{L2}+C_{D72L}) + 3\,(C_{L3}+C_{D23L}) \qquad (V.74)$$

Equations V.66 through V.72 were substituted into eqns.V.73, V.74 and the latter were solved for the monomer concentrations C_D, C_L in the range $1.10^{-5} \leq \bar{C}_{DT} \leq 5.10^{-2}$ and at $\bar{C}_{LT} = 1.10^{-3}$, 5.10^{-3}, and 1.10^{-2}kmolm^{-3}. The Numerical Algorithms Group (NAG) routine C05NBF was used to evaluate C_D and C_L from eqns.V.109, V.110 at each $\bar{C}_{DT}$, $\bar{C}_{LT}$ point. A listing of the computer code (NORG) is included in appendix H.

The concentration of the various aggregates was then computed by back-substitution. The speciation maps obtained in this way are shown in figures V.10 and V.11, as log(species) vs log $\bar{C}_{DT}$, at two values of [LIX63]. It is shown in figure V.10 that the mixed dimer DL is the main aggregate in the lower half-range, where micellar concentrations are negligible. DL is important in the upper half-range, where it is in higher concentration than either monomer. In the latter region, however, micelles are significant. The "pure" micelle D_7 predominates at the upper end of the range. The mixed micelle $D_7.2L$ is nowhere relevant. The concentration of $D_7.L$ varies as that of D_7, particularly at higher $\bar{C}_{LT}$.

Breaks can be seen in the C_{D7} and in the C_{D7L} versus $\bar{C}_{DT}$ curves in both figures, at $\bar{C}_{DT}$ values somewhat higher than the respective CMCs. The concentration of $D_2.3L$ peaks near those breaks at both values of $\bar{C}_{LT}$.

The one prediction by the analysis which cannot be readily explained is the high value of C_L at the lower end of the range. At $\bar{C}_{DT}=1.10^{-5}$kmolm^{-3}, $C_L \cong \bar{C}_{LT}=1.10^{-3}$, whereas C_{L2} and C_{L3} are between (0.01 and 0.001) $\bar{C}_{LT}$. Thus at $\bar{C}_{LT}=1 .10^{-3}$ kmolm^{-3} the free oxime is mainly as a monomer when DNNSA is in solution, according to the model. At $\bar{C}_{LT} = 5.10^{-3}$kmolm^{-3}, and $\bar{C}_{DT}=1.10^{-5}$kmolm^{-3}, C_{L3} is around $\bar{C}_{LT}/20$, consistent with the higher aggregation expected at higher LIX63 concentration.

It is shown in figure V.10 that C_{L2} crosses above C_{L3} as $\bar{C}_{DT}$ is increased past the CMC. Besides, the concentrations of the three free oxime species (L, L_2, and L_3) fall more sharply at $\bar{C}_{DT}$> CMC, consistent with the proposed solubilization of the oxime by

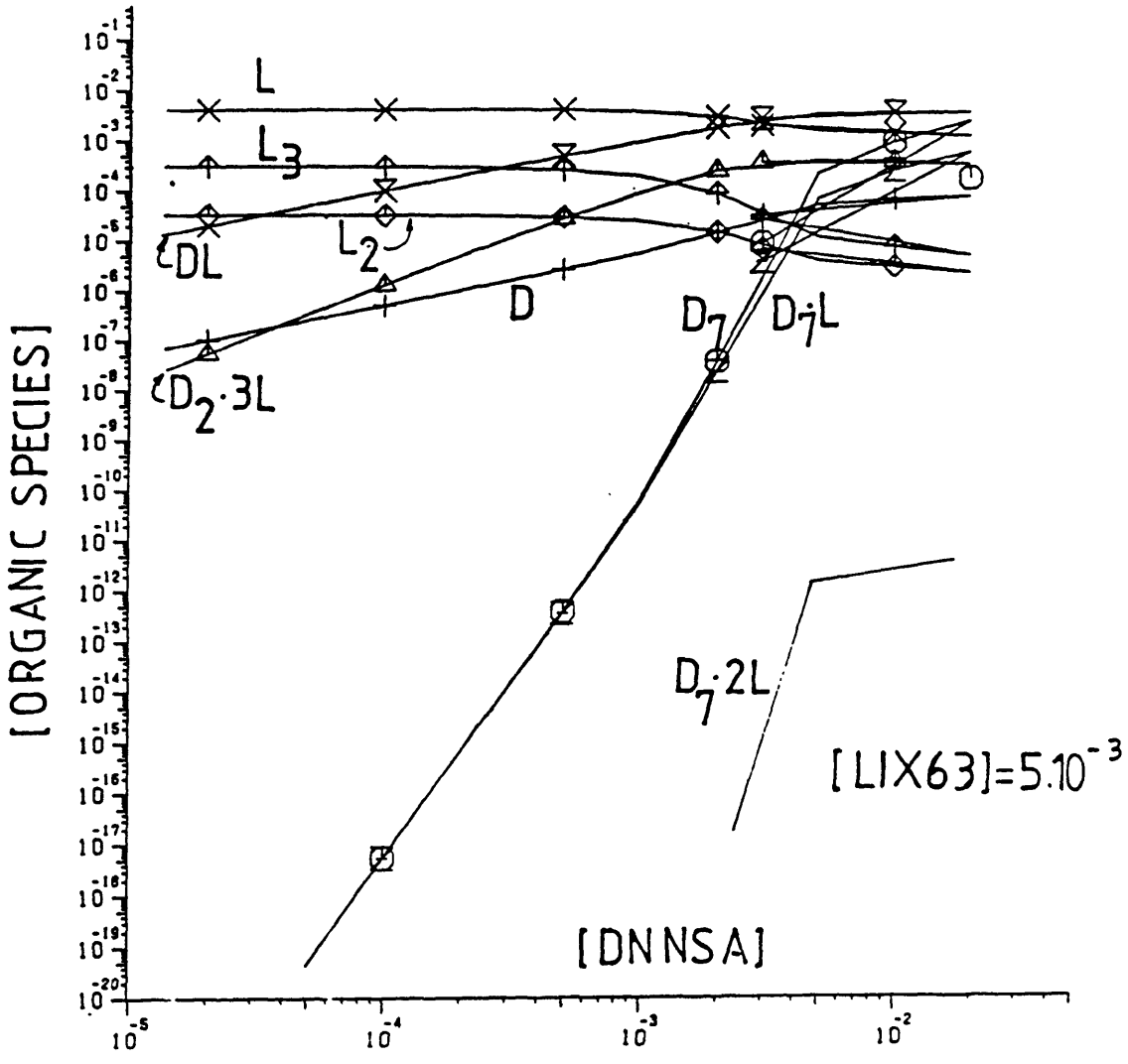


Figure V.10 Speciation of DNNSA-LIX63 mixtures at $[LIX63] = 5.10^{-3}$ kmolm^{-3}.

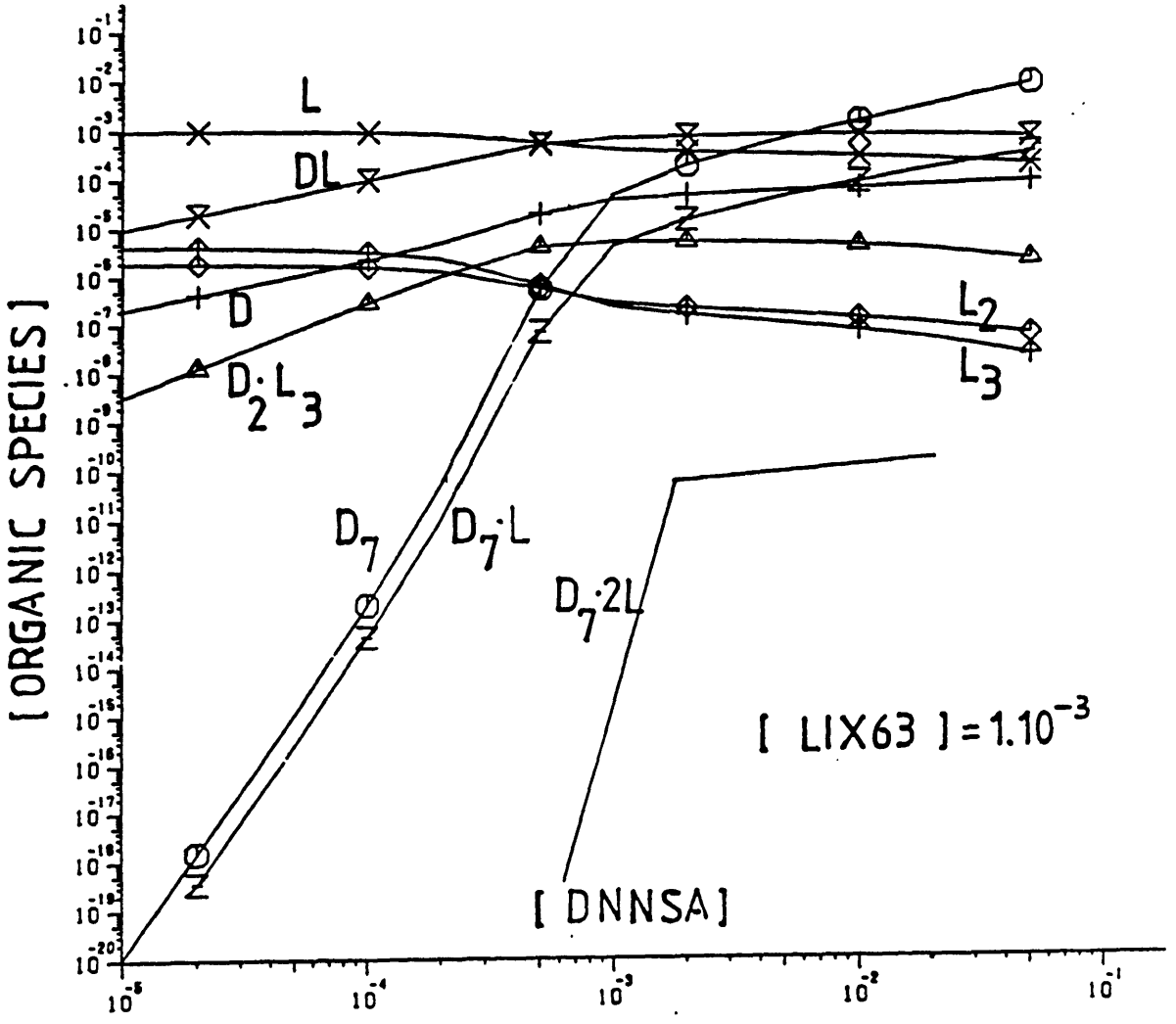


Figure V.11 Speciation of DNNSA-LIX63 mixtures at $[LIX63]=1.10^{-3}$ kmolm^{-3}.

DNNSA micelles (Osseo-Asare and Zheng, 1987; Osseo-Asare and Keeney, 1980a).

V.8. KINETIC MODEL FOR EXTRACTION BY MIXTURES

An attempt is made in this section to find a quantitative explanation to the pH and organic composition effects on J_M presented in section IV.9. The rate model will draw inputs from the π-A isotherms calculated in subsection IV.1 .2, the interfacial potentials corrected in subsection IV.1 .3, the cation exchange equilibrium reported in subsection IV.4.1, the single-reagent models derived in sections V.3 and V.6, and the organic speciation computed in section V.7.

It was concluded in section V.3 that the rate of interaction between reversed micelles and the adsorbed film determines the rate of nickel complex desorption and phase transfer under plateau conditions with DNNSA alone. In that case, all the experiments were done at $\bar{C}_{DT}$>CMC, where the interfacial density (Γ_D) was approximately constant. The concentration of discrete particles (DP, micelles in this case) changed as $\bar{C}_{DT}^{\cong 1}$, because the concentration of micelles was much larger than the monomer concentration and the aggregation number is constant.

When LIX63 was added to DNNSA solutions, the interfacial density of the mixtures (Γ_M) was found to be smaller than Γ_D (section IV.1), and the speciation of the system changed (section V.7). The decrease to Γ_M from Γ_D means a dilution of the adsorbed mosaic, thus the interfacial complexation of nickel must be slower in mixtures than with DNNSA alone. The concentration of DPs able to interact with the adsorbed film, however, increased as more LIX63 was added due to the formation of *sub-micellar aggregates* (SMA). Thus the rate of interfacial interactions causing renovation of the interfacial film is expected to increase.

The combination of slower conversion and faster desorption may shift the overall rate control to the former mechanism in mix-

ed systems. An attempt is now made to translate the model into mathematical terms. Two assumptions are made:

1) The rate at which an adsorbed film desorbs depends mainly on the concentration of aggregates that interact with the film. The film properties are a factor of lesser importance.

2) The various aggregates are similarly efficient to interact with and desorb the interfacial film. In other words, the spread of DP-interface collision frequencies is small, and it is accepted that a single frequency describes the interfacial mechanics.

A factor F is now defined as the ratio of DPs concentrations in both systems:

$$F = \frac{\text{Concentration of DPs in mixtures}}{\text{Concentration of DPs with DNNSA}} \qquad (V.75)$$

The numerator in eqn.V.75 is the sum of the concentrations of micellar species (MIC) and of SMAs (SMA) in the mixed system:

$$MIC + SMA = (C_{D7} + C_{D7L} + C_{D72L}) + (C_{DL} + C_{D23L} + C_{L2} + C_{L3})$$

The denominator in eqn.V.75 is simply $\bar{C}_{DT}/m$ since $\bar{C}_{DT}$>CMC in the concentration range chosen. Values of F are shown vs $\bar{C}_{DT}$ in figure V.13 at $\bar{C}_{LT}=1.10^{-3}$kmolm^{-3} and 5.10^{-3} kmolm^{-3}. F was computed by program NORG, listed together with sample output in appendix H.3.

In figure V.12, F is seen to decrease at $\bar{C}_{LT}=1.10^{-3}$M from around 12 to around 9 as $\bar{C}_{DT}$ was increased up to the CAC. F decreased slightly in the range CAC $\leq \bar{C}_{DT} \leq$ CMC, and it fell again more sharply at $\bar{C}_{DT}$>CMC to F$\cong$1 at $\bar{C}_{DT}= 1.10^{-2}$kmolm^{-3}. Three regions are identified accordingly. In region I the concentration of monomers decreases as more DNNSA is available to form SMAs. MIC $\cong$ 0, and the denominator in eqn.V.75 grows faster than the numerator as $\bar{C}_{DT}$ was increased toward the CAC of the mixture.

In region III the oxime was solubilized by micelles forming appreciably above the mixture's CMC (Osseo-Asare and Keeney, 1980, Zheng and Osseo-Asare, 1987) thus SMA decreased while MIC increased. The reason for the saddle point in region II is less obvious, one possibility being the depletion in L_2 and L_3 at the expense of D_2L_3 (figure V.11).

The flux enhancement ratio (E) also shown in figure V. 12 was defined as follows

$$E=J_M/J_D \qquad (V.76)$$

The partition in three regions also applies to the E vs $\bar{C}_{DT}$ curve. Results presented in figure IV.37 as J_D, J_M versus $\bar{C}_{DT}$, $\bar{C}_{LT}$ are reproduced in figure V.13, where the three regions are shown. It is interesting to compare figures V.12 and V.13. The horizontal stretch at $\bar{C}_{DT}$<CAC in figure V.12 at $E\cong 9$ corresponds to region I, where J_D and J_M vary as $\bar{C}_{DT}^{\cong 1}$. J_M was nearly constant in region II, thus E fell to around 2 at $\bar{C}_{DT}\cong$CMC. E was almost constant in region III as the curves J_D vs $\bar{C}_{DT}$ and J_M vs $\bar{C}_{DT}$ were again parallel.

The large value of F at $\bar{C}_{DT}$<CAC and the fact that $\Gamma_M<\Gamma_D$ suggest the possibility that the rate of interfacial complexation be lower, thus rate-determining, than the rate of desorption in regions I and II. This hypothesis is substantiated by the following argument. The rate models derived in sections V.3 and V.5 included the concentration of micelles explicitly. If similar mechanisms of interaction between aggregates and the interface control the rate in this case, the flux equation must be of the form

$$J_M=k\Gamma_M\theta_{Ni}(MIC+SMA) \qquad (V.77)$$

where $k=k'/\lambda$, and the factor including the surface renewal frequency s in eqn.V.50 (section V.5) is assumed equal to one. The sum MIC +SMA increased as $\bar{C}_{DT}^{\cong 1}$ between the CAC and the CMC of the mixtures (region II), while the fraction θ_M is not expected to vary significantly. Γ_M also increased in the region (figure IV.4), thus values of J_M strongly affected by $\bar{C}_{DT}$ would be predicted.

That variation was not found experimentally. Instead J_M increased slightly, its variation resembling that of Γ_M. In region II, therefore, the results suggest that complex formation instead of desorption was the RDS with mixtures. This step does not involve organic aggregates, i.e. it is an interaction between aqueous and interfacially adsorbed species.

Because Γ_M^I is smaller than Γ_M^{II} and because F^I is larger than F^{II}, the above conclusion about the RDS is even more obvious in region I.

Now the reactions controlling the extraction kinetics in regions I and II may be written. The assumption is obvious that oxime and sulphonate adsorb. The former is assumed undissociated from the ψ measurements (Osseo-Asare et al., 1983) and loaded with NO_3^- as confirmed by experiments in this work.

$$M^{2+}{}^{i} + D^{-}{}^{ad} \longrightarrow MD^{ad} \qquad (V.78)$$

$$NO_3^- + H_2L^{ad} \Leftrightarrow NO_3^-.H_2L^{ad}$$

$$M^{2+}{}^{i} + NO_3^-.H_2L^{ad} \longrightarrow (NO_3)MHL^{ad} + H^{+}{}^{i} \qquad (V.79)$$

The contribution by DNNSA to the total flux is

$$J_D = vk'_D\ C_M^i\ C_D^{ad} \qquad (V.80)$$

and the contribution due to LIX63 is

$$J_L = vk'_L\ C_M^i\ C_L^{ad}/C_H^i \qquad (V.81)$$

The superscript i in this case indicates that bulk concentrations are to be corrected for electrostatic effects and for gradients due to mass transfer resistances. The observed flux is simply the sum of both contributions:

$$J_M = J_D + J_L \qquad (V.82)$$

The concentrations of adsorbed reagents are estimated from the assumption of an interfacial mosaic equilibrated with a nickel-free aqueous phase. For LIX63, the following simple approximation allows estimating C_L^{ad} from the results shown in table IV.2 and figure IV.4:

$$C_L^{ad} \cong \theta_L \Gamma_M / \lambda \qquad (V.83)$$

Due to the low selectivity of DNNSA, estimating its interfacial concentration is less simple than for LIX63. C_D^{ad} is approximated neglecting the FC by nickel complexes in the following balance about the adsorbed film:

$$\theta_D \cong \theta_s + \theta_{HD} + \theta_{KD} = \frac{\Sigma C_j^{ad}}{\Gamma_M / \lambda} = A\,\theta_s \qquad (V.84)$$

where A was defined before (section V.3) as eqn.V.26, and the FC by ionized sulphonate was defined in eqn.V.23, rewritten as

$$\theta_s = C_D^{ad} \lambda / \Gamma_M \qquad (V.85)$$

The FC by nickel complexes was estimated in section V.3 to be smaller than 10%. Since the complexes were at equilibrium concentration then whereas they form at a finite rate now, their coverage must be even smaller than before. Besides, a fraction of the interface is now covered by LIX63, further reducing the FC by nickel-DNNSA complexes. Thus neglecting the FC by metal complexes seems in this case justified. Substitutions into eqn V.82 lead to the following model:

$$J_M = \left(k_D \frac{\theta_D}{A} + k_L \frac{\theta_L}{C_H^i}\right) \Gamma_M\, C_M^i \qquad (V.86)$$

where $k_D = \frac{k'_D}{\lambda}$, $k_L = \frac{k'_L}{\lambda}$, and

$$C_H^i = (C_H + 2J_M / K_{aq}) \exp(-F\psi/RT)$$

$$C_M^i = (C_M - J_M / K_{aq}) \exp(-2F\psi/RT)$$

Model V.86 predicts that the data cluster on a straight line when plotted versus A/C_H^i, rearranged as eqn.V.87.

$$\frac{J_M A}{\Gamma_M C_M^i} = k_D\theta_D + k_L\theta_L(A/C_H^i) \qquad (V.87)$$

The prediction was confirmed (figure V.14). The values $K_a = 0.27$, $K_s = 0.31$ were used in the computations. An average value of K_{aq} was estimated from the DNNSA solubilization work as $1.10^{-4}ms^{-1}$. The constants obtained from fitting the data by eqn.V.87 were used to predict values of J_M, shown as curves I, II in figure V.13 at $\bar{C}_{LT} = 1.10^{-3}kmolm^{-3}$. The model mimics the experimental results well in the range $2.10^{-5} \leq \bar{C}_{DT} \leq 4.10^{-4}kmolm^{-3}$.

In region III the value of F fell to around one, and Γ_M was relatively high and nearly constant, thus intuition suggests that extraction by mixed and single reagents was similarly rate-controlled in this region by film desorption instead of by interfacial complexation. A film is assumed of composition again described by eqns.V.83 through V.85, but now equilibrated with the aqueous subphase containing nickel. Each aggregate in concentration $\bar{C}_j$ able to interact with the interfacial film contributes a fraction J_{ij} of the observed flux when it hits the ith adsorbed nickel complex. Thus

$$J_{ij} = k'_{ij} C_{Mi}^{ad} \bar{C}_j = k_{ij}\Gamma_M \theta_{Ni}^i \bar{C}_j \quad ; \text{ where } k_{ij} = k'_{ij}/\lambda \qquad (V.88)$$

The total contribution to J_M by the jth aggregate thus is

$$J_j = k_j \Gamma_M \bar{C}_j \theta_{Ni}; \text{ where } \theta_{Ni} = \sum_i \theta_{Ni}^i = \theta_{Ni,L} + \theta_{Ni,D}$$

The total flux is the sum of all these contributions, thus

$$J_M = \sum_j J_j = k_M \Gamma_M \theta_{Ni} \sum_j \bar{C}_j \qquad (V.89)$$

A unique value k_M for the kinetic constants k_j was assumed. The sum over the concentrations of aggregates is the same value

used to calculate F, i.e. MIC+SMA, evaluated at the sublayer adjacent to the interface. Γ_M was estimated experimentally. The difficulty here lies, as in section V.3, with the evaluation of the FCs by metal complexes (θ_{Ni}) in eqn.V.89. For LIX63 alone, it was found in section V.6, eqn. V.63, that

$$\theta_{Ni,L}^{single} \cong 2\left[\frac{C_M^i C_a^i / C_H^i}{1+2C_M^i C_a^i / C_H^i}\right] \qquad (V.90)$$

where 2 $m^3 kmol^{-1}$ was the value found for the constant K_{53} in eqn.V.63. With mixed reagents, the FC by nickel oximate is assumed equal to the fraction $\theta_{Ni,L}^{single}$ of the fraction of mixed film covered by oxime and oximate, θ_L. In other words,

$$\theta_{Ni,L} = \theta_L . \theta_{Ni,L}^{single} \cong$$

$$\cong 2\left[\frac{\theta_L C_M C_a / C_H}{1+2 C_M C_a / C_H}\right]$$

The superscripts were dropped because the exponential corrections due to ψ cancel out. In section V.3, the complex coverage with DNNSA alone was in model C:

$$\theta_{Ni,D}^{single} = \frac{K_a^{i2}}{K_1^i K_2^i} C_M^i \frac{\theta_H^2}{C_H^2} \cong \frac{K_a^2}{K_1 K_2} C_M \frac{(1-X)^2}{C_H^2}$$

where the bulk selectivity factor X is used to approximate the FC by adsorbed acid. Also for DNNSA it is assumed that the FC in mixtures is proportional to the FC by the reagent alone. Thus

$$\theta_{Ni,D} = \theta_D . \theta_{Ni,D}^{single} = \frac{K_a^2}{K_1 K_2} \frac{\theta_D C_M \theta_H^2}{C_H^2} \qquad (V.92)$$

Substitutions lead to the following model for the total flux

$$J_M = k_M \Gamma_M \left[\frac{2\,\theta_L C_M C_a / C_H}{1+2\,C_M C_a / C_H} + \frac{K_a^2}{K_1 K_2} \frac{\theta_D C_M (1-X)^2}{C_H^2}\right] (MIC+SMA)^i \qquad (V.93)$$

The pH effect on J_M at varying $\bar{C}_{DT}$, $\bar{C}_{LT}$ can be identified in eqn. V.93 for the following two limiting cases:

i) $\bar{C}_{LT}=\theta_L=0 \longrightarrow J_M = J_D \alpha \left[\frac{1-X}{C_H}\right]^2 \alpha\ 0.43pH$

ii) $\bar{C}_{DT}=\theta_D=0 \longrightarrow J_M = J_L \alpha \frac{C_M C_a/C_H}{1 + 2C_M C_a/C_H}$

At C_a=0.5M, $C_M=5.10^{-3}$kmolm^{-3} and at pH<2, $2C_MC_a/C_H$ is smaller than 0.5, and J_M is roughly proportional to C_H^{-1}. The constants in model V.93 were evaluated using the values of (MIC+SMA) listed in appendix H, and the dependence of θ_D, θ_L on $\bar{C}_{LT}$ estimated from the results by Al Diwan et al. (1977) listed in table IV.2. θ_D, θ_L were considered constant at given values of $\bar{C}_{LT}$. The model was rewritten as eqn. V.94 to evaluate the parameters by data fitting

$$\frac{J_M}{\Gamma_M(MIC+SMA)} = k_M \frac{2\,\theta_L C_M C_a/C_H}{(1+2\,C_M C_a/C_H)} + \frac{K_a^2}{K_1K_2}\,\frac{\theta_D C_M (1-X)^2}{C_H^2} \qquad (V.94)$$

The constants returned by bivariable regression analysis by the MINITAB statistical package at $\bar{C}_{LT}=1.10^{-3}$kmolm^{-3} were $k_M\theta_L$=266, thus k_M= 1900, and $k_M K_a^2\theta_D/K_1K_2$=307, thus $K_1K_2 \cong 0.56$. For these values of the constants K_1,K_2, the metal FC roughly was $\theta_{Ni} \cong 0.004\theta_H$, thus no large error was introduced by the approximation done in eqn. V.84 when it was assumed θ_{Ni}=0.

Predictions by the models are shown as line III at $\bar{C}_{LT}=1.10^{-3}$ kmolm^{-3} and variable $\bar{C}_{DT}$ in figure V.13. The predicted line in figure IV.35 mimics well the effect of pH on J_M at $\bar{C}_{LT}$= 1.10^{-3}kmol m^{-3}.

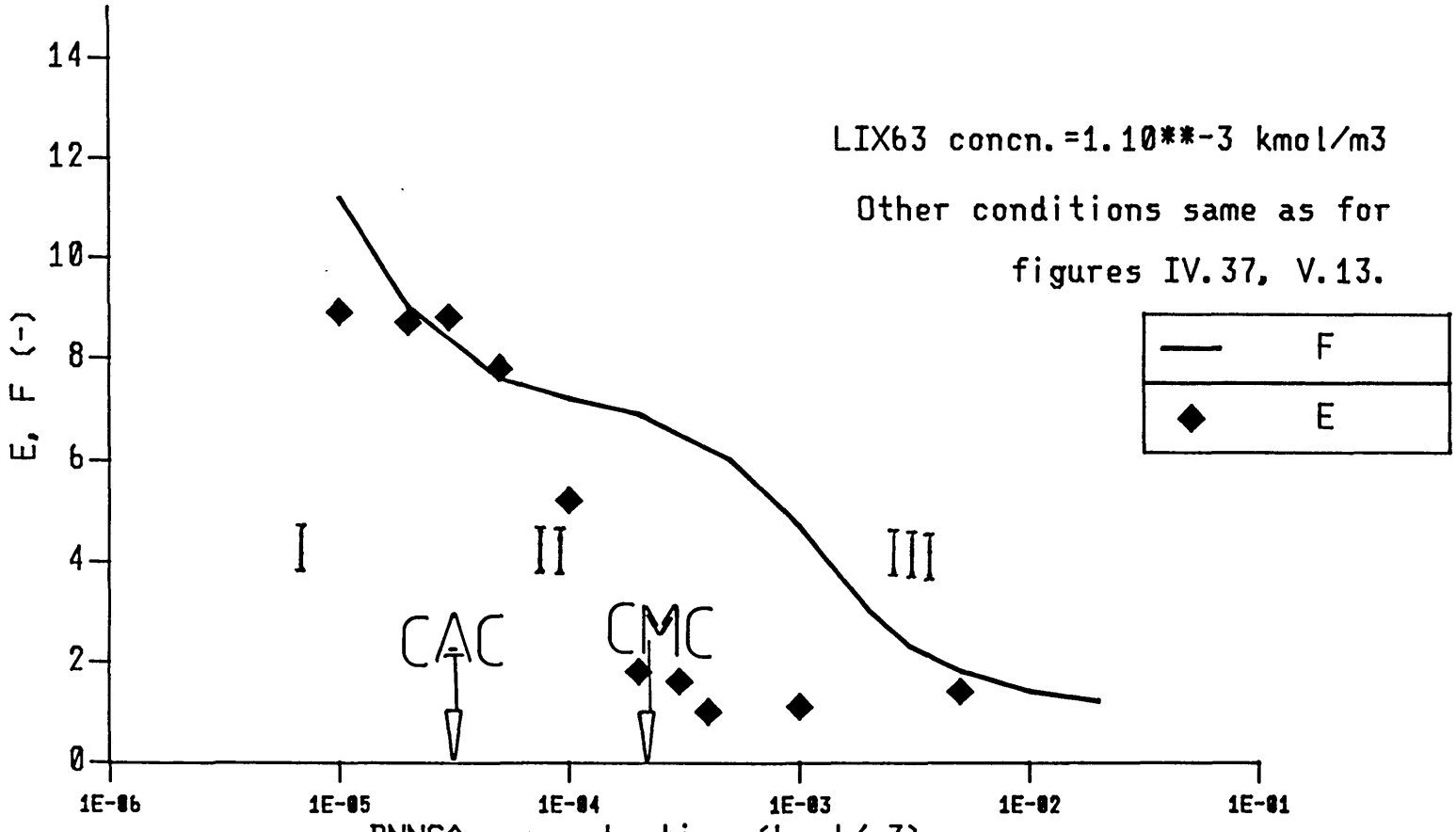


Figure V.12 Enhancement factors of nickel flux (E) and of particles-interface collisions rate (F).

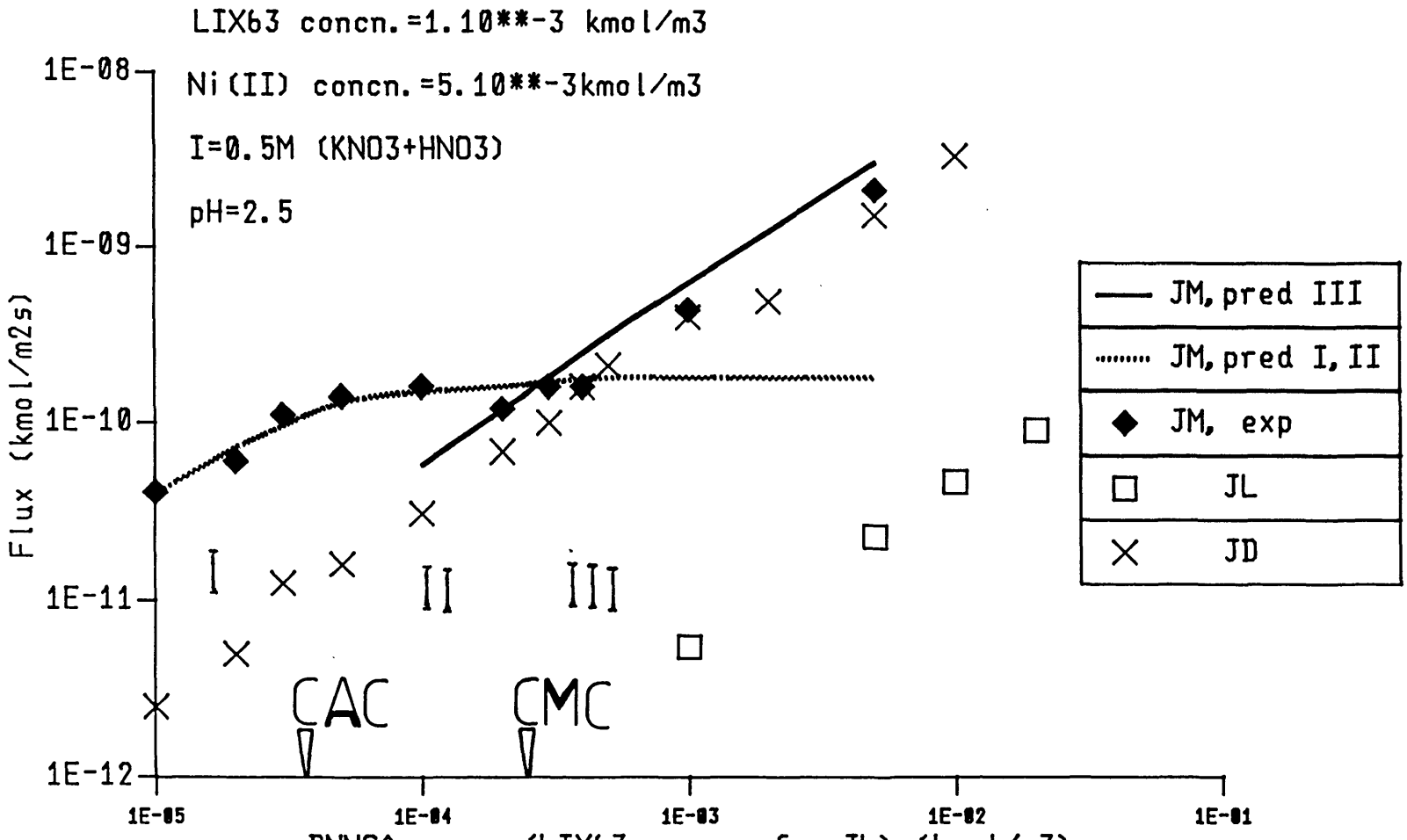


Figure V.13. Experimental and predicted nickel extraction fluxes by DNNSA (JD) and by mixtures (JM).

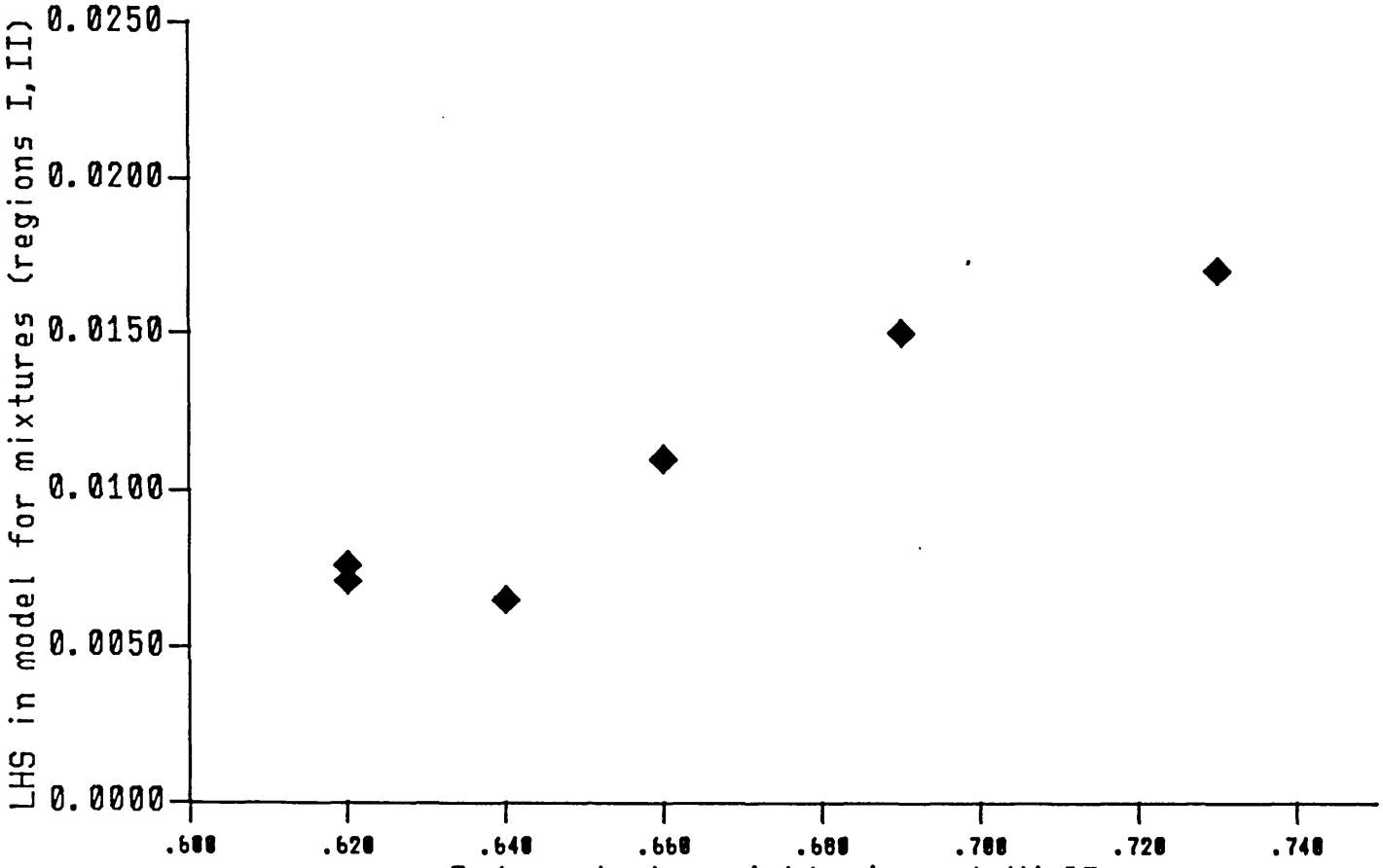


Figure V.14 Fit of extraction fluxes by mixtures to model for regions I, II (eqn. V.87)

CHAPTER VI. CONCLUSIONS AND SUGGESTIONS FOR FURTHER WORK

VI.1. CONCLUSIONS

The rate of Ni(II) extraction from nitrate media by DNNSA solutions in hexane in a NDSC was controlled by heterogeneous reactions, or by transport resistances, or by a combination of both depending on hydrodynamic conditions.

Under chemical control the locus of the RDS was identified as the interface. A criterion based on the dynamic dissolution of DNNSA into the aqueous phase was developed and used to rule out the possibility of a RDS in the aqueous bulk. A second criterion based on DNNSA equilibrium partition demonstrated that the RDS was not located in the aqueous diffusion film. The RDS was found to be the interaction between DNNSA reversed micelles and nickel complexes adsorbed as part of the interfacial mosaic. Water dynamic solubilization experiments indicated that reversed micelles interact with the o/w interface.

It was observed that values of nickel flux became constant as the stirring speed was increased beyond certain value. Those plateaux started at higher speeds and laid at higher values of flux as the reaction rate was increased. Reasoning along the lines of the two-film theory of mass transfer proved that the plateaux are of true kinetic origin.

By solving the second Fick law in planar geometry with the 'radiation' boundary condition at the interface, an expression was obtained for the flux of desorbed nickel complexes into organic phase fluid elements. Averaging of the fluxes according to Danckwerts' frequency of surface renewal resulted in a model able to predict the plateaux observed under varying hydrodynamic conditions.

Solutions of LIX63 in hexane extract nitrates from strong HNO_3 media. A value for the LIX63 dimerization constant was estimated similar to a literature value for LIX65N.

It was shown that omission of physical preequilibration of organic feeds may result in errors when rate experiments involving aggregating extractants are carried out using short contact time techniques. An estimate of those errors in single-drop experiments was obtained.

Micellar transport coefficients were estimated from experimental results independently from chemical reactions. The processes of electrolyte solubilization and of DNNSA dynamic transfer were found to be mass transfer-controlled. The mechanism of initial solubilization by reversed micelles and the mechanism of core exchange by saturated micelles were investigated and their rates were compared.

The synergic effects observed by previous workers with DNNSA -LIX63 mixtures were confirmed. An explanation of the synergism was found from thermodynamic principles in the Gibbs free energy change resulting from variations in the aggregation status and the desolubilization of water which took place with mixed extractants.

Extraction rate enhancements by mixtures were observed. Reasons for this effect were proposed based on the bulk organic phase speciation and interfacial properties. Depending on the value of the $\bar{C}_{DT}/\bar{C}_{LT}$ ratio, three regions were identified with well characterized relationships between fluxes and bulk and interfacial compositions. At $\bar{C}_{DT} \leq$CAC of a mixture, single DNNSA micelles break down into larger numbers of smaller SMAs which enhance the rate of film desorption. The conversion of the adsorbed layer controlled the rate in this region. The same RDS was found for region II (CAC $\leq\bar{C}_{DT}\leq$CMC), but almost constant fluxes were observed in this region consistent with an almost invariant adsorption density at $\bar{C}_{DT}>$CAC. In the third region (at $\bar{C}_{DT}>$CMC) the bulk speciation was similar to that of DNNSA alone and the RDS shifted to the desorption of the interfacial film. Models not requiring formation of nickel complexes with mixed reagents were able to simulate the effect of changing concentrations on the flux.

VI.2. SUGGESTIONS FOR FURTHER WORK

When this work was started, the emphasis was expected to be placed on the already classical problems of heterogeneous chemical reactions found in the liquid extraction of metal ions. It was expected that, from all interfacial parameters, electrostatic potentials and adsorption densities would be incorporated in the kinetic models eventually derived. As the work progressed, the significance and also the potential of physical solubilization became clear. Water in oil microemulsions look poised to gain a place of their own among Separation Processes. Used as conventional liquid-liquid extractants, or in combination with one of the techniques which conventional extraction spawned such as liquid membrane permeation, microemulsions will most probably find widespread application.

Further understanding of transport processes involving micelles is required to support those potential uses. Among the problems that must be tackled is that of interactions between micelles and macro-interfaces. The core exchange mechanisms in bulk phases will probably also receive much attention. The link between solubilization, concentrative effects, and catalytic effects will have to be sought with increasingly powerful analytical tools.

Little work has been so far reported on aging of micelles and the resulting changes in their shape and size. Such changes can lead to apparent inconsistencies when comparing dynamic and equilibrium results.

Understanding the speciations of bulk phases and interface is essential to explain synergic and rate enhancement effects in mixed reagent systems. It is felt that no satisfactory attempt to study problems involving interfacial transport reactions may be done without an *a priori* knowledge of the chemistry involved. Further, consistency between bulk speciation and interfacial properties is required.

Efforts invested in the investigation of the composition and behaviour of interfacially adsorbed mosaics will surely be rewar-

ded. Besides work in Langmuir and other troughs with stagnant sublayers, experiments are needed under transport conditions in the presence of bulk phases. Dynamic interfacial tensions provide information on the relaxation of adsorbed films and it is felt that their measurement and analysis could be profitably incorporated to the modelling of liquid-liquid extraction with surface-active reagents. The effect of reactions on the changes in composition of the interfacial mosaic may further our understanding of interfacial mechanisms.

BIBLIOGRAPHY

Adamsom, A.W., "Physical Chemistry of Surfaces" , 2nd.ed., Wiley, NY (1967).

Aguilar, M., Elizalde, M.P., and Castresana, J.M., Proc. Int. Solv. Extr. Conf. (ISEC) '83 , 491-492 (1983).

Ajawin, L.A., Doctoral Thesis, London University, 1980.

Akiba, K., and Freiser, H., Anal. Chim. Acta , 136 (1982) 329-337.

Albery, W.J., and Fisk, P.R., Proc. Hydrometallurgy '81 , Soc. Chem. Ind. Symp., U.M.I.S.T. ,30June-3July 1981, F5/1-F5/15.

Albery, W.J., Choudhery, R.A., Zerguep, N.A., and Robinson, B.H., J. Chem. Soc. Faraday Trans. , 1(1987) 83 (8) 2407-2419.

Al-Diwan, T.A.B., Hughes, M.A., and Whewell, R.J., J. Inorg. Nucl. Chem. , 39 (1977) 1419-1424.

Ashbrook, A.W., Anal. Chim. Acta , 58 (1972) 115-121.

Astarita, G., "Mass Transfer with Chemical Reaction" , Elsevier, Amsterdam, 1967.

Atwood, R.L., Thatcher, D.N., and Miller, J.D., Met. Trans. B , 6B (1975) 465-473.

Austin, L.J., Doctoral Thesis, London University, 1966.

Aveyard, R., Chem. & Ind. , 20 July 1987, 474-478.

Baes, C.F., McDowell, W.J., and Bryan, S.A., Solv. Extn. Ion Exch. 5(1)1-28 (1987).

Bauer, G.L., and Chapman, T.W., Met. Trans. B , 7B, 519(1976).

Bauer, D., and Komornicki, J., Proc. Int. Solv. Extn. Conf. (ISEC) '83 , 315- 316 (1983).

Bauer, D., and Komornicki, J., Actes Summer School on Extraction , E.N.S.I.G.C., Toulouse, D-I-1/D-I-11 (September 1987).

Baht, S.N., Smith, G.A., Tucker, E.E., Christian, S.D., Scamehorn, J.F., and Smith, W., Ind. Eng. Chem. Res. ,26 (1987) 1217-1222.

Balasubramanian, D., J. Indian Chem. Soc. , vol. 58 (1981) 633-639.

Berezin, I.V., Martinek, K., and Yatsimirskii, A.K., Russian Chemical Reviews , 42 (10) 787-802 (1973).

Blumberg, R., and Gai, J.E., Proc. Int. Solv. Extn. Con. (ISEC) '77 , (1)9-15 (1977).

Bowcott, J.E., and Schulman, J.H., Z. Elektrochem. , 59(1955)283.

Caldin, E.F., "Fast Reactions in Solution" , Blackwell Scientific Publications, 288-289 (1964).

Cante, C.J., McDermott, J.E., Saleeb J.Z., and Rosano, H.L., J. Colloid Interface Sci. , 50 (1) 1-11 (1975).

Carroll, B.J., J. of Colloid Interface Sci. , 79 (1) 126-135 (1981)

Carroll, B.J., O'Rourke, B.G.C., and Ward, A.J.I., J. Pharm. Pharmacol. , 34 (1982) 287-292.

Carslaw, H.S., and Jaeger, J.C., "Conduction of Heat in Solids" , Clarendon Press, Oxford, 1959.

Chaiko, D.J., and Osseo-Asare, Proc. Int. Solv. Extn. Conf.(ISEC) '83, 276-277 (1983).

Chaiko, D.J., and Osseo-Asare, K., Proc. Int. Solv. Extn. Conf. (ISEC) '86 , 409 - 414 (1986a).

Chaiko, D.J., and Osseo-Asare, K., submitted to J.Colloid Interface Sci. (July 1986b).

Chaiko, D.J., and Osseo-Asare, K., Solv. Extn. Ion Exch. , 5(2)277-286(1987a).

Idem, 287-300 (1987b).

Chan, A.F., Evans, D.F., and Cussler, E.L., A. I. Ch. E. J. , 22 (6) 1006-1013 (1976).

Chiarizia, R., Danesi, P.R., D'Alessandro, G., and Scuppa, B., J. Inorg. Nucl. Chem. , 38 (1976) 1367-1369.

Chiarizia, R., and Danesi, P.R., J. Inorg. Nucl. Chem. , (39) 525-530 (1977).

Cohen, J.A., and Cohen, M., Biophysical Journal , (36) 623-651 (1981).

Coleman, C. F., and Roddy, J. W., Solvent Extraction Revs. , 1(1)63-91 (1971).

Corkill, J.M., Goodman, J.F., and Walker, T., Discuss. Faraday Soc. , 589 - 593 (1964).

Cox, M., Elizalde, M.P., Castresana, J.M., and Miralles, N., Proc. Int. Solv. Extn, Conf. (ISEC) '83 , 268-269 (1983).

Cox, M., and Flett D.S., Proc. Int. Solvent Extraction Conference (ISEC) '77 , 1 (1977) 63-72.

Crank, J., "The Mathematics of Diffusion" , Clarendon Press, Oxford, 2nd. ed. (1979) p.36.

The Chemical Rubber Co. (CRC) Handbook of Chem. and Phys., 64th Ed. (1983-1984) p. D-156.

Cussler, E.L., "Multicomponent Diffusion" , Elsevier, NY, 1976.

Cussler, E.L., "Diffusion: Mass Transfer in Fluid Systems" , Cambridge University Press, 1986.

Dalton, R.F., Hauxwell, F., and Tumilty, J.A., Chem. Ind. , 181-184 (1978).

Danesi, P.R., Chiarizia, R., and Scibona J., J. Inorg. Nucl. Chem. , 35 (1973) 3926-3928.

Danesi, P.R., Chiarizia, R., and Saltelli, A., J. of Inorg. Nucl. Chem. , 38 (1976) 1687-1693.

Danesi, P.R., and Chiarizia, R., Proc. Int. Solv. Extn. Conf. (ISEC) '77 , 1(219-227) 1977.

Danesi, P.R., Chiarizia, R., and Sanad, W.A., J. Inorg. Nucl. Chem. , 39 (1977) 519-523.

Danesi, P.R., and Chiarizia, R., CRC Critical Reviews in Analytical Chemistry , 10 (1) 1980.

Danesi, P.R., Proc. Int. Solv. Extn. Conf. (ISEC) '83 , 1-3(1983).

Danesi, P.R., Solv. Extn. Ion Exch. , 2(1)29-44(1984).

Danckwerts, P.V., Ind. Eng. Chem. , 43(1460)1951.

Davies, J.T., and Rideal, E.K., "Interfacial Phenomena" , Academic Press, N.Y., 1963.

Demopoulos, G.P., and Gefvaert, D.L., Hydrometallurgy, 12(1984)299-315.

Dobson, S., and van der Zeeuw, A.J., Chem. and Ind. , 1976, 175.

Duyckaerts, G., and Desreux, J.F., Proc. Int. Solv. Extn. Conf. (ISEC) '77 , 73-86(1977).

Eicke, H.-F., and Christen, H., Helv. Chim. Acta , 61 (1978) 2258-2263.

Eicke, H.-F., and Christen, H., J. Colloid Interface Sci. , 46(1974a)417-427.

Eicke, H.-F., and Christen, H., J. Colloid Interface Sci. , 48 (2) 281-290 (1974b).

Eicke,H.-F., Shepherd, J.C.W., and Steinmann, J., J. Colloid Interface Sci. 56 (1976) 168.

Eicke, H.-F., "Micellization, Solubilization, and Microemulsions" ,

(K.L. Mittal, ed.) 1 (1977) 429-443.

Eicke, H.-F., Pure Appl. Chem. , 52 (1980) 1349-1357.

Eisenberg, M., Tobias, C.W., and Wilke, C.R., AIChE Progr. Symp. Ser. 16(51) 1-16(1955).

El Seoud, O.A., and Shimizu, M.R., Colloid Polymer Sci. , 260 (1982a) 794-798.

El Seoud, O.A., Chinelatto, A.M., and Shimizu, M.R., J. Colloid Interface Sci. , 88 (2) 420-427 (1982b).

El Seoud, O.A., and Chinelatto, A.M., J. Colloid Interface Sci. , 95 (1) 163-171 (1983).

Elworthy, P.H., Florence, A.T., and Macfarlane, C.B., "Solubilization by Surface-Active Agents" , The Chancer Press, England, 1968.

England, D.C., and Berg, J.C., AIChE J. , 17(2)313-322(1971).

Evans, D.F., Mukherjee, S., Mitchell, D.J., and Ninham, B.W., J. Colloid Interface Sci. , 93(1)184-204(1983).

Fendler, J.H., and Fendler, E.J., "Catalysis in Micellar and Macromolecular Systems" , Academic Press, 1975.

Fleming, C.A., Nat. Inst. Met. S. Africa , report no. 1793 (1976).

Fletcher, P.D.I., and Robinson, B.H., Ber. Bunsenges Phys. Chem. , 85(1981) 863.

Fletcher, P.D.I., Howe, A.M., and Robinson, B.H., J. Chem. Soc. Faraday Trans. , 1, 83, 985-1006 (1987).

Flett, D.S., and Jaycock, M.J., "Ion Exchange and Solvent Extraction", (Marinsky, J., and Marcus, Y., eds.) vol.3, ch.1 (1973)1-50.

Flett, D.S., Okuhara, D.N., and Spink, D.R., J. Inorg. Nucl. Chem. , 35 (1973) 2471-2487.

Flett, D.S., Cox, M., and Heels, J.D., Proc. Int. Solv. Extn. Conf. (ISEC) '74 , 2559-2575 (1974).

Ibid, J. Inorg. Nucl. Chem. , 37 (1975a) 2197-2201.

Idem, 37 (1975b)

Flett, D.S., Acct. Chem. Res. , 10 (1977) 99-104.

Freeman, R.W., and Tavlarides, L.L., Chem. Eng. Sc., 37(10)1547-1556(1982).

Freiser, H., Proc. Int. Solv. Extn. Conf. (ISEC) '83 , 4-5 (1983).

Friberg, S.E., Nortensen, M., and Neogy, P., Sep. Sci. Tech. , 20 (4)

285-296 (1985).

Friberg, S., "Microemulsions - Theory and Practice" , Academic Press, New York, 1977.

Froment, G.F., and Bischoff, K.B., "Chemical Reactor Analysis and Design" , Wiley, NY, 1979.

Fromherz, P., and Masters, B., Biochim. Biophys. Acta , 356 (1974) 270-275.

Fyles, T.M., J. of Membrane Sci. , (24) 229-243 (1985).

Fyles, T.M., J. Chem. Soc., Faraday Transactions , 1 (82) 617-633 (1986).

Gaonkar, A.G., and Neuman, R.D., Proc. Int. Solv. Extr. Conf. (ISEC) '86 , II-361, 1986.

Gallacher, L.V., "Solution Behaviour of Surfactants" , (K.L. Mittal, ed.) 2 (1982) 791-801.

Gershfeld, N.L., and Patlak, C.S., J. Phys. Chem. , 70(1966)286-288.

Goklen K.E., and Hatton, T.A., Biotechnol. Prog. , 1(1)69-74(1985).

Goklen, K.E., and Hatton, T.A., Proc. Int. Solv. Extn. Conf. (ISEC) '86 , Vol.III, 587- 595 (1986).

Grandi, C., Smith, R.E., and Luisi, P.L., J. Biol. Chem. , 256 (2) 837-843 (1981).

Hall, D.G., and Tiddy, G,J,T., in "Anionic Surfactants, Physical Chemistry of Surfactant Action" , (E.H. Lucassen-Reynders, ed.) ch. 2 (1981) 55-108 (M. Dekker).

Harada, M., and Miyake, Y., J. of Chemical Eng. of Japan , 19 (3) 193-207 (1986).

Hartley, G.S., "Aqueous Solutions of Paraffin Chain Salts" , Hermann et Cie., Paris, 1936.

Hartley, G.S., and Roe, J.W., Trans. Far. Soc. , 36 (1940) 101-109.

Hicks, J.R., and Reinsborough, V.C., Aust. J. Chem. , 35(1982)15-19.

Ibid, Can. J. Chem. , 62(1984)990-994.

Högfeldt, E., Nature , 5039 (May 28, 1966) 941-942.

Högfeldt, E., Kuvaeva, Z.I., and Soldatov, V., J. Inorg. Nucl. Chem. , 40 (1978) 1405-1407.

Högfeldt, E., Chiarizia, R., Danesi, P.R., and Soldatov, V., Chemica Scripta , (18) 13-43 (1981).

Huang, C., Evans, D.F., and Cussler, E.L., J. Colloid Interface Sci. , 82 (2) 499-507 (1981).

Hughes, M.A., and Rod, V., Proc. Int. Solv. Extn. Conf. (ISEC) '83 , 14-15 (1983).

Hughes, M.A., and Rod, V., Faraday Discussions Chem. Soc. , (77) 7 (1984a).

Hughes, M.A., and Rod, V., Hydrometallurgy , 12 (1984b) 1267.

Hummelstedt, L., Proc. Int. Solv. Extn. Conf. (ISEC) '77 , 86-93(1977).

Inoue, K., Tomita, S., and Maruuchi, T., J. Chem. Eng. Jpn. , 18 (5) 445-449 (1985).

Inoue, K., Tsunomachi, H., Tomita, S., and Maruuchi, Proc. Int. Solv. Extn. Conf. (ISEC) '83 , 303-304 (1983a).

Inoue, K., and Tsunomachi, H., Hydrometallurgy , 13 (1984) 73-87.

Inoue, K., Watanabe, H., and Nose, Y., J. Colloid Interface Sci. , 94 (1) 229- 236 (1983b).

Hutchinson, M.H., and Sherwood, T.K., Ind. Eng. Chem. , 29 (7) 836-840 (1937).

Irandoust, S., and Andersson, B., Can. J. Chem. Eng. , 64(1986) 954-959.

James, A.D., and Robinson, B.H., J. Chem. Soc. Far. Trans. I , 74 (1978) 10-21.

Jenson, V.G., and Jeffreys, G.V., "Mathematical Methods in Chemical Engineering" , Academic Press, NY, 1977.

Kandil, A.T., and Choppin, G.R., J. Inorg. Nucl. Chem. , 37(1975)1787-1789.

Kaufman, S., and Singleterry, C.R., J. Colloid Sci. , 10 (1955) 139-150.

Idem, 12 (1957) 465.

Keeney, M.E., and Osseo-Asare, K., Polyhedron , 1 (5) 453-455 (1982).

Keeney, M.E., and Osseo-Asare, K., Hydrometallurgy , 12 (1984) 255-265.

Kertes, A.S., and Gutmann, H., "Surface and Colloid Science" , (E. Matijevic, ed.) 8, ch. 3, 193-295 (1976).

Kertes, A.S., "Micellization, Solubilization, and Microemulsions" , (K.L. Mittal, ed.) vol. 1(1977) 445-454.

Komasawa, I., Otake, T., and Muraoka, T., J. Chem. Eng. Jpn. , 13 (3) 204-208 (1980a).

Komasawa, I., Otake, T., and Yamada, A., J. Chem. Eng. Jpn. , 13 (3) 209-213 (1980b).

Lakhsmanan, V.I., and Lawson, G.J., J. Inorg. Nucl. Chem. , 35(1973) 4285-4294.

Lakhsmanan, V.I., Lawson, G.J., and Tomliens, J.L., J. Inorg. Nucl. Chem. , 37 (1975)2181-2185.

Lee, C.K., and Tavlarides, L.L., Polyhedron , 4(1985)47-51.

Lee, C.K., and Tavlarides, L.L., I. E. C. Fund. , 25 (1986) 96-102.

Levich, V.G., "Physicochemical Hydrodynamics" , Prentice Hall, 1962.

Lewis, J.B., Chem. Eng. Sci. , 3 (1954) 248-259.

Lewis, W.K., and Whitman, W.G., Ind. Eng. Chem. , 16(1924)1215.

Lianos, P., Viriot, M.L., and Zana, R., J. Phys. Chem. , (88) 1098-1101 (1984).

Li, N.N., Ind. Eng. Chem. Proc. Des. Dev. , 10(1971)215.

Lin, K.L., and Osseo-Asare, K., Proc. Int. Solv. Extn. Conf. (ISEC) '83" , 278 -279 (1983).

Lin, K.L., and Osseo-Asare, K., Solvent Extraction and Ion Exchange , 2(3) 365-380 (1984).

Lin, K.L., Doctoral Dissertation, The Pennsylvania State University, 1984.

Lucassen-Reynders, E.H., in "Anionic Surfactants. Physical Chemistry of Surfactant Action" , (E. H. Lucassen-Reynders, ed.) ch.1 (1981) 1-54 (M. Dekker).

Luisi, P.L., and Wolf,R., in "Solution Behaviour of Surfactants" , (K. L. Mittal, ed.) 2 (1982) 887-905.

Luisi, P.L., and Laane, C., Trends in Biotech. , 153-160 (June 1986).

Markus, Y., and Kertes, A.S., "Ion Exchange and Solvent Extraction of Metal Complexes" , J. Wiley, 1969.

Markovitz, G.Y., and Choppin, G.R., Ion Exchange Solvent Extraction , (J.A. Marinsky and Y. Markus, eds.) ch.2, 51-81, 1973.

MacRitchie, F., in "Interfacial Synthesis" , (Millich, F., and Carraher, C.E., Jr., eds.) M. Dekker Inc., N.Y., 1977.

Matijevic, E., and Pethica, B.A., Trans. Far. Soc. , 54(1958) 1390-1399.

McQueen, D. H., and Hermans, J. J., J. Colloid Interface Sci. , 39 (389) 1972.

Mickley, H.S., Sherwood, T.K., and Reed, C.E., "Applied Mathematics in Chemical Engineering" , McGraw-Hill Book Co., 2nd Ed., 1957.

Miller, J.D., and Atwood, R.L., J. Inorg. Nucl. Chem. , 37 (1975) 2539-2542.

Miyake, M., Takenoshita, Y., and Teramoto, M., J. of Chemical Eng. of Japan , 16 (203) 1983.

Miyake, Y., Imanishi, Y., Katayama, Y., Hamatani, T., and Teramoto, M., J. Chem. Eng. Jpn. , 19 (2) 117-125 (1986).

Morris, D.F.C., and Jones, M.W., Electrochim. Acta , 14 (1969) 1233.

Mukherjee, P., J. Pharm. Sci. , 63(6)972-981(1974).

Murthy, C.V.R., Ph.D. Thesis, London University, 1987.

Nagarajan, R., and Ruckenstein, E., J. Colloid Interface Sci. , 71 (3) 580-604 (1979).

Nagarajan, R., Chaiko, M.A., and Ruckenstein, E., J. Phys. Chem. , 88(1984) 2916-2922.

Nagarajan, R., Langmuir , 1 (1985) 331-341.

Nagy, J.B., in "Solution Behaviour of Surfactants" , (K. L. Mittal, ed.) 2 (1982) 743-766.

Neogy, P., Kim, M., and Friberg, S.E., Sep. Sci. Tech. , 20 (7 and 8) 613-622 (1985).

Nitsch, W., and Kruis, B.J., J. Inorg. Nucl. Chem. , 40 (1978) 857-864.

Nitsch, W., and Hoffman, A., Chem.-Ing.-Tech. , 53(1981)367.

Ortiz, E.S.P. de, J. Appl. Chem. Biotechnol. , 28 (1978) 149-156.

Ortiz, E.S.P. de, Cox, M., and Flett, D.S., Proc. Int. Solv. Ext. Conf. (ISEC) '77 , (1)198-203(1977).

Ortiz, E.S.P. de, in "Ion Exchange Science and Technology" , (A. Rodrigues, ed.) NATO ASI Series E, No.107, 575-584 (1985).

Osseo-Asare, K., and Keeney, M.E., Metallurgical Trans. B , IIB (1980a) 63-67.

Osseo-Asare, K., and Keeney, M.E., Separation Sci. Technol. , 15 (4) 999-1011 (1980b).

Osseo-Asare, K., and Chaiko, D.J., Proc. Int. Solv. Extn. Conf. (ISEC)

'83 , 276-277 (1983).

Osseo-Asare, K., Renninger, D.R., and Wagner, J.D., Sol. Extr. Ion Exch. , 1 (2) 337-347 (1983a).

Osseo-Asare, K., Lin, K.L., and Chaiko, D.J., Proc. Int. Solv. Extn. Conf. (ISEC) '83 , 313-314 (1983b).

Osseo-Asare, K., and Renniger, D.R., Hydrometallurgy , (13) 45-62 (1984).

Osseo-Asare, K., in "Hydrometallurgical Process Fundamentals" ,NATO Conference Series VI, vol.10 (R. Bautista, ed.) 357-407(1984) Plenum, NY.

Osseo-Asare, and Chaiko, D.J., submitted to J. Membrane Sci. , August 1986.

Osseo-Asare, K., and Zheng, Y., submitted to Colloids and Surfaces , February 1987.

Paatero, E.Y.O., and Golding, J.A., Proc. Int. Solv. Extn. Conf. (ISEC) '83 , 295-296 (1983).

Patlak, C.S., and Gershfeld, N.L., J. Colloid Interface Sci. , 25(503-513)1967.

Plucinski, P., Int. J. Heat Mass Transfer , 28 (2) 451-458 (1985).

Preston, J.S., J. Inorg. Nucl. Chem. , 37 (1975) 1235-1242.

Preston, J.S., and Whewell, R.J., J. Inorg. Nucl. Chem. , 39 (1977) 1675.

Price, R., "Separation Processes in Hydrometallurgy" ,(G.A. Davies, Ed.) Proc. of Hydrometallurgy '87 , 143-147, UMIST, Soc. Chem. Ind., London, 1987.

Raterman, K.T., and Shaeiwitz, J.A., J. Colloid Interface Sci. , 98 (2) 394-405 (1984).

Reid, R.C., Prausnitz, J.M., and Sherwood, T.K., "The Properties of Gases and Liquids" , McGraw-Hill Book Co., 3rd ed., 1977.

Renninger, D.R., and Osseo-Asare, K., Metall. Trans. B , 14B (1983) 41-47.

Robinson, R.A., and Stokes, R.H., "Electrolyte Solutions" , 2nd. Edition, Butterworths Pub. 1959.

Rod, V., Sir, Z., Guberova,A., Chem. Eng. Res. Dev. , 63(1985)89-100.

Rodriguez de Carvalho, J.M., and Slater, M., Proc. Int. Solv. Extn. Conf. (ISEC) '83 , 297-298.

Rosen, M.J., "Surfactants and Interfacial Phenomena" , J. Wiley &

Sons, N.Y., 1978.

Savastano, M. Sc. Thesis, Syracuse University, Syracuse, New York, USA, 1984.

Savastano, C.A., Osseo-Asare, K., and Ortiz, E.S.P.de, Proc. Int. Solv. Extn. Conf. (ISEC) '86 , II345-II352, 1986.

Ibid, "Separation Processes in Hydrometallurgy" , (G.A. Davies, Ed.) Proc. of Hydrometallurgy '87 , UMIST, Soc. Chem. Ind., London, 7-10 July 1987.

Sawistowski, H., in "Recent Advances in Liquid-Liquid Extraction" , (C. Hanson, ed.) , Ch.9, Pergamon Press, Oxford, 1971, 293-366.

Sawistowski, H., in "Technologically Important Aspects of Interface Science" . Course offered at Imperial College, 28-29 June 1982, paper E.

Seidell, A., "Solubilities of Organic Compounds" , D. van Nostrand Co., Ny, 1941, p.148.

Shaeiwits, J. A., Chan, A. F. C. , Cussler, E. L., and Evans, D. F., J. Colloid Interface Sci. , 84 (1) 47-56 (1981).

Sherwood, T.K., Pigford, R.L., and Wilke, C.R., "Mass Transfer" , McGraw-Hill Book Co., USA, 1975.

Smith, J.M., "Chemical Engineering Kinetics" , 3rd.ed., McGraw-Hill Book Co., USA, 1981.

Smith, R.M., and Martell, A.E., "Critical Stability Constants, vol.4: Inorganic Complexes" , Plenum, NY, 1976.

Stowe, L.R., and Shaeiwitz, J.A., J. of Colloid Interface Sci. , 90(2)495 -508 (1982).

Tammi, T.T., Hydrometallurgy , 2 (1976/7) 371-380.

Tanford, C., "The Hydrophobic Effect" , J. Wiley & Sons, 1973.

Tavlarides, L.L., Lee, C.K., Mukhavilli, S., Bae, J., and Hahn, I., presented at the Fourth Symposium on Separation Sci. and Technol. for Energy Applications , October 20-24, 1985, Knoxville, Tennessee, USA.

Ter Minassian-Saraga, L., J. Chim. Phys. , 52(1955)181.

Tondre, C., and Xenakis, A., Colloid and Polymer Sci. , 260(1982) 232-233.

Tondre, C., and Xenakis, A., Far. Disc. Chem. Soc. , 77(1984)115-126.

Van Dalen, A., Gerritsma, K.W., and Wijstra, J., J. of Colloid Interface Sci. , 48(1) 122-126 (1974a).

Idem, 48 (1) 127-133 (1974b).

Van der Zeuuw, A.J., and Kok, R., Proc. Int. Solv. Extn. Conf. (ISEC) '77 , 1 (17-23)1977.

Van Krevelen, D.W., and Hoftjizer, P.J., Rec. Trav. Chim. , 67 (1947) 563.

Van Voorst Vader, F., Trans. Far. Soc. , 57 (1961) 2263-2271.

Wang, S.M., and Li, N.C., J. Inorg. Nucl. Chem. , 27 (1965) 2093.

Weinheimer, R.M., Evans, D.F., and Cussler, E.L., J. Colloid Interface Sci. , 80(1981)357.

Whewell, R.J., Hughes, M.A., and Hanson, C., J. Inorg. Nucl. Chem. , 37 (1975) 2303-2307.

Whewell, R.J., Hughes, M.A., and Hanson, C., Proc. Int. Solv. Extn. Conf. (ISEC) '77 , 1(185-192) 1977.

Whewell, R.J., and Hanson, C., in "Ion Exchange and Solvent Extraction" , (J.A. Marinsky and Y. Markus, Eds.), M.Dekker, NY, 1981.

Wu, C.K., Kao, H.-C., Chen, T., Li, S.-C., King, T.-C., and Hsu, K.-H, Proc. Int. Solv. Extn. Conf. (ISEC) '80 , paper 80-23 (1980).

Zapatero, M.J., Elizalde, M.P., and Castresana, J.M., Solv. Extn. Ion Exch. , 5 (1) 83-101 (1987).

Zheng, Y., and Osseo-Asare, K., Solv. Extn. Ion Exch. , 3(6)825-837 (1985).

Zheng, Y., and Osseo-Asare, K., unpublished research (1987).

APPENDICES

APPENDIX A. Purification of DNNSA.

The extractant was received as a 40% v/v n-heptane solution. The diluent was evaporated under vacuum in a rotary evaporator at 58 to 62° until gel consistency. A fraction was diluted in rectified ethanol, then it was loaded onto Dowex-1X ion exchange resin. The resin was stored in Cl^- form, it was converted to the HO^- form with 1M NaOH, again to Cl^- with 1M HCl, and to HO^- again before loading. Impurities without ion-exchanging properties were not fixed by the bed and were washed with ethanol, together with the NH_4Cl produced.

DNNSA was eluted from the resin by 1M HCl in ethanol, using around twenty bed volumes. The eluate was rotary-evaporated at 25°C under full vacuum of the pump. Further additions of ethanol were evaporated to eliminate residual HCl. The diluent left was removed by drying under vacuum at 65°C. The dark brown, gelly product was kept in a dessicator over P_2O_5. Stock solutions were kept in a refrigerator.

Appendix B. Purification of LIX63.

As-received LIX63 was diluted to 50% v/v with hexane 95%+ pure. Ammoniacal $CuSO_4$ approx. 0.6M Cu(II) was prepared under fume cupboard as follows: 5 cc of concentrated H_2SO_4 were added to 800 ml water to obtain pH ≅ 3. Then ammonia solution was added until pH ≅ 9.5. $CuSO_4.nH_2O$ was then dissolved in.

200 cc of the LIX63 solution was added to 400 cc of Cu(II) solution in a 800 ml beaker and the dispersion was stirred during 30 min under fume hood. It was then transferred to a separatory funnel and the aqueous phase was drained and kept. The extract was washed twice to remove traces of the base, each wash of 200 cc distilled water. The extract was then added dropwise to 400 cc acetone in a 800 cc beaker. The copper oximate precipitated whereas the inactive isomer and other non-copper-complexing impurities remained in solution. The oximate was separated by filtration and air-dried. The acetone solution of impurities was discarded. The precipitated oximates ranged from a green powder to a green amorphous gel. Once dried, the oximate was dissolved in anhydrous diethyl ether, which proved to be the best to dissolve the product. The precipitation step was repeated by adding fresh acetone drop by drop to the stirred ether solution, followed by the removal of 50% solvents by rotary evaporation. The oximate recrystallized, and the product was filtered, air-dried, and dissolved in hexane. The metal was stripped in 3 or 4 short contacts with 4M H_2SO_4 in a 1/1 volume ratio. The oxime solution was washed twice with distilled water to remove traces of acid, and it was rotary evaporated until a viscous product that was kept in a dessicator over P_2O_5. The rest of diluent was removed by storing the product in a vacuum oven at 65°C and around 1mm Hg residual pressure. A waxy, almost white product resulted.

Appendix C. Operation of the Non-Dispersive Reactor.

C.1. Start of an experiment.

(Numbers of items refer to figure III.1.a)

.Load aqueous feed (AF) in cylinders 9.

.Rinse with AF the external flow circuit and lower half of the NDSC 1.

.Close drain valves 10 and 12.

.Start peristaltic pump 11, filling with the AF the lower half of the NDSC with around 0.3l. All air bubbles from the flow circuit must be removed.

.Check that the thermostatic bath is at the desired temperature (T)

.Start lower stirrer 3 to shorten the thermal equilibration time. When the experiment is to be run at T>Tambient, air will desorb from the AF, because the solubility of N_2 in water is 2.33cm^3/100 cm^3at 0°C and 1.02cm^3/100cm^3at 45°C (CRC Handbook of Chem. and Phys., 23rd ed., p.447). Air bubbles collect under the lower mesh 6. To remove the bubbles transfer some AF back to 9 with pump 11. The rotation of the pump must be inverted with this aim.

.Refill the lower half, start stirrers to detach and coalesce remaining bubbles. Repeat the last two steps as necessary until no more bubbles collect under the lower mesh.

.Measure the required volume of organic diluent.

.Pour the diluent slowly down the orifice 7 with a funnel fitted with a piece of tubing on the stem. The diluent must not reach the lower mesh.

.Allow time for thermosthatization while stirring both phases.

.Stop stirrers and tap upper mesh with a long needle or similar to remove trapped air bubbles.

.Set the desired speed to the stirrers.

.Inject the required volume of concentrated extractant stock through orifice 7. Start the stopwatch simultaneously.

C.2. Sampling.

.Organic phase: with pipette from orifice 7.

.Aqueous phase: by opening 3-way valve while pump turns slowly.

C.3 Cleaning

.Stop stirrers at end of the run.

.Open drain valves 10 and 12. Drain empty the NDSC.

.Load lower half with distilled water from the orifice 7 to remove the bulk of dissolved solids.

.Fill NDSC with coktel of 50% ethanol and 50%acetone. Stirr both halves, drain.

.Rinse with distilled water several times.

.Rinse with acetone.

.Dry with air via the pump 11 or sparging compressed N_2 through a fine tubing inserted through 7.

APPENDIX D. SOLUTION TO THE PROBLEM OF DIFFUSION AND ACCUM ULATION IN A BOUNDARY LAYER.

Austin (1966) solved the problem of unsteady diffusion in a boundary layer where the solute accumulates thereby reducing the driving force for mass transfer. That author made the following assumptions:

1) Solutions were diluted, thus Fick's laws applied and phase volumes were constant.
2) Instantaneous partition equilibrium at the interface.
3) Perfectly mixed bulk.
4) Stagnant films of thickness δ near the interface, thus the solute transferred by molecular diffusion only.
5) The mass of solute accumulated in the film could be neglected in the macroscopic balances.
6) Concentration independent diffusivity.

Mathematical statement of the problem:

The mass conservation equation in the film is Fick's second law in planar geometry:

$$\frac{\partial C}{\partial t} = \mathcal{D} \frac{\partial^2 C}{\partial x^2} \; ; \; t>0; \; 0<x\leq\delta \qquad (D.1)$$

with the following BCs:

$$\begin{aligned} &C=0 \text{ at } t\leq 0, \; x\geq 0 \\ &C=C^{*} \text{at } t>0, \; x=0 \\ &C=C^{b} \text{at } t>0, \; x=\delta \end{aligned} \qquad (D.2)$$

The solute balance relate the bulk concentration (C^b) and the gradient across the film:

$$V \frac{\partial C^b}{\partial t} = -A\mathcal{D}(\partial C/\partial x)_{x=\delta} \; ; \; t>0. \qquad (D.3)$$

Eqns. D.1 through D.3 were solved by Laplace transformation. The solution is eqn. D.4:

$$C^b = C^* \left[1 - 2k \left[\frac{\exp(-\mathfrak{D}\alpha t/\delta^2)}{(\alpha + k + k^2)\cos(\alpha^{1/2})} + \text{SUM} \right] \right] \qquad \text{(D.4)}$$

where:

$$k = \delta A/V;$$

$$\alpha = (2.25 + 3k)^{1/2} - 1.5, \text{ and}$$

$$\text{SUM} = \sum_{n=1}^{\infty} \frac{(-1)^n \exp(-\mathfrak{D}[n\pi + k/n\pi]^2 t/L^2)}{(n\pi + k + k^2/n\pi)\cos(k/n\pi)}$$

APPENDIX E. INTERFACIAL REACTION AND SURFACE RENEWAL.

The solution of eqn.V.46 is obtained here. Then the expression for the instantaneous flux is obtained and averaged. Dimensionless concentrations will be used, chosen as follows:

$$C^+ = \frac{\bar{C}_M - \bar{C}_M^b}{(L\bar{C}_{DT}/m) - \bar{C}_M^b}$$

where bars superscripted are omitted for simplicity, although all species are in the organic phase. Equation V.46 thus converts to:

$$\frac{\partial C^+}{\partial t} = \mathcal{D}\,\frac{\partial^2 C^+}{\partial x^2} \quad ; \; C^+=0; \; t=0, \; x \geq 0. \tag{E.1}$$

$$C^+=0; \; t>0, \; x \longrightarrow \infty.$$

$$\frac{\partial C^+}{\partial x} = h(C^+ - 1) \; ; \; x=0, \; t>0.$$

The Laplace transform of eqn.E.1 is

$$s\bar{C} - C^+(0) = \mathcal{D}\,\frac{\partial^2 \bar{C}}{\partial x^2}$$

and its solution is :

$$\bar{C} = A\exp(px) + B\exp(-px) \tag{E.2}$$

where $p=\pm\sqrt{s/\mathcal{D}}$. From the first BC, A=0. The Laplace transform of the second BC is

$$\frac{\partial \bar{C}}{\partial x} = h(\bar{C} - 1/s) \; ; \; x=0. \tag{E.3}$$

from eqn.E.2: $$\left.\frac{\partial \bar{C}}{\partial x}\right|_{x=0} = -pB \tag{E.4}$$

also from eqn.E.2: $$\left.\bar{C}\right|_{x=0} = B \tag{E.5}$$

Substitution of E.4 and E.5 into E.3 leads to:

$$-pB=h(B-1/s)$$

thus: $$B=\frac{h/s}{h+p}$$

and the solution E.2 becomes:

$$\bar{C}=\frac{h\sqrt{\mathfrak{D}}}{s(h\sqrt{\mathfrak{D}}+\sqrt{s})}\exp(-\sqrt{s/\mathfrak{D}}\,x) \qquad (E.6)$$

The translation of equation E.6 into the time domain is immediate. The antitransform is the No.86 in Jenson and Jeffreys (1975), with $a=h\sqrt{\mathfrak{D}}$ and $k=x/\sqrt{\mathfrak{D}}$:

$$C^{+}=\operatorname{erfc}(x/2\sqrt{\mathfrak{D}t})-\exp(hx)\exp(h^2\mathfrak{D}t)\operatorname{erfc}\left[h\sqrt{\mathfrak{D}t}+\frac{x}{2\sqrt{\mathfrak{D}t}}\right]$$

The "surface" concentration of complex is found by taking x=0:

$$C_M^s=\bar{C}_M\Big|_{x=0}=\bar{C}_M^b+(L\bar{C}_{DT}/m-\bar{C}_M^b)(1-\exp(h^2\mathfrak{D}t)\operatorname{erfc}(h\sqrt{\mathfrak{D}t}))$$

thus at t=0, $C_M^s(0)=\bar{C}_M^b$, meaning that the FE is at bulk complex concentration at the time it reaches the interface. The instantaneous flux (J^i) into each fluid element due to molecular diffusion of the nickel complex forming at the surface is evaluated as the derivative of E.6 at x=0:

$$J^i=h\mathfrak{D}(L\bar{C}_{DT}/m-C_M^b)\exp(h^2\mathfrak{D}t)\operatorname{erfc}(h\sqrt{\mathfrak{D}t}) \qquad (E.7)$$

The coefficient $h\mathfrak{D}=\frac{\delta k\theta_M}{\mathfrak{D}}\mathfrak{D}$ is independent of the diffusion coefficient. The same comment applies to J^i at t=0, which is a kinetic function given by:

$$J^i(0)=\delta k\theta_M\left(\frac{L\bar{C}_{DT}}{m}-\bar{C}_M^b\right)$$

The fluxes are now averaged over all the FEs. Calling the average flux J_D, then

$$J_D = \int_0^{\infty} J_i \, \phi(t) \, dt$$

Where $\phi(t)=s \exp(-st) \, dt$. The integral

$$\int_0^{\infty} s \exp(-st) \exp(h^2 \mathfrak{D} t) \operatorname{erfc}(h\sqrt{\mathfrak{D} t}) \, dt$$

is done by parts. In the formula $\int_a^b u \, dv = uv\Big|_a^b - \int_a^b v \, du$,

it was taken $dv=\exp(-(s-h^2\mathfrak{D})t)dt$. The solution to the integral is:

$$\frac{s - h\sqrt{\mathfrak{D} s}}{s^2 - h \mathfrak{D}}$$

Appendix F Experimental Data

Table F.1 Equilibrium solubilities of the ternary system water/ethanol/hexane. (Seidell, 1941)

EQUILIBRIUM IN THE SYSTEM ETHYL ALCOHOL, HEXANE AND WATER.
(Tarassenkow and Paulsen. 1937.)

Results at 0°

Gms. per 100 gms. homogeneous mixture		
C_2H_5OH	C_6H_{14}	H_2O
6.53	92.70	0.77
44.30	54.10	1.60
53.32	45.39	1.29
63.34	35.18	1.48
74.01	21.67	4.32
79.22	11.86	8.92
78.74	7.96	13.30
79.08	7.32	13.60
76.82	4.00	19.18
69.85	2.13	28.02
69.43	1.57	29.00
60.04	0.94	39.02
43.12	0.42	56.46

Results at 25°

Gms. per 100 gms. homogeneous mixture		
C_2H_5OH	C_6H_{14}	H_2O
3.10	95.92	0.98
18.52	79.90	1.51
36.28	61.64	2.08
37.82	59.70	2.48
51.94	45.91	2.15
68.03	28.11	3.86
73.84	17.61	8.55
74.73	12.93	12.34
73.52	8.00	18.48
67.49	3.61	28.90
53.81	1.86	44.38
36.68	1.21	62.11

The composition of the following conjugate layers at 25° was also determined.

Gms. per 100 gms. upper layer		
C_2H_5OH	C_6H_{14}	H_2O
0.08	99.31	0.61
1.75	97.71	0.54

Gms. per 100 gms. lower layer		
C_2H_5OH	C_6H_{14}	H_2O
37.67	0.23	62.10
56.92	2.91	40.47

ETHYL ALCOHOL C_2H_5OH.

RECIPROCAL SOLUBILITY OF ETHYL ALCOHOL AND WATER AT LOW TEMPERATURES, DETERMINED BY THE FREEZING-POINT METHOD.
(Pictet and Altschul, 1895; Pickering, 1893.)

t°. of Freezing.	Sp. Gr. Sat. Sol.	Gms. C_2H_5OH per 100 Gms. Sat. Sol.	Solid Phase.	t°. of Freezing.	Sp. Gr. Sat. Sol.	Gms. C_2H_5OH per 100 Gms. Sat. Sol.	Solid Phase.
— 1	0.9962	2.5	Ice	— 23.6	0.9512	33.8	Ice
— 2	0.9916	4.8	"	— 28.7	0.9417	39	"
— 3	0.9870	6.8	"	— 33.9	0.9270	46.3	"
— 5	0.9824	11.3	"	— 41	0.9047	56.1	"
— 6.1	0.9793	13.8	"	— 50	...	68	"
— 8.7	0.9747	17.5	"	— 60	...	75	"
— 9.4	0.9732	18.8	"	— 70	...	80	"
—10.6	0.9712	20.3	"	— 80	...	83.5	"
—12.2	0.9689	22.1	"	—100	...	89.5	"
—14	0.9662	24.2	"	—118 Eutec.	...	93.5	" + C_2H_5OH
—16	0.9627	26.7	"	—115	...	96	C_2H_5OH
—18.9	0.9578	29.9	"	—110.5	...	100	"

The result for the eutectic and for the f.-pt. of C_2H_5OH are by Puschin and Glagoleva, 1914, 1915; the other data for concentrations of C_2H_5OH above 70% were obtained by exterpolation. Additional data for the freezing-point lowering are given by Rozsa (1911).

Later determinations of the freezing-points of Ethyl Alcohol Water Mixtures by Tarassenkow, 1928, and Laland, 1934, gave an average curve from which the following values were taken.

t° of freezing	Gms. C_2H_5OH per 100 gms. sat. sol.	Solid Phase	t° of freezing	Gms. C_2H_5OH per 100 gms. sat. sol.	Solid Phase
- 2.0	5.0	Ice	-38.0	50	Ice
- 4.5	10.	"	-43.5	60	"
- 7.2	15	"	-50.5	70	"
-11.0	20	"	-67.0	80	"
-15.8	25	"	-87.5	85	"
-20.5	30	"	-113.0	90	"
-30.5	40	"	-125 Eutec.	92.5	" + C_2H_5OH
			-120	95	C_2H_5OH
			-114.5	100	"

Table F.3 Density of extractant solutions in hexane at 25°C.

Hexane : ρ = 0.654 g cc^{-1}			
$\bar{C}_{LT}$ (kmol m^{-3})	$\bar{C}_{DT}$ (kmol m^{-3})		
	1.10^{-4}	1.10^{-3}	1.10^{-2}
0.	0.654	0.654	0.656
5.10^{-3}	0.654	0.655	0.661
1.10^{-2}	0.658	0.658	0.662
2.10^{-2}	0.662	0.662	0.665

Table F.4 Viscosity of organic feeds at 25°C.

$\bar{C}_{DT}$	$\bar{C}_{LT}$	t(s)	ν_2(cS)	ρ_2(g cc^{-1})	μ_2(mPa.s)	$\frac{N_o}{N}_a$
hexane		43.4	0.474	0.654	0.310	0.47
1.10^{-4}	0.	43.4	0.474	0.654	0.310	0.47
	5.10^{-3}	44.0	0.480	0.654	0.314	0.48
	1.10^{-2}	45.0	0.491	0.658	0.323	0.49
	2.10^{-2}	46.6	0.509	0.662	0.337	0.51
1.10^{-3}	1.10^{-2}	44.7	0.488	0.658	0.321	0.49
	2.10^{-2}	46.3	0.506	0.662	0.334	0.50
1.10^{-2}	0.	44.0	0.480	0.656	0.315	0.48
	5.10^{-3}	44.8	0.489	0.661	0.323	0.49
	1.10^{-2}	48.2	0.526	0.662	0.348	0.53
	2.10^{-2}	51.2	0.559	0.665	0.372	0.56

Table F.5 Data and calculations for the π-A isotherm of DNNSA.

$\bar{C}_{DT} \times 10^6$ kmol/m^3	σ mNm^{-1}	π mNm^{-1}	$-(d\sigma/d\ln\bar{C}_{DT})^{-1}$ mmN^{-1}(1)	A(2) 10^{-9} m^2/kmol	A(2) nm^2/molec	Γ_D(2) 10^9 kmol/m^2
0.1	46	5	0.534	1.33	2.22	0.75
0.2	44	7	0.207	0.52	0.86	1.93
0.3	42.5	8.5	0.153	0.38	0.64	2.63
0.5	39	12	0.115	0.29	0.48	3.45
0.8	33	18	0.094	0.23	0.39	4.35
1.0	30	21	0.086	0.22	0.36	4.54
2.0	23	29	0.069	0.17	0.29	5.88
3.0	14	37	0.062	0.15	0.26	6.67
5.0	8	43	0.054	0.14	0.24	7.14
10.	7.5					
20.	3.9					
50.	4.3					
100.	2.8					
200.	3.					
300.	3.					

(1) Calculated fron the polynomial fitting of the data, as follows: $\sigma = -532. - 69.9 \ln(\bar{C}_{DT}) - 2.11 \ln(\bar{C}_{DT})^2$

(2) From eqn. IV.4.

Table F.6 Data and calculations for the π-A isotherms of DNNSA-LIX63 mixtures.

a) $\bar{C}_{LT}=1.10^{-3}$kmolm^{-3}

$\bar{C}_{DT}$	σ	π	A	A	$\Gamma x10^{9}$
10^{5}kmol/m^{3}	mNm^{-1}	mNm^{-1}	10^{-9}m^{2}kmol^{-1}	nm^{2}molec^{-1}	kmol m^{-2}
1.	26.4	24.6	2.41	4.01	0.42
2.	25.2	25.8	0.64	1.07	1.55
5.	20.5	30.5	0.44	0.73	2.28
10.	13.	38.			
20.	12.9	38.1			
30.	11.1	39.9			
50.	10.1	40.9			
100.	8.5	42.5	0.29	0.48	3.50
500.	3.2				

b) $\bar{C}_{LT}= 5.10^{-3}$kmol m^{-3}

$\bar{C}_{DT}$	σ	π	A	A	$\Gamma x10^{9}$
10^{5}kmol/m^{3}	mNm^{-1}	mNm^{-1}	10^{-9} m^{2}kmol^{-1}	nm^{2}molec^{-1}	kmol m^{-2}
1.	23.6	27.4	4.85	8.1	0.21
2.	24.0	27.0	1.54	2.6	0.65
3.	22.7	28.3	1.1	1.8	0.91
5.	22.7	28.2	0.81	1.34	1.24
10.	18.1	32.9	0.59	0.99	1.69
20.	15.2	35.8	0.47	0.78	2.13
30.	13.0	38.0	0.42	0.70	2.38
50.	9.9	41.1	0.37	0.61	2.70
100.	5.5	45.5	0.32	0.53	3.13
200.	5.3				
300	5.3				

Table F.6 Continued

c) $\bar{C}_{LT} = 1.10^{-2}$kmol m^{-3}

$\bar{C}_{DT}$	σ	π	A	A	$\Gamma x10^{9}$
10^{5}kmol/m^{3}	mNm^{-1}	mNm^{-1}	$10^{-9}m^{2}kmol^{-1}$	$nm^{2}molec^{-1}$	kmol m^{-2}
10.	22.	29.	1.97	3.3	0.51
20.	22.	29.	0.95	1.6	1.05
30.	21.	30.	0.73	1.2	1.37
50.	20.	31.	0.57	0.94	1.77
100.	12.	39.	0.43	0.72	2.31
200.	6.	45.	0.35	0.58	2.86
500.	3.8				

Polynomial fitting of the data

$\sigma = a_0 + a_1 \ln(\bar{C}_{DT}) + a_2 \ln^2(\bar{C}_{DT}) + a_3 \ln^3(\bar{C}_{DT})$

	$\bar{C}_{LT} = 1.10^{-3}M$	$5.10^{-3}M$	$1.10^{-2}M$
a_0	-186.	-87.7	-141.
a_1	-29.7	-19.	-35.7
a_2	-0.748	-0.803	-1.94
a_3	-0.012	–	–

Table F.7 Data and calculations for the π-A isotherm of LIX63. (Data from this work).

$\bar{C}_{LT}$	σ	π	A	A	$\Gamma \times 10^9$
10^3kmol/m^3	mNm^{-1}	mNm^{-1}	10^{-9}m^{2}kmol^{-1}	nm^{2}molec^{-1}	kmol m^{-2}
0.1	41.7	9.3	7.34	12.23	0.14
0.2	43.1	7.9	2.56	4.27	0.39
0.5	41.2	9.8	0.76	1.26	1.32
1.	36.	15.	0.58	0.96	1.0
4.	23.8	27.2	0.17	0.28	5.9
10.	23.2				
20.	21.7/20.9				
50.	20.8				

$$\sigma = -233. - 88.1 \ln(\bar{C}_{LT}) - 9.42 \ln^2(\bar{C}_{LT}) - 0.337 \ln^3(\bar{C}_{LT})$$

Table F.8 Data and calculations for the π-A isotherm of LIX63 (Data of Al-Diwan et al., 1977).

$\bar{C}_{LT}$	σ	π	A		$\Gamma \times 10^9$
10^3kmol/m^3	mNm^{-1}	mNm^{-1}	10^{-9}m^{2}kmol^{-1}	nm^{2}molec^{-1}	kmol m^{-2}
0.02	47.1	3.9	2.94	4.9	0.34
0.1	45.7	5.3	1.37	2.28	0.73
0.2	44.4	6.6	0.96	1.6	1.04
0.5	41.8	9.2	0.74	1.2	1.34
1.	39.1	11.9	0.675	1.13	1.48
2.	36.4	14.6	0.65	1.08	1.54
20.	28.1	22.9	0.83	1.38	1.20

$$\sigma = 26.4 + 3.20 \ln(\bar{C}_{LT}) + 1.18 \ln^2(\bar{C}_{LT}) + 0.0656 \ln^3(\bar{C}_{LT})$$

Table F.9 Interfacial potentials at $\bar{C}_{LT}=0$.

$\bar{C}_{DT}$	-EM(1)	$-\zeta$	$-\psi$	π	A	$-\psi$	$\exp(-F\psi/RT)$
$10^4 \frac{kmol}{m^3}$	$\frac{\mu m}{V}$	(1) V	(2) mV	mNm^{-1}	$\frac{nm^2}{molec}$	(3) mV	—
100	7.8	0.100	100	49	0.22	41	4.94
32			94			39	4.58
10	7.0	0.090	87	48.5	0.22	36	4.07
5			82			34	3.77
3.2			80			33	3.62
2			74			30	3.22
1	5.0	0.064	64	48	0.225	26	2.76
0.5	4.2	0.054	54	47.5	0.23	23	2.45
0.2	3.0	0.039	39	47	0.23	16	1.87
0.1	2.0	0.026	26	43.5	0.24	11	1.54

(1) at $I=4.10^{-3}M$ (Lin, 1984)

(2) interpolated from polynomial fitting of Lin's data:

$$\psi = -66.1 - 32736\,\bar{C}_{DT} + 0.969.10^{-7}.\bar{C}_{DT}^{2} - 0.676.10^{9}\bar{C}_{DT}^{3}$$

(3) at I= 0.5M, from eqn. IV.10.

Table F.10 Interfacial potentials in mixed reagent systems. I=0.5.

$\bar{C}_{LT} = 1.10^{-3}M$		$\bar{C}_{LT} = 1.10^{-2}M$	
-EM μm/V	$-\psi$ mV	- EM μm/V	$-\psi$ mV
1.	5.2	0.7	3.6
1.6	8.3	1.2	6.2
2.0	10.4	1.6	8.3
3.6	18.7	3.0	15.6
4.0	20.8	3.2	16.6
4.7	24.4	4.0	20.8
5.5	28.9	4.6	23.9
6.8	35.4	6.0	31.2

MALVERN AUTOSIZER IIc

Table F.11.a

sample : B in hexane
Imperial College
H. J. Simpson 22/12/86Live Data from Correlator
Temperature 25.0 Viscosity 0.2940 Refractive Index 1.375 Angle 90.0

Particle size distribution (nm.) Graph of Intensity distribution

2.2	-	2.6	|----------+
2.6	-	3.2	|----------+
3.2	-	3.9	|----------+
3.9	-	4.7	|----------+
4.7	-	5.7	|----------+
5.7	-	6.9	|----------+
6.9	-	8.3	|----------+
8.3	-	10.1	|----------+
10.1	-	12.2	|----------+
12.2	-	14.8	|----------+
14.8	-	17.9	|----------+
17.9	-	21.7	|----------+
21.7	-	26.3	|+
26.3	-	31.9	|+
31.9	-	38.7	|+
38.7	-	46.8	|+
46.8	-	56.7	|+
56.7	-	68.7	|+
68.7	-	83.3	|+
83.3	-	100.9	|+
100.9	-	122.2	|+
122.2	-	148.1	|+
148.1	-	179.4	|+
179.4	-	217.4	|+

Size Class			% by Intensity			% by mass			% by number		
			Under	In	Above	Under	In	Above	Under	In	Above
2.2	-	2.6	0.0	13.7	86.3	0.0	42.8	57.2	0.0	65.9	34.1
2.6	-	3.2	13.7	12.7	73.6	42.8	28.0	29.2	65.9	24.3	9.8
3.2	-	3.9	26.4	11.3	62.3	70.8	14.3	14.9	90.2	7.0	2.8
3.9	-	4.7	37.7	10.1	52.2	85.1	7.2	7.7	97.2	2.0	0.8
4.7	-	5.7	47.8	9.3	42.9	92.3	3.7	4.0	99.2	0.6	0.2
5.7	-	6.9	57.1	9.0	33.9	96.0	2.0	2.0	99.8	0.2	0.1
6.9	-	8.3	66.1	9.2	24.7	98.0	1.1	1.0	99.9	0.1	0.0
8.3	-	10.1	75.3	7.2	17.5	99.0	0.5	0.4	100.0	0.0	0.0
10.1	-	12.2	82.5	5.9	11.6	99.6	0.2	0.2	100.0	0.0	0.0
12.2	-	14.8	88.4	4.6	7.0	99.8	0.1	0.1	100.0	0.0	0.0
14.8	-	17.9	93.0	3.8	3.1	99.9	0.0	0.0	100.0	0.0	0.0
17.9	-	21.7	96.9	3.1	0.0	100.0	0.0	0.0	100.0	0.0	0.0
21.7	-	26.3	100.0	0.0	0.0	100.0	0.0	0.0	100.0	0.0	0.0
26.3	-	31.9	100.0	0.0	0.0	100.0	0.0	0.0	100.0	0.0	0.0
31.9	-	38.7	100.0	0.0	0.0	100.0	0.0	0.0	100.0	0.0	0.0
38.7	-	46.8	100.0	0.0	0.0	100.0	0.0	0.0	100.0	0.0	0.0
46.8	-	56.7	100.0	0.0	0.0	100.0	0.0	0.0	100.0	0.0	0.0
56.7	-	68.7	100.0	0.0	0.0	100.0	0.0	0.0	100.0	0.0	0.0
68.7	-	83.3	100.0	0.0	0.0	100.0	0.0	0.0	100.0	0.0	0.0
83.3	-	100.9	100.0	0.0	0.0	100.0	0.0	0.0	100.0	0.0	0.0
100.9	-	122.2	100.0	0.0	0.0	100.0	0.0	0.0	100.0	0.0	0.0
122.2	-	148.1	100.0	0.0	0.0	100.0	0.0	0.0	100.0	0.0	0.0
148.1	-	179.4	100.0	0.0	0.0	100.0	0.0	0.0	100.0	0.0	0.0
179.4	-	217.4	100.0	0.0	0.0	100.0	0.0	0.0	100.0	0.0	0.0

z Average Mean 4.9 Poly 0.167 Dist. mean 6.4 St.Dev. 4.4
Analysis range 100 :fit : 0.1674
[illegible] • scints/1000 • % resid : % n-range: Count rate 1000's /sec

MALVERN AUTOSIZER IIc

Table F.11.b

sample : B in hexane
Imperial College
H. J. Simpson 22/12/86Live Data from Correlator
Temperature 25.0 Viscosity 0.2940 Refractive Index 1.375 Angle 90.0

Particle size distribution (nm.) Graph of Intensity distribution

2.2	-	2.6	I----------+
2.6	-	3.2	I----------+
3.2	-	3.9	I----------+
3.9	-	4.7	I----------+
4.7	-	5.7	I----------+
5.7	-	6.9	I----------+
6.9	-	8.3	I----------+
8.3	-	10.1	I----------+
10.1	-	12.2	I----------+
12.2	-	14.8	I----------+
14.8	-	17.9	I----------+
17.9	-	21.7	I----------+
21.7	-	26.3	I+
26.3	-	31.9	I+
31.9	-	38.7	I+
38.7	-	46.8	I+
46.8	-	56.7	I+
56.7	-	68.7	I+
68.7	-	83.3	I+
83.3	-	100.9	I+
100.9	-	122.2	I+
122.2	-	148.1	I+
148.1	-	179.4	I+
179.4	-	217.4	I+

Size Class			% by Intensity			% by mass			% by number		
			Under	In	Above	Under	In	Above	Under	In	Above
2.2	-	2.6	0.0	13.4	86.6	0.0	42.4	57.6	0.0	65.7	34.3
2.6	-	3.2	13.4	12.6	74.0	42.4	27.9	29.7	65.7	24.4	9.9
3.2	-	3.9	26.0	11.4	62.6	70.3	14.4	15.3	90.1	7.1	2.9
3.9	-	4.7	37.4	10.2	52.3	84.7	7.3	8.0	97.1	2.0	0.8
4.7	-	5.7	47.7	9.4	43.0	92.0	3.8	4.2	99.2	0.6	0.3
5.7	-	6.9	57.0	9.8	33.2	95.8	2.1	2.1	99.7	0.2	0.1
6.9	-	8.3	66.8	9.4	23.8	97.9	1.1	1.0	99.9	0.1	0.0
8.3	-	10.1	76.2	7.4	16.4	99.0	0.6	0.4	100.0	0.0	0.0
10.1	-	12.2	83.6	5.8	10.6	99.6	0.2	0.2	100.0	0.0	0.0
12.2	-	14.8	89.4	4.4	6.2	99.8	0.1	0.1	100.0	0.0	0.0
14.8	-	17.9	93.8	3.5	2.7	99.9	0.0	0.0	100.0	0.0	0.0
17.9	-	21.7	97.3	2.7	0.0	100.0	0.0	0.0	100.0	0.0	0.0
21.7	-	26.3	100.0	0.0	0.0	100.0	0.0	0.0	100.0	0.0	0.0
26.3	-	31.9	100.0	0.0	0.0	100.0	0.0	0.0	100.0	0.0	0.0
31.9	-	38.7	100.0	0.0	0.0	100.0	0.0	0.0	100.0	0.0	0.0
38.7	-	46.8	100.0	0.0	0.0	100.0	0.0	0.0	100.0	0.0	0.0
46.8	-	56.7	100.0	0.0	0.0	100.0	0.0	0.0	100.0	0.0	0.0
56.7	-	68.7	100.0	0.0	0.0	100.0	0.0	0.0	100.0	0.0	0.0
68.7	-	83.3	100.0	0.0	0.0	100.0	0.0	0.0	100.0	0.0	0.0
83.3	-	100.9	100.0	0.0	0.0	100.0	0.0	0.0	100.0	0.0	0.0
100.9	-	122.2	100.0	0.0	0.0	100.0	0.0	0.0	100.0	0.0	0.0
122.2	-	148.1	100.0	0.0	0.0	100.0	0.0	0.0	100.0	0.0	0.0
148.1	-	179.4	100.0	0.0	0.0	100.0	0.0	0.0	100.0	0.0	0.0
179.4	-	217.4	100.0	0.0	0.0	100.0	0.0	0.0	100.0	0.0	0.0

z Average Mean 4.6 Poly 0.140 Dist. mean 6.3 St.Dev. 4.2
Analysis range 100 :fit : 0.1553

Run : counts/1000	: % merit	: % in-range:	Count rate 1000's /sec
7 1312.6	49.8	87.9	6.3

MALVERN AUTOSIZER IIc

Table F.11.c

sample : B in hexane
Imperial College
H. J. Simpson 22/12/86Live Data from Correlator
Temperature 25.0 Viscosity 0.2940 Refractive Index 1.375 Angle 90.0

Particle size distribution (nm.) Graph of Intensity distribution

2.2	-	2.6	|----------+
2.6	-	3.2	|----------+
3.2	-	3.9	|----------+
3.9	-	4.7	|----------+
4.7	-	5.7	|----------+
5.7	-	6.9	|----------+
6.9	-	8.3	|----------+
8.3	-	10.1	|----------+
10.1	-	12.2	|----------+
12.2	-	14.8	|----------+
14.8	-	17.9	|----------+
17.9	-	21.7	|----------+
21.7	-	26.3	|+
26.3	-	31.9	|+
31.9	-	38.7	|+
38.7	-	46.8	|+
46.8	-	56.7	|+
56.7	-	68.7	|+
68.7	-	83.3	|+
83.3	-	100.9	|+
100.9	-	122.2	|+
122.2	-	148.1	|+
148.1	-	179.4	|+
179.4	-	217.4	|+

Size Class			% by Intensity			% by mass			% by number		
			Under	In	Above	Under	In	Above	Under	In	Above
2.2	-	2.6	0.0	14.3	85.7	0.0	43.0	57.0	0.0	66.1	33.9
2.6	-	3.2	14.3	13.1	72.6	43.0	28.0	29.0	66.1	24.2	9.7
3.2	-	3.9	27.4	11.6	61.1	71.0	14.2	14.9	90.3	6.9	2.8
3.9	-	4.7	38.9	10.4	50.6	85.1	7.1	7.7	97.2	1.9	0.8
4.7	-	5.7	49.4	9.6	41.1	92.3	3.7	4.0	99.2	0.6	0.2
5.7	-	6.9	58.9	10.7	30.4	96.0	2.1	1.9	99.8	0.2	0.1
6.9	-	8.3	69.6	8.4	22.0	98.1	1.1	0.8	99.9	0.1	0.0
8.3	-	10.1	78.0	6.7	15.3	99.2	0.5	0.4	100.0	0.0	0.0
10.1	-	12.2	84.7	5.3	10.0	99.6	0.2	0.2	100.0	0.0	0.0
12.2	-	14.8	90.0	4.1	5.8	99.8	0.1	0.1	100.0	0.0	0.0
14.8	-	17.9	94.2	3.3	2.6	99.9	0.0	0.0	100.0	0.0	0.0
17.9	-	21.7	97.4	2.6	0.0	100.0	0.0	0.0	100.0	0.0	0.0
21.7	-	26.3	100.0	0.0	0.0	100.0	0.0	0.0	100.0	0.0	0.0
26.3	-	31.9	100.0	0.0	0.0	100.0	0.0	0.0	100.0	0.0	0.0
31.9	-	38.7	100.0	0.0	0.0	100.0	0.0	0.0	100.0	0.0	0.0
38.7	-	46.8	100.0	0.0	0.0	100.0	0.0	0.0	100.0	0.0	0.0
46.8	-	56.7	100.0	0.0	0.0	100.0	0.0	0.0	100.0	0.0	0.0
56.7	-	68.7	100.0	0.0	0.0	100.0	0.0	0.0	100.0	0.0	0.0
68.7	-	83.3	100.0	0.0	0.0	100.0	0.0	0.0	100.0	0.0	0.0
83.3	-	100.9	100.0	0.0	0.0	100.0	0.0	0.0	100.0	0.0	0.0
100.9	-	122.2	100.0	0.0	0.0	100.0	0.0	0.0	100.0	0.0	0.0
122.2	-	148.1	100.0	0.0	0.0	100.0	0.0	0.0	100.0	0.0	0.0
148.1	-	179.4	100.0	0.0	0.0	100.0	0.0	0.0	100.0	0.0	0.0
179.4	-	217.4	100.0	0.0	0.0	100.0	0.0	0.0	100.0	0.0	0.0

z Average Mean 4.1 Poly 0.136 Dist. mean 6.2 St.Dev. 4.1
Analysis range 100 :fit : 0.1498

Run : counts/1000	: % merit	: % in-range:	Count rate 1000's /sec
5 925.9	51.1	88.1	6.2

MALVERN AUTOSIZER IIc

Table F.11.d

sample : C in hexane

Filed data from b:1130 : block 12

Temperature 25.0 Viscosity 0.2940 Refractive Index 1.375 Angle 90.0

Particle size distribution (nm.) Graph of Intensity distribution

2.2	-	2.6	|----------
2.6	-	3.2	|----------+
3.2	-	3.9	|----------+
3.9	-	4.7	|----------+
4.7	-	5.7	|----------+
5.7	-	6.9	|----------+
6.9	-	8.3	|----------+
8.3	-	10.1	|----------+
10.1	-	12.2	|----------+
12.2	-	14.8	|----------+
14.8	-	17.9	|----------+
17.9	-	21.7	|----------+
21.7	-	26.3	|+
26.3	-	31.9	|+
31.9	-	38.7	|+
38.7	-	46.8	|+
46.8	-	56.7	|+
56.7	-	68.7	|+
68.7	-	83.3	|+
83.3	-	100.9	|+
100.9	-	122.2	|+
122.2	-	148.1	|+
148.1	-	179.4	|+
179.4	-	217.4	|+

Size Class			% by Intensity			% by mass			% by number		
			Under	In	Above	Under	In	Above	Under	In	Above
2.2	-	2.6	0.0	8.6	91.4	0.0	39.0	61.0	0.0	64.4	35.6
2.6	-	3.2	8.6	8.1	83.3	39.0	26.1	34.9	64.4	24.2	11.4
3.2	-	3.9	16.7	8.1	75.2	65.1	14.5	20.3	88.6	7.6	3.8
3.9	-	4.7	24.8	9.1	66.1	79.7	8.7	11.7	96.2	2.5	1.3
4.7	-	5.7	33.9	9.5	56.7	88.3	5.2	6.4	98.7	0.9	0.4
5.7	-	6.9	43.3	9.8	46.9	93.6	3.0	3.4	99.6	0.3	0.1
6.9	-	8.3	53.1	9.3	37.7	96.6	1.7	1.8	99.9	0.1	0.0
8.3	-	10.1	62.3	8.6	29.1	98.2	0.9	0.9	100.0	0.0	0.0
10.1	-	12.2	70.9	8.0	21.1	99.1	0.5	0.4	100.0	0.0	0.0
12.2	-	14.8	78.9	7.4	13.7	99.6	0.2	0.2	100.0	0.0	0.0
14.8	-	17.9	86.3	7.0	6.6	99.8	0.1	0.1	100.0	0.0	0.0
17.9	-	21.7	93.4	6.6	0.0	99.9	0.1	0.0	100.0	0.0	0.0
21.7	-	26.3	100.0	0.0	0.0	100.0	0.0	0.0	100.0	0.0	0.0
26.3	-	31.9	100.0	0.0	0.0	100.0	0.0	0.0	100.0	0.0	0.0
31.9	-	38.7	100.0	0.0	0.0	100.0	0.0	0.0	100.0	0.0	0.0
38.7	-	46.8	100.0	0.0	0.0	100.0	0.0	0.0	100.0	0.0	0.0
46.8	-	56.7	100.0	0.0	0.0	100.0	0.0	0.0	100.0	0.0	0.0
56.7	-	68.7	100.0	0.0	0.0	100.0	0.0	0.0	100.0	0.0	0.0
68.7	-	83.3	100.0	0.0	0.0	100.0	0.0	0.0	100.0	0.0	0.0
83.3	-	100.9	100.0	0.0	0.0	100.0	0.0	0.0	100.0	0.0	0.0
100.9	-	122.2	100.0	0.0	0.0	100.0	0.0	0.0	100.0	0.0	0.0
122.2	-	148.1	100.0	0.0	0.0	100.0	0.0	0.0	100.0	0.0	0.0
148.1	-	179.4	100.0	0.0	0.0	100.0	0.0	0.0	100.0	0.0	0.0
179.4	-	217.4	100.0	0.0	0.0	100.0	0.0	0.0	100.0	0.0	0.0

z Average Mean 3.1 Poly 0.088 Dist. mean 8.0 St.Dev. 5.1

Analysis range 100 :fit : 0.2561

Run	: counts/1000	: % merit	: % in-range:	Count rate 1000's /sec
0	1364.2	44.6	77.3	2.8

MALVERN AUTOSIZER IIc

Table F.11.e

sample : C in hexane
Imperial College
H. J. Simpson 22/12/86Live Data from Correlator
Temperature 25.0 Viscosity 0.2940 Refractive Index 1.375 Angle 90.0

Particle size distribution (nm.) Graph of Intensity distribution

2.2	-	2.6	|----------+
2.6	-	3.2	|----------+
3.2	-	3.9	|----------+
3.9	-	4.7	|----------+
4.7	-	5.7	|----------+
5.7	-	6.9	|----------+
6.9	-	8.3	|----------+
8.3	-	10.1	|----------+
10.1	-	12.2	|----------+
12.2	-	14.8	|----------+
14.8	-	17.9	|----------+
17.9	-	21.7	|----------+
21.7	-	26.3	|+
26.3	-	31.9	|+
31.9	-	38.7	|+
38.7	-	46.8	|+
46.8	-	56.7	|+
56.7	-	68.7	|+
68.7	-	83.3	|+
83.3	-	100.9	|+
100.9	-	122.2	|+
122.2	-	148.1	|+
148.1	-	179.4	|+
179.4	-	217.4	|+

Size Class			% by Intensity			% by mass			% by number		
			Under	In	Above	Under	In	Above	Under	In	Above
2.2	-	2.6	0.0	10.6	89.4	0.0	41.2	58.8	0.0	65.2	34.8
2.6	-	3.2	10.6	10.0	79.4	41.2	27.3	31.5	65.2	24.3	10.4
3.2	-	3.9	20.6	9.4	70.0	68.5	14.5	17.0	89.6	7.3	3.2
3.9	-	4.7	30.0	9.1	60.9	83.0	7.8	9.2	96.8	2.2	1.0
4.7	-	5.7	39.1	8.8	52.1	90.8	4.2	4.9	99.0	0.7	0.3
5.7	-	6.9	47.9	8.5	43.6	95.1	2.3	2.6	99.7	0.2	0.1
6.9	-	8.3	56.4	8.2	35.5	97.4	1.2	1.4	99.9	0.1	0.0
8.3	-	10.1	64.5	7.8	27.6	98.6	0.7	0.7	100.0	0.0	0.0
10.1	-	12.2	72.4	7.4	20.2	99.3	0.4	0.3	100.0	0.0	0.0
12.2	-	14.8	79.8	7.1	13.1	99.7	0.2	0.2	100.0	0.0	0.0
14.8	-	17.9	86.9	6.8	6.4	99.8	0.1	0.0	100.0	0.0	0.0
17.9	-	21.7	93.6	6.4	0.0	100.0	0.0	0.0	100.0	0.0	0.0
21.7	-	26.3	100.0	0.0	0.0	100.0	0.0	0.0	100.0	0.0	0.0
26.3	-	31.9	100.0	0.0	0.0	100.0	0.0	0.0	100.0	0.0	0.0
31.9	-	38.7	100.0	0.0	0.0	100.0	0.0	0.0	100.0	0.0	0.0
38.7	-	46.8	100.0	0.0	0.0	100.0	0.0	0.0	100.0	0.0	0.0
46.8	-	56.7	100.0	0.0	0.0	100.0	0.0	0.0	100.0	0.0	0.0
56.7	-	68.7	100.0	0.0	0.0	100.0	0.0	0.0	100.0	0.0	0.0
68.7	-	83.3	100.0	0.0	0.0	100.0	0.0	0.0	100.0	0.0	0.0
83.3	-	100.9	100.0	0.0	0.0	100.0	0.0	0.0	100.0	0.0	0.0
100.9	-	122.2	100.0	0.0	0.0	100.0	0.0	0.0	100.0	0.0	0.0
122.2	-	148.1	100.0	0.0	0.0	100.0	0.0	0.0	100.0	0.0	0.0
148.1	-	179.4	100.0	0.0	0.0	100.0	0.0	0.0	100.0	0.0	0.0
179.4	-	217.4	100.0	0.0	0.0	100.0	0.0	0.0	100.0	0.0	0.0

z Average Mean 2.8 Poly 0.085 Dist. mean 7.7 St.Dev. 5.1
Analysis range 100 :fit : 0.2092

Run	: counts/1000	: % merit	: % in-range:	Count rate 1000's /sec
8	2330.7	57.8	72.3	2.9

MALVERN AUTOSIZER IIc

Table F.11.f

sample : C in hexane
Imperial College
H. J. Simpson 22/12/86Live Data from Correlator
Temperature 25.0 Viscosity 0.2940 Refractive Index 1.375 Angle 90.0

Particle size distribution (nm.) Graph of Intensity distribution

2.2	-	2.6	I----------+
2.6	-	3.2	I----------+
3.2	-	3.9	I----------+
3.9	-	4.7	I----------+
4.7	-	5.7	I----------+
5.7	-	6.9	I----------+
6.9	-	8.3	I----------+
8.3	-	10.1	I----------+
10.1	-	12.2	I----------+
12.2	-	14.8	I----------+
14.8	-	17.9	I----------+
17.9	-	21.7	I----------+
21.7	-	26.3	I+
26.3	-	31.9	I+
31.9	-	38.7	I+
38.7	-	46.8	I+
46.8	-	56.7	I+
56.7	-	68.7	I+
68.7	-	83.3	I+
83.3	-	100.9	I+
100.9	-	122.2	I+
122.2	-	148.1	I+
148.1	-	179.4	I+
179.4	-	217.4	I+

Size Class			% by Intensity			% by mass			% by number		
			Under	In	Above	Under	In	Above	Under	In	Above
2.2	-	2.6	0.0	11.0	89.0	0.0	41.2	58.8	0.0	65.2	34.8
2.6	-	3.2	11.0	10.3	78.7	41.2	27.3	31.4	65.2	24.3	10.5
3.2	-	3.9	21.3	9.8	68.9	68.6	14.6	16.8	89.5	7.3	3.2
3.9	-	4.7	31.1	9.7	59.3	83.2	7.9	8.9	96.8	2.2	1.0
4.7	-	5.7	40.7	9.0	50.3	91.1	4.3	4.7	99.0	0.7	0.3
5.7	-	6.9	49.7	8.5	41.8	95.3	2.2	2.4	99.7	0.2	0.1
6.9	-	8.3	58.2	7.8	34.0	97.6	1.2	1.3	99.9	0.1	0.0
8.3	-	10.1	66.0	7.4	26.7	98.7	0.6	0.7	100.0	0.0	0.0
10.1	-	12.2	73.3	7.1	19.5	99.3	0.3	0.3	100.0	0.0	0.0
12.2	-	14.8	80.5	6.7	12.8	99.7	0.2	0.1	100.0	0.0	0.0
14.8	-	17.9	87.2	6.6	6.3	99.9	0.1	0.0	100.0	0.0	0.0
17.9	-	21.7	93.7	6.3	0.0	100.0	0.0	0.0	100.0	0.0	0.0
21.7	-	26.3	100.0	0.0	0.0	100.0	0.0	0.0	100.0	0.0	0.0
26.3	-	31.9	100.0	0.0	0.0	100.0	0.0	0.0	100.0	0.0	0.0
31.9	-	38.7	100.0	0.0	0.0	100.0	0.0	0.0	100.0	0.0	0.0
38.7	-	46.8	100.0	0.0	0.0	100.0	0.0	0.0	100.0	0.0	0.0
46.8	-	56.7	100.0	0.0	0.0	100.0	0.0	0.0	100.0	0.0	0.0
56.7	-	68.7	100.0	0.0	0.0	100.0	0.0	0.0	100.0	0.0	0.0
68.7	-	83.3	100.0	0.0	0.0	100.0	0.0	0.0	100.0	0.0	0.0
83.3	-	100.9	100.0	0.0	0.0	100.0	0.0	0.0	100.0	0.0	0.0
100.9	-	122.2	100.0	0.0	0.0	100.0	0.0	0.0	100.0	0.0	0.0
122.2	-	148.1	100.0	0.0	0.0	100.0	0.0	0.0	100.0	0.0	0.0
148.1	-	179.4	100.0	0.0	0.0	100.0	0.0	0.0	100.0	0.0	0.0
179.4	-	217.4	100.0	0.0	0.0	100.0	0.0	0.0	100.0	0.0	0.0

z Average Mean 3.1 Poly 0.097 Dist. mean 7.6 St.Dev. 5.1
Analysis range 100 :fit : 0.2168

Run :	counts/1000 :	% merit :	% in-range:	Count rate 1000's /sec
7	2067.6	50.3	64.7	3.0

Table F.12 Partition of DNNSA.

$\bar{C}_{DT}$	I (M, HNO_3)	C_{DT}, $x10^4$M	P	log P
2.10^{-2}	1.10^{-5}	2.7	73	1.86
	1.10^{-4}	2.6	76	1.88
	1.10^{-3}	2.5	79	1.90
	1.10^{-2}	1.7	116	2.07
	5.10^{-2}	0.90	221	2.34
	0.1	0.65	307	2.49
	0.5	0.24	832	2.92
1.10^{-2}	0.5	0.18	569	2.75
5.10^{-3}	1.10^{-5}	0.95	52	1.71
	1.10^{-4}	0.90	55	1.74
	1.10^{-3}	0.90	55	1.74
	1.10^{-2}	0.65	76	1.88
	0.1	0.33	151	2.18
	0.5	0.16	312	2.49
1.10^{-3}	1.10^{-5}	0.30	32	1.51
	1.10^{-4}	0.30	32	1.51
	1.10^{-3}	0.27	36	1.56
	1.10^{-2}	0.20	49	1.69
	5.10^{-2}	0.13	76	1.88
	0.1	0.09	110	2.04
	0.5	0.04	249	2.40
		0.08	119	2.07
1.10^{-4}	2.10^{-3}	0.036	27	1.43
	0.03	0.025	39	1.59
	0.1	0.016	61	1.79
	0.5	0.012	82	1.92
		0.014	70	1.85
1.10^{-5}	1.10^{-3}	0.005	19	1.28
	1.10^{-2}	0.004	24	1.38
	0.1	0.004	24	1.38
	0.5	0.003	32	1.51
		0.0014	69	1.84

Table F.13 Effect of changing aqueous phase composition at constant I on the solubility of DNNSA. I=0.5 M(KNO_3+ HNO_3).

$\bar{C}_{DT}$ (kmol m^{-3})	pH_{equil}	$C_{K,in}$ (kmol m^{-3})	P
2.10^{-2}	1.67	0.5	1005
	1.62	0.497	889
	0.76	0.35	873
5.10^{-3}	4.8	0.5	400
	2.2	0.497	301
	0.82	0.35	278
1.10^{-3}	2.2	0.497	128
	0.82	0.35	118

Table F.14 Rates and fluxes in DNNSA transfer.

EXP. N°	$\bar{C}_{DT} x1.10^{-2}$ (kmolm^{-3})	I (kmolm^{-3})	N rpm	$r_a x10^5$(1) moldm^{-3}min^{-1}	$J_a x10^9$(2) kmolm^{-2}s^{-1}
MVI	1.	4.10^{-3}	300	0.54	6.4
MII	1.	4.10^{-3}	250	0.49	5.8
MI	1.	4.10^{-3}	200	0.48	5.7
EI	1.	0.5	300	0.10	1.2
E7	1.	4.10^{-3}	200	0.49	5.8
E8	1.	0.5	200	0.07	0.86
MIV	0.5	4.10^{-3}	300	0.34	4.0
MV	0.5	4.10^{-3}	250	0.28	3.3
MIII	0.5	4.10^{-3}	200	0.24	2.8
E2	0.1	4.10^{-3}	300	0.054	0.64
E3	0.1	4.10^{-3}	250	0.044	0.52
E4	0.1	4.10^{-3}	200	0.041	0.48
E5	0.01	0.1	300	0.004	0.048
E6	0.01	0.1	250	0.0035	0.042
MXIV	0.01	0.1	200	0.0021	0.025
MVIII	0.5	0.1	300	0.18	2.2
MXIII	0.5	0.5	300	0.080	0.91
MXI(3)	0.5	0.1	300	0.17	2.0
MVII	0.5	0.1	200	0.16	1.9
MX(3)	0.5	0.1	200	0.14	1.7
MIX(4)	0.5	0.1	200	0.092	1.1
MXII(4)	0.5	0.5	200	0.065	0.77

(1) from eqn. IV.14
(2) from eqn. IV.15
(3) preequilibrated organic feed
(4) With 5.10^{-3}M nickel in solution

Table F.15 Moisture content of purified DNNSA.

Sample n°	drying time (h)	$\bar{C}_{DT}$ (1) kmol/m³	C_W kmol/m³	C_E kmol/m³	W_1 —	W_2 —	E —
1	0	0.24	0.81	0.51	3.4	3.1	2.1
2	15	0.14	0.45	0.14	3.2	2.8	1.0
3	39	0.081	0.30	0.047	3.7	3.0	0.58
4	63	0.067	0.21	0.048	3.1	2.3	0.72
5	87	0.068	0.24	0.045	3.5	2.7	0.66

(1) after dilution in hexane.

Table F.16 Equilibration of DNNSA solutions with ^{32}P. I=0.1 M HNO_3 (pH=1.), W^s=12.

$\bar{C}_{DT}$ M	0.1 cm³	0.5 cm³	1 cm³	1 cm³ average ± σ	100σ / average %	C_W^s= 12 $\bar{C}_{DT}$
	Counts / 30s					
5.10^{-3}	2096		20960			
	2132		20130	20863	2.4	0.06
		10613	21226	± 501		
		10567	21134			
1.10^{-2}	2592		25920			
	2554		25540	25315	2.0	0.12
		12425	24850	± 505		
		12475	24950			
5.10^{-2}	27046		270460			
	26955		269550	268508	0.7	0.60
		133655	267310	± 1999		
		133355	266710			
0.1	79872		798720			
	79191		791910	780934	2.2	1.2
		383596	767192	± 16846		
		382956	765912			

Table F.17 Water solubilization across a membrane. N=1200rpm, C_W^h= 0.057M. Total water, kmol water m^{-3} (uncorrected for C_W^H)

time	$\bar{C}_{DT}=2.10^{-2}$	$\bar{C}_{DT}=1.10^{-2}$	$\bar{C}_{DT}=5.10^{-3}$	$\bar{C}_{DT}=2.5.10^{-3}$
min	M	M	M	M
0	0.103	0.080	0.069	0.063
1	0.161	0.109	0.074	0.064
2	0.187	0.122	0.073	
3	0.234	0.131	0.085	0.077
4	0.225	0.145	0.098	
5	0.240	0.140		0.078
6	0.222	0.148		
7		0.125	0.100	
10	0.225	0.140	0.093	0.074
12		0120	0.094	0.072
15	0.252			
20	0.227	0.148		0.080
30	0.243	0.145		
120	0.224	0.143	0.090	
∞	0.24	0.14	0.093	0.077

Table F.18 Saturation loadings and rates in membrane transfer.

$\bar{C}_{DT}$	C_W^s	$V\, r_W \times 10^8$
$\frac{\text{kmolDNNSA}}{m^3}$	$\frac{\text{kmol } H_2O}{m^3}$	$\frac{\text{kmol } H_2O}{s}$
2.10^{-2}	0.23	1.3
1.10^{-2}	0.14	0.57
5.10^{-3}	0.093	0.25
$2.5.10^{-3}$	0.097	0.12
1.10^{-2}(1)	0.14	0.23

(1) at N=780 rpm.

Table F.19 Data from electrolyte solubilization in the NDSC.

$\bar{C}_{DT}$	1.10^{-2}			5.10^{-3}			5.10^{-3}	
C_W^o	0.022M			0.011M			0.011M	
I	4.10^{-3}M(HNO_3)			4.10^{-3}M(HNO_3)			0.1	0.1
N_o	100	125	150	100	125	150	200	300
EXP	I	VI	II	III	V	IV	VII	VIII
time (min)	Water concentration in organic phase, C_W x10^{-2} (kmol m^{-3})							
0	2.2	2.2	2.2	1.5	2.0	2.0	1.1	1.1
0.5	-	3.5	3.1	1.7	2.5	2.7	1.3	-
1	3.5	-	4.5	-	3.1	-	-	1.3
2	4.1	4.8	-	1.9	-	4.3	1.9	2.0
3	4.6	-	6.0	2.2	3.8	-	2.4	-
4	4.7	-	6.3	2.7	4.1	5.0	2.8	-
5	5.3	6.1	-	3.0	-	-	2.7	3.0
6	5.2					5.2		
7	5.4			3.2				
8	5.6							
9	6.4							
J_W(1)	1.7	3.0	4.8	0.90	1.5	1.8	0.65	0.84
Rex10^{-3}	8.4	10.5	12.6	8.4	10.5	12.6	16.8	25.2

(1) x 10^5 kmol H_2O $m^{-2}s^{-1}$

Table F.20a Data from ^{32}P dynamic solubilization by dry and pre-equilibrated micelles. $\bar{C}_{DT}=5.10^{-2}M$. Activity decay correction factor f= 0.559.

time	counts/30s	C_w^i	counts/30s	C_w^e
(min)	(1)	(2)	(1)	(2)
0	81	0.026	81	0.026
0.5	404	0.096	88	0.027
1	583	0.134	101	0.030
2	732	0.167	146	0.040
5	802	0.183	182	0.048
10	926	0.210	262	0.065
15	1027	0.232	362	0.087
20	1013	0.229	367	0.088
30	1070	0.241	435	0.103
40	1246	0.280	685	0.157
50	1357	0.304	843	0.192
60	1499	0.335	840	0.191

(1) corrected for background (86 counts/30s), average of four countings. 1/100 dilution of tracer.

$$(2)((1)x\frac{100}{0.100} \times \frac{1}{0.559})1.2.10^{-7} + 0.00786$$

Table F.20b Data from ^{32}P dynamic solubilization by dry and pre-equilibrated micelles. $\bar{C}_{DT}=2.10^{-2}M$. Activity decay correction factor f= 0.533 (dry, i), 0.507 (prequilibrated, e).

time	counts/30s	C_w^i	counts/30s	C_w^e
(min)	(1)	(2)	(1)	(2)
0	111	0.032		
0.5	375	0.090		
1	597	0.138	239	0.065
2	671	0.154	292	0.078
5	838	0.191	305	0.081
10	866	0.197	339	0.089
15	909	0.206	379	0.099
20	1049	0.237	466	0.110
30	1062	0.239	486	0.125
40	1110	0.250	563	0.143
50	1133	0.255	603	0.153
60	1166	0.262		

Table F.20c Data from ^{32}P solubilization rates by dry and pre-equilibrated micelles. $\bar{C}_{DT}$=0.013M. Activity decay correction factor f= 0.507.

time	counts/30s	C_w^i	counts/30s	C_w^e
(min)	(1)	(2)	(1)	(2)
0	75	0.026	67	0.024
0.5	147	0.043	105	0.033
1	291	0.078	171	0.049
2	371	0.097	202	0.056
5	519	0.133	264	0.071
10	603	0.152	336	0.089
15	761	0.191	362	0.095
20	768	0.193	453	0.117
30	962	0.239	465	0.120
40	827	0.207	526	0.134
50	849	0.220	558	0.142
60	890	0.222		

Table F.20d Data from ^{32}P solubilization rates by dry and pre-equilibrated micelles. $\bar{C}_{DT}=5.10^{-3}M$. Activity decay correction factor f= 0.483.

time	counts/30s	C_w^i	counts/30s	C_w^e
(min)	(1)	(2)	(1)	(2)
0	13	0.011	11	0.013
0.5	63	0.024	70	0.026
1	83	0.029	76	0.027
2	114	0.037	100	0.033
5	175	0.052	156	0.047
10	192	0.056	178	0.052
15	208	0.060	200	0.059
20	226	0.065	221	0.064
30	231	0.066	217	0.062
40	248	0.0704	235	0.067
50	255	0.072	247	0.070
60	256	0.072	252	0.071

Table F.21 Potassium-Hydrogen exchange by DNNSA. I=0.5M (HNO_3+ KNO_3), $\bar{C}_{DT}$= 0.1 $kmolm^{-3}$.

pH	$C_{K,feed}$	X(1)	$C_{H,eq}^{(2)}$	pH_{eq}	$\bar{C}_{KD,eq}$	X(3)	X(4)	X(5)
-	$kmolm^{-3}$	-	$kmolm^{-3}$	-	$kmolm^{-3}$	-	-	-
4.0	0.485	1.00	0.0625	1.20	0.074	0.74	0.62	0.68
3.5	0.485	1.00	0.0694	1.16	0.069	0.69	0.69	0.69
3.0	0.484	0.99	0.067	1.19	0.076	0.65	0.76	0.71
2.5	0.482	0.98	0.070	1.15	0.058	0.58	0.65	0.62
2.0	0.475	0.94	0.073	1.14	0.063	0.63	0.61	0.62
1.5	0.453	0.85	0.096	1.0	-	-	0.59	-
1.0	0.385	0.68	0.16	0.80	0.051	0.51	0.48	0.495
0.5	0.169	0.33	0.34	0.47	0.023	0.23	0.24	0.235
(6)				2.0	0.095	0.92	-	-
(6)				3.0	0.099	0.99	-	-

(1) eqn. IV.21

(2) titrated with HONa 0.05N

(3) $X = \bar{C}_{KD} / \bar{C}_{DT}$ (atomic emission spectrophotometry)

(4) $X = \dfrac{C_{H,eq} - C_{H,feed}}{\bar{C}_{DT}}$ (titration)

(5) average of (3) and (4)

(6) from the organic feed of nickel extraction rate experiments with pH as variable (preequilibrated with blank of appropriate pH)

Table F.22 Equilibrium distribution of Ni(II) extracted by (K-H)DNNS. I= 1M (HNO_3+KNO_3), pH ≅ 0.5.

[Ni(II)]	$\bar{C}_{DT}$ ($kmolm^{-3}$)							
in feed	0.0667				0.0813			
$x10^3 kmolm^{-3}$	a	b	c	d	a	b	c	d
0.1	7.0	5.9	0.20	0.200	6.68	5.58	0.16	0.197
0.5	34.4	27.7	1.2	0.242	34.0	26.9	1.0	0.264
1.0	65.5	53.8	2.1	0.217	65.0	51.5	2.0	0.262
5.0	-	-	-	-	338	271	9.1	0.228
10.	-	-	-	-	620	517	15	0.200
50.	3113	2563	81	0.215	4164	3083	96	0.351
f	0.220				0.228 ± 0.030			
g							13	

a= $C_{M,feed}$, average (ppm)

b= $C_{M,equilibrium}$, average (ppm)

c= loading % = $7 \frac{\bar{C}_M}{\bar{C}_{DT}} = 7 (C_{M,f} - C_{M,eq}) / \bar{C}_{DT}$ (%)

d= $D_D = (C_{M,f} - C_{M,eq})/\bar{C}_{DT}$

f = D_D ± std. dev. at constant $\bar{C}_{DT}$

g= relative error at 1 *sd* = $(sd/D_D)x100$ (%)

Table F.22 (continued)

[Ni(II)] in feed	$\bar{C}_{DT}$ (kmolm^{-3})							
	0.135				0.236			
x10^{3}kmolm^{-3}	a	b	c	d	a	b	c	d
0.1	10.5	7.5	0.27	0.394	6.18	3.70	0.13	0.670
0.5	47.6	32.8	1.3	0.452	30.1	18.0	0.62	0.682
1.0	89.7	63.7	2.3	0.408	55.3	30.	1.3	0.843
					60.1	34.	1.3	0.773
5.	466	323	12.6	0.443	288	181	5.4	0.600
					325	172	7.7	0.893
10.	860	627	21	0.372	529	302	12.	0.755
50.	4164	3083	96	0.351	2636	1635	51	0.612
f	0.407 ± 0.035				0.728 ± 0.107			
g	8.5				15			

[Ni(II)] in feed x10^{3}kmolm^{-3}	e	R
0.1	$\log D_D = 0.474 + 1.03 \log \bar{C}_{DT}$	0.9540
0.5	$\log D_D = 0.448 + 0.92 \log \bar{C}_{DT}$	0.9897
1.0	$\log D_D = 0.570 + 1.05 \log \bar{C}_{DT}$	0.9941
5.	$\log D_D = 0.366 + 0.90 \log \bar{C}_{DT}$	0.9700
10.	$\log D_D = 0.670 + 1.26 \log \bar{C}_{DT}$	0.9999
50.	$\log D_D = 0.416 + 0.99 \log \bar{C}_{DT}$	0.9988

e= linear regression of D_D on $\bar{C}_{DT}$ at constant $C_{M,feed}$.

R= correlation coefficient.

Table F.23 Calculations to estimate the aggregation number of DNNSA from nickel distribution data. I=1M (HNO_3 + KNO_3), pH=0.5.

$\bar{C}_{DT}$	$\bar{C}_M$	$\frac{\bar{C}_M}{\bar{C}_{DT}}$	D_D	$\frac{D_D}{\bar{C}_{DT}}$
$kmol\,m^{-3}$	ppm	$\frac{ppm}{kmol/m^3}$	–	$m^3/kmol$
0.0667	6.7	100	0.242	3.63
	11.7	175	0.217	3.25
0.0813	7.1	87.3	0.264	3.25
	13.5	166	0.262	3.22
	67	824	0.228	2.80
	103	1267	0.200	2.46
0.135	14.8	110	0.452	3.35
	26.	193	0.408	3.02
	143	1059	0.443	3.28
	233	1726	0.372	2.76
0.236	25.3	107	0.843	3.57
	26.1	111	0.773	3.28
	107	453	0.600	2.54

Table F.24 Equilibrium distribution of Ni(II) extracted by LIX63. Aqueous feed conditions: C_M=5.10^{-3}M, I=0.5M (HNO_3+ KNO_3), pH=2.5, 20°C.

$\bar{C}_{LT}$ x10^3	D_L	$D_{L,\ avge}$	s.d.	(s.d./$D_{L,avge}$) x100	pH_{eq}
20	0.0230	0.0214	0.0023	10.6	-
	0.0198				
10.	0.0124	0.0137	0.0018	13.4	2.61
	0.015				
8.	0.0106				
7.	0.0086				
5.	0.0072				2.49
3.	0.0046				
2.	0.0039	0.0047	0.00113	24.0	2.54
	0.0055				
1.	0.0030	0.0033	0.00035	10.6	2.49
	0.0035				
0.5	0.0031				2.53
0.2	0.0027				2.55
0.1	0.0015				2.55

Table F.25 Effect of pH on distribution in Ni(II) extraction by LIX63. Feed conditions: $C_M=5.10^{-3}M$, I=0.5M (HNO_3+KNO_3), $\bar{C}_{LT}=0.01M$.

pH_{feed}	$\bar{C}_M x10^3$ kmolm^{-3}	D_L	$D_L(1)$	$\bar{C}_{Me}/\bar{C}_{Ms}$
3.0				20
2.5	0.125	0.025	0.036	6
2.0	0.091	0.018	0.015	2
1.4	0.045	0.009	0.0075	0.6
0.5	0.025	0.005	0.0053	0.06

(1) predicted by eqn. IV.61 with a=0.005, b=0.0001

Table F.26 Equilibrium distribution of Ni(II) in the mixed extractants system. [Ni(II)]=5.10^{-3}kmolm^{-3}, I=0.5M (HNO_3+ KNO_3), pH=2.5.

$\bar{C}_{LT}$(M)=	0.0	1.10^{-3}	5.10^{-3}	1.10^{-2}
$\bar{C}_{DT}$x 10^4 (kmolm^{-3})	D_D	D_M	D_M	D_M
0.1		0.0034	0.0062	
0.5		0.012	0.0138	0.019
1.		0.035	0.0225	
2.		0.018	0.028±0.006	0.034
3.		0.031	0.043±0.013	0.044
4.			0.045	
5.		0.080	0.060±0.008	0.083
6.			0.080	
7.		0.084		
10.	0.0018	0.114	0.39±0.08	
20.	0.0035		0.59	
50.	0.009	0.52		
100.	0.100			
670	0.283			
1350	0.443			
2360	0.593			

Table F.27 Equilibrium constants for nickel extraction by mixtures. $\bar{C}_{LT}=5.10^{-3}$kmolm^{-3}, $C_M=5.10^{-3}$ kmolm^{-3}, I=0.5, pH=2.5.

$\bar{C}_{DT}x10^3$	D_2	K_2'	D_1	K_1'	K_2'/K_1'
1.	0.39	0.075	0.11	0.0275	3.5
2.	0.59	0.148	0.18	0.045	3.3
5.	1.38	0.345	0.38	0.095	3.6

Table F.28 Effect of N and $\bar{C}_{DT}$ on J_D ($x10^{10}$kmolm^{-2}s^{-1}). [Ni(II)]=5.10^{-3}kmolm^{-3}, I=0.5M (HNO_3 +KNO_3), pH=2.5.

	N (rpm)				
$\bar{C}_{DT}$ $x10^4$kmolm^{-3}	150	200	250	300	350
1.			0.23	0.36	0.35
4.			1.3	1.6	1.5
5.		1.8	2.3	2.2	
10.	2.5	4.6	4.4	4.0	3.9
50.	14.	16.		17./15.	
100.	24.	29.	36.		

Table F.29 Effect of $\bar{C}_{DT}$, C_M, and pH on J_D($\times 10^{10}$ kmolm^{-2}s^{-1})

$\bar{C}_{DT}$= VARIABLE C_M=5.10^{-3}kmolm^{-3} pH=2.5		1.10^{-3}kmolm^{-3} VARIABLE 2.5		5.10^{-3}kmolm^{-3} 5.10^{-3}kmolm^{-3} VARIABLE	
$\bar{C}_{DT}\times 10^4$M	J_D	$C_M\times 10^3$kmolm^{-3}	J_D	pH	J_D
0.1	0.035	0.5	0.33±0.12	0.5	2.8/2.9
0.2	0.055	1.	0.55±0.06	1.0	5.1/5.1
0.3	0.10	2.5	1.4	1.5	7.5
0.5	0.16	4.	2.3	2.0	12.
1.	0.31±0.02			2.5	15.3
2.	0.69±0.15			3.0	16.4
3.	1.0			3.5	15.1
4.	1.6±0.1				
5.	2.1±0.1				
10.	4.0±0.7				
20	4.9				
50	15.1±4.1				
100	32.7±4.4				

Table F.30 Effect of extractant concentration on the nickel flux with LIX63 alone. [Ni(II)]=5.10^{-3} kmolm^{-3}, I=0.5M (HNO_3+ KNO_3), pH=2.5.

$\bar{C}_{LT}$x10^{3}kmolm^{-3}	J_Lx10^{10}kmolm^{-2}s^{-1}
20	0.91
10	0.47
5	0.23
1	0.055

Table F.31 Effect of pH on the nickel flux with LIX63 alone. [Ni(II)]=5.10^{-3}kmolm^{-3}, I=0.5M (HNO_3+ KNO_3). (J_Lx10^{10}kmolm^{-2}s^{-1})

pH	$\bar{C}_{LT}$	
	1.10^{-3}kmolm^{-3}	1.10^{-2}kmolm^{-3}
1.5		0.05
2.0	0.013	0.16
2.5	0.055	0.47
3.0	0.21	0.50/0.65

Table F.32 Nickel fluxes in mixed reagents systems. [Ni(II)]=5 .10^{-3}kmolm^{-3}, I=0.5M (HNO_3+KNO_3), pH=2.5, N=300 rpm. ($J_M x10^{10}$kmol $m^{-2}s^{-1}$)

$\bar{C}_{DT}$	$\bar{C}_{LT} x10^3$kmolm^{-3}		
$x10^4$kmolm^{-3}	1.	5.	10.
0.1	0.41		
0.2	0.61		
0.3	1.1		
0.5	1.4	1.6	1.9
1.	1.6		
2.	1.2	3.3/3.9	
3.	1.6	3.6	5.0
4.	1.6		
10.	4.4	3.6	4.7
20.	9.	8.0	5.5
50	21.	16.7	15.7/15.9

Table F.33 Effect of pH on nickel flux ($J_M x10^{10}$ kmolm^{-2}s^{-1}) in mixed reagents sistems. $\bar{C}_{DT}$= 5.10^{-3}kmolm^{-3}, C_M=5.10^{-3}kmolm^{-3}, I=0.5M (HNO_3+ KNO_3), N=300rpm

pH	$\bar{C}_{LT}$=1.10^{-3}kmolm^{-3}	$\bar{C}_{LT}$=1.10^{-2}kmolm^{-3}
1.0	1.8	
1.5	4.51.9	
2.0	9.5	4.2
2.5	21.	15.7/15.9
3.0	26.0/26.8	28.1/27.3

Table F.34 Effect of [Ni(II)] on the nickel flux in mixed systems. I=0.5M (HNO_3+ KNO_3), pH=2.5, N=300 rpm.

$\bar{C}_{DT}$ x10^{-3}kmolm^{-3}	$\bar{C}_{LT}$ x10^{-3}kmolm^{-3}	$C_M x10^{-3}$kmolm^{-3} 0.5	1.	5.
1.	0.	0.26/0.33	0.60	2.9
	1.	0.98	1.6	4.4
	5.	0.40	0.72	3.6
	10.	0.49		4.7
0.3 0.	0.16	0.26	1.0	
	1.	0.21	0.33	1.6
	5.	0.33	0.49	3.6
	10.	0.41	0.53	5.0

Table F.35 Mass transfer coefficients in the NDSC (aqueous phase). I=0.004 M HNO_3.

$\bar{C}_{DT} \times 10^2$ kmolm^{-3}	N rpm	$K_{aq} \times 10^5$ ms^{-1}	$K_{aq} \alpha Re^{EXP}$ EXPONENT	correlation coefficient
1.	300	5.7		
1.	250	4.9		
1.	200	3.7	1.06	0.9962
0.5	300	6.6		
0.5	250	5.3		
0.5	200	3.9	1.28	0.9999
0.1	300	7.5		
0.1	250	5.6		
0.1	200	4.6	1.21	0.9779

Table F.36 Mass transfer coefficients in the NDSC (organic phase), $K_o \times 10^{-5}$ ms^{-1}. Parameter is $\bar{C}_{DT}$(kmolm^{-3})/W^s(-).

N/2 rpm	Re	5.10^{-3}/14 kmolm^{-3}	5.10^{-3} /10 kmolm^{-3}	1.10^{-2}/13 kmolm^{-3}
100	8400	7.6		7.3
125	10500	10.1		9.9
150	12600	12.9		13.5
200	16800		14.4	
300	25200		16.0	

Table F.37 Solubilization contribution to Ni(II) extraction fluxes. [Ni(II)]=3.10^{-3}. N_o=150rpm.

$\bar{C}_{DT}x10^3$	$J_D x10^{10}$	$J_W x10^6$	$J_W x10^6$	$J_{DS} x10^{10}$	J_{DS}/J_D	$1.3J_D x10^{10}$
$kmolm^{-3}$	$kmolm^{-2}s^{-1}$	$kmolm^{-2}s^{-1}$	$kmolm^{-2}s^{-1}$	$kmolm^{-2}s^{-1}$	--	$kmolm^{-2}s^{-1}$
	NDSC	I=0.004	I=0.5	NDSC		
1.	4.1	3.[1]	1.2[2]	1.1	0.27	5.3
5.	17.	18.	6 [3]	5.4	0.32	22.
10.	37.	48.	16 [3]	14.	0.38	48.

(1) From transfer through membrane, at I=0.1.

(2) Corrected as $W^s \cong 10$ at I=0.1, $W^s \cong 4$ at I=0.5.

(3) Corrected as $W^s \cong 12$ at I=0.004, $W^s \cong 4$ at I=0.5.

Appendix G Estimation of diffusion coefficients.

Rates of sublayer renewal were estimated in section V.4 from MTCs found from initial water solubilization and micellar core exchange experiments in the NDSC, and an estimate of the diffusion coefficient $\mathcal{D}$. This appendix shows how $\mathcal{D}$ was evaluated.

In their work on DNNSA monolayers dissolution in a Langmuir trough, Chaiko and Osseo-Asare (1986 .) estimated the diffusion coefficient of DNNSA monomers in the aqueous sublayer (at 0.1M KNO_3 , pH=6, and at 18°C) as $\mathcal{D}_{m,w}=3.10^{-10}\ m^2s^{-1}$. The diffusion coefficient of monomers in hexane, $\mathcal{D}_{m,o}$, may be evaluated from this estimate and the correlations available in the literature (Reid et al., 1970, p.570; Sherwood et al., 1975). The correlations by Wilke-Chang, Scheibel, and Reddy and Doraiswami were found to predict similar values of $\mathcal{D}_{m,o}$. The Wilke-Chang correlation predicts that

$$\mathcal{D}^{o}_{AB} \alpha \frac{M_B^{1/2}}{\mu_B} \qquad (G.1)$$

where M_B is the molecular weight of the diluent, μ_B is its viscosity, and A refers to the solute. A ratio may thus be written for both diluents as follows:

$$\frac{\mathcal{D}_{m,o}}{\mathcal{D}_{m,w}} = \left[\frac{M_o}{M_w}\right]^{1/2} \frac{\mu_w}{\mu_o} = \left[\frac{86}{18}\right]^{1/2} \frac{1}{0.336}$$

It results $\mathcal{D}_{m,o}=6.5\mathcal{D}_{m,w}=2.10^{-9}m^2s^{-1}$. It is now desired to estimate the diffusion coefficient of the reversed micelle in hexane, $\mathcal{D}_{rm}$. McQueen and Hermans (1972) showed that the Stokes-Einstein equation related satisfactorily the values of $\mathcal{D}_{m,o}$ and $\mathcal{D}_{rm}$. The diffusion coefficients of two particles of different volume are proportional to their hydraulic radii, and assuming that micellar volumes depend linearly on mean aggregation numbers (m), those authors stated eqn.G.2:

$$\mathcal{D}_{rm} = \frac{\mathcal{D}_{m,o}}{m^{1/3}} \qquad (G.2)$$

Thus $\mathcal{D}_{rm} = 2.10^{-9}/7^{1/3} \cong 1.05.10^{-9} m^2 s^{-1}$.

As the RM solubilizes water, a water pool forms at its core and the diffusion coefficient changes because the change in size. The coefficient for the saturated micelle is $\mathcal{D}_{rms}$. The mean diameter of dry and saturated micelles measured by PCS were respectively around 3 and 4.5 nm. Thus

$$\frac{\text{Volume micelle, satd.}}{\text{Volume micelle, dry}} = \left[\frac{4.5}{3.}\right]^3 = 3.4$$

Although the solubilization capacity depends on the solubilizate ionic strength, only one value of the saturated micelle diameter will be considered here. Now the effect of the size change on the diffusion coefficient may be evaluated by the Wilke-Chang or the Reddy-Doraiswami correlations. Both predict the ratio G.3:

$$\frac{\mathcal{D}_{rms}}{\mathcal{D}_{rm}} = \left[\frac{1/Vs}{1/Vd}\right]^{1/3} = 0.67 \qquad (G.3)$$

The result is $\mathcal{D}_{rms} = 7.10^{-10} m^2 s^{-1}$.

Appendix H Computer codes and output samples.

File name	Section	Page
FIT	V.5	326
REWAL	V.5	327
OUTPUT OF REWAL	V.5	329
NORG	V.7	332
OUTPUT OF NORG	V.7	335

```
00100      PROGRAM FIT(DATA,OUTPUT,TAPE5=DATA,TAPE6)
00110 C    THIS PROGRAM FITS THE NICKEL FLUX VERSUS (N,CDT)DATA
00120 C    TO ESTIMATE THE PARAMETER DELTA*K IN THE RENEWAL -
00130 C    REACTION MODEL, USING THE NAG ROUTINE E04FDF.
00140 C
00150      DIMENSION AJCDT(20),S(20)
00152      DIMENSION W(109),IW(1)
00160      REAL X, FSUMSQ,W
00170      INTEGER I,IFAIL,LW,LIW,M,N,IW
00180      COMMON AJCDT,S
00190      DO 30 I=1,20
00200      READ (5,*)AJCDT(I),S(I)
00210      WRITE(6,32)AJCDT(I),S(I)
00220      32 FORMAT (1X,'J/CDT=',E15.10,2X,'S=',F5.2)
00230      30 CONTINUE
00240 C
00250      M=20
00260      N=1
00270      X=1.E-5
00280      LW=109
00290      LIW=1
00300      IFAIL=1
00310      CALL E04FDF(M,N,X,FSUMSQ,IW,LIW,W,LW,IFAIL)
00320      IF(IFAIL.NE.0)WRITE(6,104)IFAIL
00330      IF(IFAIL.EQ.1)GO TO 40
00340      WRITE(6,105)FSUMSQ
00350      WRITE(6,106)X
00360      104 FORMAT(1X,'ERROR EXIT TYPE',I3)
00370      105 FORMAT(1X,'SUM OF SQUARES ON EXIT=',E15.8)
00380      106 FORMAT(1X,'DELTA*K=',E8.3)
00390      40 STOP
00400      END
00410 C
00420 C
00430      SUBROUTINE LSFUN1(M,N,XC,FVECC)
00440      DIMENSION FVECC(M)
00444      REAL XC
00450      DIMENSION AJCDT(20),S(20)
00460      INTEGER I,M,N
00465      REAL AA,BB
00470      COMMON AJCDT,S
00480      DO 46 I=1,20
00490      AA=S(I)-0.378E4*XC*SQRT(S(I))
00500      BB=S(I)-0.14E8*XC*XC
00510      FVECC(I)=0.00143*XC*AA/BB-AJCDT(I)
00520      46 CONTINUE
00530      RETURN
00540      END
```

```
00100      PROGRAM REWAL (INPUT,OUTPUT,TAPE6)
00110 C    THIS PROGRAM IMPLEMENTS THE SOLUTION TO THE
00120 C    PROBLEM OF DIFFUSION AND REACTION WITH THE
00130 C    "RADIATION HEAT TRANSFER" BOUNDARY CONDITION
00140 C    AT X=0. IT MAPS THE METAL COMPLEX CONCENTRATION
00150 C    IN SPACE AND TIME USING THE DIFFUSION FILM.
00152 C    IT COMPUTES THE SURFACE COMPLEX CONCENTRATION
00160 C    "SURFACE". IT COMPUTES INSTANTANEOUS FLUXES
00170 C    INTO THE FLUID ELEMENT, AND THE AVERAGE FLUX
00175 C    AS A FUNCTION OF REACTION RATE CONSTANT AND
00180 C    SURFACE RENEWAL FREQUENCY.
00185      REAL CDT,D,DD,AK,DELTA,CMB0,THETA,CPLUS
00186      REAL H,HH,X,XT,T,TT,A,AA,B,BB,C,E,F
00190      REAL S,CS,AL,DKL
00200      REAL DELTK
00210      AL=0.1
00220      DD=7.E-10
00225      CMB0=0.
00230      1007 CONTINUE
00232      PRINT *,'ENTER DELTK'
00234      READ *,DELTK
00236      IF(DELTK.GT.10.)GO TO 125
00240      PRINT*,'ENTER CDT'
00245      READ*,CDT
00270      THETA=0.10
00280      CPLUS=0.
00290      H=DELTK*THETA/DD
00300 C    HH=H*H
00310      D=SQRT(DD)
00340       COMPUTATION OF CONCNC. IN DIFFUSION FILM
00350      WRITE(6,101)
00360      101 FORMAT(10X,"X",10X,"T",12X,"CPLUS",14X,"X/SQRT(D*T)")
00370      X=1.E-7
00380      105 CONTINUE
00390      TT=1.
00400      1002 CONTINUE
00410      T=SQRT(TT)
00420      XT=X/(D*T)
00430      A=ERFC(XT/2)
00440      B=EXP(H*X+HH*DD*TT)
00450      C=ERFC(H*D*T+XT/2)
00460      CPLUS=A-B*C
00470      WRITE(6,102)X,TT,CPLUS,XT
00480      102 FORMAT(1X,F15.10,2X,F8.5,2X,F15.10,2X,F15.10)
00490      TT=2*TT
00500      IF(TT.GE.10.)GO TO 103
00510      GO TO 1002
00520      103 CONTINUE
00530      X=10*X
00540      IF(X.GT.1.E-4)GO TO 104
00550 C    GO TO 105
```

```
00560     104 CONTINUE
00590      COMPUTATION OF SURFACE CONCENTRATIONS
00600     WRITE(6,110)
00610     110 FORMAT(10X,"T",5X,"CS DIMENSIONLESS")
00620     TT=1.
00630     113 CONTINUE
00640     T=SQRT(TT)
00650     E=EXP(HH*DD*TT)
00660     F=ERFC(H*D*T)
00670     CS=1-E*F
00680     WRITE(6,111)TT,CS
00690     111 FORMAT(5X,F8.2,2X,E8.3)
00700     TT=10*TT
00710     IF(TT.GE.1.E3)GO TO 112
00720     GO TO 113
00730 C   112 CONTINUE
00732     129 CONTINUE
00760      COMPUTATION OF AVGE. FLUXES
00770     WRITE(6,120)
00780     120 FORMAT(1X,"S",30X,"JD")
00790     S=2.
00800     126 CONTINUE
00810     AA=S-H*SQRT(S)*D
00820     BB=1./(S-HH*DD)
00830     CC=DELTK*THETA*AL*CDT/7.
00840     AJD=CC*AA*BB
00850     WRITE(6,121)S,AJD
00860     121 FORMAT(1X,F8.3,10X,E15.8)
00862     DKL=DELTK*AL
00870     S=S*2
00880     IF(S.GT.150)GO TO 127
00890     GO TO 126
00891     127 CONTINUE
00892     WRITE(6,1008)DELTK,CDT
00893     1008 FORMAT(1X,'DONE FOR DELTA*K=',E8.3,2X,'CDT=',F8.5,/)
00894     WRITE (6,1111)DKL
00895     1111 FORMAT(1X,'DELTA*K*L=',E15.10/)
00896     GO TO 1007
00900     125 STOP
00910     END
```

REWAL OUTPUT

X	T	CPLUS	X/SQRT(D*T)
.0000001000	1.00000	.6274894737	.0037796447
.0000001000	2.00000	.7134188525	.0026726124
.0000001000	4.00000	.7860892137	.0018898224
.0000001000	8.00000	.8438054518	.0013363062
.0000010000	1.00000	.6119948696	.0377964473
.0000010000	2.00000	.7014673467	.0267261242
.0000010000	4.00000	.7771544175	.0188982237
.0000010000	8.00000	.8372756169	.0133630621
.0000100000	1.00000	.4666842760	.3779644730
.0000100000	2.00000	.5861990468	.2672612419
.0000100000	4.00000	.6895467149	.1889822365
.0000100000	8.00000	.7726511912	.1336306210
.0001000000	1.00000	.0026790183	3.7796447301
.0001000000	2.00000	.0295164611	2.6726124191
.0001000000	4.00000	.1164201812	1.8898223650
.0001000000	8.00000	.2603102125	1.3363062096

T	CS DIMENSIONLESS
1.00	.629E+00
10.00	.860E+00
100.00	.954E+00

S	JD
2.000	.24928322E-11
4.000	.28872124E-11
8.000	.32508832E-11
16.000	.35687385E-11
32.000	.38337973E-11
64.000	.40463031E-11
128.000	.42113662E-11

DONE FOR DELTA*K=.327E-03 CDT= .00001

DELTA*K*L=.3270000000E-04

X	T	CPLUS	X/SQRT(D*T)
.0000001000	1.00000	.6274894737	.0037796447
.0000001000	2.00000	.7134188525	.0026726124
.0000001000	4.00000	.7860892137	.0018898224
.0000001000	8.00000	.8438054518	.0013363062
.0000010000	1.00000	.6119948696	.0377964473
.0000010000	2.00000	.7014673467	.0267261242
.0000010000	4.00000	.7771544175	.0188982237
.0000010000	8.00000	.8372756169	.0133630621
.0000100000	1.00000	.4666842760	.3779644730
.0000100000	2.00000	.5861990468	.2672612419
.0000100000	4.00000	.6895467149	.1889822365
.0000100000	8.00000	.7726511912	.1336306210
.0001000000	1.00000	.0026790183	3.7796447301
.0001000000	2.00000	.0295164611	2.6726124191
.0001000000	4.00000	.1164201812	1.8898223650
.0001000000	8.00000	.2603102125	1.3363062096

T	CS DIMENSIONLESS
1.00	.629E+00
10.00	.860E+00
100.00	.954E+00

S	JD
2.000	.24928322E-10
4.000	.28872124E-10
8.000	.32508832E-10
16.000	.35687385E-10
32.000	.38337973E-10
64.000	.40463031E-10
128.000	.42113662E-10

DONE FOR DELTA*K=.327E-03 CDT= .00010

DELTA*K*L=.3270000000E-04

X	T	CPLUS	X/SQRT(D*T)
.0000001000	1.00000	.6274894737	.0037796447
.0000001000	2.00000	.7134188525	.0026726124
.0000001000	4.00000	.7860892137	.0018898224
.0000001000	8.00000	.8438054518	.0013363062
.0000010000	1.00000	.6119948696	.0377964473
.0000010000	2.00000	.7014673467	.0267261242
.0000010000	4.00000	.7771544175	.0188982237
.0000010000	8.00000	.8372756169	.0133630621
.0000100000	1.00000	.4666842760	.3779644730
.0000100000	2.00000	.5861990468	.2672612419
.0000100000	4.00000	.6895467149	.1889822365
.0000100000	8.00000	.7726511912	.1336306210
.0001000000	1.00000	.0026790183	3.7796447301
.0001000000	2.00000	.0295164611	2.6726124191
.0001000000	4.00000	.1164201812	1.8898223650
.0001000000	8.00000	.2603102125	1.3363062096

T	CS DIMENSIONLESS
1.00	.629E+00
10.00	.860E+00
100.00	.954E+00

S	JD
2.000	.24928322E-09
4.000	.28872124E-09
8.000	.32508832E-09
16.000	.35687385E-09
32.000	.38337973E-09
64.000	.40463031E-09
128.000	.42113662E-09

DONE FOR DELTA*K=.327E-03 CDT= .00100

DELTA*K*L=.3270000000E-04

X	T	CPLUS	X/SQRT(D*T)
.0000001000	1.00000	.6274894737	.0037796447
.0000001000	2.00000	.7134188525	.0026726124
.0000001000	4.00000	.7860892137	.0018898224
.0000001000	8.00000	.8438054518	.0013363062
.0000010000	1.00000	.6119948696	.0377964473
.0000010000	2.00000	.7014673467	.0267261242
.0000010000	4.00000	.7771544175	.0188982237
.0000010000	8.00000	.8372756169	.0133630621
.0000100000	1.00000	.4666842760	.3779644730
.0000100000	2.00000	.5861990468	.2672612419
.0000100000	4.00000	.6895467149	.1889822365
.0000100000	8.00000	.7726511912	.1336306210
.0001000000	1.00000	.0026790183	3.7796447301
.0001000000	2.00000	.0295164611	2.6726124191
.0001000000	4.00000	.1164201812	1.8898223650
.0001000000	8.00000	.2603102125	1.3363062096

T	CS DIMENSIONLESS
1.00	.629E+00
10.00	.860E+00
100.00	.954E+00

S	JD
2.000	.24928322E-08
4.000	.28872124E-08
8.000	.32508832E-08
16.000	.35687385E-08
32.000	.38337973E-08
64.000	.40463031E-08
128.000	.42113662E-08

DONE FOR DELTA*K=.327E-03 CDT= .01000

DELTA*K*L=.3270000000E-04

```
      PROGRAM NORG(INPUT,OUTPUT,TAPE6,TAPE62)
C     THIS PROGRAM CALCULATES THE ORGANIC PHASE SPECIA-
C     TION IN THE
C     MIXED HDNNS-LIX63 SYSTEM, USING THE CONSTANTS DETER-
C     MINED BY
      ZHENG AND OSSEO-ASARE FROM VPO MEASUREMENTS. THE
     NAG ROUTINE
      C05NBF DOES THE JOB, IT DOES NOT REQUIRE SUPLYING OF
     JACOBIAN.
      COMMON /CONOO  / CXX,CLT,KP,KB,KM
      COMMON/COOO/ KM1,KM2,KL2,KL3
      DIMENSION C(14,10),CDT(20),Z(20)
      DIMENSION X(2),FVEC(2),WA(19),XCDT(20),XCP(20),XCD23L(20)
      REAL KP,KB,KM1,KM2,KL2,KL3,KM
      REAL
     LCDT(20),LCD,LCL,LCP,LCL2,LCL3,LCDL,LCD7L,LCD72L,LCD23L
      EXTERNAL FCN
      CALL BORDOFF
      CALL START(2)
      CALL SCALEZ (1.5)
      N=2
      KP=6.47E26
      KL2=2.03
      KL3=4.68E3
      KB=4.84E4
      KM1=249
      KM2=1.58
      KM=1.27E-13
      SMA=0.
      SMIC=0.
      F=0.
      LWA=19
      XTOL=1.E-10
      IFAIL=0
      WRITE(6,101)
101   FORMAT(4X,'CDT',15X,'CLT',15X,'SMA',15X,'SMIC',15X,'F')
29    CONTINUE
      I=0
      PRINT *,'ENTER CLT'
      READ *,CLT
      IF(CLT.GT.0.1)GO TO 104
38    CONTINUE
      I=I+1
      PRINT *,'ENTER CDT'
      READ *,CDT(I)
      X(1)=CDT(I)
      X(2)=CLT
      CXX=CDT(I)
      CALL C05NBF(FCN,N,X,FVEC,XTOL,WA,LWA,IFAIL)
```

```
      GO TO 108
      WRITE(6,10)IFAIL,X(1),X(2)
10    FORMAT(1X,'IFAIL=',I5,/,'CD=',E15.8,2X,'CL=',E15.8,/)
108   CONTINUE
      CD=X(1)
      CL=X(2)
      CP=KP*(CD**7)
      CL2=KL2*CL*CL
      CL3=KL3*CL*CL*CL
      CDL=KB*CD*CL
      CD7L=KM1*CP*CL
      CD72L=KM2*CP*CL*CL
      CD23L=KM*KP*CD*CD*CL*CL*CL
      LCDT(I)=ALOG10(CDT(I))
      LCD=ALOG10(CD)
      LCL=ALOG10(CL)
      LCP=ALOG10(CP)
      LCL2=ALOG10(CL2)
      LCL3=ALOG10(CL3)
      LCDL=ALOG10(CDL)
      LCD7L=ALOG10(CD7L)
      LCD72L=ALOG10(CD72L)
      LCD23L=ALOG10(CD23L)
      GO TO 103
      WRITE(6,11)CDT,LCDT,CLT,CD,LCD,CL,LCL,CP,LCP,CD23L,
     1LCD23L
11    FORMAT(5X,'CDT=',E12.5,5X,'LCDT=',F8.5,5X,'CLT=',F8.5,
     1 5X,/,'CD=',E12.5,5X,'LCD=',F8.5,5X,'CL=',E12.5,5X,'LCL='
     1 ,F8.5,5X,/,'CP=',E12.5,5X,'LCP=',F8.5,5X,'CD23L=',E12.5,
     1 5X,'LCD23L=',F8.5)
      WRITE(6,12)CL2,LCL2,CL3,LCL3,CDL,LCDL,CD7L,LCD7L,
     1 CD72L,LCD72L
12    FORMAT(1X,'CL2=',E12.5,5X,'LOG CL2=',F8.5,5X,'CL3=',E12.5,5X,
     1 'LOG CL3=',F8.5/,1X,'CDL=',E12.5,5X,'LOG CDL=',F8.5,5X,
     1 'CD7L=',E15.5,5X,'LOG CD7L=',F8.5,5X,'CD72L=',E15.8,5X,
     1 'LOG CD72L=',F8.5/)
103   CONTINUE
      SMA=CL2+CL3+CDL+CD23L
      SMIC=CP+CD7L+CD72L
      F=(SMA+SMIC)*7./CDT(I)
      WRITE(6,102)CDT(I),CLT,SMA,SMIC,F
102   FORMAT(1X,E10.5,2X,E10.5,2X,E10.5,2X,E10.5,2X,F8.5)
      C(I,1)=CP
      C(I,2)=CD23L
      C(I,3)=CD
      C(I,4)=CL
      C(I,5)=CL2
      C(I,6)=CL3
```

```
      C(I,7)=CDL
      C(I,8)=CD7L
      IF(I.LT.12)GO TO 38
      CALL PLOT(2.,0.,-3)
      CALL LOGAX(0.,0.,2,.8,20,-20,2,2,1)
      CALL LOGAX(0.,0.,1,4.,5,-5,1,1,1)
      WRITE(7,1111) (CDT(IU),(C(IU,IOO),IOO=1,8) ,IU=1,12)
1111  FORMAT(1X,9(E10.3,2X))
      DO 223 J=1,8
      DO 99 J1=1,12
      Z(J1)=C(J1,J)
99    CONTINUE
      CALL POINTS(CDT,Z,I)
      CALL SYMBOL(10.,2.,.42,'CDT (KMOLE/M3)',0.,0)
      CALL SYMBOL(1.,4.,.42,'CONC. SPECIES (KMOLE/M3)',90.,0)
      CALL SYMBOL(2.,3.,.42,'CLT=',0.,0)
      CALL NUMBER(4.,3.,.42,CLT,0.,6)
      DO 414 ITR=2,I,2
      CALL LOCATE(CDT(ITR),C(ITR,J),ZW,ZQ,1)
      CALL SYMBOL(ZW,ZQ,.35,J,0.,-1)
414   CONTINUE
223   CONTINUE
      CALL NEWPAGE
      GO TO 29
104   CONTINUE
      CALL ENPLOT
      STOP
      END
      SUBROUTINE FCN(N,X,FVEC,IFLAG)
      COMMON /CONOO / CXX,CLT,KP,KB,KM
      COMMON/COOO/ KM1,KM2,KL2,KL3
      INTEGER IFLAG,N
      REAL FVEC(2),X(2)
      REAL KP,KB,KM1,KM2,KL2,KL3,KM
      N=2
      FVEC(1)=X(1)*(1.+KB*X(2))+2.*KM*KP*X(2)*X(2)*X(2)*X(1)
     1 *X(1)+7.*KP*(X(1)**7)*(1.+KM1*X(2)+KM2*X(2)*X(2))-CXX
      FVEC(2)=X(2)*(1.+KB*X(1)+KM1*KP*(X(1)**7))+2.*X(2)*X(2)
     1 *(KM2*KP*(X(1)**7)+KL2)+3.*(X(2)**3)*(KL3+KM*KP*X(1)
     1 *X(1))-CLT
      RETURN
      END
```

NORG OUTPUT

CDT	CLT	SMA	SMIC	F
.10000E-04	.10000E-02	.16029E-04	.13407E-19	11.22029
.20000E-04	.10000E-02	.25648E-04	.18219E-17	8.97676
.50000E-04	.10000E-02	.54460E-04	.13371E-14	7.62446
.10000E-03	.10000E-02	.10234E-03	.23663E-12	7.16369
.20000E-03	.10000E-02	.19757E-03	.62034E-10	6.91503
.50000E-03	.10000E-02	.47420E-03	.60221E-06	6.64728
.10000E-02	.10000E-02	.62364E-03	.48101E-04	4.70217
.20000E-02	.10000E-02	.66042E-03	.18462E-03	2.95762
.50000E-02	.10000E-02	.67841E-03	.60952E-03	1.80309
.10000E-01	.10000E-02	.67343E-03	.13237E-02	1.39801

.50000E-04	.50000E-02	.37949E-03	.87940E-19	53.12870
.10000E-03	.50000E-02	.42116E-03	.10799E-16	29.48113
.20000E-03	.50000E-02	.50280E-03	.12944E-14	17.59788
.50000E-03	.50000E-02	.73780E-03	.72893E-12	10.32919
.10000E-02	.50000E-02	.11123E-02	.11123E-09	7.78586
.20000E-02	.50000E-02	.18612E-02	.54750E-07	6.51427
.50000E-02	.50000E-02	.30015E-02	.23556E-03	4.53185
.10000E-01	.50000E-02	.30963E-02	.93732E-03	2.82355